MOLECULAR MECHANISMS OF TYROSINE KINASE INHIBITORS-ASSOCIATED HEPATOTOXICITY

Inauguraldissertation

zur

Erlangung der Würde eines Doktors der Philosophie

vorgelegt der

Philosophisch-Naturwissenschaftlichen Fakultät

der Universität Basel

von

Franziska Paech

aus Deutschland

2019

Genehmigt von der Philosophisch-Naturwissenschaftlichen Fakultät

auf Antrag von

Prof. Stephan Krähenbühl

Prof. Alex Odermatt

Basel, den 14. November 2017

Prof. Dr. Martin Spiess

TABLE OF CONTENTS

ACKNOWLEDGMENT

At the end of the long journey, I would like to thank all those who have supported me during my PhD study.

First of all, I would like to express my sincere gratitude to Prof. Stephan Krähenbühl for given me the opportunity to start my PhD in his lab, for continuous support of my PhD study, for his patience, motivation and extensive knowledge. I appreciate your support and scientific discussion we had. Thank you for your encouragement and advice how to reach my scientific goals!

Besides my advisor, I would like to thank the rest of my thesis committee: Prof. Alex Odermatt and Prof. Jörg Huwyler for being part of my jury.

My sincere thank also goes to my PhD supervisor Jamal Bouitbir for his insightful comments, suggestions, and encouragement. You had always an open door for all my questions. Merci beaucoup pour ton aide!

I want to thank Cécile and Vanessa for being such motivated master students. I enjoyed working with you. Thanks for your great scientific contribution!

A big thanks goes to Andrea, Anna, Annalisa, Bea, Benji, David, Deborah, Dino, Fabio, François, Gerda, Miljenko, Patrizia, Riccardo, Urs, Xun and all other master students in Lab 410 and Lab 411 for your stimulating scientific discussions. It was a pleasure to know you all and to work in such an inspiring atmosphere. I enjoyed the good talks during lunch breaks and other group activities.

Last but not least, I would like to thank my parents for supporting me during all my studies and PhD study. Vielen Dank für eure Unterstützung in meinem Leben!

At the end I would like to express appreciation to my beloved boyfriend Christian who was always a good listener for all my problems. Vielen Dank für all deine Unterstützung und Liebe vor allen in den letzten stressigen Monaten!

ABBREVIATIONS

ABL1	Abelson murine leukemia viral oncogene homolog 1
ADP	Adenosine diphosphat
ALK	Anaplastic lymphoma kinase
ALP	Alkaline phosphatase
ALT	Alanine Aminotransferase
AMPK	AMP-activated protein kinase
Apaf-1	Apoptotic protease activating factor-1
APAP	Acetaminophen
AST	Aspartate Aminotransferase
ATP	Adenosine triphosphate
BCR	Breakpoint cluster region
CACT	Carnitine acylcarnitine translocase
CML	Chronic myelogenous leukemia
CO_2	Carbon dioxide
CoA	Coenzyme A
CPT1	Carnitine palmitoyltransferase 1
DILI	Drug-induced liver injury
DISC	Death-inducing signaling complex
DNA	Desoxyribonucleic acid
Drp1	Dynamin-related protein 1
EGFR	Epidermal growth factor receptor
EML4	Echinoderm microtubule-associated protein-like 4
ETC	Electron transport chain
FADH$_2$	Flavin adenine dinucleotide
Fas	First apoptosis signal
FDA	Food and Drug Administration
FGFR	Fibroblast growth factor receptor
FLT3	Foetal liver tyrosine kinase receptor 3

FMN	Flavin mononucleotide
GIST	Gastrointestinal stromal tumors
GPx	Glutathione peroxidase
GSH	Reduced glutathione
GSSG	Oxidized glutathione
GWAS	Genome-wide association studies
HER2	Human epidermal growth factor receptor 2
HLA	Human leukocyte antigen
HLC	Hepatocyte-like cells
H_2O	Water
H_2O_2	Hydrogen peroxide
KIT	Tyrosine-protein kinase
Mfn	Mitofusin
MPTP	Mitochondrial permeability transition pore
mtDNA	Mitochondrial DNA
NADH	Nicotinamide adenine
NRF	Nuclear respiratory factor
O$_2$	Dioxygen
$\bullet O_2^-$	Superoxide anion radical
•OH	Hydroxyl radical
Opa1	Optic atrophy 1
OXPHOS	Oxidative phosphorylation
PARP	Poly ADP-ribose polymerase
PDGFR	Platelet-derived growth factor receptor
PGC-1	Peroxisome proliferator-activated receptor-γ-coactivator-1
Ph+ ALL	Philadelphia chromosome-positive acute lymphoblastic leukemia
PRC	PGC-1 related coactivator
RM	Reactive metabolite
ROS	Reactive oxygen species
SOD	Superoxide dismutase

TCA	Tricarboxylic acid cycle
TFAM	Mitochondrial transcription factor A
TIM	Translocase of the inner membrane
TK	Tyrosine kinase
TKI	Tyrosine kinase inhibitor
TNF	Tumor necrosis factor
TOM	Translocase of the outer membrane
ULN	Upper limit of normal
UPC	Uncoupling protein
VDAC	Voltage-dependent anion channels
VEGFR	Vascular endothelial growth factor receptor

SUMMARY

Tyrosine kinase inhibitors (TKIs) have revolutionized the treatment of certain cancers. They are usually well-tolerated, but can cause adverse reaction including liver injury. Currently, mechanisms of hepatotoxicity associated with TKIs are only partially clarified. We therefore aimed at investigating the *in vitro* mechanisms of hepatotoxicity of 10 TKIs that have been reported to cause liver injury in patients in our first three papers. We treated HepG2 cells, HepaRG cells, and mouse liver mitochondria with TKIs (concentrations 0.5-100 µM) for different periods of time and assessed toxicity.

In the first paper, we investigated erlotinib, imatinib, lapatinib, and sunitinib. In HepG2 cells, all TKIs showed a time- and concentration-dependent cytotoxicity and, except erlotinib, a drop in intracellular ATP. For imatinib, lapatinib, and sunitinib, cytotoxicity increased in HepaRG cells induced with rifampicin, suggesting formation of toxic metabolites. Imatinib, lapatinib, and sunitinib reduced the mitochondrial membrane potential in HepG2 cells and in mouse liver mitochondria. In HepG2 cells, these compounds increased reactive oxygen species (ROS) production, impaired glycolysis, and induced apoptosis. In addition, imatinib and sunitinib impaired oxygen consumption and activities of complex I and/or III of the electron transport chain, and reduced the cellular GSH pool. In conclusion, imatinib and sunitinib are mitochondrial toxicants after acute and long-term exposure and inhibit glycolysis. Lapatinib affects mitochondria only weakly and inhibits glycolysis, whereas the cytotoxicity of erlotinib could not be explained only by a mitochondrial mechanism.

In the second paper, we investigated crizotinib, dasatinib, pazopanib, ponatinib, regorafenib, and sorafenib. Regorafenib and sorafenib strongly inhibited oxidative metabolism and glycolysis, decreased the mitochondrial membrane potential, and induced apoptosis and/or necrosis of HepG2 cells at concentrations similar to steady-state plasma concentrations in humans. In HepaRG cells, pretreatment with rifampicin decreased membrane toxicity and dissipation of ATP stores, indicating that toxicity was associated mainly with the parent drugs. Ponatinib strongly impaired oxidative metabolism but only weakly glycolysis, and induced apoptosis of HepG2 cells at concentrations higher than steady-state plasma concentrations in humans. Crizotinib and dasatinib did not significantly affect mitochondrial functions and inhibited glycolysis only weakly, but induced apoptosis of HepG2 cells.

Pazopanib was associated with a weak increase in mitochondrial ROS formation and inhibition of glycolysis without being cytotoxic. In conclusion, regorafenib and sorafenib are strong mitochondrial toxicants and inhibitors of glycolysis at clinically relevant concentrations. Ponatinib affects mitochondria and glycolysis at higher concentrations than reached in plasma (but possibly in liver), whereas crizotinib, dasatinib and pazopanib show no relevant toxicity.

In the third paper, we wanted to better characterize the mechanisms underlying the mitochondrial impairment observed with the multikinase inhibitors ponatinib, regorafenib, and sorafenib in our second paper. The multikinase inhibitors impaired the activity of different complexes of the respiratory chain. As a consequence, they decreased the mitochondrial membrane potential concentration-dependently. They induced mitochondrial fission and mitophagy as well as mitochondrial release of cytochrome *c* associated with apoptosis and/or necrosis. In conclusion, ponatinib, regorafenib, and sorafenib impair the function of the respiratory chain, which is associated with increased ROS formation and a drop in the mitochondrial membrane potential. Despite mitochondrial fission and mitophagy, some cells are eliminated concentration-dependently by apoptosis or necrosis. Mitochondrial dysfunction may represent a toxicological mechanism of hepatotoxicity associated with certain kinase inhibitors.

In the fourth paper, we switched to the *in vivo* situation and aimed to investigate the *in vivo* mechanisms of hepatotoxicity of sunitinib in mice. We treated mice with 7.5 mg/kg sunitinib for 14 days. Sunitinib did not affect nutrient intake or body weight, but was associated with a six-fold increase in plasma ALT. Enzyme activity of the mitochondrial electron transport chain was decreased in liver tissue and significantly for complex III in isolated liver mitochondria. The decreased complex activity was associated with mitochondrial ROS formation and increased SOD2 expression. In addition, the citrate synthase activity and protein expression of PGC-1α were reduced. Caspase 3 cleavage and TUNEL-positive hepatocytes were increased, compatible with hepatocyte apoptosis and increased plasma ALT. In conclusion, mice treated with 7.5 mg/kg sunitinib for 14 days had an impaired mitochondrial function leading to hepatocyte apoptosis with the key regulator of mitochondrial proliferation and function PGC-1α may an important mechanistic factor for these findings.

INTRODUCTION

1 LIVER AND DRUG-INDUCED LIVER INJURY

The liver is a vital organ that is part of the digestive system found in all vertebrates. In humans, it is located in the upper-right quadrant of the abdomen, under the rib cage and below the diaphragm. The liver has different important functions such as detoxification of metabolites, protein synthesis, production of biochemicals that are important for digestion, regulation of glycogen storage, metabolism, decomposition of red blood cells, hormone production, and storage of vitamins A, D, E, K, and B12.

The liver has two major blood sources: the portal vein and the hepatic artery. The portal vein is responsible for 75% of the liver blood supply and carries blood from the digestive system to the liver and has therefore nutrients from the digestive system. The hepatic artery supplies the liver with oxygen-rich blood from the heart. In addition, liver cells produce bile, a yellow-green fluid important for fat digestion. The bile is transported to the liver through a series of ducts to the small intestine or to the gallbladder for storage.

The liver is the most important organ for the metabolism of virtually every foreign substance. Most drugs and xenobiotics are lipophilic and thus enable crossing the membranes of intestinal cells. Due to biochemical processes in the hepatocytes, drugs become more hydrophilic and are excreted in urine or bile. The hepatic biotransformation includes oxidative pathways, primarily through the cytochrome P450 enzyme system (Xie et al. 2016). Afterwards, conjugation to a glucuronide, a sulfate or glutathione takes place and the hydrophilic product is exported into plasma or bile by transporters on the hepatocyte membrane and is excreted by the kidney or the gastrointestinal tract (Zamek-Gliszczynski et al. 2006).

Because the liver is the responsible for drug absorption, metabolism and elimination, it is a preferential target organ for drug toxicity. Indeed, drug-related hepatotoxicity and, more specifically, idiosyncratic drug-induced liver injury is the most frequent reason for acute liver failure in the USA (Amacher 2012; Lee 2013). In addition, hepatotoxicity is the major cause of drug withdrawal from the market and non-approval by regulatory authorities in the past five decades (Regev 2014). Because drug induced hepatotoxicity occurs rarely, it often remains undetected during drug development, where only a few thousand subjects are treated.

The following sections will describe the drug-induced liver injury in more detail focusing on the definition, types, risk factors, and targets of cell injury.

1.1 Definition of drug-induced liver injury

Drug-induced liver injury (DILI) is defined as a liver injury that is caused by various medications, herbs, or other xenobiotics that leads to abnormalities in liver tests or liver dysfunction, with reasonable exclusion of other reasons (Suk and Kim 2012). DILI can present in several clinical forms, varying from asymptomatic and transient elevations in liver biochemical tests to jaundice and severe life threatening acute liver failure, but seldom ends in chronic liver disease (Devarbhavi 2012). DILI is clinically defined according to the DILI Expert Working Group as the occurrence of any one of the following: more than five-fold elevation above the upper limit of normal (ULN) for alanine aminotransferase (ALT), more than two-fold elevation above the ULN for alkaline phosphatase (ALP) or more than three-fold elevation in ALT together with a bilirubin elevation of more than two-fold ULN (Aithal et al. 2011). Clinical presentations of DILI are hepatocellular, cholestatic or mixed forms and are defined by the ratio of ALT elevation to ALP elevation (see Table 1). Antimicrobials and drugs for the central nervous system are the most common causes of DILI (Suk and Kim 2012).

Table 1: Liver injury patterns according to (Weiler et al. 2015).

Type of liver injury	Cholestatic	Mixed	Hepatocellular
	Injury to bile ducts or affecting bile flow	Hepatocellular and cholestatic injury	Injury predominantly to hepatocytes
R value	≤2	>2 and <5	≥5

$$\text{R value} = \frac{\text{ALT level/ALT ULN}}{\text{ALP level/ALP ULN}}$$

1.2 Types of drug reactions

DILI can be classified into intrinsic (Type A) and idiosyncratic (Type B) reactions (see Table 2). Intrinsic reactions are dose-dependent, predictable, and experimentally reproducible, having a high incidence. The pain medication acetaminophen (APAP) is the most prominent drug for intrinsic DILI and is responsible for almost half of the cases of acute liver failure in the USA (Gunawan and Kaplowitz 2007). APAP causes dose-related hepatotoxicity in humans and animals through the toxic metabolite N-acetyl-p-benzoquinone imine that

covalently binds to cellular constituents, which depletes the glutathione content and ultimately leads to mitochondrial dysfunction and hepatocellular necrosis (Roth and Ganey 2010). In contrast, idiosyncratic drug reactions occur at therapeutic doses in susceptible individuals at rates from 1 in every 1000 to 1 in every 100 000 patients, with a drug-consistent pattern (Devarbhavi 2012). Idiosyncratic drug reactions are unexpected, not strictly dose-dependent, occur rarely, and currently cannot be predicted by conventional clinical toxicology tests (Fontana 2014). The delay or latency period is between 5 to 90 days from the first ingestion of the drug and idiosyncratic reactions are frequently fatal if the drug is continued once the reaction has started (Hussaini and Farrington 2014). Because of the unpredictability of idiosyncratic toxicity in *in vivo* and *in vitro* models, idiosyncratic DILI remains the major issue for new drug entities (Regev 2014).

Table 2: Intrinsic vs. idiosyncratic DILI (Roth and Ganey 2010).

Characteristics	Intrinsic	Idiosyncratic
Affected patients	Affects all individuals at some dose	Attacks only susceptible individuals
Dose	Clearly dose-related	Obscure relation to dose
Exposure	Predictable latent period after exposure	Variable onset relative to exposure
Physiopathology	Distinctive liver lesion	Variable liver pathology
Prediction	Predictable using routine animal testing	Not predictable using routine animal testing

1.3 Risk factors for idiosyncratic DILI

The traditional thinking is that idiosyncratic DILI is not dose-related. However, a recent study suggested that drugs with a daily dose higher than 50 mg can predispose for idiosyncratic DILI (Lammert et al. 2008). In addition, multifactorial mechanisms appear to underlie DILI, including drug-related risk factors (chemical features of the drug, dose, route, and duration), host-related risk factors (age, sex, genetics, and underlying diseases) and environmental risk factors (diet type, alcohol, coffee, smoking, multidrug therapy, immune state, and nutritional status) (Figure 1) (Licata 2016). Moreover, genetic factors have an important role concerning underlying mechanisms and susceptibility. Polymorphisms in genes involved in drug

metabolism may increase the drug plasma concentrations. Such genetic variations include CYP2E1, N-acetyltransferase 2, UDP-glucuronosyltransferase 2B7, and glutathione S-transferase M1/T1 (Stephens et al. 2012). In addition, patients with genetic variations in the antioxidant enzymes mitochondrial superoxide dismutase 2 (SOD2) and glutathione peroxidase 1 (GPX1) are at higher risk to develop DILI (Lucena et al. 2010). An association between specific human leukocyte antigen (HLA) alleles and idiosyncratic DILI has been reported for several drugs (Kim and Naisbitt 2016). For example, the HLA-B*5701 allele increases the risk for flucloxacillin-induced DILI by 80-fold (Daly et al. 2009). Lapatinib is another example, where DQA1*02:01 and DRB1*07:01 alleles were found more often in patients with elevated transaminases than in patients with normal transaminases (Spraggs et al. 2011; Spraggs et al. 2012).

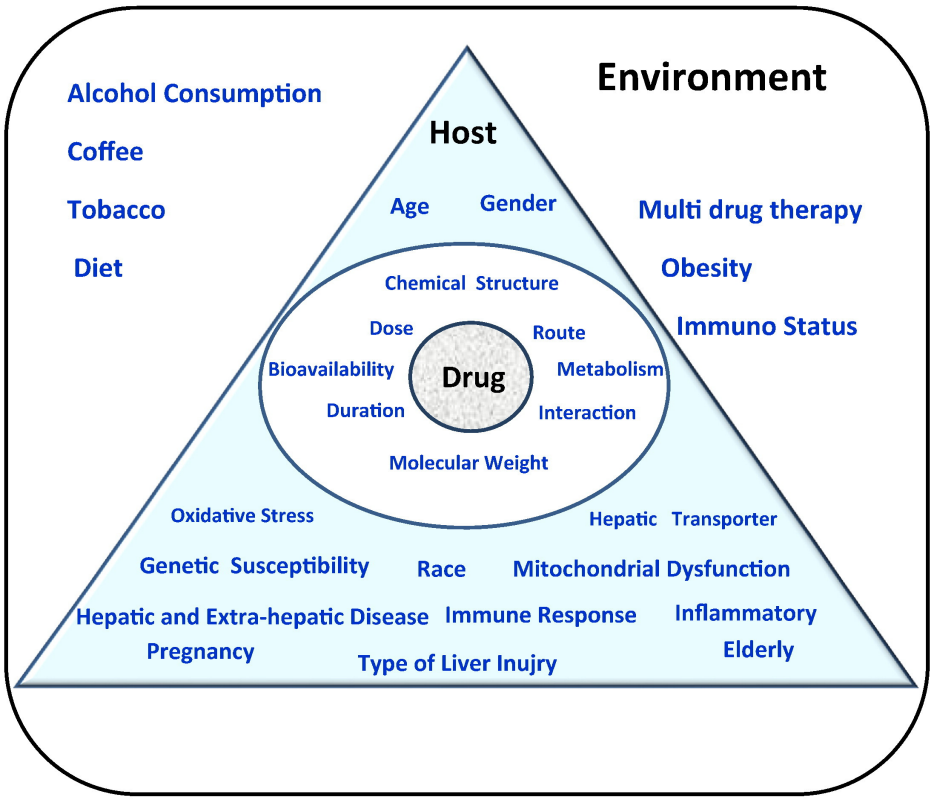

Figure 1: DILI is multifactorial and depends on complex interplay of drug, host, and environmental factors (Licata 2016).

1.4 Targets of cell injury

According to Lee (2003), at least six mechanisms are involved in the development of DILI (see Figure 2). Cytochrome P450 enzymes are lead to covalent binding of the drug to intracellular proteins, consequently producing intracellular dysfunction resulting in the loss of ionic gradient, reduced ATP levels, actin disruption, cell swelling, and cell rupture (Yun et al. 1993) (Figure 2A). If drugs affect transporter proteins at the canalicular membrane, they can interrupt bile flow and cause cholestasis (Trauner et al. 1998) (Figure 2B). Normally, drugs are relatively small molecules and are unlikely to cause an immune response. Nevertheless, biotransformation of the drug can result in the formation of drug-enzyme-adducts. These adducts can be large enough to serve as immune targets, and if they migrate to the surface of the hepatocyte, they can induce the formation of antibodies (antibody-mediated cytotoxicity) or direct cytolytic T-cell response (Robin et al. 1997) (Figure 2C and D). The secondary cytokine response can potentially cause an inflammation and neutrophil-mediated hepatotoxicity (Jaeschke et al. 2002). Another mechanism of DILI is through programmed cell death (apoptosis) together with immune-mediated injury, destroying hepatocytes by tumor necrosis factor and the Fas pathways, including cell shrinkage and fragmentation of nuclear chromatin (Reed 2001) (Figure 2E). If the drug activates pro-apoptotic molecules, they will compete with protective anti-apoptotic survival pathways within the cell. This dynamic interaction may shift the balance to or against cell damage. The last possible DILI-pathway is the damage of mitochondria, disrupting fatty-acid oxidation and energy production of the cell. Drugs can inhibit respiratory-chain enzymes or mitochondrial DNA, resulting in oxidative stress and subsequently anaerobic metabolism, lactic acidosis, and triglyceride accumulation (Pessayre et al. 2001) (Figure 2F). Clearly, more than one of the mentioned cellular pathways to liver injury is possible.

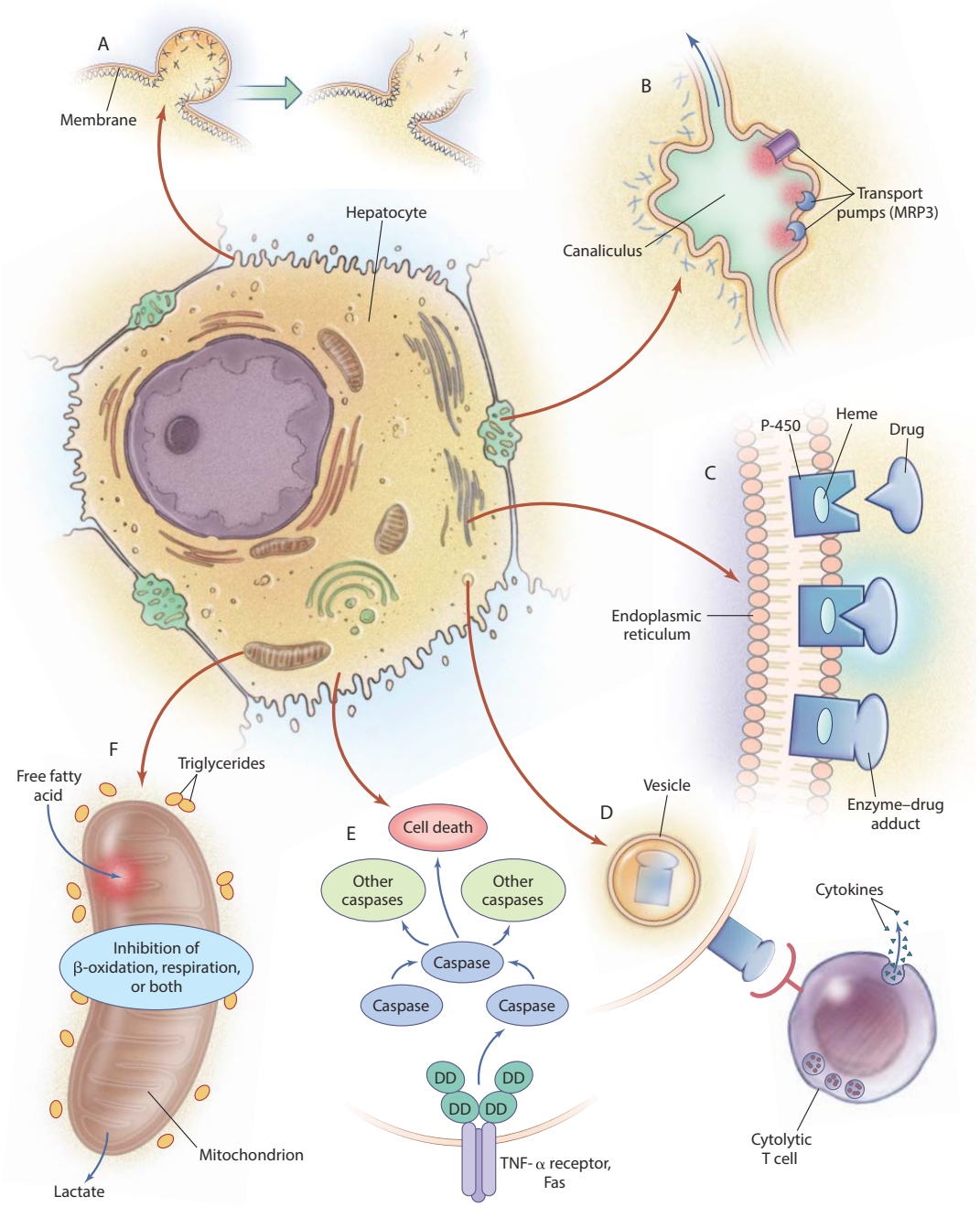

Figure 2: Six mechanisms of drug-induced liver injury. Injury to liver cells occurs in patterns specific to intracellular organelles affected. (A) Blebbing of cell membrane, rupture and cell lysis. (B) Interruption of bile flow and cholestasis. (C) High-energy reactions through the cytochrome P450 system. (D) Enzyme-drug adducts migrate to the cell surface and induce the formation of antibodies or direct cytolytic T-cell response. (E) Apoptosis together with immune-mediated injury. (F) Damage of mitochondria, disrupting fatty-acid oxidation and energy production of the cell. According to (Lee 2003).

1.5 In vitro models

Cell-based screening models are important in early drug development stages to detect hepatotoxicity *in vitro* before testing the new compounds *in vivo* in animals or humans. In the following section, different cellular models and their advantages and disadvantages will be described.

1.5.1 Human hepatocytes

Human hepatocytes in monolayer culture are the gold standard *in vitro* model for testing toxicity and drug metabolism (Zeilinger et al. 2016). They preserve key hepatic-specific functions such as carbohydrate metabolism, plasma protein synthesis and secretion, lipid metabolism and transport, bile acid synthesis and uptake, and drug biotransformation by cytochrome P450 and conjugation enzymes that are still inducible (Gomez-Lechon et al. 2014). In addition, intact cells are used and therefore the plasma membrane is conserved and uptake and excretion mechanisms remain active (Castell et al. 2006). However, limitations of human hepatocytes are their short viability, rapid changes in structure once they are in culture, large variability of different donors, and last but not least, their high costs (Gomez-Lechon et al. 2014).

1.5.2 Isolated mitochondria

Isolating mitochondria from different species such as mice or rat is another approach to estimate hepatotoxicity. After acute drug exposure, isolated mitochondria can be used to measure the activity of oxidative phosphorylation, mitochondrial membrane potential and other mitochondrial functions (Brand and Nicholls 2011; Felser et al. 2013). Nevertheless, isolated mitochondria have no contact to the plasma membrane, cytosol and other organelles and have no access to substrates and inhibitors coming from the cytoplasm and are therefore not in their physiological environment.

1.5.3 Hepatoma cell lines

Human hepatic cell lines created from tumor tissue or by genetic engineering of primary human liver cells are widely used *in vitro* models due to their good availability and high proliferation capacity under standardized and reproducible conditions (Zeilinger et al. 2016). HepG2, HepaRG, Hep3b, and Huh7 cells have been used as hepatic cell lines to study hepatotoxicity *in vitro*. Hepatoma cell lines have several advantages versus human hepatocytes as they grow continuously with an almost unlimited lifespan, have a quite stable phenotype, are easily available and are simple to culture (Castell et al. 2006). Drawbacks are the limited biotransformation activities (Donato et al. 2013). HepG2 cells are the most often used human hepatoma cell line and in addition with another human hepatoma cell line, HepaRG, that expresses drug metabolism and transport abilities and retains the possibility to differentiate *in vitro*, they are the most relevant cell lines to study drug-induced hepatotoxicity.

1.5.3.1 HepG2 cells

HepG2 cells (Figure 3) are an excellent model to study mitochondrial toxicity because of their high content of organelles and mitochondrial DNA (Pinti et al. 2003). HepG2 cells have similar characteristics as normal hepatocytes but the major drawback is the lack of relevant liver cytochrome P450 enzymes (Castell et al. 2006). HepG2 cells are normally grown in media containing 25 mM glucose which is five-fold higher than in physiological conditions (Swiss and Will 2011). However, under these conditions, the cells derive almost all of their energy from glycolysis rather than *via* mitochondrial oxidative phosphorylation, the so-called Crabtree effect (Marroquin et al. 2007). Therefore, mitochondrial toxicants have little effect on cell growth, viability, or cell death. By replacing the glucose with galactose (10 mM), HepG2 cells are forced to rely on mitochondrial oxidative phosphorylation to generate sufficient ATP because the oxidation of galactose to pyruvate *via* glycolysis yields no net ATP (Marroquin et al. 2007). These HepG2 cells under galactose conditions will be more susceptible to mitochondrial toxicants. Nevertheless, interpretation of data has to be done carefully because continuously growing tumor cells differ from normal, resting, and non-neoplastic cells in patients.

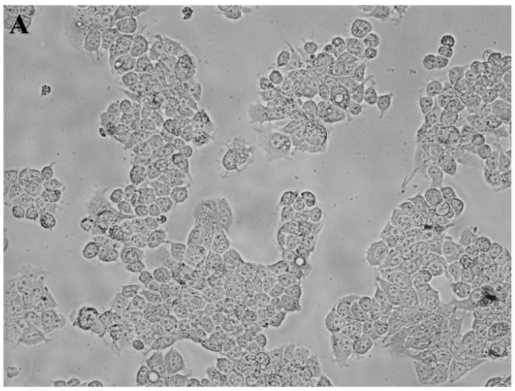

Figure 3: HepG2 cells under the microscope (Elshafie et al. 2017). The photographs were taken at a magnification x40.

1.5.3.2 HepaRG cells

The HepaRG cell line (Figure 4) is one of the most advanced hepatocyte cell culture models because it combines easy handling with physiological drug metabolism (Mueller et al. 2015). HepaRG cells were obtained from a liver tumor of a female patient suffering from hepatocarcinoma (Guillouzo et al. 2007). HepaRG cells can differentiate from a progenitor state to mature hepatocytes and primitive biliary cells which are stable over several weeks (Josse et al. 2008). HepaRG cells express between 81% and 92% of human hepatocyte genes including metabolizing enzymes (Mueller et al. 2015).

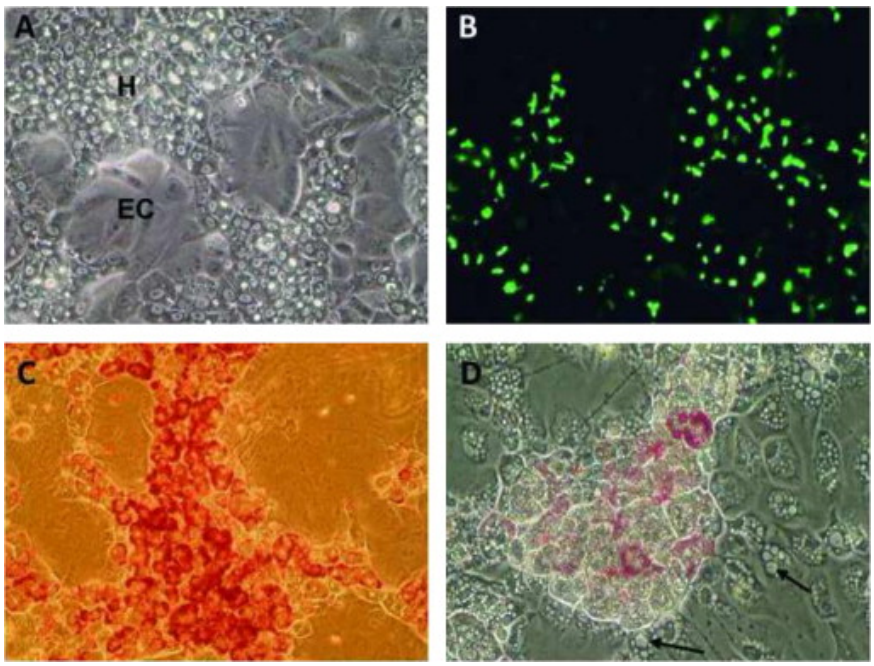

Figure 4: Light microscopy of differentiated HepaRG cells. (A) HepaRG cells treated with standard medium observed under phase-contrast microscopy, H: hepatocyte-like cells, EC: epithelial-like cells. (B) Staining of bile canaliculi. (C) Staining by Oil Red O for 14 days. Lipid droplet accumulation in hepatocyte-like cells. (D) HepaRG cells were treated with amiodarone for 24 h followed by Oil Red O staining. Unstained vesicles corresponding to lamellar bodies are visible in both hepatocyte-like and biliary epithelial-like cells. (Antherieu et al. 2012)

1.5.3.3 3D cell culture

The drawback of all the aforementioned *in vitro* models is the lack of 3D organization of hepatocytes. Several 3D liver culture strategies are available, one of which is the human 3D micro-tissue spheroid culture from InSphero. They use a gravity-enforced cellular assembly that enables the formation of cellular contacts (Messner et al. 2013). After formation of the microtissue, they can be cultured up to 5 weeks with stable function including cell-cell contacts and transporter activity. A recent study demonstrated that the 3D human liver microtissues outperformed human hepatocytes in identifying clinically relevant hepatotoxins (Proctor et al. 2017).

2 MITOCHONDRIA

Mitochondria has been recognized as an important drug biosensor, being a key off-target of drugs inducing idiosyncratic DILI (Han et al. 2013). A lot of drugs causing metabolic failure are highly associated with impaired mitochondrial function (Chan et al. 2005; Hargreaves et al. 2016). Therefore, mitochondrial toxicity has become a major topic in drug development, being the reason for many drug candidate failures, black box warnings or drug withdrawal from the market (Wallace 2015). Mitochondria play a key role in the regulation of cellular function as they supply 90% of the overall cellular energy through oxidative phosphorylation. Consequently, damage at a specific or different mitochondrial targets leads to multi-tissue toxicity. Especially mitochondria-rich organs such as the heart, brain, muscle, and liver that are working under highly aerobic conditions and relying on the energy-producing metabolism of the mitochondria are more susceptible to mitochondrial toxicants. Mitochondrial dysfunction thus can be induced by xenobiotics or by drugs via a direct interaction of mitochondrial function, by an interference with mitochondrial transcription, mitochondrial translation, or by increased superoxide anion formation leading to oxidative stress.
In the following chapter, basic principles of mitochondrial structure, bioenergetics, biogenesis and different mechanisms leading to an impairment of mitochondrial function will be described in more detail.

2.1 Structure

Mitochondria are highly specialized organelles that are organized in a dynamic complex network. Mitochondria (Figure 5) are organized by two membrane systems, the outer and the inner mitochondrial membranes, both formed of phospholipid bilayers. Mitochondria are differentiated into distinct compositional and functional regions, where diverse transporting and enzymatic proteins are integrated. The space between these two membranes is called intermembrane space, in which essential proteins (e.g. cytochrome *c*, creatine kinase) are housed, playing a major role in cell homeostasis and mitochondrial energetics. Moreover, in the inner mitochondrial membrane, multiple invaginations increasing the surface area are formed into the matrix compartment that houses assembled respiratory complexes, proteins for ATP synthesis, and transport.

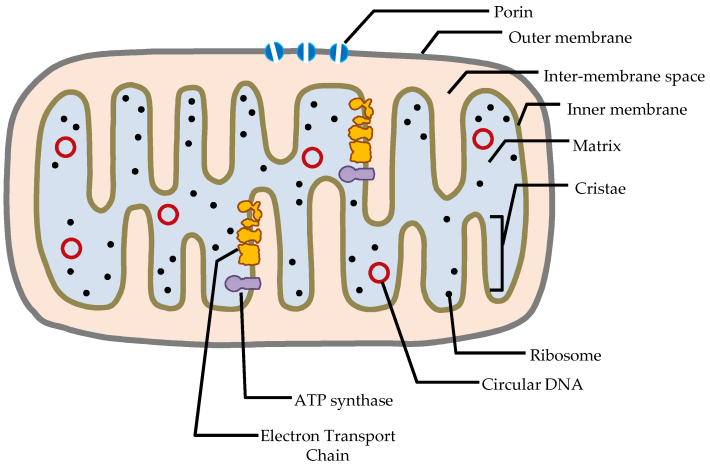

Figure 5: Schematic representation of a mitochondrion. The outer mitochondrial membrane encloses the entire organelle to separate it from the cytosol. The intermembrane space is the space between the outer and the inner mitochondrial membrane. The inner mitochondrial membrane separates the mitochondrial matrix from the intermembrane space. The mitochondrial matrix is the space enclosed by the inner mitochondrial membrane. (Yusoff and Jaafar 2015)

2.1.1 Outer membrane

The outer mitochondrial membrane encloses the entire organelle to separate it from the cytosol. It contains a large number of integral membrane proteins, so called Voltage-dependent anion channels (VDAC), to form pores that allow the transfer of small molecules up to 5000 Da. VDACs are diffusion pores for small hydrophilic molecules to facilitate the exchange of ions between mitochondria and cytosol. The VDACs play a key role in regulating energetic and metabolic flux across the outer mitochondrial membrane by transporting ions such as Ca^{2+}, Na^{+}, K^{+}, Cl^{-} or OH^{-} and ATP, ADP, pyruvate, malate and other metabolites (Blachly-Dyson and Forte 2001). Mitochondrial pro-proteins are imported through specialized translocation complexes – translocases of the outer membrane (TOM). Short-chain fatty acids can simply diffuse through the outer mitochondrial membrane, but long-chain fatty acids transport involves the carnitine palmitoyltransferase 1 (CPT1). A disruption of the outer mitochondrial membrane permits proteins from the intermembrane space to leak into the cytosol, leading to cell death.

2.1.2 Intermembrane space

The intermembrane space is the space between the outer and the inner mitochondrial membrane. Because the outer mitochondrial membrane is permeable to small molecules, the composition of the intermembrane space of ions and sugar is equal to the one of the cytosol.

2.1.3 Inner membrane

The inner mitochondrial membrane separates the mitochondrial matrix from the intermembrane space. The inner mitochondrial membrane is – contrary to the outer mitochondrial membrane – impermeable for small molecules. Only oxygen, water, and carbon dioxide can freely pass the inner mitochondrial membrane. Therefore, the inner mitochondrial membrane is a chemical barrier and an electrical isolator. Transporters of the inner membrane (translocase of the inner membrane, TIM) are needed to import proteins to the mitochondrial matrix. The TIM23 complex facilitates the transport of proteins across the inner mitochondrial membrane whereas the TIM22 complex integrates the proteins to the inner mitochondrial membrane.

The inner mitochondrial membrane consists of 80% proteins and 20% lipids, in contrast to the outer mitochondrial membrane, which consist of 50% proteins and 50% lipids. This membrane is constituted by a highly specialised lipid bilayer, containing cardiolipin in high quantities (Ikon and Ryan 2017). The inner mitochondrial membrane folds extensively to the mitochondrial cristae, increasing the total membrane surface area. For typical liver mitochondria, the area of the inner mitochondria membrane is about five times that of the outer mitochondrial membrane.

The mitochondrial electron transport chain (ETC) consists of five complexes that are located in the inner mitochondrial membrane and produces ATP via oxidative phosphorylation. The ETC will be explained in detail later. The ETC pumps protons from the matrix to the intermembrane space across the inner mitochondrial membrane to produce a proton gradient that is used by the ATP synthase to produce ATP. Uncoupling proteins (UCP) are regulated proton channels in the inner mitochondrial membrane that dissipate the proton gradient by pumping the protons back from the intermembrane space to the mitochondrial matrix and producing heat. UCPs play a role in the generation of reactive oxygen species (ROS). ADP and ATP cannot cross the inner mitochondrial membrane. Therefore, ADP/ATP translocases

enable the import of ADP into the mitochondria and the export of new-formed ATP out of the mitochondria. CPT2 together with a translocase transfer fatty acids inside the matrix, where the β-oxidation takes place.

2.1.4 Matrix

The mitochondrial matrix is the space enclosed by the inner mitochondrial membrane. The matrix contains the mitochondrial DNA, ribosomes, soluble enzymes, small organic molecules, nucleotide cofactors, and inorganic ions. The matrix contains enzymes for the tricarboxylic acid cycle (TCA), β-oxidation, and the urea cycle.

2.1.5 mtDNA

Mitochondria have their own independent circular DNA located in the matrix (see Figure 6). Each mitochondrion contains several copies of mitochondrial DNA (mtDNA), approximately 100-10,000 per cell (Schon et al. 1997). In humans, the 16,569 base pairs of the mtDNA encode for only 37 genes: 13 are for polypeptides, 22 for transfer RNA and 2 for small and large subunits of ribosomal RNA (see table 3). All 13 polypeptides are used in the ETC. The remaining proteins of the ETC are encoded by the nuclear DNA. Mitochondria are lacking protective histones and have relatively lacking repair mechanisms (Meyer et al. 2013). In addition, mitochondria are in direct proximity to the ETC, where the majority of ROS is produced (Fruehauf and Meyskens 2007). Therefore, the mutation rate of the mtDNA is 5-10 times higher than in the nuclear DNA (Tao et al. 2014). The high number of mtDNA is the only working buffering system against stressors.

The mtDNA is only inherited from the mother. Mitochondria are the only organelles that are under genetic control of both nuclear DNA and its own mitochondrial genome.

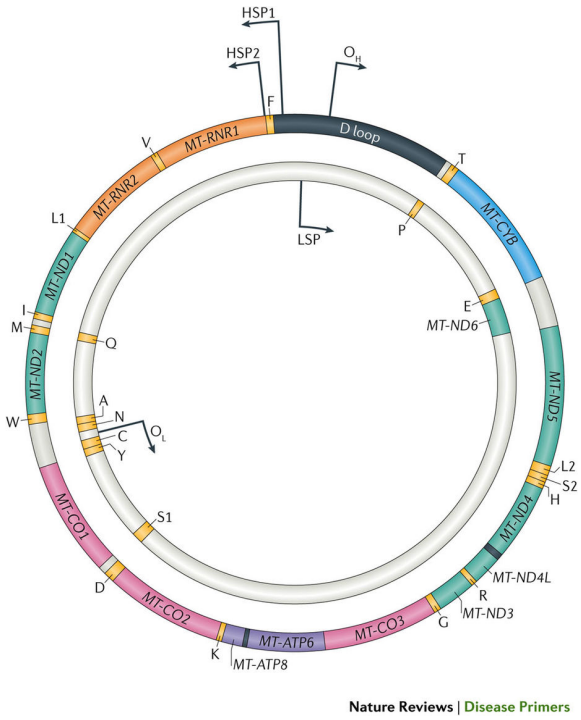

Figure 6: Human mtDNA. The human mitochondrial genome is a 16.6 kb double-stranded and circular DNA molecule. The displacement loop (D loop), a 1.1 kb non-coding region, is involved in the regulation of transcription and replication of mtDNA. The rest encodes 37 genes: 13 are for polypeptides, 22 for transfer RNA and two for small and large subunits of ribosomal RNA. (Gorman et al. 2016)

Table 3: Mitochondrial-encoded genes: 13 proteins, 2 ribosomal RNAs (rRNA) and 22 transfer RNAs (TRNA). Adapted from (Schon et al. 2012).

Proteins	rRNAs	tRNAs	
ATP synthase 6	12S rRNA	tRNA-Ala	tRNA-Met
ATP synthase 8	16S rRNA	tRNA-Arg	tRNA-Phe
COX I		tRNA-Asn	tRNA-Pro
COX II		tRNA-Asp	tRNA-Ser1
COX III		tRNA-Cys	tRNA-Ser2
Cytochrome *b*		tRNA-Gln	tRNA-Thr
ND1		tRNA-Glu	tRNA-Trp
ND2		tRNA-Gly	tRNA-Tyr
ND3		tRNA-His	tRNA-Val
ND4		tRNA-Ile	
ND4L		tRNA-Leu1	
ND5		tRNA-Leu2	
ND6		tRNA-Lys	

2.2 Mitochondrial bioenergetics

Mitochondria are the main organelles for energy production in the cell as they convert the energy produced by the oxidation of pyruvate and fatty acid and from the TCA cycle into ATP through oxidative phosphorylation. Glycolysis in the cytosol is the other pathway for ATP production. However, glycolysis produces only 2 molecules of ATP per glucose molecule whereas oxidative phosphorylation produces more than 30 molecules of ATP per glucose molecule. Mitochondria are also the main organelles involved in fat oxidation. The following sections explain the three main energy-producing pathways of mitochondria.

2.2.1 Tricarboxylic acid cycle

The tricarboxylic acid cycle is the key metabolic pathway that connects carbohydrate, fat, and protein metabolism and consists of a series of eight enzyme-catalyzed reactions taking place in the mitochondrial matrix. The TCA cycle oxidizes acetyl-CoA from carbohydrates, fats and proteins into CO_2 and water and produces ATP, nicotinamide adenine dinucleotide (NADH), and flavin adenine dinucleotide ($FADH_2$) as described in Figure 7. The intermediates of the TCA cycle are used by many essential energy consuming biosynthetic pathways such as amino acids, cholesterol, porphyrin, or nucleotide bases (Williamson and Cooper 1980).

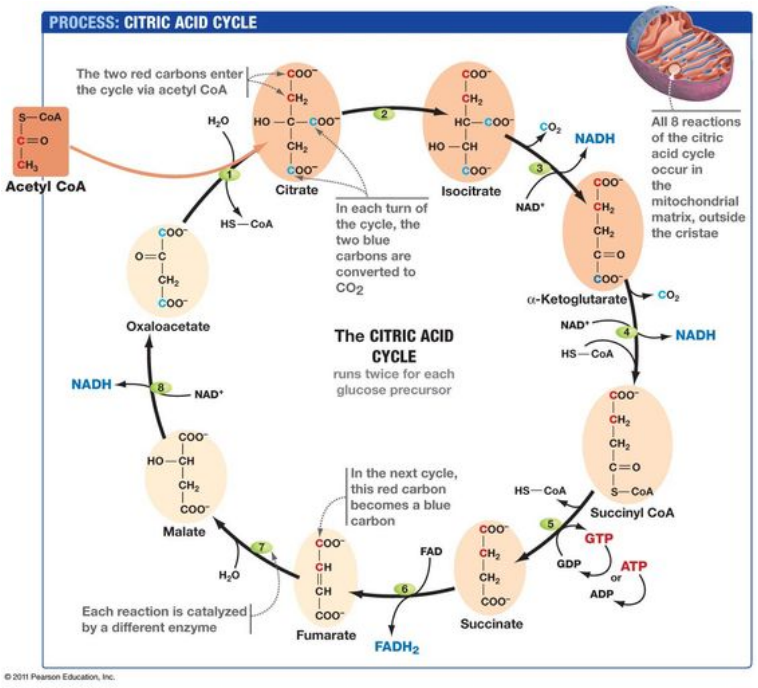

Figure 7: The tricarboxylic acid cycle. The TCA cycle oxidize acetyl-CoA from carbohydrates, fats and proteins into CO_2 and water and producing ATP, NADH, and $FADH_2$.

2.2.2 β-oxidation

Mitochondria are the main organelle for the degradation of fatty acids as they carry out more than 90% of the cellular β-oxidation, the prime pathway for the degradation of fatty acids. The residual 10% are realized in the peroxisomal pathway. In order to enter mitochondria, long-chain fatty acyl-CoAs (C14-C18) require a carnitine shuttle, as the mitochondrial membranes are impermeable to these acyl-CoAs. In contrast, short-chain (C4-C6) and medium-chain (C6-C14) fatty acids are able to freely cross the inner and outer mitochondrial membranes. The first step of the carnitine shuttle is performed by CPT1 in the outer mitochondrial membrane that converts an acyl-CoA into an acylcarnitine. The carnitine acylcarnitine translocase (CACT) exchanges acylcarnitines for free carnitine molecules from the inside. After entering the mitochondria, CPT2 at the inner mitochondrial membrane reconverts the acylcarnitines into the CoA-esters, which can undergo β-oxidation (Houten and Wanders 2010).

Mitochondrial β-oxidation is a cyclic four-enzyme reaction in the mitochondrial matrix where acyl-CoAs are shortened and two carboxy-terminal carbon atoms are released as acetyl-CoA unit each time a cycle is fully completed (see Figure 8). In the first step of the β-oxidation, an

acyl-CoA-ester is dehydrogenated to procedure a trans-2-enoyl-CoA. Afterwards, the double bond is hydrated to a L-3-hydroxy-acy-CoA and in the third step dehydrogenated to 3-keto-acyl-CoA. Finally, this is thiolytic cleaved to a two-carbon chain-shortened acyl-CoA and an acetyl-CoA. The shortened acyl-CoA undergoes another cycle of β-oxidation. In addition to the acetyl-CoA, each cycle produces one NADH and one $FADH_2$ that deliver electrons as electron carriers to the ETC. The produced acetyl-CoA enters the TCA cycle.

As a result of inhibition of β-oxidation or fatty acid oxidation, free fatty acids and triglycerides are accumulating in the cytoplasm forming small vesicles and leading to microvesicular steatosis in patients (Jaeschke et al. 2002).

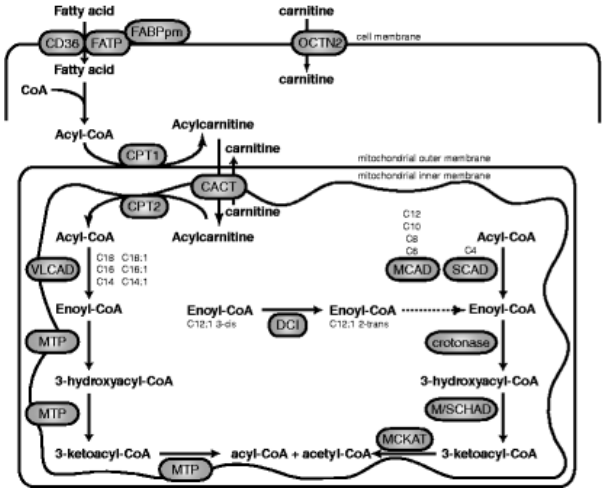

Figure 8: β-oxidation in humans. Fatty acids get activated to acyl-CoAs after transport across the plasma membrane. CPT1 converts the acyl-CoA into an acylcarnitine which is transported across the mitochondrial membrane by CACT. CPT2 converts the acylcarnitine back into the acyl-CoA. Long chain acyl-CoAs are metabolized by membrane bound enzymes, the VLCAD (very long chain acyl-CoA dehydrogenase), MTP (mitochondrial trifunctional protein), LCHAD (long chain hydroxyacyl-CoA dehydrogenase) and thiolase activity. Short and medium chain fatty acids are metabolized in the mitochondrial matrix by MCAD (medium chain acyl-CoA dehydrogenase), SCAD (short chain acyl-CoA dehydrogenase), crotonasa, M/SCHAD (medium and short chain hydroxyacyl-CoA dehydrogenase), and MCKAT (medium chain 3-ketoacyl-CoA thiolase). (Houten and Wanders 2010)

2.2.3 Mitochondrial electron transfer chain and oxidative phosphorylation

The ETC is located in the inner mitochondrial membrane and is composed of five complexes with multiple protein subunits (Figure 9). Briefly, electrons are transferred from NADH to complex I and from $FADH_2$ to complex II. Both complexes transfer their electrons to coenzyme Q, which transports the electrons to complex III. Complex III delivers the electrons to cytochrome *c*, which will then transfer the electrons to complex IV to reduce oxygen to water. In addition, complexes I, III, and IV pump protons across the inner mitochondrial membrane and therefore producing an electrochemical proton gradient – the mitochondrial membrane potential. The membrane potential is used by the ATP synthase (Complex V) to phosphorylate ADP to ATP. This process is called oxidative phosphorylation (OXPHOS) and produces most of the ATP within the cell. The single complexes of the ETC will be described in the next sections in more detail.

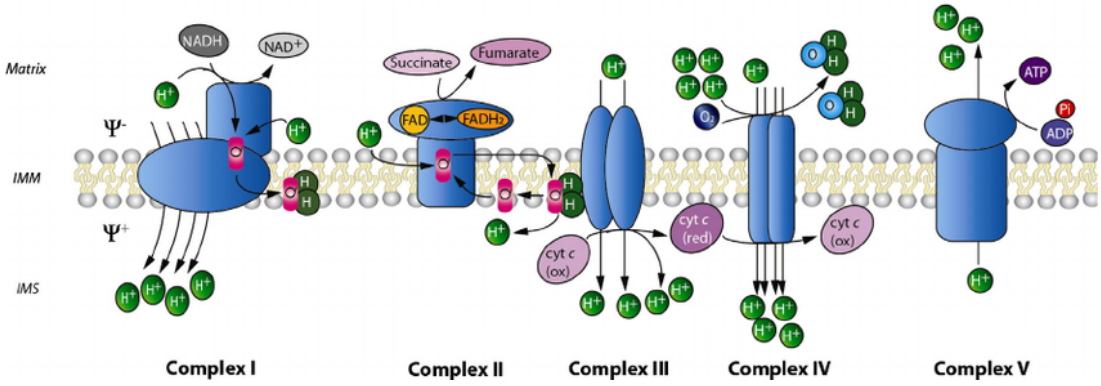

Figure 9: The mitochondrial electron transport chain (Bird et al. 2014). Electrons enter the ETC by oxidation of NADH at complex I and succinate at complex II. They are transferred by the mobile electron carrier coenzyme Q to complex III and afterwards via cytochrome *c* (cyt *c*) to complex IV, where they are used to reduce oxygen to form water. Complex V utilizes the electrochemical gradient to couple proton flow through the complex with ATP synthesis from ADP and phosphate (Pi). In addition, complexes I, III, and IV are pumping protons (H^+) across the inner mitochondrial membrane into the intermembrane space to maintain the mitochondrial membrane potential. IMM: inner mitochondrial membrane; IMS: intermembrane space; ox: oxidized; red: reduced; Ψ: charge.

2.2.3.1 Complex I

The complex I of the ETC is known as the NADH:ubiquinone oxidoreductase or NADH:dehydrogenase. Complex I is composed of 49 subunits, 42 encoded by the nucleus and 7 by the mtDNA (Wirth et al. 2016). Complex I contains 14 central subunits, 7 hydrophilic and 7 hydrophobic polypeptides. The hydrophilic central subunits comprise all redox active prosthetic groups, namely one flavin mononucleotide (FMN) and eight iron-sulfur clusters (Figure 10) (Wirth et al. 2016).

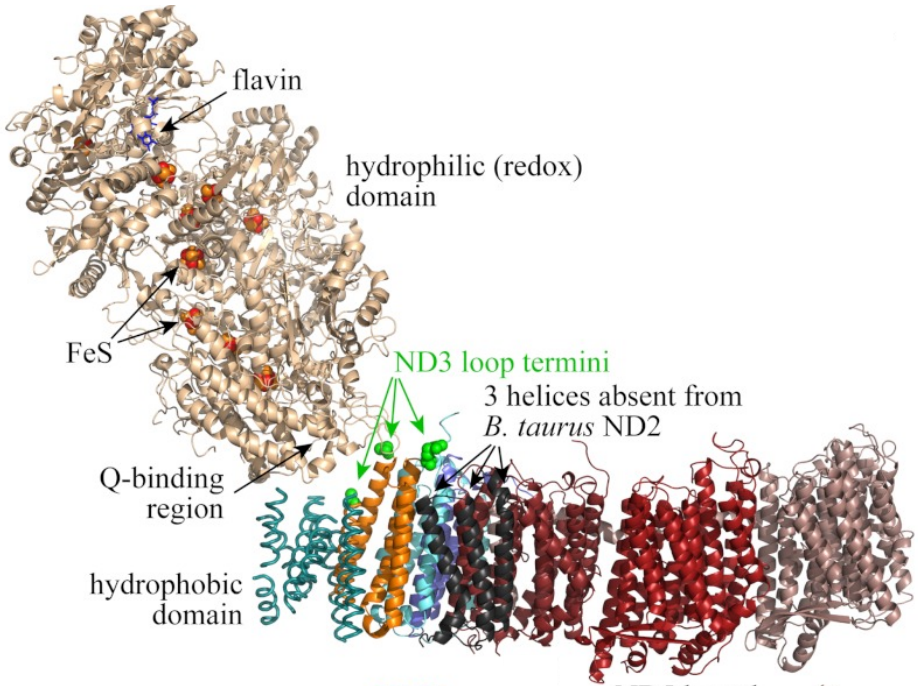

Figure 10: Structure of complex I. Complex I is an L-shaped enzyme, with a large hydrophilic domain containing the flavin mononucleotide, iron-sulfur (FeS) clusters, and the binding site for the ubiquinone headgroup. (Roberts and Hirst 2012)

Complex I catalyzes the transfer of two electrons from NADH to the lipid-soluble carrier ubiquinone (Q) reducing it to ubiquinol (QH_2) and translocates four protons across the inner mitochondrial membrane. The reaction can be described as follow:

$$NADH \leftrightarrow NAD^+ + H^+ + 2\ e^-$$

$$NADH + Q + 5H^+ \leftrightarrow NAD^+ + QH_2 + 4H^+$$

Complex I is one of the main sites where premature electron leakage to oxygen occurs. Complex I can be inhibited by rotenone as it inhibits the transfer of electrons from iron-sulfur centers in complex I to ubiquinone by blocking the quinone-binding site of complex I. Therefore, complex I is unable to pass off its electrons to ubiquinone and is creating a back-

up of electrons within the mitochondrial matrix (Brand 2010). Consequently, the rate of superoxide formation at complex I is increased several-fold through rotenone.

2.2.3.2 Complex II

The complex II is known as succinate:ubiquinone oxidoreductase or succinate dehydrogenase. It is composed of four nuclear encoded subunits. Complex II can be competitively inhibited by malonate by binding to the active site of the enzyme without reacting to it and therefore competing with succinate, the normal substrate of complex II. Complex II catalyzes the oxidation of succinate to fumarate with the reduction of ubiquinone to ubiquinol using two electrons and two protons. Complex II is a parallel electron transport to complex I, but unlike complex I, no protons are pumped across the inner mitochondrial membrane. The reaction can be described as follow:

$$\text{Succinate} + Q \leftrightarrow \text{Fumarate} + QH_2$$

2.2.3.3 Complex III

The complex III is known as ubiquinone-cytochrome *c* oxidoreductase or cytochrome *c* reductase. It is composed of 10 nuclear and 1 mtDNA encoded subunits. Three subunits have prosthetic groups – the cytochrome *b* subunit has two b-type hemes (b_L and b_H), the cytochrome *c* has one *c*-type heme (c_1), and the Rieske Iron Sulfur Protein (ISP) subunit has an iron-sulfur cluster. The Q cycle mechanism postulates two separate quinone-binding sites – one for quinol oxidation (Q_o site) and the other for quinone reduction (Q_i site). One electron from the substrate quinol is transferred at the Q_o site and further to the ISP, to cytochrome c_1 and the soluble electron acceptor cytochrome *c*. The second electron is transferred to heme b_L and b_H ending at the Q_i site (Gao et al. 2003). The fully reduced quinone at the Q_i site picks up two protons from the mitochondrial matrix and moves to the Q_o site for reoxidation. Therefore, a complete Q cycle consumes two quinol-molecules at the Q_o site, generates one quinol-molecule at the Q_i site, and translocates four protons to the intermembrane space (Figure 11).

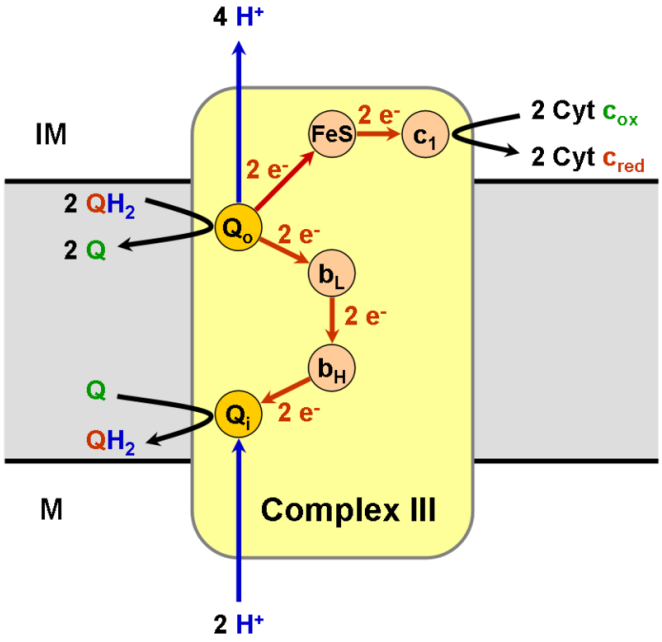

Figure 11: Structure of complex III including the binding site for quinol oxidation (Q_o site), the binding site for quinone reduction (Q_i site). A complete Q cycle consumes two quinol-molecules at the Q_o site, generates one quinol-molecule at the Q_i site, and translocates four protons to the intermembrane space.

Overall, complex III catalyzes the transfer of two electrons from ubiquinol to two molecules of cytochrome *c*, a water-soluble electron carrier located within the intermembrane space. The reaction can be described as follow:

$$QH_2 + 2\ \text{cyt}\ c^{3+} + 2\ H^+ \leftrightarrow Q + 2\ \text{cyt}\ c^{2+} + 4\ H^+$$

Complex III can be inhibited by antimycin A by binding to the Q_i site and therefore inhibiting the electron transfer from the heme b_H to quinone. When the electron transfer is reduced, complex III also leaks electrons to molecular oxygen, resulting in ROS formation.

2.2.3.4 Complex IV

The complex IV is known as cytochrome *c* oxidase and is composed of 10 nuclear and 3 mtDNA encoded subunits. Complex IV transfer four electrons from cytochrome *c* to the terminal electron acceptor – molecular oxygen producing two molecules of water. The reaction can be described as follow:

$$4\ \text{cyt}\ c^{2+} + 8\ H^+ + O_2 \leftrightarrow 4\ \text{cyt}\ c^{3+} + 4\ H^+ + 2\ H_2O$$

Complex IV translocates four protons across the inner mitochondrial membrane and can be inhibited by cyanide. Cyanide prevents the transport of electrons from cytochrome *c* to oxygen.

2.2.3.5 Complex V

The complex V is known as F_1F_0-ATPase or ATP synthase and is composed of 16 nuclear and 2 mtDNA encoded subunits. Complex V uses the electrochemical proton gradient across the inner mitochondrial membrane created by complexes I, III, and IV to produce ATP. The reaction can be described as follow:

$$ADP + P_i + H^+ \leftrightarrow ATP + H_2O + H^+$$

The ATP synthase (Figure 12) consists of two main subunits, F_0 and F_1. F_0 consists of mainly hydrophobic regions embedded in the inner mitochondrial membrane to allow the protons to translocate the inner mitochondrial membrane. The proton flow will be converted to a rotation of the F_1 part. F_1 consists of six hydrophilic subunits, three of them are binding ADP and the other three catalyze the ATP synthesis.

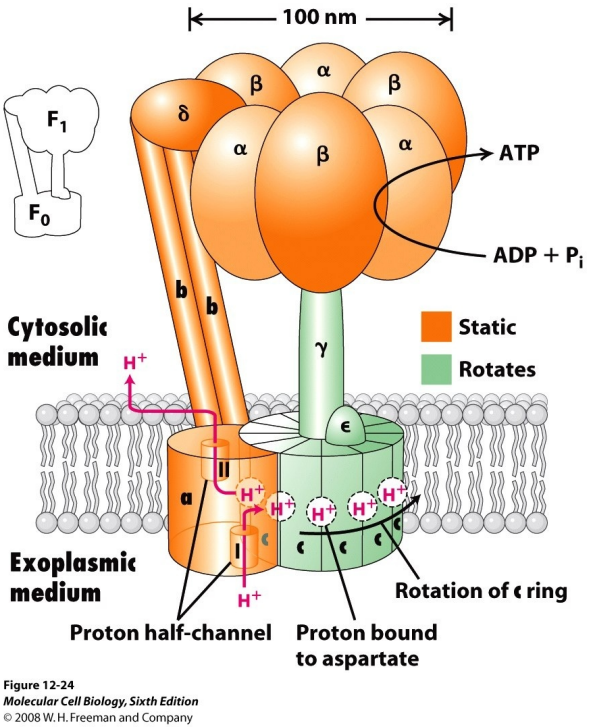

Figure 12: The ATP synthase. The ATP synthase consists of the F_0 and F_1 subunits. F_0 is mainly embedded in the inner mitochondrial membrane to allow the protons to translocate the inner mitochondrial membrane. The proton flow will be converted to F_1-rotation.

2.3 Reactive oxygen species

Oxygen exists in two different forms: as its molecular form (O_2) and as a free radical. A free radical is an atom, molecule or ion that has unpaired valence electrons. These unpaired electrons make free radicals highly chemically reactive towards other molecules. Oxygen has two unpaired electrons in separate orbitals in the valence shell making it especially susceptible to radical formation. Sequential reduction of molecular oxygen leads to the formation of a group of reactive oxygen species: superoxide anion radical ($\bullet O_2^-$), hydrogen peroxide (H_2O_2) and hydroxyl radical ($\bullet OH$) (Figure 13). One electron reduction of oxygen generates the superoxide anion radical ($\bullet O_2^-$), which is not a very reactive species and its chemical reactivity depends on the site of generation in the cell and on the collision with suitable substrates. Further addition of one electron to superoxide will form hydrogen peroxide (H_2O_2), which is non-radical, but can diffuse long distances, cross membrane and can react with transition metals by a hemolytic cleavage yielding the highly reactive hydroxyl radical ($\bullet OH$). Hydrogen peroxide can also be formed by two electrons reduction of oxygen. Addition of one electron to hydrogen peroxide forms a hydroxyl anion and a hydroxyl radical ($\bullet OH$), the most reactive oxygen species because it reacts with almost all biological compounds. The hydroxyl radical will only mediate direct effects close to its site of generation and cannot diffuse long distances. The reactions can be described as follow:

$$O2 + e^- \rightarrow \bullet O_2^-$$

$$2\ H^+ + \bullet O_2^- + \bullet O_2^- \rightarrow H_2O_2 + O_2$$

$$O_2 + 2\ e^- \rightarrow O_2^{2-}$$

$$H_2O_2 + e^- \rightarrow HO^- + \bullet OH$$

$$2\ H_2O_2 \rightarrow 2\ H_2O + O_2$$

Another type of ROS is singlet oxygen ($^1O_2$), which is produced from triplet oxygen ($^3O_2$) through energy input. Singlet oxygen is not a free radical but is highly reactive, especially with organic compounds that contain double bonds. The next sections will explain the biological role and cellular sources of ROS as well as the resulting oxidative stress and the antioxidant system.

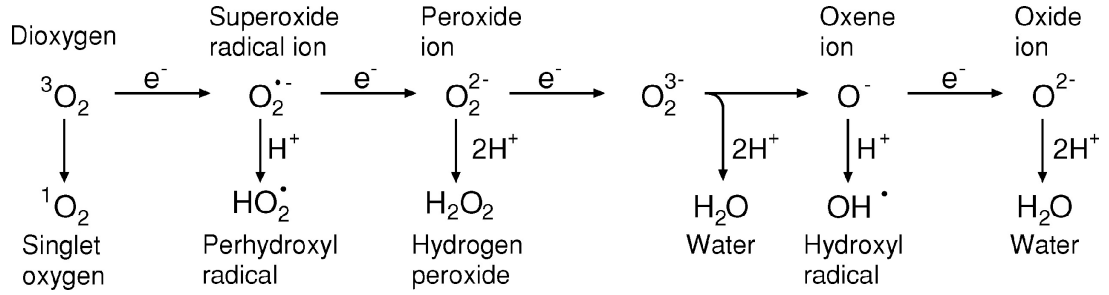

Figure 13: Generation of different ROS by energy transfer or sequential univalent reduction of ground state triplet oxygen (Apel and Hirt 2004).

2.3.1 Biological role of free radicals

Oxygen radicals are not always bad. Indeed, they are produced in a number of essential reactions. ROS are involved in intra- and intercellular signaling and used by the immune system to attack and kill pathogens (Wilson et al. 2017b). Short-term oxidative stress is important in the prevention of aging by the induction of mitohormesis (Gems and Partridge 2008). On the other hand, ROS can be harmful to cells because they are able to damage all macromolecules, including lipids, proteins and nucleic acids (Wilson et al. 2017a).

2.3.2 Cellular sources of ROS

ROS are produced intracellularly through multiple mechanisms: enzymatic reactions – such as NADPH oxidase, NADPH-cytochrome P450 reductase and xanthine oxidase; cellular sources – such as mitochondrial ETC, microsomal monooxygenase, leukocytes, and macrophages; and environmental factors – such as ultraviolet light, radiation, toxic chemicals, aromatic hydroxylamines and aromatic nitro compounds.

NADPH oxidases contain cytosolic FAD- and NADPH-binding domains, six transmembrane domains, and two heme groups (Togliatto et al. 2017). The heme groups transfer the electrons from cytosolic NAD(P)H across the membrane to oxygen to produce superoxide anion outside the cell or in phagosomes to kill bacteria and fungi (Nguyen et al. 2017). The reaction can be described as follow:

$$NADPH + 2\ O_2 \rightarrow NADP^+ + 2\ \bullet O_2^- + H^+$$

NADPH-cytochrome P450 reductase is composed of multiple domains that transport electrons from NADPH to cytochrome P50 via flavin cofactors in the endoplasmic reticulum (Gray et al. 2010). NADPH-cytochrome P450 reductase has the ability to autooxidize and generate ROS (Mishin et al. 2010).

Xanthine oxidases are enzymes that catalyze the oxidation of hypoxanthine to xanthine and the oxidation of xanthine to uric acid. Xanthine oxidase can reduce molecular oxygen with formation of superoxide radical anion and hydrogen peroxide (Bonini et al. 2004).

Most of the electrons transferred to the ETC safely react with protons and oxygen to form water, but some electrons directly react with oxygen at complexes I and III and form superoxide anion radical that afterwards can generate other ROS (Ott et al. 2007). Therefore, mitochondria are the main endogenous source of ROS in the normal cell and produce around 90% of cellular ROS (Balaban et al. 2005). Under normal conditions less thea 0.1% of electrons passing through the ETC leak and form superoxide (Brand 2010). Superoxide can be produced in complex I in two different situations. The first one is when electrons back up in the chain of iron-sulfur clusters. This is the case when NADH is present but the downstream ETC is blocked by rotenone (complex I), antimycin A (complex III), cyanide (complex IV) or other inhibitors. The second situation is the reverse electron transfer, when electrons flow back from complex II via ubiquinone to complex I leading to a reduction of complex I and ROS formation (Drose and Brandt 2012). Superoxide formation at complex III takes place at the Q_o ubiquinone site releasing ROS to both sides of the inner mitochondrial membrane. The rate of ROS formation is strongly increased under oxidant-induced reduction conditions – in the presence of a Q_i site inhibitor like antimycin A, sufficient amount of reducing equivalents and an oxidized downstream respiratory chain. In addition, a high mitochondrial membrane potential can increase the ROS formation at the Q_o site. Inhibition of reducing ubiquinone at the Q_i site and slowing it down by a high mitochondrial membrane potential result in a backup of electrons and an accumulation of semiquinone radical at the Q_o site transferring the electrons to oxygen forming superoxide (Drose and Brandt 2012).

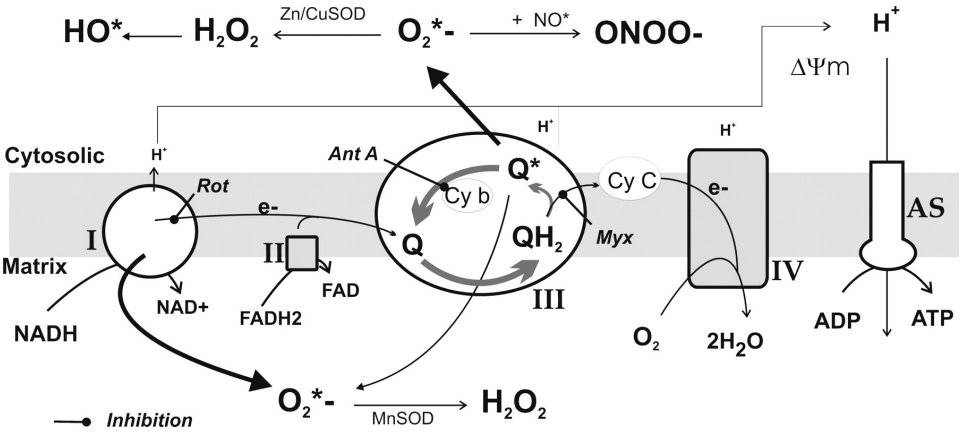

Figure 14: Main mechanisms for mitochondrial ROS generation. The main centers of mitochondrial superoxide formation are complex I and III, although small amounts can be formed at complex II and IV. In addition, the main routes of superoxide transformation are prepresented. SOD: superoxide dismutase, H_2O_2: hydrogen peroxide, $ONOO^-$: peroxynitrite, NO*: nitric oxide, $\Delta\Psi_m$: mitochondrial potential, AS: ATP synthase. Only the inner mitochondria membrane is represented. (Camello-Almaraz et al. 2006)

2.3.3 Oxidative stress

Oxidative stress occurs with an over-formation of ROS or a decreased antioxidant system within the cell. Therefore, oxidative stress can be described as an imbalance between ROS formation and the ability to detoxify the ROS or to repair the resulting damage. Cells can tolerate mild to moderate oxidative stress leading to increased antioxidant defense. High oxidative stress will lead to damages within the cell including proteins, lipids and nucleic acids. One of the best known toxic effects of ROS is the damage of cellular membranes by lipid peroxidation of polyunsaturated fatty acids present in membrane phospholipids, particularly arachidonic and linoleic acid (Ademowo et al. 2017). As a consequence, the membrane fluidity, which is essential for proper function of membranes, decreases. Unless superoxide is quickly dismutated, it can react with nitric oxide (NO) to form DNA- and protein-damaging peroxynitrite (Pessayre et al. 2012). The DNA can be damaged by base damage or strand breaks, which can cause long-term effects when the damage is inside a coding region. mtDNA is 10 times more susceptible for DNA damage than nuclear DNA because 90% of ROS are produced within mitochondria and mitochondria are lacking protective histones and have an incomplete repair mechanisms (Meyer et al. 2013). Protein damage by ROS can lead to peptide chain breaks and the thereby modified protein length and

protein structure may induce a loss of catalytic function of the protein. Normally, any damage to cells is repaired rapidly but severe oxidative stress can cause cell death. Moderate oxidative stress triggers apoptosis while more intense oxidative stress causes ATP depletion, preventing controlled apoptotic death leading to necrosis.

2.3.4 Antioxidant system

Cells developed several antioxidant defense mechanisms to protect themselves against ROS. An antioxidant inhibits the oxidation of other molecules. The enzymatic scavenger system is composed of superoxide dismutase (SOD), catalase, glutathione peroxidase and peroxiredoxin. The antioxidant systems are described in more detail in this section.

2.3.5 Superoxide dismutase

SODs are a class of enzymes that catalyze the dismutation of the superoxide radical into oxygen and hydrogen peroxide:

$$2\ {\bullet}O_2^- + 2\ H^+ \rightarrow H_2O_2 + O_2$$

As described before, superoxide is produced as a by-product of several reactions and by complex I and III of the ETC of mitochondria. If superoxide is not regulated, it can cause different types of cell damage (Hayyan et al. 2016). Hydrogen peroxide can also damage cells and is degraded by other enzymes such as catalase. Therefore, SOD is an important antioxidant defense in nearly all living cells exposed to oxygen. The importance of SODs is illustrated by several knock-out mice models. Mice lacking SOD2 survive only for a short time due to massive oxidative stress (Joe et al. 2015). Mice with a SOD1 knock-out develop a range of different pathologies such as hepatocellular carcinoma, acceleration of age-related muscle mass loss, earlier incidence of cataracts, and reduced lifespan (Elchuri et al. 2005; Muller et al. 2006).

In humans, three forms of SODs (SOD1 to SOD3) are present. SOD1 is mainly located in the cytosol of cells and in the intermembrane space and contains a copper-zinc cofactor. SOD2 is located in the mitochondrial matrix and contains a manganese cofactor. SOD3 is extracellular and contains also a copper-zinc cofactor (Mates et al. 1999).

2.3.5.1 Catalase

Catalase is concentrated in peroxisomes, whereas liver mitochondria contain no catalase. Catalase catalyzes the formation of water and oxygen out of hydrogen peroxide:

$$2\ H_2O_2 \rightarrow 2\ H_2O + O_2$$

Catalase contains four iron-containing heme groups that allow reacting with hydrogen peroxide.

2.3.5.2 Glutathione peroxidase

Glutathione peroxidase (GPx) reduces hydrogen peroxide to water by transferring the energy of the reactive peroxides to a very small sulfur-containing protein called glutathione (GSH) to oxidized glutathione (GSSG):

$$H_2O_2 + 2\ GSH \rightarrow GSSG + 2\ H_2O$$

The sulfur of GSH acts as the reactive center, carrying reactive electrons from the peroxide to the glutathione. Five different forms of GPx exist in mammals. GPx1 and GPx4 are found in most tissues, whereas GPx2 and GPx3 can be found in the gastrointestinal tract and kidney, and GPx5 is specifically expressed in mouse epididymis. GPx1 and GPx2 are located in the cytosol, GPx 3 is extracellular and GPx4 is located in the cytosol and membrane fraction (Mates et al. 1999). As GPx consumes GSH, it is necessary to restore the GSH pool. The glutathione reductase converts GSSG back to GSH.

2.3.5.3 Glutathione

Glutathione (GSH) is an important antioxidant that is used in the reaction of glutathione peroxidase. GSH is a tripeptide with a glutamate, cysteine, and glycine amino acids where the thiol group of cysteine serves as reducing agent (Figure 15). The GSH-structure is unique as the peptide bond linking glutamate and cysteine is through the γ-carboxyl group of glutamate and not through the conventional α-carboxyl group. The only enzyme that can hydrolyze this unusual bond is γ-glutamyltranspeptidase, which is only present on external surfaces of certain cell types (Kunutsor and Laukkanen 2017). Therefore, GSH is resistant to intracellular degradation and is only metabolized extracellularly by cells that express γ-glutamyltranspeptidase.

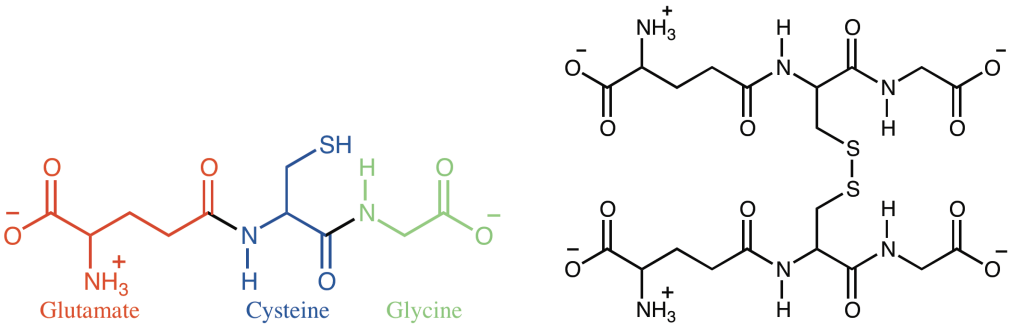

Figure 15: Structure of GSH (left) and GSSG (right). GSH is the tripeptide γ-L-glutamyl-L-cysteinylglycine and GSSG is the oxidized form of GSH.

GSH is present in all mammalian tissues at 1-10 mM with the highest concentration in the liver (Lu 2013). In addition to the antioxidant function by the GPx, GSH regulates the redox-depending cell signaling by modifying the oxidative state of critical protein cysteine residues (Figure 16) (Forman et al. 2009). GSH can bind to the –SH generating glutathionylated proteins, which can either activate or inactivate the protein and protects sensitive thiols from irreversible oxidation (Dalle-Donne et al. 2009).

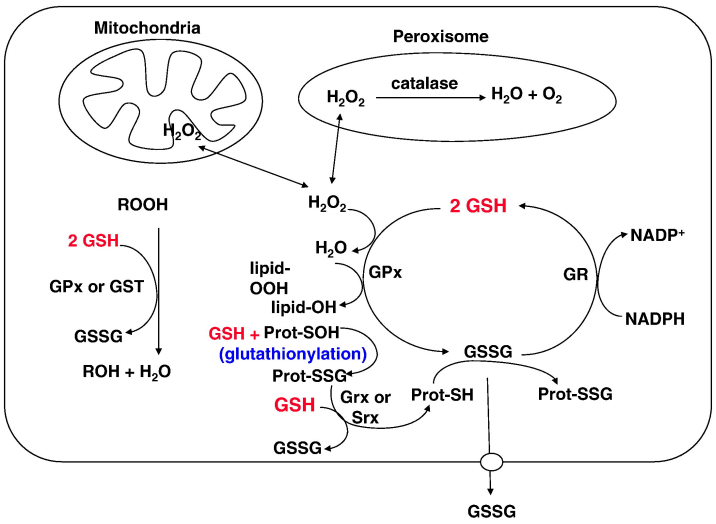

Figure 16: Antioxidant function of GSH. Hydrogen peroxide (H_2O_2) can be metabolized by GSH peroxidase (GPx) in the cytosol and mitochondria and by catalase in the peroxisome. GSSG can be reduced back to GSH by glutathione reductase (GR) using NADPH and thereby forming a redox cycle. Organic peroxides (ROOH) can be reduced by either GPx or GSH S-transferase (GST). In addition, GSH plays a role in protein redox signaling as it can react with oxidized proteins to sulfenic acid (Prot-SOH) during oxidative stress and forms protein mixed disulfides Prot-SSG which can be reduced back to the Prot-SH. Oxidative stress may leads to an accumulation of GSSG, therefore GSSG can either be actively transported out of the cell or react with Prot-SH to form a mixed disulfide Prot-SSG. (Lu 2013)

Once oxidized, GSSG can be reduced back to GSH by glutathione reductase using NADPH as an electron donor (Couto et al. 2013). In addition, the ratio of GSH to GSSG is often used as a marker for cellular oxidative stress (Lu 2013). Under normal conditions, the reduced GSH accounts for more than 98% of total GSH (Forman et al. 2009). Most of the cellular GSH is in the cytosol (80-85%), 10-15% is stored in mitochondria and a small percentage is in the endoplasmic reticulum (Lu 2013).

The synthesis of GSH from its precursor amino acids involves two enzymatic steps with ATP consumption: formation of γ-glutamylcysteine from glutamate and cysteine by γ-glutamylcysteine synthetase, the rate-limiting step, and formation of GSH from γ-glutamylcysteine and glycine by GSH synthetase.

2.3.5.4 Peroxiredoxins

Peroxiredoxins also degrade hydrogen peroxide to water within mitochondria, cytosol and nucleus.

2.4 Mitochondrial biogenesis

Mitochondrial biogenesis can be described as growth and division of pre-existing mitochondria. Mitochondrial biogenesis is stimulated by environmental stress such as oxidative stress, caloric restriction, cold exposure, cell division, and exercise by activating the transcription cascade of mitochondrial biogenesis (Jornayvaz and Shulman 2010). Accurate mitochondrial biogenesis requires coordinated synthesis and import of 1000-1500 nuclear encoded proteins (Baker et al. 2007). The peroxisome proliferator-activated receptor-γ-coactivator-1 (PGC-1) family stands at the beginning of the biosynthesis cascade with the members PGC-1α, PGC-1β, and PRC (PGC-1 related coactivator). PGC-1α is the master regulator of mitochondrial biogenesis (Lynch et al. 2017). It induces the nuclear respiratory factor 1 (NRF1) and NRF2, which together activate the mitochondrial transcription factor A (Tfam). Tfam transcribes mitochondrial-encoded proteins. PGC-1β is structurally similar to PGC-1α and is also involved in mitochondrial biogenesis but is not up-regulated in response to exercise. AMP-activated protein kinase (AMPK) acts as an energy sensor of the cell and

works as a key regulator of mitochondrial biogenesis by phosphorylating and activating PGC-1α (Jornayvaz and Shulman 2010).

The following sections will describe fission, fusion, and mitophagy that are important mechanisms for healthy mitochondria, in more detail.

2.4.1 Fission and fusion

Mitochondria are highly dynamic organelles undergoing fission and fusion, which are essential for maintaining healthy mitochondria. Fission is the event of a single mitochondrion breaking apart, whereas fusion is the event of two or more mitochondria joining to form a whole (Figure 17) (Mishra and Chan 2016). Increased fission creates fragmented mitochondria, which is helpful for the elimination of damaged mitochondria and for creating smaller mitochondria for transport (Youle and van der Bliek 2012). Therefore, balance between fusion and fission permits the cell to have the right mitochondrial network organization during biogenesis.

Three large GTPases of the dynamin superfamily mediate mitochondrial fusion: Mitofusin 1 (Mfn1), Mfn2 and optic atrophy 1 (Opa1) (Chan 2012). Mitochondrial fusion is a two-step process with outer-membrane fusion by Mfn1 and Mfn2 followed by inner-membrane fusion by Opa1. Complete loss of fusion through removal of bath mitofusin and Opa1 results in a dramatic decrease in mtDNA content, heterogeneous loss of mtDNA nucleoids and membrane potential and reduced respiratory chain function (Chen et al. 2005). Fusion is required for embryonic development and for cell survival at later development stages (Youle and van der Bliek 2012). In addition, Mfn2 maintains coenzyme Q levels (Mourier et al. 2015) and Opa1 maintains mitochondrial cristae structure and is critical for respiratory chain supercomplex assembly (Cogliati et al. 2013). High OXPHOS activity correlates with mitochondrial fusion (Mishra et al. 2014). Oxidative stress can increase fusion due to elevated GSH levels promoting disulfide-mediated dimerization of mitofusin molecules (Shutt et al. 2012).

Mitochondrial fission is mediated by Dynamin-related protein 1 (Drp1), a large cytosolic GTPase that is recruited to the outer mitochondrial membrane via collection of receptor protein and is forming a spiral around mitochondria to break the outer and the inner mitochondrial membrane. Fission has multiple functions such as facilitate mitochondrial transport, mitophagy and apoptosis (Mishra and Chan 2016). Inhibition of OXPHOS is associated with fission.

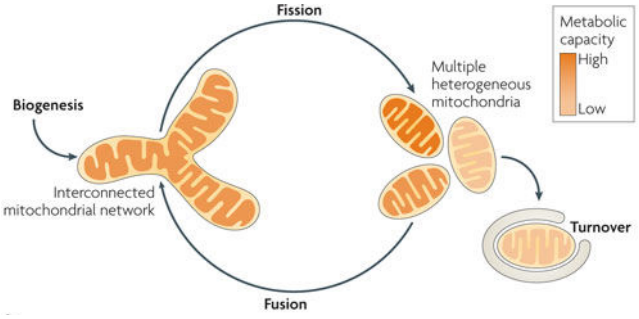

Figure 17: Fission and Fusion. The mitochondrial life cycle starts with growth and division of pre-existing mitochondria by biogenesis and ends with degradation of impaired mitochondria by mitophagy. In between, mitochondria undergo frequent cycles of fission and fusion that allow the cell to generate multiple heterogeneous mitochondria (fission) or interconnected mitochondrial networks (fusion) depending on the physiological conditions. (Westermann 2010)

2.4.2 Mitophagy

Autophagy is a well-established mechanism of degrading cellular components and protects cells from deleterious protein aggregates by encapsulating and degrading them (Youle and van der Bliek 2012). Autophagy is also required for maintaining a healthy mitochondrial network by eliminating old and damaged mitochondria and preventing an accumulation of dysfunctional mitochondria, which can lead to cellular degeneration. Mitophagy, the autophagic elimination of mitochondria, is also used for the adjustment of mitochondrial numbers to react to changing metabolic needs and during certain cellular development stages (Figure 18). A study showed that one out of five mitochondria are eliminated via mitophagy (Twig et al. 2008). Mitophagy is linked to mitochondrial fission and fusion – fission is required for mitophagy (Twig et al. 2008). Mitophagy is regulated by PINK1 and parkin, genes that are responsible for some familiar Parkinson's disease cases (Youle and van der Bliek 2012). PINK1 is a mitochondrial-localized kinase that is imported and degraded under normal conditions. The import, like for all proteins, is dependent on the mitochondrial membrane potential. Therefore, a depolarization results in PINK1 accumulation in the outer mitochondrial membrane and phosphorylates other proteins including ubiquitin to recruit and activate the cytosolic parkin (Matsuda et al. 2010; Okatsu et al. 2015). Activated parkin results in ubiquitination of proteins of outer mitochondrial membrane proteins including Mfn1

and Mfn2, whose degradation is required for directing the mitochondrion to the autophagic membrane (Chan et al. 2011). Ubiquitination recruits the autophagy adaptor LC3 that is leading to mitophagy. Another mitophagy pathway is mitophagy receptors on the outer mitochondrial membrane such as NIX1, BNIP3 and FUNDC1. These receptors bind LC3 and therefore leading to mitochondria degradation.

Mitophagy can be activated under certain cellular stress like energy stress, hypoxic conditions and metabolic conditions promoting increased mitochondrial function.

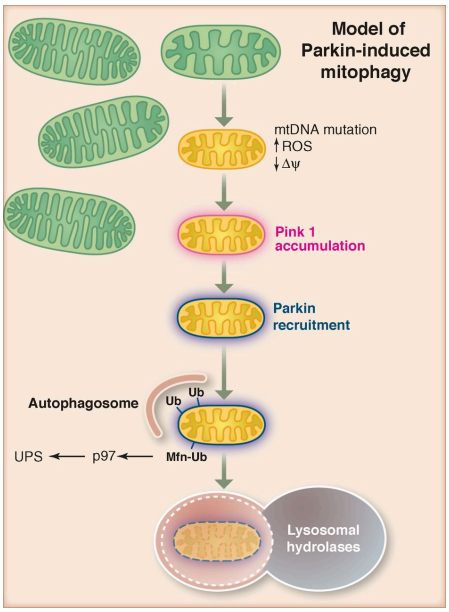

Figure 18: Model of parkin-induced mitophagy. In healthy mitochondria, PINK1 is permanent degradated by the inner mitochondrial membrane protease. PINK1 is accumulated to the outer mitochondrial membrane is damaged mitochondria with depolarized membrane potential. Accumulated PINK1 is recruiting the E3 ligase parkin from the cytosol and resulting in ubiquitination of several outer membrane proteins and elimination of Mfn1 and Mfn2. Finally, parkin induces autophagic elimination of damaged mitochondria. (Youle and van der Bliek 2012)

2.5 Apoptosis

Mitochondria play a central role in most forms of cell death (Pessayre et al. 2010). An impairment of mitochondrial function by oxidative stress or other factors ultimately leads to cell death by apoptosis or necrosis. Two pathways can initiate apoptosis: the intrinsic pathway

is triggered by oxidative stress, cytosolic calcium overload, endoplasmic reticulum stress, and DNA stress and the extrinsic pathway is triggered by signals of other cells (Figure 19). The intrinsic apoptotic pathway leads to the opening of the MPTP (mitochondrial permeability transition pore), which spans the inner and outer mitochondrial membrane and releases the pro-apoptotic factor cytochrome *c* into the cytosol. Cytochrome *c* binds to Apaf-1 (Apoptotic protease activating factor-1) and pro-caspase-9 to form an apoptosome, which cleaves the pro-caspase-9 to its active form caspase-9 and subsequently activates caspase-3. The extrinsic pathway is activated through TNF (tumor necrosis factor) or Fas (First apoptosis signal) signaling, resulting in the formation of the DISC (death-inducing signaling complex) and activation of caspase-8, which activates caspase-3. Both pathways activate the effector caspase-3 that can activate other effector caspases and cleaves PARP (poly ADP-ribose polymerase) preventing further DNA repair (Los et al. 2002). Activation of effector caspases kills the cell by protein degradation and phagocytosis of the cell. The activation of caspases is an ATP-dependent process, where a certain functioning of the mitochondria is still required (Wang and Youle 2009). The cell goes to necrosis if ATP depletion occurred where the cell membrane integrity is lost and an uncontrolled release of cell products into the extracellular space occurs.

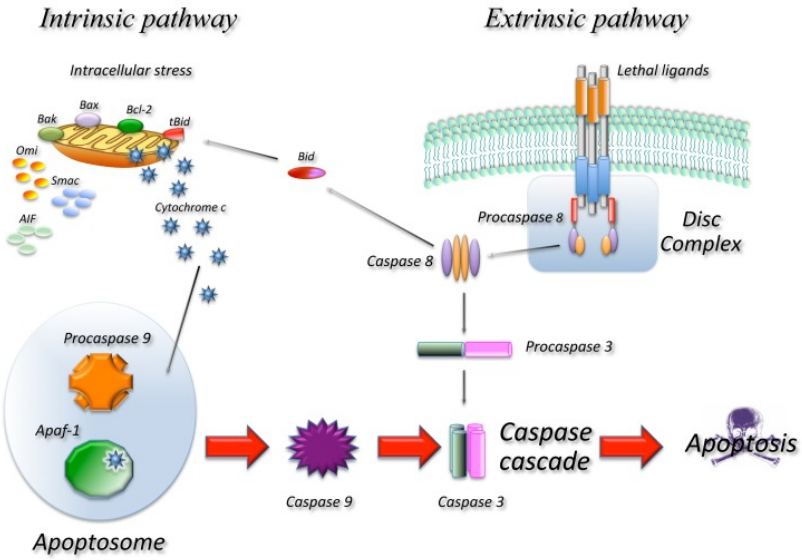

Figure 19: Intrinsic and extrinsic apoptosis pathway. The release of cytochrome *c* from mitochondria results in the formation of the apoptosom and activation of caspase-9 in the intrinsic pathway. The DISC complex is formed in the extrinsic pathway upon ligand binding to specific receptors and caspase-8 is activated. Caspase-8 and caspase-9 activate downstream caspases such as caspase-3 resulting in cell death. (Favaloro et al. 2012)

2.6 Drug induced mitochondrial toxicity

Proper mitochondrial function is dependent upon the impermeability of the inner mitochondrial membrane and the integrity of the respiratory complexes. In addition, mitochondrial replication requires the capacity to replicate and express mtDNA (Dykens and Will 2007). Several drugs are known to inhibit mitochondrial function. The following paragraph will discuss the possible targets of drug-induced mitochondrial toxicity (Figure 20). Some fibrates and thiazolidinediones acutely impair mitochondrial function by inhibition of the ETC or by uncoupling the electron transport from ATP production (Brunmair et al. 2004). Therefore, the mitochondrial membrane potential is decreased and ATP production reduced. Acetaminophen, doxorubicin, and ethanol produce oxidative stress via redox cycling or via glutathione depletion, CYP2E1-derived ROS generation, or reactive metabolite formation (Dykens and Will 2007). Some thiazolidinediones and statins induce mitochondrial permeability transition causing an irreversible collapse of the mitochondrial membrane potential and the release of pro-apoptotic factors (Bova et al. 2005; Kaufmann et al. 2006). Moreover, inhibition of metabolic pathways as fatty acid β-oxidation or Krebs cycle which deliver cofactors for the ETC will impair ATP production (Pessayre et al. 1999). In case of impairment of the fatty acid oxidation, the free fatty acids in the liver are insufficiently oxidized and are esterified into triglycerides that accumulate in the cytoplasm of hepatocytes as small vesicles or larger vacuoles. Acute impairment causes microvesicular steatosis with numerous tiny lipid vesicles. In contrast, in chronic impairment mixed forms of steatosis with tiny lipid vesicles and large fat vacuoles occur. Long-term chronic impairment results in macrovacuolar steatosis (Fromenty and Pessayre 1995). Inhibition of any of the mitochondrial membrane transporters that exchange metabolites across the impermeable inner mitochondrial membrane will also impair ATP production (Stewart and Steenkamp 2000).

Nucleotide reverse transcriptase inhibitors prevent mitochondrial replication through inhibition of the mitochondrial polymerase. Therefore, they result in reduction of mitochondrial function in various tissues like muscle and liver (Lai et al. 1991). Certain aminoglycoside antibiotics result in long-term mitochondrial dysfunction to impaired protein synthesis, leading to ototoxicity and nephrotoxicity (Fischel-Ghodsian 2005).

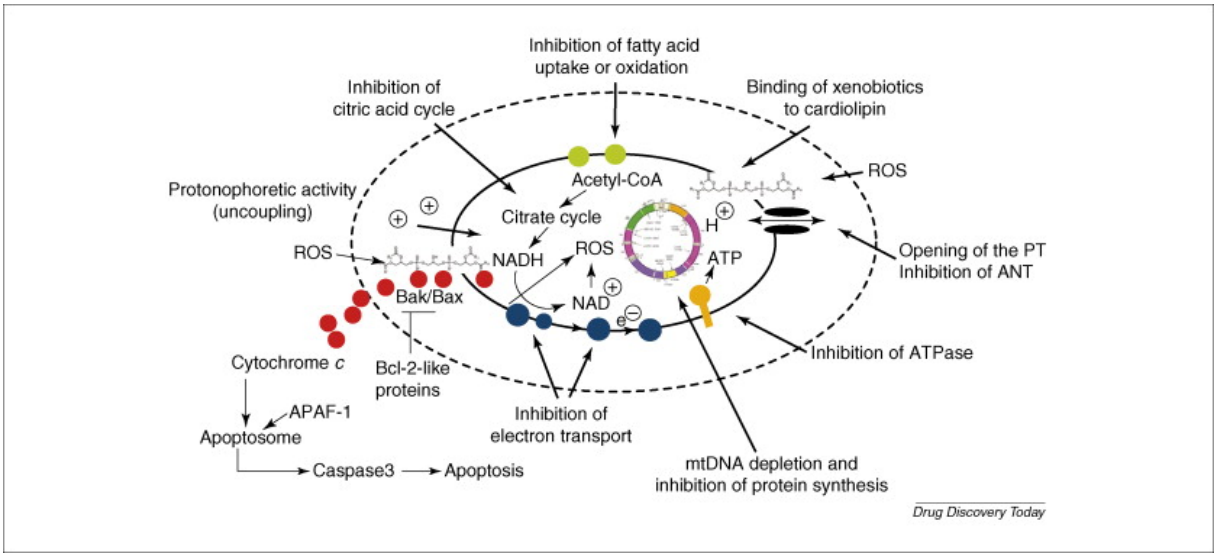

Figure 20: Possible ways for the inhibition of mitochondrial function (Dykens and Will 2007).

3 TYROSINE KINASE INHIBITORS

3.1 Tyrosine kinases

Kinases are enzymes that catalyze the transfer of a phosphate group from high-energy donor molecules, e.g. ATP, to specific substrates. Protein kinases phosphorylate proteins resulting in functional changes of the target protein. The human genome encodes for 518 protein kinases (Manning et al. 2002), 90 of them belong to the group of tyrosine kinases (TKs). Six other groups of protein kinases exist primarily phosphorylating serine and threonine residues. The TK group comprise approximately 30 families such as the vascular endothelial growth factor receptor (VEGFR) family and the fibroblast growth factor receptor (FGFR) family (Gotink and Verheul 2010). TKs can also be categorized into receptor and non-receptor (cytoplasmic) TKs. Receptor TKs are crucial in the transduction of extracellular signals into the cell while non-receptor TKs are essential in intracellular communication. A monomer of a receptor TK is composed of a N-terminal extracellular ligand-binding, a transmembrane, and a C-terminal intracellular domain with the TK activity. Ligand binding to the extracellular domain of the receptor TK stimulates receptor dimerization and a conformational change resulting in autophosphorylation of specific tyrosine residues of the intracellular kinase domain (Figure 21) (Schlessinger 2000). Activation of signaling pathways leads to biological responses such as cell activation, proliferation, differentiation, migration, survival, and vascular permeability (Pawson 2004).

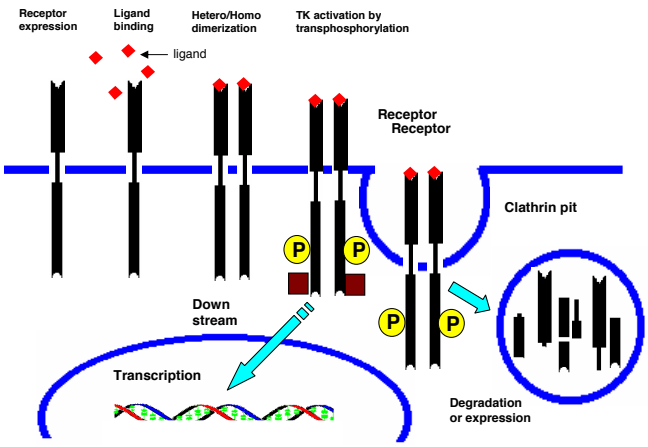

Figure 21: Mechanism of action of tyrosine kinase. After Ligand binding, dimerization is leading to TK activation and tyrosine transphosphorylation, signal transduction, and down-stream effects. Afterwards, receptor internalization and receptor degradation or re-expression occurs. (Paul and Mukhopadhyay 2004)

3.2 Tyrosine kinase inhibitors

Overexpression or mutation in TKs pathways can cause and exaggerate many types of cancer. Currently, there are two different classes of targeted treatments of deregulated TKs: therapeutic monoclonal antibodies such as cetuximab or necitumumab, or tyrosine kinase inhibitors (TKIs) such as imatinib or sunitinib (Figure 22). TKIs are a relatively new class of drugs with imatinib, initially for the treatment of patients with chronic myeloic leukemia, being the first on the market in 2001 (Mealing et al. 2013). The Food and Drug Administration (FDA) had approved a total of 31 small-molecule kinase inhibitors as of November 2016 (Zhang et al. 2017b). The TKIs can be classified according to the most important receptor, which they inhibit. Families of TKIs include Bcr-abl inhibitors (dasatinib, imatinib, nilotinib), ErbB inhibitors (erlotinib, gefitinib, lapatinib), VEGFR inhibitors (axitinib, pazopanib, sorafenib, sunitinib), and miscellaneous inhibitors (crizotinib, ruxolitinib, vemurafenib) (Josephs et al. 2013).

TKIs can also be subdivided in three groups according to their mechanism of TK-inhibition: type I TKIs recognize the active conformation of the TK, type II TKIs recognize the inactive conformation of the TK and the covalent TKIs bind covalently to cysteines at specific sites of the TK (Gotink and Verheul 2010). Type I TKIs bind to the ATP-binding site of a TK by presenting one to three hydrogen bonds imitating the hydrogen bonds that are normally formed by ATP (Zhang et al. 2009). Sunitinib, inhibiting the VEGF pathway, is an example of a type I TKI. Type II TKIs indirectly compete with ATP by occupying the hydrophobic pocket that is in direct neighborhood to the ATP-binding site. Sorafenib, a type II TKI, uses a hydrophobic pocket to compete with ATP and therefore blocks the phosphorylation of VEGFR, platelet-derived growth factor receptor (PDGFR), Raf, and tyrosine-protein kinase (KIT) (Wan et al. 2004). A covalent TKI has an electrophilic group that reacts with the electron-rich sulfur in the cysteine residue and therefore irreversibly binds the inhibitor to the cysteine residue, blocking the ATP binding and TK activity (Kwak et al. 2005). Vandetanib is an example of a covalent TKI. The kinase domain and ATP-binding site of TKs have a high degree of similarity. Therefore, it is difficult to develop highly selective type I inhibitors because they occupy the ATP-binding site. Type II inhibitors can be more selective since kinases in the inactive conformation are more variable (Mol et al. 2004). Covalent inhibitors can be very selective because of their irreversible mechanism of binding to a cysteine residue of the TK.

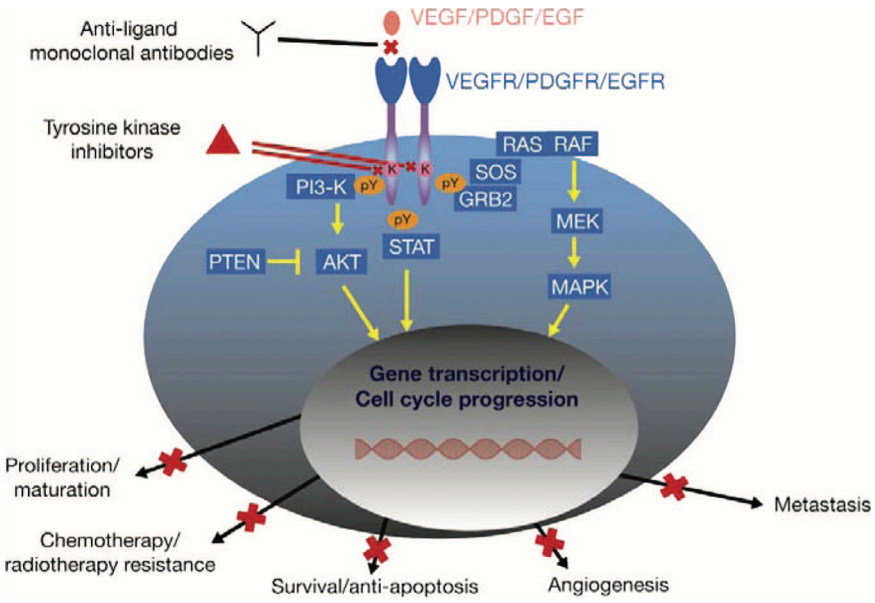

Figure 22: Pathways blocked by tyrosine kinase inhibitors and monoclonal antibodies (Scagliotti and Govindan 2010).

Abbreviations: EGF, endothelial growth factor; EGFR, endothelial growth factor receptor; GRB2, growth factor receptor-bound protein-2; MAPK, mitogen-activated protein kinase; MEK, MAPK/extracellular signal–related kinase kinase; PI3K, phos- phoinositide 3-kinase; PDGF, platelet-derived growth factor; PTEN, phosphatase and tensin homologue deleted on chromosome ten; SOS, son of sevenless; STAT, signal transducer and activator of transcription; VEGF, vascular endothelial growth factor; VEGFR, vascular endothelial growth factor receptor.

TKIs are lipophilic low molecular drugs and can therefore, in contrast to monoclonal antibodies, enter the cell easily (Imai and Takaoka 2006). Once inside the cell, TKIs can interact with the intracellular receptor domain and intracellular signaling molecules resulting in a blockage of the activation of various signaling pathways (Gotink and Verheul 2010). TKIs can be taken orally once or twice daily at a fixed dose because the pharmacokinetics of TKIs is not significantly affected by weight (Houk et al. 2009). TKIs undergo intense hepatic metabolism with N-dealkylation mainly by CYP3A4 as the first metabolic step (Josephs et al. 2013). TKIs as targeted treatments offer big advantages compared to traditional anti-cancer therapies because they are more specific, and therefore expected to have less side effects.

However, they still have a narrow therapeutic window with dose-limiting adverse reactions, including in particular skin, intestinal, liver, and cardiovascular toxicity (Amitay-Laish et al. 2011; Breccia and Alimena 2013; Yang and Papoian 2012), whereas bone marrow toxicity is rare. The reason for this is that many TKIs are multi-targeted kinase inhibitors, targeting a

number of different TKs which are involved in different signaling pathways. Inhibition of multiple kinases results in a broader efficacy than single-targeted inhibitor. On the other hand, inhibitors should be highly selective to minimize treatment-induced toxicities.

3.3 Investigated TKIs

This PhD project will take a deeper look at the 10 following TKIs and their unexpected liver toxicity.

3.3.1 Crizotinib

Crizotinib (Xalkori, Pfizer, Figure 23) acts as an anaplastic lymphoma kinase (ALK) and c-ros oncogene 1 (ROS1) inhibitor. It was approved in August 2011 by the FDA for the treatment of locally advanced or metastatic non-small cell lung cancer that expresses the abnormal ALK gene. In March 2016, crizotinib was also approved for ROS1-positive non-small cell lung cancer. About 5% of patients suffering from non-small cell lung cancer have a chromosomal rearrangement that generates a fusion gene between ALK and echinoderm microtubule-associated protein-like 4 (EML4) resulting in constant kinase activity and carcinogenesis (Gerber and Minna 2010). Crizotinib inhibits the kinase activity of the fusion protein by competitive binding within the ATP-binding pocket.

The bioavailability of crizotinib is 32-66% after administration of a single 250 mg dose with C_{max} after 4-6 hours. The volume of distribution of crizotinib is 25 L/kg and 90% are bound to plasma proteins (Josephs et al. 2013). Crizotinib is primarily metabolized by CYP3A4 and CYP3A5 to O-desalkymetabolites and eliminated in feces (63%) and urine (22%). The most common adverse events associated with crizotinib are visual disorders, nausea, vomiting, constipation, and diarrhea (Josephs et al. 2013). The trough plasma concentration in patients is on average 1.1 µM and maximal 1.9 µM (Kurata et al. 2015).

Crizotinib was associated with elevated serum aminotransferase levels in up to 57% of treated patients in clinical trials with 6% of these patients having more than five times the ULN (Shah et al. 2013). In a phase 3 clinical trail, 16% of patients reported an ALT/AST elevation of grade 3-4 (Shaw et al. 2013). Serum aminotransferase elevation begins after 4-12 weeks of

treatment with minimal or non-symptomatic liver injury. However, fatal cases of liver injury with crizotinib treatment have been reported (van Geel et al. 2016). Therefore, the FDA labeled crizotinib for hepatotoxicity and routine liver monitoring during therapy is recommended. Crizotinib suppresses state 3 respiration driven by succinate and induces mitochondrial swelling at 100-fold Cmax, releases cytochrome *c* at 50-fold Cmax and inhibits complex I and increases ROS formation at 20-fold Cmax in isolated rat liver mitochondria (Zhang et al. 2017b).

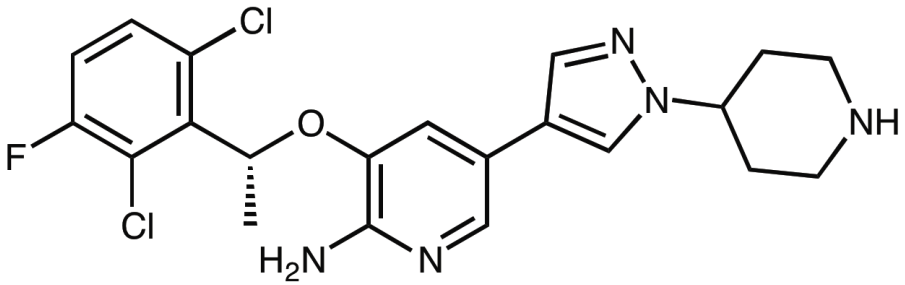

Figure 23: Chemical structure of crizotinib.

3.3.2 Dasatinib

Dasatinib (Sprycel, Bristol-Myers Squibb, Figure 24) was approved in June 2006 by the FDA for people with chronic myelogenous leukemia (CML) that is resistant or intolerant to imatinib and Philadelphia chromosome-positive acute lymphoblastic leukemia (Ph+ ALL) (Brave et al. 2008). The Philadelphia chromosome is a defective and short chromosome due to translocation of the Abelson murine leukemia viral oncogene homolog 1 (ABL1) gene on chromosome 9 and the breakpoint cluster region (BCR) gene on chromosome 22 giving the fusion gene BCR-ABL1. BCR-ABL1 codes for a hybrid protein – a TK that is always on and therefore causing the cell to divide uncontrollably. Dasatinib binds the active and inactive conformation of the ABL1 kinase domain and is 325 fold more potent than imatinib (Aguilera and Tsimberidou 2009). Dasatinib is a multi-target TKI with the main targets BCR-ABL1, Src, c-KIT, ephrin receptors and several other TKs. Dasatinib suppresses progenitor growth through inhibition of proliferation and a modest increase in apoptosis in dividing progenitors (Konig et al. 2008).

Dasatinib is absorbed rapidly with C_{max} after 0.5-3 hours. The volume of distribution of dasatinib is 30-40 L/kg and 92-97% are bound to plasma proteins (Josephs et al. 2013).

Dasatinib is primarily metabolized by CYP3A4 to active metabolites and eliminated mainly via feces. The most common adverse events associated with dasatinib are myelosuppresion, edema, nausea, rash, fatigue, and headache (Josephs et al. 2013). In October 2011, the FDA announced that dasatinib might increase the risk of pulmonary hypertension. The C_{max} plasma concentration in patients is 0.6 μM (Haura et al. 2010).

In clinical trials, 50% of dasatinib-treated patients showed elevated serum aminotransferase levels and 1-9% showed elevations above five times the ULN but cases were usually mild and self-limited (Shah et al. 2013). No cases of acute liver injury due to dasatinib therapy have occurred. Dasatinib does not cause mitochondrial toxicity in isolated rat liver mitochondria (Zhang et al. 2017b). In another study in rat hepatocytes, dasatinib was found to induce oxidative stress with ROS formation, GSH depletion, decreased mitochondrial membrane potential, and decreased superoxide dismutase (SOD) activity and induction of apoptosis (Xue et al. 2012). Another study conducted on primary human hepatocytes has shown that dasatinib induced autophagy in the liver which through the p38 signaling was protective against hepatotoxicity (Yang et al. 2015).

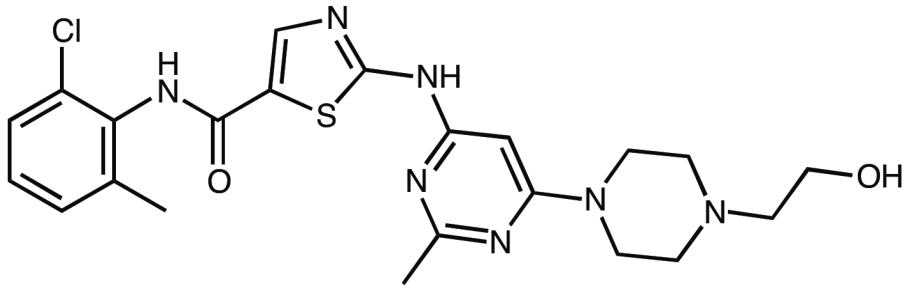

Figure 24: Chemical structure of dasatinib.

3.3.3 Erlotinib

Erlotinib (Tarceva, Genentech, Figure 25) was approved by the FDA in November 2004 for the treatment of locally advanced or metastatic non-small cell lung cancer after the failure of more than one or two previous chemotherapeutics (Smith 2005). In November 2005, erlotinib was also approved for the treatment of pancreatic cancer in combination with gemcitabine. Erlotinib is a receptor TKI acting on the epidermal growth factor receptor (EGFR) by binding reversibly to the ATP-binding site of the receptor (Raymond et al. 2000).

The bioavailability of erlotinib is 69-76% with C_{max} after 4 hours. It is highly bound to plasma proteins (92-95%) and has a volume of distribution of 3 L/kg (Josephs et al. 2013). Erlotinib undergoes extensive metabolism by CYP3A4, but also CYP3A5, CYP2D6 and CYP1A1 with O-desmethylerlotinib as the main metabolite (Li et al. 2007). Erlotinib is eliminated mainly via feces. The most common adverse events associated with erlotinib are skin toxicity and diarrhea. The C_{max} plasma concentration in patients is 7.6 μM (Haura et al. 2010).
Elevations in serum aminotransferase levels are common during erlotinib treatment (35-45%) and levels above five time ULN occur in up to 10% of the patients (Shah et al. 2013). The abnormalities are usually asymptomatic but there have been reports of clinically apparent liver injury. However, several fatal cases are reported with erlotinib treatment (Huang et al. 2009; Liu et al. 2007; Pellegrinotti et al. 2009; Schacher-Kaufmann and Pless 2010). Therefore, routine liver monitoring during therapy is recommended. Erlotinib inhibits complex V at 10-fold Cmax in isolated rat liver mitochondria (Zhang et al. 2017b).

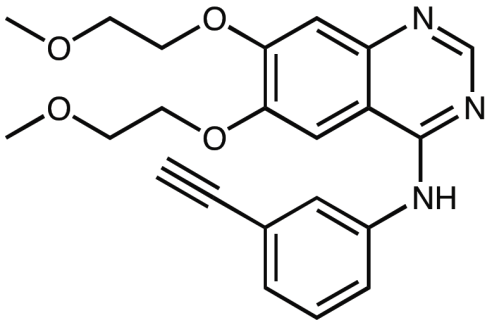

Figure 25: Chemical structure of erlotinib.

3.3.4 Imatinib

Imatinib (Gleevec, Novartis, Figure 26) was the first TKI on the market, approved by the FDA in 2001. Imatinib is used for the treatment of patients with CML, Ph+ ALL, and certain types of gastrointestinal stromal tumors (GIST), systemic mastocytosis, and myelodysplastic syndrome. Imatinib binds and stabilizes the inactive form of BCR-ABL1, therefore inhibiting autophosphorylation and inducing apoptosis of BCR-ABL1-positive cells (Gambacorti-Passerini et al. 1997). Imatinib is quite selective for BCR-ABL1 but also inhibits c-kit and PDGFR. Some patients develop a resistance to imatinib through point mutations in the kinase domain of BCR-ABL1 that impair imatinib binding but do not change the kinase activity (Shah and Sawyers 2003), by alteration of the equilibrium of ABL kinase favoring the active

state instead of the inactive state where imatinib is binding (Cowan-Jacob et al. 2004) or by overexpressing the BCR-ABL1 gene (Hochhaus et al. 2002).

The bioavailability of imatinib is 98% with a volume of distribution of 2-4 L/kg and 95% plasma protein binding (Josephs et al. 2013). Imatinib is mainly metabolized through CYP3A4, CYP3A5, and CYP2C8 to the active N-desmethylimatinib and is eliminated via feces (68%) and urine (13%). The most common adverse events associated with imatinib are myelosuppression, edema, nausea, diarrhea, musculoskeletal symptoms, fatigue, and headache. The concentration of imatinib in patients is 3.2 µM (Bolton et al. 2004).

Imatinib treatment is associated with elevated serum aminotransferase levels but levels above five times ULN occurred in just 2-4% of the patients (Shah et al. 2013). However, imatinib treatment is linked to rare cases of acute liver injury with jaundice after treatment for 6 days to several years. Imatinib is associated with three forms of acute liver injury: transient and usually asymptomatic elevations of serum transaminases, clinically apparent acute hepatitis and reactivation of an underlying chronic hepatitis B. The liver injury can be fatal (Ridruejo et al. 2007). Imatinib-associated liver injury shows immune features and responses to prednisone therapy suggest that the liver injury is possibly immunologically mediated. Imatinib suppresses state 3 respiration driven by glutamate/malate at 30-fold Cmax, releases cytochrome *c* at 50-fold Cmax and inhibits complex I at 100-fold Cmax in isolated rat liver mitochondria (Zhang et al. 2017b).

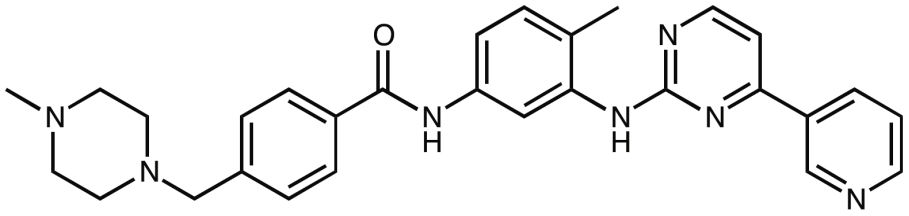

Figure 26: Chemical structure of imatinib.

3.3.5 Lapatinib

Lapatinib (Tykerb, GlaxoSmithKline, Figure 27) was approved in March 2007 by the FDA for combination therapy with capecitabine (Xeloda) for the treatment of breast cancer (Higa and Abraham 2007). In January 2010, lapatinib was also approved for the treatment of postmenopausal women with hormone receptor positive metastatic breast cancer that overexpresses the human epidermal growth factor receptor 2 (HER2). Lapatinib inhibits the

activity of HER2 and EGFR by binding to the ATP-binding pocket of the kinase domain, preventing autophosphorylation and activation of signal mechanism (Wood et al. 2004).

The bioavailability of lapatinib is variable and increased with food intake. The volume of distribution of lapatinib is 31 L/kg and more than 99% plasma protein binding (Josephs et al. 2013). Lapatinib is mainly metabolized through CYP3A4 and to a lesser degree by CYP3A5, CYP2C19, and CYP2C8 and is eliminated via feces. Most common adverse events associated with lapatinib are diarrhea, fatigue, nausea, and rash (Burris et al. 2005). The C_{max} plasma concentration in patients is 4.8 µM (Midgley et al. 2007).

Elevated serum aminotransferase levels are common during lapatinib treatment (37-53%) with values greater than five times the ULN being rare (Shah et al. 2013). But lapatinib has been linked to several cases of clinically relevant liver injury starting after one to three months of lapatinib treatment. Therefore, the FDA labeled lapatinib for hepatotoxicity and routine liver monitoring during therapy is recommended. A study suggested an HLA-associated mechanism because DQA1*02:01 and DRB1*07:01 were found more often in patients with elevated transaminases than in patients with normal transaminases suggesting an immune-mediated mechanism (Spraggs et al. 2011; Spraggs et al. 2012). Lapatinib releases cytochrome *c* at 10-fold Cmax on isolated rat liver mitochondria (Zhang et al. 2017b). A study in rats demonstrated that lapatinib triggers hepatic toxicity mainly as sinusoidal injury with transaminase level elevations (Demirci et al. 2012). Involvement of CYP3A4 induction in the hepatotoxicity induced by lapatinib via increasing reactive metabolite formation was suggested by a study in HepaRG cells (Hardy et al. 2014) and in a study in HepG2 cells where the metabolite is inducing oxidative stress, reduced oxygen consumption and decreased GSH levels (Eno et al. 2016).

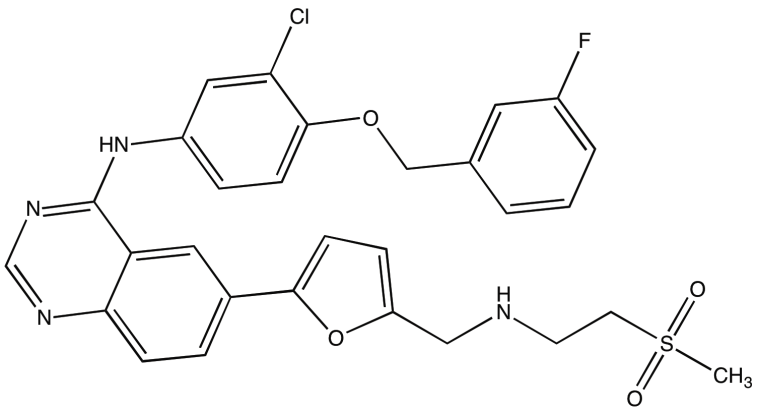

Figure 27: Chemical structure of lapatinib.

3.3.6 Pazopanib

Pazopanib (Votrient, GlaxoSmithKline, Figure 28) was approved in October 2009 by the FDA for the treatment of advanced renal cell carcinoma. In 2012, pazopanib was also approved for patients with soft tissue sarcoma who had received chemotherapy. Pazopanib binds to the ATP-binding site of VEGRF, PDGFR, and c-kit kinases resulting in pathway deactivation essential for cell survival, migration, cell permeability, and proliferation (Keisner and Shah 2011).

The bioavailability of pazopanib is low (14-39%) with C_{max} after 2-8 hours. The volume of distribution of lapatinib is 0.1-0.2 L/kg and more than 99% plasma protein binding (Josephs et al. 2013). Pazopanib is mainly metabolized through CYP3A4 and to a lesser degree by CYP1A2 and CYP2C8 and is eliminated via feces. The most common adverse events associated with pazopanib are nausea, vomiting, diarrhea, hypertension, and change in hair color. The average plasma concentration of pazopanib in patients is 93 µM (Herbrink et al. 2016).

Pazopanib was associated with elevated serum aminotransferase levels in up to 53% of treated patients and elevated total serum bilirubin in one-third of treated patients in clinical trials (Shah et al. 2013). Transaminases higher than five times the ULN occurred in 8% of patients and the combination of ALT and bilirubin elevations in 1-2% of patients. However, fatal cases of liver injury with pazopanib treatment have been reported (Klempner et al. 2012). Therefore, the FDA labeled pazopanib for hepatotoxicity and routine liver monitoring during therapy is recommended. Several possible mechanism of pazopanib-hepatotoxicity have been hypothesized such as immune mediated toxicity, UGT1A1 inhibition or on-target toxicity on VEGFR (Kapadia et al. 2013). Another study found an elevated risk for ALT elevations in pazopanib-treated patients with HLA-B*57:01 providing further evidence for the involvement of immune-mediated mechanism is pazopanib-associated hepatotoxicity (Xu et al. 2016). In addition, Pazopanib affects oxygen consumption and inhibits complex I at Cmax concentrations in isolated rat liver mitochondria (Zhang et al. 2017b). Another study with patient-specific hepatocyte-like cells showed that pazopanib induces oxidative stress and disruption of iron metabolism (Choudhury et al. 2017).

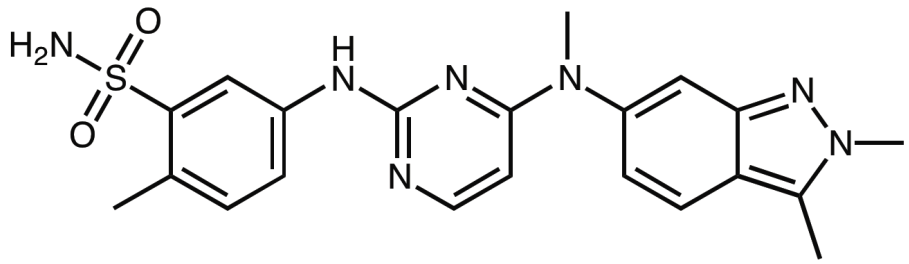

Figure 28: Chemical structure of pazopanib.

3.3.7 Ponatinib

Ponatinib (Iclusig, ARIAD Pharmaceuticals, Figure 29) was approved by the FDA in December 2012 but temporarily suspended from October to December 2013 because blood clots were observed in patients. Pazopanib was reintroduced into the market after additional warning labels and postmarket investigation was performed (Prasad and Mailankody 2014). Ponatinib is used for the treatment of chronic, accelerated or blast phase CML and Ph+ ALL. Ponatinib inhibits the BCR-ABL1 fusion protein even with the T315I mutation that is responsible for therapy resistance with imatinib, nilotinib, and dasatinib. The T315I mutation blocks the access of the drug to the ATP-binding site and confers a high degree of resistance to all currently approved TKIs (O'Hare et al. 2007). Ponatinib contains a novel triple-bond linkage that avoids the steric hindrance caused by the T315I mutation (Cortes et al. 2012).
Ponatinib reaches the C_{max} after 6 hours and is more than 99% bound to plasma proteins (Price et al. 2013). Ponatinib is mainly metabolized through CYP3A4 and minor by CYP2C8, CYP2D6, and CYP3A5 and is eliminated via feces. The main adverse events associated with ponatinib are hypertension, rash, fatigue, and headache. The mean peak concentration at steady state in patients is 1.4 µM (Price et al. 2013).
In clinical trials, 56% of ponatinib-treated patients showed elevated serum aminotransferase levels and 8% showed elevations above five times the ULN, but these were usually reversible (Shah et al. 2013). However, fatal cases of liver injury with ponatinib treatment have been reported (Price et al. 2013). Therefore, the FDA labeled pazopanib for hepatotoxicity and routine liver monitoring during therapy is recommended. Ponatinib does not cause mitochondrial toxicity in isolated rat liver mitochondria (Zhang et al. 2017b).

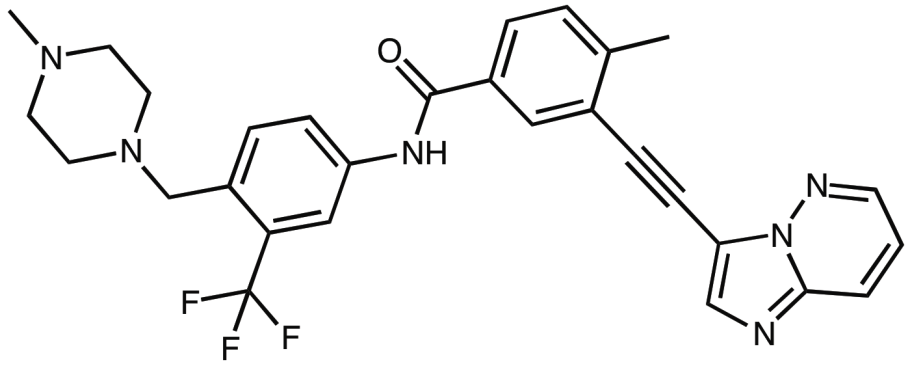

Figure 29: Chemical structure of ponatinib.

3.3.8 Regorafenib

Regorafenib (Stivarga, Bayer, Figure 30) was approved by the FDA in September 2012 for the treatment of metastatic colorectal cancer. The approval was expanded for patients with advanced GIST in February 2013 (Waddell and Cunningham 2013). Regorafenib is a multi-kinase inhibitor with anti-angiogenic activity due to inhibition of VEGFR, PDGFR, FGFR, RAF, c-kit, and other TKs.

Regorafenib reaches the C_{max} after 1-6 hours (Mross et al. 2012). Regorafenib is mainly metabolized by CYP3A4 and UGT1A9 (Teo et al. 2015). The main adverse effects associated with regorafenib are fatigue, loss of appetite, hand-food skin reaction, diarrhea, and high blood pressure. The average patient plasma concentration is 6.2 μM (Strumberg et al. 2012).

Elevations in serum aminotransferase levels are common during regorafenib treatment (45-65%) and levels above five time the ULN occur in 3-6% of the patients (Shah et al. 2013). Regorafenib-treatment is associated with fatal liver injury (Raissouni et al. 2015; Sacre et al. 2016). For this reason, the FDA labeled pazopanib for hepatotoxicity and routine liver monitoring during therapy is recommended. In rat hepatocytes, regorafenib uncouples the oxidative phosphorylation, disrupts the mitochondrial membrane potential and induces necrosis and autophagy (Weng et al. 2015). In addition, regorafenib affects oxygen consumption, reduces the mitochondrial membrane potential, induces mitochondrial swelling and cytochrome *c* release at Cmax concentrations and inhibits complex II at 10-fold Cmax in isolated rat liver mitochondria (Zhang et al. 2017b).

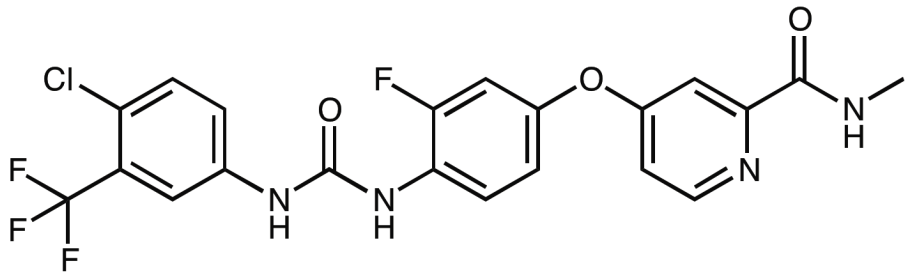

Figure 30: Chemical structure of regorafenib.

3.3.9 Sorafenib

Sorafenib (Nexavar, Bayer and Onyx Pharmaceuticals, Figure 31) was approved in December 2005 by the FDA for the treatment of renal cell carcinoma. Later, the approval was extended for patients with advanced hepatocellular carcinoma and locally recurrent or metastatic, progressive differentiated thyroid carcinoma refractory to radioactive iodine treatment (Llovet et al. 2008). Sorafenib is a multi-kinase inhibitor acting on Raf-1 and B-Raf serine-threonine kinases playing a major role in proliferation and differentiation of the cell and is often deregulated in tumors (Strumberg et al. 2007) and on the receptor TKs VEGFR, PDGFR (Wilhelm et al. 2008). Inhibition of tumor cell proliferation and of angiogenesis is considered to contribute to the antitumor effect of sorafenib (Josephs et al. 2013).

The bioavailability of sorafenib is less than 50% with C_{max} after 2-14 hours. The volume of distribution of sorafenib is 3-6 L/kg and more than 99% are bound to plasma proteins (Josephs et al. 2013). Sorafenib undergoes oxidative metabolism by CYP3A4 and is glucoronidated by UTG1A9 and is eliminated mainly via feces (77%). The most common adverse events associated with sorafenib are diarrhea, rash, nausea, vomiting, hand-foot syndrome, and fatigue. The concentration of sorafenib in patients is up to 21 µM (Strumberg et al. 2007).

In clinical trials, 21-25% of sorafenib-treated patients showed elevated serum aminotransferase levels and 2% showed elevations above five times the ULN but were usually reversible (Shah et al. 2013). However, fatal cases of acute liver injury with sorafenib treatment have been reported (Fairfax et al. 2012). For sorafenib, it is known that it can induce ROS accumulation and GSH depletion in HepG2 cells (Chiou et al. 2009). Sorafenib affects oxygen consumption and reduces the mitochondrial membrane potential at Cmax concentrations, induces mitochondrial swelling at 2.5-fold Cmax and induces cytochrome *c*

release and inhibits complex V at 5-fold Cmax in isolated rat liver mitochondria (Zhang et al. 2017b). In another study, sorafenib inhibits complex II, III, and V, activates Parkin and apoptosis (Zhang et al. 2017a).

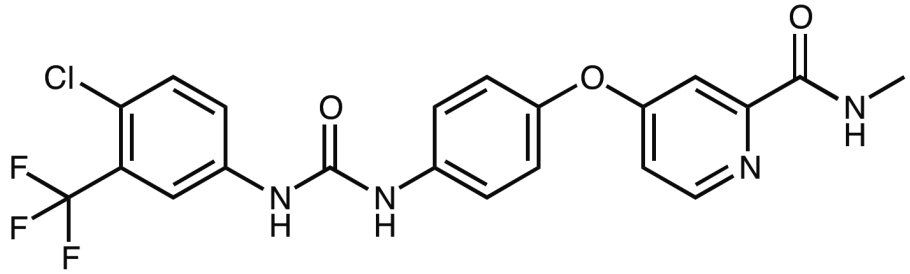

Figure 31: Chemical structure of sorafenib.

3.3.10 Sunitinib

Sunitinib (Sutent, Pfizer, Figure 32) was approved in January 2006 by the FDA for the treatment of renal cell carcinoma and imatinib-resistant gastrointestinal stromal tumor. Sunitinib inhibits various receptor tyrosine kinases such as the VEGFR 1-3 (Mendel et al. 2003), PDGRF α and β (Roskoski 2007), foetal liver tyrosine kinase receptor 3 (FLT3) (O'Farrell et al. 2003), stem cell factor receptor (c-kit) (Abrams et al. 2003), and colony stimulating factor 1 receptor (CSF1R) (Murray et al. 2003). Accordingly, Sunitinib inhibits angiogenesis, tumor growth, and metastasis (Faivre et al. 2006).

Sunitinib is well absorbed with C_{max} of 6-12 hours. The volume of distribution of sorafenib is around 30 L/kg and 95% are bound to plasma proteins (Josephs et al. 2013). Sunitinib is mainly metabolized by CYP3A4 to the active metabolite N-desethylsunitinib and is mainly eliminated via feces. The main adverse events associated with sunitinib are fatigue, diarrhea, nausea, hypertension, hand-foot syndrome, and stomatitis. The average plasma concentration of patients treated with sunitinib is between 0.1 µM and 0.3 µM (Di Gion et al. 2011).

Elevated serum aminotransferase levels are common during sunitinib treatment (40-60%) with values greater than five times the ULN occurring in 2-3% of the patients, but the elevations are normally asymptomatic (Shah et al. 2013). Rare reports of clinically apparent liver injury and even fatalities have been reported under sunitinib therapy (Weise et al. 2009). In addition, sunitinib has also been reported to cause hyperammonemia and encephalopathy (Lee et al. 2011). Sunitinib induces loss in mitochondrial membrane potential and inhibition

of complex II in mouse liver mitochondria (Porceddu et al. 2012). Another study in isolated rat liver mitochondria showed no mitochondrial toxicity due to sunitinib (Zhang et al. 2017b).

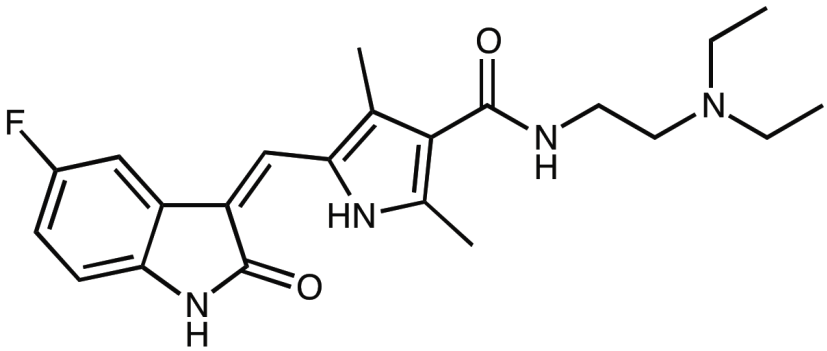

Figure 32: Chemical structure of sunitinib.

3.4 TKIs and hepatotoxicity

Present clinical evidence suggests that TKIs are associated with idiosyncratic hepatotoxicity. A meta-analysis demonstrated that patients receiving TKIs were four-times more likely to experience high-grade hepatic adverse events than patients receiving placebo (Teo et al. 2013). Several hypotheses about the mechanisms of TKI-induced hepatotoxicity have been proposed. A large percentage of drugs that induce idiosyncratic hepatotoxicity are capable of forming reactive metabolites (RM) (Leung et al. 2012; Walgren et al. 2005). In general, RMs are highly reactive and can therefore interfere with cellular molecules via covalent interactions and thus affect critical cell function and promote cell death. Hence, several scientist have postulated that hepatotoxicity due to TKIs is responsible for the formation of RM (Li et al. 2009; Li et al. 2010; Teng et al. 2010). This RM formation is probably enhanced due to changes in drug metabolism, either due to genetic polymorphisms in drug metabolizing enzymes or due to drug-drug-interaction (Teo et al. 2015). For lapatinib, it was demonstrated that metabolites induced oxidative stress, reduced oxygen consumption, and decreased GSH levels (Eno et al. 2016; Hardy et al. 2014). Other hypotheses include immune-mediated mechanisms (Spraggs et al. 2011). In addition, mitochondrial mechanisms of TKI-induced hepatotoxicity have been postulated mainly for dasatinb (Xue et al. 2012), pazopanib (Choudhury et al. 2017; Zhang et al. 2017b), regorafenib (Weng et al. 2015; Zhang et al. 2017b), sorafenib (Chiou et al. 2009; Zhang et al. 2017a; Zhang et al. 2017b), and sunitinib

(Porceddu et al. 2012). Mitochondrial toxicity was mostly due to oxidative stress, inhibition of oxidative phosphorylation, and reduction of the mitochondrial membrane potential.

4 GOAL OF THE THESIS

The goal of this thesis was to contribute to an increased and comprehensive understanding of the mechanisms of TKI-induced hepatotoxicity. The project focused on mitochondrial toxicity in human hepatocyte cell lines and isolated mitochondria *in vitro* and on sunitinib-induced hepatotoxicity in mice *in vivo*. We aimed to find out susceptibility factors for the idiosyncratic hepatotoxicity of TKIs.

The purpose of the first study was to investigate the mechanisms of hepatotoxicity for erlotinib, imatinib, lapatinib, and sunitinib *in vitro* in more detail. We wanted to consider the question whether mitochondrial toxicity contributed to the hepatotoxicity seen in patients treated with these TKIs. Therefore we focused on energy metabolism, oxidative stress, and mechanism of cell death in HepG2 cells, HepaRG cells, and mouse liver mitochondria.

In a second study, we investigated six more TKIs that are associated with hepatotoxicity in patients – crizotinib, dasatinib, pazopanib, ponatinib, regorafenib, and sorafenib. We wanted to answer the question if the mechanisms of hepatotoxicity of these TKIs are similar to the mechanisms of the previous four TKIs or not. Therefore, we used similar conditions and end points as in the first study.

In the third project, we focused on the three most hepatotoxic TKIs of the second study – ponatinib, regorafenib, and sorafenib. We wanted to investigate the question what is the exact mechanism behind the demonstrated mitochondrial toxicity with decreased mitochondrial membrane potential, inhibited mitochondrial oxidative metabolism, and induction of apoptosis and/or necrosis. Therefore, we focused on single complexes of the mitochondrial electron transport chain and on events in fission, fusion, mitophagy, and apoptosis.

The goal of the last study was to investigate the sunitinib-induced hepatotoxicity *in vivo* because so far the effects of sunitinib on liver mitochondria has been investigated in isolated rat liver mitochondria *ex vivo* and not *in vivo*. We wanted to consider the question whether the mechanisms of sunitinib-induced hepatotoxicity *in vitro* and *in vivo* are the same or whether there are specific effects in different species. Therefore, we investigated liver morphology and function as well as the function of the respiratory chain and mechanism of death in liver mitochondria in mice.

RESULTS

1 PAPER 1

HEPATOCELLULAR TOXICITY ASSOCIATED WITH TYROSINE KINASE INHIBITORS: MITOCHONDRIAL DAMAGE AND INHIBITION OF GLYCOLYSIS

Within this article, we will investigate the mechanisms of hepatotoxicity for erlotinib, imatinib, lapatinib and sunitinib *in vitro*.

frontiers in Pharmacology

ORIGINAL RESEARCH
published: 14 June 2017
doi: 10.3389/fphar.2017.00367

Hepatocellular Toxicity Associated with Tyrosine Kinase Inhibitors: Mitochondrial Damage and Inhibition of Glycolysis

*Franziska Paech[1,2], Jamal Bouitbir[1,2,3] and Stephan Krähenbühl[1,2,3]**

[1] Division of Clinical Pharmacology and Toxicology, University Hospital Basel, Basel, Switzerland, [2] Department of Biomedicine, University of Basel, Basel, Switzerland, [3] Swiss Centre of Applied Human Toxicology, Basel, Switzerland

Tyrosine kinase inhibitors (TKIs) are anticancer drugs with a lesser toxicity than classical chemotherapeutic agents but still with a narrow therapeutic window. While hepatotoxicity is known for most TKIs, underlying mechanisms remain mostly unclear. We therefore aimed at investigating mechanisms of hepatotoxicity for imatinib, sunitinib, lapatinib and erlotinib *in vitro*. We treated HepG2 cells, HepaRG cells and mouse liver mitochondria with TKIs (concentrations 1–100 μM) for different periods of time and assessed toxicity. In HepG2 cells maintained with glucose (favoring glycolysis), all TKIs showed a time- and concentration-dependent cytotoxicity and, except erlotinib, a drop in intracellular ATP. In the presence of galactose (favoring mitochondrial metabolism), imatinib, sunitinib and erlotinib showed a similar toxicity profile as for glucose whereas lapatinib was less toxic. For imatinib, lapatinib and sunitinib, cytotoxicity increased in HepaRG cells induced with rifampicin, suggesting formation of toxic metabolites. In contrast, erlotinib was more toxic in HepaRG cells under basal than CYP-induced conditions. Imatinib, sunitinib and lapatinib reduced the mitochondrial membrane potential in HepG2 cells and in mouse liver mitochondria. In HepG2 cells, these compounds increased reactive oxygen species production, impaired glycolysis, and induced apoptosis. In addition, imatinib and sunitinib impaired oxygen consumption and activities of complex I and III (only imatinib), and reduced the cellular GSH pool. In conclusion, imatinib and sunitinib are mitochondrial toxicants after acute and long-term exposure and inhibit glycolysis. Lapatinib affected mitochondria only weakly and inhibited glycolysis, whereas the cytotoxicity of erlotinib could not be explained by a mitochondrial mechanism.

Keywords: tyrosine kinase inhibitor, hepatotoxicity, mitochondrial toxicity, glycolysis, ROS, apoptosis

OPEN ACCESS

Edited by:
Eleonore Fröhlich, Medical University of Graz, Austria

Reviewed by:
Nick Plant, University of Surrey, United Kingdom
Mele Antonietta, Università degli studi di Bari Aldo Moro, Italy
Joerg Huwyler, University of Basel, Switzerland

****Correspondence:***
Stephan Krähenbühl
stephan.kraehenbuehl@usb.ch

Specialty section:
This article was submitted to Predictive Toxicology, a section of the journal Frontiers in Pharmacology

Received: *31 October 2016*
Accepted: *26 May 2017*
Published: *14 June 2017*

Citation:
Paech F, Bouitbir J and Krähenbühl S (2017) Hepatocellular Toxicity Associated with Tyrosine Kinase Inhibitors: Mitochondrial Damage and Inhibition of Glycolysis. Front. Pharmacol. 8:367. doi: 10.3389/fphar.2017.00367

Abbreviations: $\Delta\psi_m$, mitochondrial membrane potential; AK, adenylate kinase; BSO, buthionine sulfoximine; CCCP, carbonyl cyanide-chlorophenyl hydrazone; DMSO, dimethyl sulfoxide; DPBS, Dulbecco's phosphate buffered saline; FCCP, carbonyl cyanide-4-(trifluoromethoxy)phenylhydrazone; GSH, glutathione (reduced form); OCR, oxygen consumption rate; PBS, phosphate buffered saline; ROS, reactive oxygen species; SOD1, superoxide dismutase 1; SOD2, superoxide dismutase 2; TK, tyrosine kinase; TKI, tyrosine kinase inhibitor; TMRM, tetramethylrhodamine methyl ester.

INTRODUCTION

Tyrosine kinases (TK) are important enzymes that phosphorylate target proteins, leading to activation of signal transduction pathways. TK play a critical role in a variety of biological processes, including cell proliferation and cell death (Josephs et al., 2013). Mutations or structural alterations of TK can lead to uncontrolled activation of TK, possibly favoring the development of cancer (Krause and Van Etten, 2005). The critical role of TK in the regulation of cell proliferation has led to the development of a new generation of anticancer agents, the TKIs. Imatinib was the first TKI entering the market and was approved initially for the treatment of patients with chronic myeloid leukemia (Mealing et al., 2013). Many other TKIs have since then been approved inhibiting different kinases and for different indications, and many more are under development.

Compared to classical chemotherapeutic agents, TKIs are generally less toxic. Nevertheless, they still have a narrow therapeutic window, with adverse effects mainly affecting the skin, gastrointestinal tract, pancreas, lungs, the cardiovascular system including the heart, skeletal muscle and the liver (Breccia and Alimena, 2013; Bauer et al., 2016). Grade 3 to 4 toxicity, which is potentially dose- or treatment-limiting, has been described for most of the above-mentioned organs, and, with different frequencies, for all TKIs currently used (Caldemeyer et al., 2016). Hepatotoxicity has been reported for several TKIs, including crizotinib, erlotinib, gefitinib, imatinib, lapatinib, nilotinib, pazopanib, ponatinib, regorafenib, sunitinib, and vemurafenib (Josephs et al., 2013; Shah et al., 2013; Spraggs et al., 2013). The frequency of liver injury varies from 11% for gefitinib (Liu and Kurzrock, 2014) to more than 50% of patients treated with pazopanib (Shah et al., 2013). Severe liver injury has been reported to affect approximately 5% of the patients (Iacovelli et al., 2014) and liver failure 0.8% of patients treated with sunitinib, sorafenib, pazopanib, axitinib, vandetanib, cabozantinib, ponatinib, or regorafenib (Ghatalia et al., 2014). Fatalities are rare, but were reported for crizotinib (Sato et al., 2014), erlotinib (Huang et al., 2009), imatinib (Ridruejo et al., 2007), lapatinib, pazopanib (Klempner et al., 2012), ponatinib (Price et al., 2013), regorafenib, and sunitinib (Gore et al., 2009). Liver injury was hepatocellular in most cases, but also cholestasis has been reported (Shah et al., 2013). In most cases, liver injury develops 2–8 weeks after initiating therapy and features of hypersensitivity are usually absent (Teng et al., 2010; Shah et al., 2013).

Studies regarding the mechanism for hepatotoxicity of TKIs are rare. Since the spectrum of the kinases inhibited varies between the different compounds, a class effect is unlikely. For lapatinib, a study suggested a HLA-associated mechanism (Spraggs et al., 2012). The DQA1*02:01 allele was found in 71% of patients with elevated but only in 21% of patients with normal transaminases (Spraggs et al., 2011), suggesting an immune-mediated mechanism. For CP-724,714, a TKI whose clinical development was stopped because of hepatotoxicity, proposed mechanisms were mitochondrial toxicity and inhibition of canalicular and basolateral transport proteins (Feng et al., 2009). Recent publications suggested mitochondrial toxicity for dasatinib (Xue et al., 2012) and regorafenib (Weng et al., 2015). Another theory for TKI induced hepatotoxicity is the formation of reactive metabolites that can interfere with critical cell functions (Teo et al., 2015), since most TKIs undergo intense hepatic metabolism by CYP3A4 (Josephs et al., 2013).

Since the exact mechanisms underlying hepatotoxicity of TKIs are currently unclear, we decided to investigate the effects of different TKIs in human hepatocyte cell lines and in isolated mouse liver mitochondria in more detail. We focused on energy metabolism, since ATP is essential for cell survival and mitochondrial toxicity is one of the main mechanisms of non-immunologic drug-associated liver injury (Lee, 2003).

MATERIALS AND METHODS

Chemicals

Erlotinib mesylate, imatinib mesylate, lapatinib, and sunitinib were purchased from Sequoia research products (Pangbourne, United Kingdom). We prepared stock solutions in DMSO and stored them at −20°C. All other chemicals were supplied by Sigma–Aldrich (Buchs, Switzerland), except where indicated.

Cell Culture

The human hepatocellular carcinoma cell line HepG2 was provided by American type culture collection (ATCC, Manassas, VA, United States). HepG2 cells were cultured under two different conditions – low glucose and galactose.

HepG2 cells under low glucose conditions were cultured in Dulbecco's Modified Eagle Medium (DMEM containing 1 g/l [5.55 mM] glucose, 4 mM L-glutamine, and 1 mM pyruvate from Invitrogen, Basel, Switzerland) supplemented with 10% (v/v) heat-inactivated fetal bovine serum, 2 mM GlutaMax, 10 mM HEPES buffer, 10 mM non-essential amino acids, 100 units/ml penicillin, and 100 µg/ml streptomycin.

HepG2 cells under galactose conditions were cultured in Dulbecco's Modified Eagle Medium (DMEM, containing no glucose but 4 mM L-glutamine) from Invitrogen (Basel, Switzerland) supplemented with 10% (v/v) heat-inactivated fetal bovine serum, 10 mM galactose, 10 mM HEPES buffer, 1 mM sodium pyruvate, 100 units/ml penicillin, and 100 µg/ml streptomycin.

The HepaRG cell line was provided by Biopredic International (Saint-Gregoire, France). Cells were cultured and differentiated as described earlier (Gripon et al., 2002). Induction of CYP3A4 was achieved by preincubation of differentiated HepaRG cells with 20 µM rifampicin for 72 h, with medium change every 24 h.

All cells were kept at 37°C in a humidified 5% CO_2 cell culture incubator and passaged using trypsin. The cell number was determined using a Neubauer hemacytometer and viability was checked using the trypan blue exclusion method.

Isolation of Mouse Liver Mitochondria

The experiments were performed in accordance with the institutional guidelines for the care and use of laboratory animals. Male C57BL/6 mice (n = 12, age 7–10 weeks) were purchased from Charles River Laboratories (Sulzfeld, Germany) and housed

in a standard facility with 12 h light–dark cycles and controlled temperature (21–22°C). The mice were fed a standard pellet chow and water *ad libitum*. The mice did not receive any treatment and were sacrificed by cervical dislocation.

Liver mitochondria were isolated by differential centrifugation as described before (Hoppel et al., 1979). The mitochondrial protein content was determined using the Pierce BCA protein assay kit from Merck (Zug, Switzerland).

Cytotoxicity and Cellular ATP Content

Cytotoxicity, a marker for plasma membrane integrity, was assessed by using the ToxiLight assay from Lonza (Basel, Switzerland) as described previously (Felser et al., 2013). The intracellular ATP content, a marker for metabolic cell activity and cell viability, was determined using a CellTiter Glo kit from Promega (Wallisellen, Switzerland) as described before (Felser et al., 2013).

Incubations with culture medium containing 0.1% DMSO were used as negative and incubations containing 0.5% Triton X as positive controls.

Glycolysis

The glycolytic flux was determined via the conversion of [^{3}H]-glucose to ^3H_2O as described before (Vander Heiden et al., 2001). HepG2 cells were seeded in 6-well plates (500,000 cells/well) and treated with drugs for 48 h. The positive control was 20 mM 2-deoxy-D-glucose. After treatment, HepG2 cells were resuspended in 1 ml Krebs buffer (115 mM sodium chloride, 2 mM potassium chloride, 25 mM sodium bicarbonate, 1 mM magnesium chloride, 2 mM calcium chloride, 0.25% FBS, pH 7.4) and incubated for 30 min at 37°C. After centrifugation, cell pellets were resuspended in 0.5 ml Krebs buffer containing 10 mM glucose and 0.5 µl D-^{3}H(U) glucose (60 Ci/mmol, 0.5 µCi/assay, Perkin Elmer, Schwerzenbach, Switzerland) and incubated for 1 h at 37°C. After centrifugation, 50 µl supernatant were transferred to tubes containing 50 µl 0.2 N HCl. Tubes were transferred to scintillation vials containing 0.5 ml water and sealed. ^3H_2O was allowed to evaporate from the tube and to condense in the 0.5 ml water for 1 week. Afterward, the tube was removed and the radioactivity of the water was measured using a Packard 1900 TR liquid scintillation analyzer. The data were normalized to the protein content.

Mitochondrial Membrane Potential in Isolated Mouse Liver Mitochondria

The $\Delta\psi_m$ in freshly isolated mouse-liver mitochondria was determined using the [phenyl-^{3}H]-tetra-phenylphosphonium bromide uptake assay as described previously (Felser et al., 2013). Mitochondria were treated with test compounds for 15 min at 37°C. The radioactivity of the samples was measured on a Packard 1900 TR liquid scintillation analyzer.

Mitochondrial Membrane Potential in HepG2 Cells

Mitochondrial membrane potential in HepG2 cells was determined using TMRM (Invitrogen, Basel, Switzerland). In brief, HepG2 cells were seeded in 24-well plates (200,000 cells/well) and treated with drugs for 48 h. Cells were washed with DPBS and suspended in PBS with 100 nM TMRM. After 15 min incubation in the dark, cells were centrifuged and resuspended in PBS for analyzing them with flow cytometry using a FACSCalibur (BD Bioscience, Allschwil, Switzerland). Data were analyzed using CellQuest Pro 6.0 software (BD Bioscience, Allschwil, Switzerland).

Cellular Oxygen Consumption

Cellular respiration in intact cells was measured with a Seahorse XF24 analyzer (Seahorse Biosciences, North Billerica, MA, United States) as described before (Felser et al., 2013). Cellular respiration in intact cells was measured with a Seahorse XF24 analyzer (Seahorse Biosciences, North Billerica, MA, United States). HepG2 cells were seeded in Seahorse XF 24-well culture plates at 100,000 cells/well in DMEM growth medium and allow to adhere overnight. Cells were treated for 48 h with drugs. Before assessing the cellular respiration, the medium was replaced with 750 µl unbuffered DMEM medium (4 mM L-glutamate, 1 mM pyruvate, 1 g/l glucose, 63.3 mM sodium chloride, pH 7.4) and equilibrated at 37°C in a CO_2-free incubator for at least 30 min. Afterward, plates were transferred to the XF24 analyzer. Basal OCR was determined in the presence of glutamate/pyruvate (4 and 1 mM, respectively). The oxidative leak (a marker for uncoupling) was determined after inhibition of the mitochondrial phosphorylation by adding 1 µM oligomycin. The mitochondrial electron transport chain was stimulated maximally by the addition of 2 µM FCCP. Finally, the extramitochondrial respiration was determined after the addition of complex I inhibitor rotenone (1 µM). For the determination of the basal respiration, the oxidative leak, and the maximum respiration, the extramitochondrial respiration was subtracted. Respiration was expressed as OCR per minute.

Activity of Specific Enzyme Complexes of the Mitochondrial Electron Transport Chain

The activity of specific enzyme complexes of the respiratory chain was analyzed using an Oxygraph-2k high-resolution respirometer equipped with DataLab software (Oroboros instruments, Innsbruck, Austria). HepG2 cells were treated for 48 h with drugs. Afterward, they were suspended in MiR05 (mitochondrial respiration medium containing 0.5 mM EGTA, 3 mM magnesium chloride, 20 mM taurine, 10 mM potassium dihydrogen phosphate, 20 mM HEPES, 110 mM sucrose, 1 g/l fatty-acid free bovine serum albumin, and 60 mM lactobionic acid, pH 7.1) and transferred to the pre-calibrated Oxygraph chamber (Pesta and Gnaiger, 2012).

Respiratory capacities through complexes I, II, III, and IV were assessed in HepG2 cells permeabilized with digitonin (10 µg/1 million cells). Complexes I and III were analyzed using L-glutamate/malate (10 and 2 mM, respectively) as substrates followed by the addition of adenosine-diphosphate

(ADP; 2.5 mM) and rotenone (0.5 μM) as inhibitor of complex I. Afterward, duroquinol (500 μM) was added to investigate complex III activity.

Complexes II and IV were analyzed using succinate/rotenone (10 mM and 0.5 μM, respectively) as substrates followed by the addition of ADP (2.5 mM) and the complex III inhibitor antimycin A (2.5 μM). N,N,N′,N′-tetramethyl-1,4-phenylendiamine/ascorbate (0.5 and 2 mM, respectively) were added to investigate complex IV.

The integrity of the outer mitochondrial membrane was confirmed by the absence of a stimulatory effect of exogenous cytochrome *c* (10 μM) on respiration. Respiration was expressed as oxygen consumption per mg protein. Protein concentrations were determined using the Pierce BCA protein assay kit from Merck (Zug, Switzerland).

Freshly isolated mouse liver mitochondria were suspended in MiR06 (mitochondrial respiration medium containing 0.5 mM EGTA, 3 mM magnesium chloride, 20 mM taurine, 10 mM potassium dihydrogen phosphate, 20 mM HEPES, 110 mM sucrose, 1 g/l fatty-acid free bovine serum albumin, 60 mM lactobionic acid, and 280 units/ml catalase, pH 7.1) and 250 μg mitochondria were transferred to the pre-calibrated Oxygraph chamber and treated for 15 min with drugs. Respiratory capacities through complexes I, II, III, and IV were assessed with the same protocol as for HepG2 cells, except the permeabilization step in the beginning.

Mitochondrial β-Oxidation

Metabolism of [1-^{14}C] palmitic acid (60 mCi/mmol, PerkinElmer, Schwerzenbach, Switzerland) was assessed via the formation of ^{14}C-acid-soluble β-oxidation products (Felser et al., 2013). HepG2 cells were seeded in 6-well plates (500,000 cells/well) and treated with drugs for 48 h. The positive control was 5 μM etomoxir. After treatment, HepG2 cells were permeabilized with digitonin (10 μg/1 million cells) in 225 μl assay buffer (70 mM sucrose, 43 mM potassium chloride, 3.6 mM magnesium chloride, 7.2 mM potassium dihydrogen phosphate, 36 mM TRIS, 0.2 mM ATP, 50 μM L-carnitine, 15 μM coenzyme A, 5 mM acetoacetate, pH 7.4) and incubated for 10 min at 37°C. Afterward, 25 μl [1-^{14}C] palmitic acid (200 μM final concentration, 10 μCi/assay) was added to each sample and incubated at 37°C. The reaction was stopped after 15 min by adding 250 μl 6% perchloric acid. The samples were precipitated for 5 min on ice before centrifugation. Radioactivity was measured in the supernatant using a Packard 1900 TR liquid scintillation analyzer.

Cellular Accumulation of Reactive Oxygen Species

Generation of ROS was assessed using the ROS-Glo H_2O_2 Assay (Promega, Wallisellen, Switzerland). Briefly, cells were grown in 96-well plates and exposed to a range of TKIs for 48 h. The assay was performed according to manufacturer's manual and the luminescence was measured using a Tecan M200 Pro Infinity plate reader (Männedorf, Switzerland).

Mitochondrial Accumulation of Superoxide

Generation of mitochondrial ROS was assessed using MitoSOX Red (Invitrogen, Basel, Switzerland). HepG2 cells were seeded into black costar 96-well plates and exposed to a range of TKIs. The positive control was 100 μM amiodarone. After 48 h, cell culture medium was removed and 2.5 μM MitoSOX dissolved in 100 μl DPBS was added. After incubation for 10 min at 37°C in the dark, fluorescence was measured (excitation 510 nm, emission 580 nm) using a Tecan M200 Pro Infinity plate reader (Männedorf, Switzerland).

Glutathione (GSH) Content

The reduced form of glutathione (GSH) content was determined using the luminescent GSH-Glo Glutathione assay (Promega, Wallisellen, Switzerland). In brief, cells were grown in 96-well plates and exposed to a range of TKIs for 48 h. The positive control was 100 μM BSO. The assay was performed according to manufacturer's manual and the luminescence was measured after 15 min in the dark using a Tecan M200 Pro Infinity plate reader (Männedorf, Switzerland).

mRNA Expression

HepG2 cells were treated with TKIs for 48 h. The mRNA expression of SOD1 and SOD2 were assessed as described previously (Felser et al., 2013). Briefly, the mRNA expression was assessed using real-time PCR. RNA was extracted and purified using the Qiagen RNeasy mini extraction kit (Qiagen, Hombrechtikon, Switzerland). The quantity and purity of RNA were measured with NanoDrop 2000 (Thermo Scientific, Wohlen, Switzerland). cDNA was synthesized from 10 μg RNA using the Qiagen omniscript system. The real-time PCR was performed using SYBR Green (Roche Diagnostics, Rotkreuz, Switzerland). We used primers for SOD1 (forward: 5′-TGGCCGATGTGTCTATTGAA-3′, reverse: 5′-ACCTTTGCC CAAGTCATCTG-3′) and SOD2 (forward: 5′-GGTTGTTC ACGTAGGCCG-3′, reverse:5′-CAGCAGGCAGCTGGCT-3′) and calculated relative quantities of specifically amplified cDNA with the comparative-threshold cycle method. GAPDH was used as endogenous reference (forward: 5′-CATGGCCTTCCGTG TTCCTA-3′; reverse: 5′-CCT- GCTTCACCACCTTCTTGA-3′).

Quantification of Cytochrome c in Cytoplasm and Mitochondria

For the quantification of cytochrome *c*, cytoplasm and mitochondria were separated using a Mitochondrial/Cytosol Fractionation Kit (ab65320, Abcam, Cambridge, United Kingdom). Afterward, the cytochrome *c* content in the mitochondrial and cytosolic fraction was quantified by western blotting using Anti-cytochrome C antibody (ab133504, Abcam, Cambridge, United Kingdom). The purity of the fractions was checked by the determination of TOMM20 (a protein of the outer mitochondrial membrane) and α-tubulin (a major constituent of microtubules in the cytoplasm) by western blotting (Supplementary Figure S1). The antibodies used for western blotting were ab78547 (Abcam, Cambridge, United Kingdom) for

TOMM20 and ab76290 (Abcam, Cambridge, United Kingdom) for alpha-tubulin. Western blots were performed as described in the following section.

Western Blotting

After treatment for 48 h, HepG2 cells were lysed with RIPA buffer containing complete Mini protease inhibitor cocktail (Roche Diagnostics, Mannheim, Germany). After centrifugation, the supernatant was collected and stored at −80°C. Proteins were resolved by SDS–PAGE using commercially available 4–12% NuPAGE Bis-Tris gels (Invitrogen, Basel, Switzerland) and transferred using the Trans-Blot Turbo Blotting System (Bio-Rad, Cressier, Switzerland). The membranes were incubated with PARP (46D11) rabbit mAb (Cell Signaling Technology, Danvers, MA, United States), Anti-active Caspase-3 antibody (ab32042, Abcam, Cambridge, United Kingdom), Anti-pro Caspase 3 antibody (ab32150, Abcam, Cambridge, United Kingdom), Anti-SOD1 (ab20926, Abcam, Cambridge, United Kingdom) or Anti-SOD2 (ab16956, Abcam, Cambridge, United Kingdom) antibodies. After washing, membranes were exposed to secondary antibodies (Santa Cruz Biotechnology, Dallas, TX, United States). Immunoblots were developed using enhanced chemiluminescence (GE Healthcare, Little Chalfont, United Kingdom). Band intensities of the scanned images were quantified using the National Institutes of Health Image J program, version 1.48.

Caspase 3/7 Activity

Caspase 3/7 activity was determined using the luminescent Caspase-Glo 3/7 assay (Promega, Wallisellen, Switzerland). Cells were grown in 96-well plates and exposed to a range of TKIs for 48 h. The luminescence was measured using a Tecan M200 Pro Infinity plate reader (Männedorf, Switzerland).

Statistical Analysis

Data are given as the mean ± SEM of at least three independent experiments. Statistical analyses including calculation of EC_{50} values were performed using the GraphPad Prism 6 (GraphPad Software, La Jolla, CA, United States). For the comparison of more than two groups, one-way ANOVA was used, followed by Dunnett's post-test procedure. Differences between experiments with multiple conditions were compared using two-way ANOVA followed by Bonferroni's *post hoc* test. $^{*}P$-values < 0.05, $^{**}P$-values < 0.01, or $^{***}P$-values < 0.001 were considered significant.

RESULTS

Cytotoxicity and ATP Content in HepG2 Cells

Release of AK was determined as a marker of cytotoxicity, and the cellular ATP content as a measure for mitochondrial function and cellular integrity. As shown in **Figures 1A–C**, erlotinib (investigated up to 20 μM) and imatinib were only slightly toxic in HepG2 cells at the highest concentrations and after 24 to 48 h of incubation. While erlotinib did not affect the cellular ATP content (**Figures 1D–F**), imatinib decreased the ATP content in a time- and concentration-dependent fashion (starting at 5 μM after 24 h of incubation). In comparison, lapatinib was cytotoxic starting at 10–20 μM depending on the incubation time (**Figures 1A–C**). Lapatinib also decreased the cellular ATP content, starting at similar concentrations as cytotoxicity (**Figures 1D–F**). Sunitinib was cytotoxic starting at 5–10 μM after 24–48 h of incubation (**Figures 1A–C**) and decreased the cellular ATP content starting at 5 μM after 24 or 48 h of incubation (**Figures 1D–F**). The corresponding EC_{50} values are shown in **Table 1**. For imatinib, sunitinib and erlotinib, similar results were obtained in cells cultured with galactose instead of glucose (Supplementary Figure S2), whereas as lapatinib was less toxic under these conditions.

Cytotoxicity and ATP Content in HepaRG Cells

Cytotoxicity and ATP content were also investigated in HepaRG cells (**Figures 2A–H**). HepaRG cells contain inducible cytochrome P450 enzymes (CYPs) (Berger et al., 2016), allowing to test the possible contribution of metabolites for toxicity. After 48 h of treatment, erlotinib started to be cytotoxic at 5 μM and to decrease the intracellular ATP at 10 μM (**Figures 2A,E**). CYP induction was associated with less toxicity, suggesting that the parent compound is more toxic than the metabolites. For imatinib, cytotoxicity and reduction of intracellular ATP started at 50 μM (**Figures 2B,F**). Since cytotoxicity was significantly more accentuated after CYP induction, metabolites may have played a role. Lapatinib started to be cytotoxic at 20 μM, but caused no significant decrease of intracellular ATP (**Figures 2C,G**). At the highest concentration studied (50 μM), cytotoxicity was increased by CYP induction. Sunitinib started to be toxic at 10 μM and to decrease the ATP content starting at 50 μM (**Figures 2D,H**). Similar to imatinib and lapatinib, cytotoxicity was increased by CYP induction at the highest concentration studied (50 μM). The corresponding EC_{50} values are shown in **Table 1**.

CYP induction slightly increased cytotoxicity at high concentrations of imatinib, lapatinib and sunitinib. Since the parent compounds were also toxic themselves, we decided to continue our investigations with the parent compounds using HepG2 cells and isolated liver mitochondria.

Glycolysis and Mitochondrial Membrane Potential in HepG2 Cells and Isolated Mouse Liver Mitochondria

To investigate possible reasons for the observed decrease in the cellular ATP content, we determined the effect of the TKIs investigated on glycolysis and on the $\Delta\psi_m$ in HepG2 cells and in mouse liver mitochondria.

We determined the glycolytic flux by quantifying the conversion of [^{3}H]glucose to ^3H_2O. As shown in **Figure 3A**, imatinib, lapatinib, and sunitinib reduced the glycolytic flux in HepG2 cells starting at 50, 20, and 20 μM, respectively. Erlotinib did not impair glycolysis. The corresponding EC_{50} values are

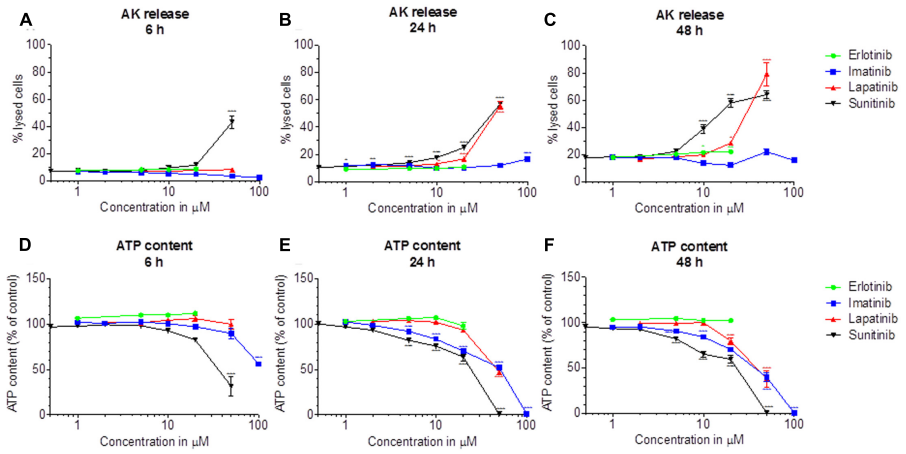

FIGURE 1 | Cytotoxicity and effect on the intracellular ATP content in HepG2 cells. Cytotoxicity was assessed by the release of AK. **(A–C)**: Cytotoxicity after drug exposure for 6, 24, and 48 h, respectively. **(D–F)**: Cellular ATP content after drug exposure for 6, 24, and 48 h, respectively. Data are expressed as % AK release in the presence of 0.5% Triton X (set at 100%) or as % ATP content in the presence of 0.1% DMSO (set at 100%). Data represent the mean ± SEM of at least three independent experiments. $^{*}p < 0.05$, $^{**}p < 0.01$ or $^{***}p < 0.001$ versus DMSO control.

given in **Table 1**. The positive control 2-deoxy-D-glucose reduced glycolysis by 75%.

Next, we quantified the effect on $\Delta\psi_m$ in HepG2 cells treated for 48 h with the TKIs (**Figure 3B**). Imatinib, lapatinib and sunitinib dissipated $\Delta\psi_m$ starting at 50, 20, and 1 µM, respectively. In contrast, erlotinib did not decrease $\Delta\psi_m$ up to 20 µM. The uncoupler CCCP (50 µM) reduced $\Delta\psi_m$ by 62% (data not shown).

As shown in **Figure 3C**, imatinib and sunitinib reduced $\Delta\psi_m$ of isolated mouse liver mitochondria after exposure for 15 min starting at 50 and 10 µM, respectively, while erlotinib and lapatinib had no significant effect. Non-radioactive tetraphenylphosphonium (positive control) apparently reduced $\Delta\psi_m$ by 38% (data not shown). The corresponding EC_{50} values are given in **Table 1**.

Effect on Oxidative Metabolism

The observed decrease in intracellular ATP and mitochondrial membrane potential could be caused by impairment of the function and/or uncoupling of the respiratory chain (Kaufmann et al., 2005). We therefore assessed the effect of TKIs on oxygen consumption by HepG2 cells using a XF24 analyzer. Cellular oxygen consumption mainly reflects mitochondrial metabolism (Felser et al., 2013). As shown in **Figures 4A–C**, exposure with erlotinib, imatinib, and lapatinib between 1 and 20 µM for 48 h did not significantly change the cellular oxygen consumption by HepG2 cells. Sunitinib decreased the maximal respiration rate (after addition of FCCP) in a concentration-dependent fashion, reaching 28% at 10 µM. Sunitinib (1–10 µM) did not increase the leak respiration after addition of oligomycin, excluding an uncoupling effect (**Figure 4D**).

In order to find out the mechanism of decreased maximal respiration, the respiratory capacities through the complexes of the electron transport chain were analyzed using a high-resolution respirometry system. Irrespective of the culture medium (low glucose or galactose), sunitinib impaired the activity of complex I in HepG2 cells exposed for 48 h in a concentration-dependent fashion, reaching significance at 10 µM for galactose (**Figure 5A** and Supplementary Figure S3). Imatinib inhibited complex III

TABLE 1 | Effect of tyrosine kinase inhibitors on different markers of toxicity.

	HepG2 (AK release)			HepG2 (ATP content)			HepaRG (AK release)		HepaRG (ATP content)		Glycolysis (HepG2 cells)	MMP (HepG2 cells)
	6 h	24 h	48 h	6 h	24 h	48 h	Induced	Non-induced	Induced	Non-induced		
Erlotinib	>20	>20	>20	>20	>20	>20	>20	>20	>20	>20	>20	>20
Imatinib	>100	>100	>100	>100	44.0	39.4	>100	>100	62.8	58.7	61.4	59.8
Lapatinib	>50	46.7	33.2	>50	34.4	24.1	>50	>50	>50	>50	>50	27.5
Sunitinib	>50	43.6	14.0	39.4	23.5	20.1	45.3	48.0	37.3	37.5	34.4	16.3

EC_{50} values were calculated using GraphPad Prism 6 as described in Methods based on the data provided in the corresponding figures. Incubation times in HepG2 cells for AK release and ATP content were as indicated and 48 h for HepaRG cells, glycolysis and the MMP. Units are µM. AK, Adenylate kinase; MMP, mitochondrial membrane potential.

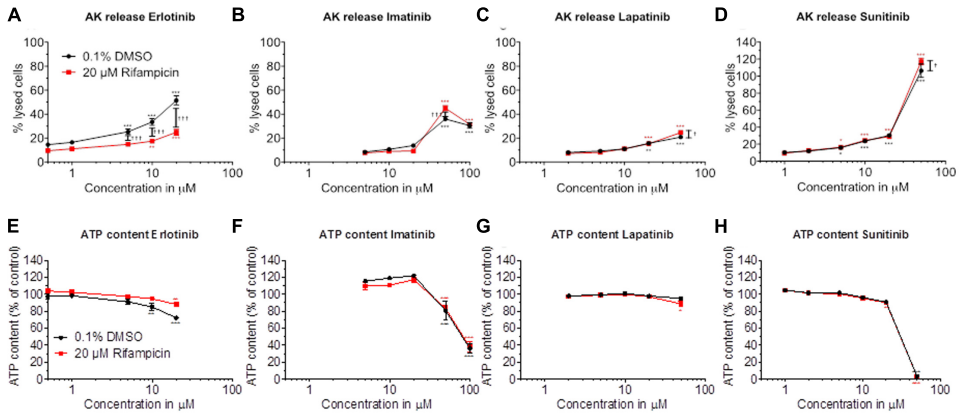

FIGURE 2 | Effect of pretreatment with rifampicin on cytotoxicity and intracellular ATP content in HepaRG cells. HepaRG cells were pretreated for 72 h with rifampicin and then exposed to drugs for 48 h. Cytotoxicity was assessed by the release of AK. **(A–D)** Cytotoxicity of erlotinib, imatinib, lapatinib, and sunitinib, respectively. **(E–H)** Intracellular ATP content of erlotinib, imatinib, lapatinib, and sunitinib, respectively. Data are expressed as % AK release in the presence of 0.5% Triton X (set at 100%) or as % ATP content in the presence of 0.1% DMSO (set at 100%). Data represent the mean ± SEM of at least three independent experiments. $^{*}p < 0.05$, $^{**}p < 0.01$ or $^{***}p < 0.001$ versus DMSO control. $^{\dagger}p < 0.05$, $^{\dagger\dagger}p < 0.01$ or $^{\dagger\dagger\dagger}p < 0.001$ rifampicin versus respective DMSO pretreatment.

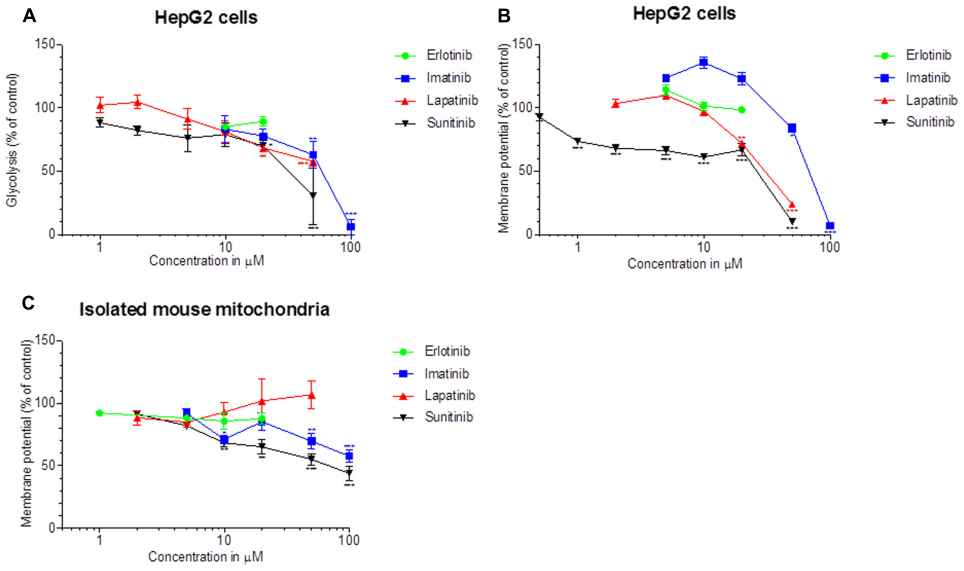

FIGURE 3 | Effect on glycolysis and on the $\Delta\psi_m$. **(A)** Glycolysis was determined using D-^{3}H(U) glucose as a substrate as described in Methods. The rate of glycolysis for the control incubations was 37.5 ± 2.6 nmoles/h/mg protein (mean ± SEM, $n = 35$ control incubations). **(B)** The $\Delta\psi_m$ was assessed in HepG2 cells by TMRM fluorescent staining after drug exposure for 48 h. **(C)** Isolated mouse liver mitochondria were labeled with [^{3}H]-tetraphenylphosphonium bromide and mitochondrial accumulation of radioactivity was determined. All data are expressed as percentage of control incubations containing 0.1% DMSO. Data represent the mean ± SEM of at least three independent experiments. $^{*}p < 0.05$, $^{**}p < 0.01$ or $^{***}p < 0.001$ versus DMSO control.

in a concentration-dependent fashion, reaching significance at 50 µM (low glucose, Supplementary Figure S3) or 10 µM (galactose, **Figure 5B**).

In isolated mouse liver mitochondria exposed for 15 min, sunitinib and imatinib were less toxic. Under these conditions, 100 µM sunitinib and 100 and 200 µM imatinib significantly decreased the respiratory capacity through complex I (**Figure 5C**).

Effect on Mitochondrial β-Oxidation

As shown in Supplementary Figure S4, erlotinib and lapatinib did not affect palmitate metabolism in HepG2 cells up to

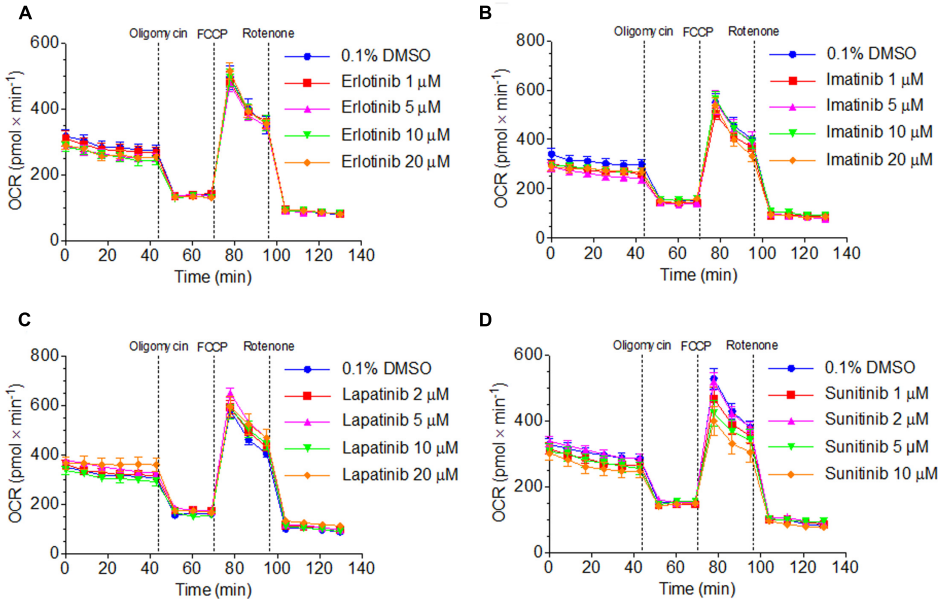

FIGURE 4 | Function of the respiratory chain in HepG2 cells. Oxygen consumption rate after exposure to **(A)** erlotinib, **(B)** imatinib, **(C)** lapatinib or **(D)** sunitinib for 48 h. Data represent the mean ± SEM of at least three independent experiments.

20 and 50 µM, respectively. Sunitinib and imatinib decreased palmitate oxidation starting at 50 and 100 µM, respectively. Since β-oxidation was inhibited at higher concentrations than glycolysis and the function of the electron transport chain, we did not assess the mechanism of this inhibition.

Effect on ROS Production, Cellular GSH and SOD Expression

Toxicants inhibiting complex I and III can stimulate superoxide production in mitochondria (Drose and Brandt, 2012). Accordingly, specific mitochondrial superoxide accumulation in HepG2 cells exposed for 48 h started at 50 µM for imatinib and 20 µM for lapatinib, but not for erlotinib up to 20 µM (**Figure 6A**). Sunitinib could not be investigated due to self-fluorescence interacting with the assay.

We therefore determined also cellular production of H_2O_2 by HepG2 cells exposed to TKIs for 48 h (**Figure 6B**). All TKIs investigated started to increase the cellular production of H_2O_2 at the lowest concentration investigated (2 µM for sunitinib and 5 µM for imatinib, lapatinib and erlotinib). For sunitinib and imatinib, there was a sharp increase in H_2O_2 production at 20 and 50 µM, respectively. The positive control 50 µM amiodarone increased the H_2O_2 accumulation 11-fold (data not shown).

Superoxide dismutases (SOD) are important for ROS defense and are located in the mitochondrial matrix (SOD2) or in the cytoplasm (SOD1) (Bresciani et al., 2015). In HepG2 cells exposed for 48 h to imatinib, mRNA expression of SOD1 and SOD2 was increased at 50 µM, reaching statistical significance for SOD1 (**Figure 6C**). Lapatinib suppressed mRNA expression of SOD2, but did not affect SOD1, whereas sunitinib increased SOD1 expression without affecting SOD2. With the exception of erlotinib, TCIs generally increased the protein expression of SOD1 and SOD2 in a concentration-dependent fashion, reaching statistical significance for sunitinib (**Figure 6D**).

Accumulating ROS can be degraded by the glutathione antioxidant system, which is an effective scavenger of free radicals (Schafer and Buettner, 2001; Fernandez-Checa and Kaplowitz, 2005). In HepG2 cells exposed for 48 h, imatinib started to decrease the GSH content at 10 µM, reaching statistical significance at 50 µM (**Figure 6E**). In cells exposed to sunitinib, the cellular GSH content was not affected at 10 µM but not different from zero at 20 µM. Cytotoxicity, which was in a range of 30% for 20 µM sunitinib, has likely contributed to this finding. For erlotinib and lapatinib, no significant decrease in GSH was found. 100 µM BSO, which served as positive control, decreased the GSH content by more than 90% (data not shown).

Mechanisms of Cell Death in HepG2 Cells

Mitochondrial toxicity associated with imatinib and sunitinib suggested involvement of mitochondria in cell death. Release of cytochrome *c* from mitochondria into the cytoplasm is an initial trigger for apoptosis (Green and Reed, 1998). As shown in **Figure 7A**, all TKIs investigated were associated with an increase of cytochrome *c* in the cytoplasm. This was associated with a concentration-dependent increase in the activity of caspases 3/7 for imatinib, lapatinib, and sunitinib starting at 50, 20, and 20 µM, respectively, but not for erlotinib (**Figure 7B**). The

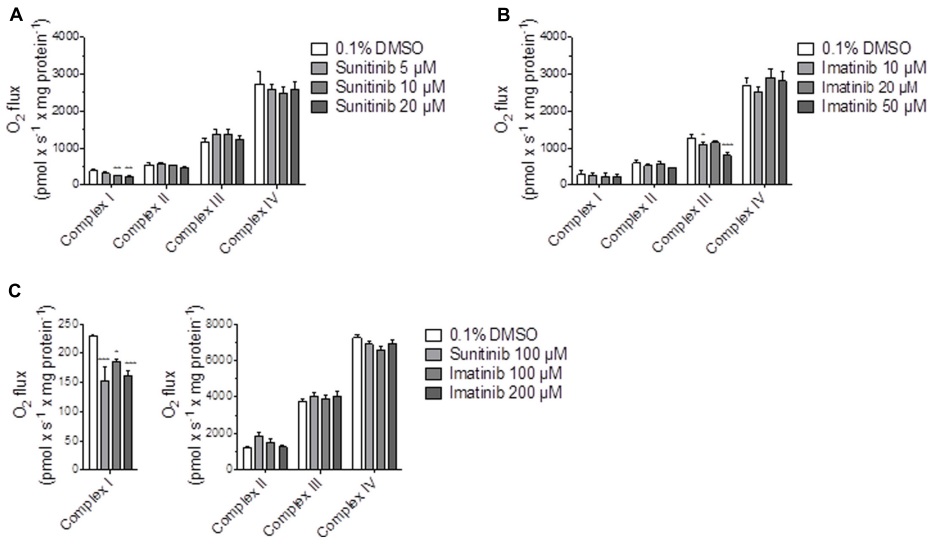

FIGURE 5 | Effect on respiratory capacities through complexes I, II, III, and IV measured on the Oxygraph-2k-high-resolution respirometer. **(A,B)** Effect on HepG2 cells cultured with galactose after sunitinib and imatinib exposure for 48 h. **(C)** Effect on isolated mouse liver mitochondria after exposure for 15 min. Data represent the mean ± SEM of at least three independent experiments. $^{*}p < 0.05$, $^{**}p < 0.01$ or $^{***}p < 0.001$ versus DMSO control.

positive control 200 nM staurosporine increased the caspases 3/7 activity sixfold (data not shown).

As shown in **Figure 7C**, the ratio of active-to-pro caspase 3 protein level was increased significantly for lapatinib and sunitinib starting at 50 and 20 µM, respectively. For imatinib there was also a threefold increase at 50 µM but without reaching statistical significance, whereas erlotinib did not affect the ratio of active-to-pro caspase 3 protein levels (**Figure 7C**). Accordingly, the protein expression of the full-length PARP was reduced for imatinib and sunitinib starting for both at 10 µM, but not for erlotinib and lapatinib (**Figure 7D**).

DISCUSSION

Our investigations demonstrated that imatinib, lapatinib, and sunitinib reduce the $\Delta\psi_m$, are associated with ROS production, impair glycolysis, and induce apoptosis in HepG2 cells. Furthermore, exposure to imatinib and sunitinib was associated with impaired cellular oxygen consumption and reduced cellular GSH levels. In HepaRG cells, CYP induction by rifampicin increased cytotoxicity of these compounds, suggesting the formation of toxic metabolites. Erlotinib, which could be investigated only up to 20 µM due to solubility problems, was slightly toxic in HepG2 and HepaRG cells. CYP induction decreased the toxicity of erlotinib, suggesting the formation of non-toxic metabolites.

The EC_{50} values in **Table 1** and the data in **Figures 1**, **2** indicate that the toxicity associated with the TKIs investigated was concentration- and time-dependent and that glycolysis was inhibited at similar concentrations than ATP production. Our data are compatible with the assumption that the mechanisms causing hepatocellular toxicity of imatinib, lapatinib and sunitinib can be explained by inhibition of certain mitochondrial functions and of glycolysis.

Indeed, imatinib inhibited complex I and III and sunitinib complex I of the electron transport chain. Inhibition of complex I and complex III is associated with increased mitochondrial ROS production (Drose and Brandt, 2012), which can reduce the cellular GSH stores and induce mitochondrial membrane permeability transition (Green and Reed, 1998; Kaufmann et al., 2005). Inhibition of complex I was shown in both HepG2 cells exposed for 48 h and in isolated mouse liver mitochondria after acute exposure. In contrast, inhibition of complex III by imatinib could only be observed in HepG2 cells. This can reflect a difference between species (humans and mice) or indicate that mitochondrial damage depends on the duration of exposure, as suggested also by the increase in the impairment of the cellular ATP pool by TKIs with time (**Table 1**).

Mitochondrial membrane permeability transition is associated with mitochondrial swelling, rupture of the outer mitochondrial membrane and release of cytochrome *c* into the cytoplasm, which induces cell death through apoptosis and/or necrosis (Antico Arciuch et al., 2012). ROS production and release of cytochrome c into the cytoplasm (suggesting mitochondrial swelling and rupture of the outer mitochondrial membrane) was demonstrated for both imatinib and sunitinib. As a consequence, sunitinib and imatinib were associated with cleavage and activation of caspase 3 and activation of caspase 7, which causes degradation of PARP and initiation of apoptosis.

For lapatinib, the mechanism of hepatotoxicity partially involved mitochondria and, possibly to a larger extent,

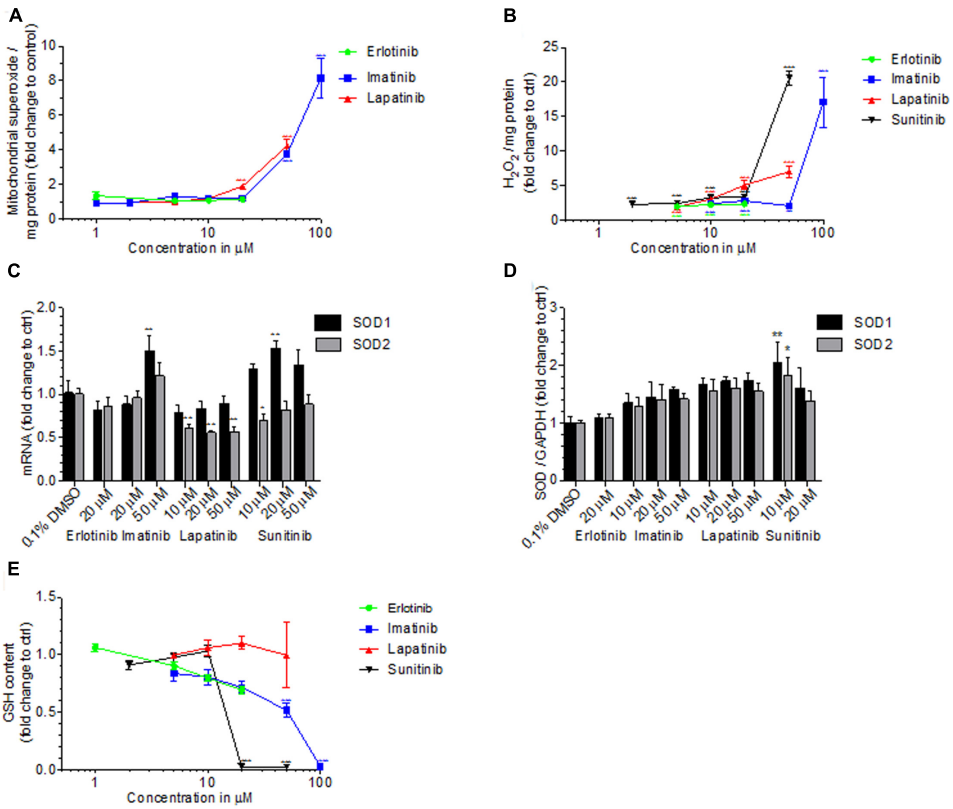

FIGURE 6 | Cellular and mitochondrial ROS production, cellular GSH content and SOD expression. **(A)** Mitochondrial ROS production by HepG2 cells after drug exposure for 48 h. **(B)** Production of H_2O_2 by HepG2 cells after drug exposure for 48 h. **(C)** mRNA expression of SOD1 and SOD2 in HepG2 cells after drug exposure for 48 h. **(D)** Protein expression of SOD1 and SOD2 in HepG2 cells after drug exposure for 48 h. **(E)** GSH content in HepG2 cells after drug exposure for 48 h. Basel GSH concentration of control incubations (0.1% DMSO) was 24.4 ± 6.0 µM. All data are expressed as fold change to control incubations containing 0.1% DMSO. Data represent the mean ± SEM of at least three independent experiments. $^*p < 0.05$, $^{**}p < 0.01$ or $^{***}p < 0.001$ versus DMSO control.

inhibition of glycolysis. In support of this assumption, lapatinib showed a more pronounced cytotoxicity and reduction in cellular ATP levels in the presence of glucose (favoring glycolysis) compared to galactose (favoring mitochondrial ATP generation) (**Figure 1** and Supplementary Figure S2). Lapatinib decreased the $\Delta\psi_m$ in mouse liver mitochondria and increased mitochondrial ROS production, but did not impair oxidative metabolism of HepG2 cells. Nevertheless, also lapatinib was associated with release of cytochrome c into the cytoplasm and induction of apoptosis. Interestingly, a recently published study suggested that mitochondrial toxicity of lapatinib is associated with the O-dealkylated metabolite of lapatinib, which can form a quinone imine after oxidation (Eno et al., 2016). These results are in agreement with the finding in the current study that CYP induction of HepaRG cells by rifampicin increased the toxicity of lapatinib (**Figure 2**).

Erlotinib was cytotoxic in HepG2 and HepaRG cells and decreased the ATP content in HepaRG but not in HepG2 cells. In agreement with these findings, erlotinib did not affect oxidative metabolism or the $\Delta\psi_m$ in HepG2 cells, excluding a mitochondrial mechanism. Based in the EC_{50} values shown in **Table 1**, HepaRG cells appear to be slightly more resistant than HepG2 cells to the toxicity associated with imatinib, lapatinib and sunitinib, but not for erlotinib. In comparison to HepG2 cells, HepaRG cells are more differentiated, as evidenced by a higher expression of CYPs in the basal state and after treatment with rifampicin (Berger et al., 2016). This may also be true for the mitochondrial antioxidative defense system, which could protect HepaRG cells from insults associated with mitochondrial generation of ROS.

Our finding that certain TKIs damage mitochondria is compatible with previous reports concerning regorafenib (Weng et al., 2015) and dasatinib (Xue et al., 2012). Regorafenib is an uncoupler of oxidative phosphorylation, and disrupts the $\Delta\psi_m$ and decreases the cellular ATP content (Weng et al., 2015). Dasatinib increases mitochondrial ROS levels, reduces the

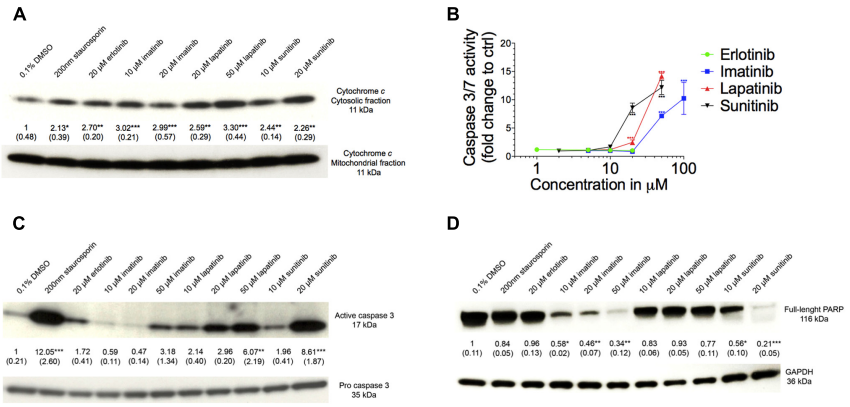

FIGURE 7 | Assessment of apoptosis. **(A)** Western blot analysis of the ratio of expression of cytochrome *c* in the cytosolic to mitochondrial fraction. **(B)** Caspase 3/7 activity in HepG2 cells after drug exposure for 48 h. **(C)** Western blot analysis of the expression of active to pro caspase 3. **(D)** Western blot analysis of the expression of full length PARP. All data are expressed as fold change to control incubations containing 0.1% DMSO. Data represent the mean ± SEM of at least three independent experiments. $*p < 0.05$, $**p < 0.01$ or $***p < 0.001$ versus DMSO control.

cellular GSH content, decreases the $\Delta\psi_m$, and induces apoptosis (Xue et al., 2012). Imatinib and sunitinib showed a similar mechanism of hepatotoxicity with ROS production, impairment of the $\Delta\psi_m$, GSH reduction, and apoptosis.

Considering the low incidence and occurrence at therapeutic dosage, TKI-induced liver injury can be regarded as an idiosyncratic (type B) adverse reaction, suggesting that affected patients have susceptibility factors (Tujios and Fontana, 2011). However, as indicated by the current study and as observed also in clinical practice, hepatotoxicity associated with TKIs appears to be dose-related, favoring intrinsic (type A) toxicity as a mechanism. At therapeutic dosages, imatinib, lapatinib, and sunitinib typically reach plasma concentrations in the range of 5, 4, and 0.3 µM, respectively (Huynh et al., 2017). As shown by data in mice, the concentrations in liver may be higher than in plasma by a factor of 2 for imatinib (Tan et al., 2011) and by a factor of at least 10 for lapatinib (Spector et al., 2015) and sunitinib (Lau et al., 2015), suggesting that toxic liver concentrations can be reached in certain patients. The data of the current study and clinical experience suggest that exposure is an important risk factor for liver toxicity associated with TKIs. Hepatic exposure is primarily dependent on the dose administered, but may also be affected by interacting drugs. Since most TKIs are metabolized (mainly *N*-dealkylation for imatinib and for sunitinib, and *O*-dealkylation for erlotinib and lapatinib) by CYP3A4 (Josephs et al., 2013; Eno et al., 2016), concomitant treatment with CYP3A4 inhibitors may increase toxicity. For imatinib, lapatinib and sorafenib, also CYP3A4 inducers could increase the risk for liver toxicity, since the metabolites formed may be more toxic than the corresponding parent compounds. Similar findings have been published for amiodarone, where the *N*-dealkylated metabolites were also more hepatotoxic than the parent compound (Zahno et al., 2011). Since imatinib, lapatinib and sunitinib are mitochondrial toxicants, mitochondrial dysfunction could be an additional susceptibility factor. The critical role of mitochondrial function regarding hepatotoxicity of mitochondrial toxicants has previously been demonstrated for valproate (Krahenbuhl et al., 2000; Knapp et al., 2008; Stewart et al., 2010) and for dronedarone (Felser et al., 2014). Furthermore, the importance of an intact hepatic mitochondrial antioxidative system has been demonstrated in $SOD2^{+/-}$ mice exposed to nimesulide (Ong et al., 2006).

The observed drop in the cellular ATP content by mitochondrial dysfunction and inhibition of glycolysis can lead to cell necrosis but can potentially damage cells also by other mechanisms. In skeletal muscle, it has recently been shown that staurosporine, a TKI which is not used as a drug, inhibits ATP-dependent potassium channels (K_{ATP} channels) at low cellular ATP levels probably by a direct interaction with the ATP binding site (Mele et al., 2014). Since liver mitochondria contain K_{ATP} channels which are important for maintaining the $\Delta\psi_m$ (Mironova et al., 1997; Seino and Miki, 2003), inhibition of these channels by TKIs may represent a mechanism of toxicity which may be important also in other organs.

CONCLUSION

Our investigations demonstrate that imatinib, lapatinib, and sunitinib were associated with mitochondrial dysfunction and inhibition of glycolysis at concentrations that may be reached in livers of affected patients. CYP induction increased the toxicity of these compounds, suggesting the formation of toxic metabolites. Hepatocellular toxicity of these compounds was concentration-dependent, corresponding with dose-dependent toxicity in patients. Erlotinib showed a slight cytotoxicity in both cell models investigated, which could not be explained by a mitochondrial mechanism or impaired glycolysis. CYP induction

reduced hepatocellular toxicity, suggesting that hepatocellular toxicity is associated mainly with the parent compound.

AUTHOR CONTRIBUTIONS

FP: Contributed to study design and data interpretation, performed lab work and helped to write paper. JB: Helped to design study, advised lab work and commented final version of manuscript. SK: Helped in study design, data interpretation and manuscript writing.

FUNDING

The study was supported by a grant from the Swiss National Science foundation to SK (SNF 31003A_156270).

SUPPLEMENTARY MATERIAL

The Supplementary Material for this article can be found online at: http://journal.frontiersin.org/article/10.3389/fphar.2017.00367/full#supplementary-material

REFERENCES

Antico Arciuch, V. G., Elguero, M. E., Poderoso, J. J., and Carreras, M. C. (2012). Mitochondrial regulation of cell cycle and proliferation. *Antioxid. Redox Signal.* 16, 1150–1180. doi: 10.1089/ars.2011.4085

Bauer, S., Buchanan, S., and Ryan, I. (2016). Tyrosine kinase inhibitors for the treatment of chronic-phase chronic myeloid leukemia: long-term patient care and management. *J. Adv. Pract. Oncol.* 7, 42–54.

Berger, B., Donzelli, M., Maseneni, S., Boess, F., Roth, A., Krahenbuhl, S., et al. (2016). Comparison of liver cell models using the Basel phenotyping cocktail. *Front. Pharmacol.* 7:443. doi: 10.3389/fphar.2016.00443

Breccia, M., and Alimena, G. (2013). Occurrence and current management of side effects in chronic myeloid leukemia patients treated frontline with tyrosine kinase inhibitors. *Leuk. Res.* 37, 713–720. doi: 10.1016/j.leukres.2013.01.021

Bresciani, G., da Cruz, I. B., and Gonzalez-Gallego, J. (2015). Manganese superoxide dismutase and oxidative stress modulation. *Adv. Clin. Chem.* 68, 87–130. doi: 10.1016/bs.acc.2014.11.001

Caldemeyer, L., Dugan, M., Edwards, J., and Akard, L. (2016). Long-term side effects of tyrosine kinase inhibitors in chronic myeloid leukemia. *Curr. Hematol. Malig. Rep.* 11, 71–79. doi: 10.1007/s11899-016-0309-2

Drose, S., and Brandt, U. (2012). Molecular mechanisms of superoxide production by the mitochondrial respiratory chain. *Adv. Exp. Med. Biol.* 748, 145–169. doi: 10.1007/978-1-4614-3573-0_6

Eno, M. R., El-Gendy Bel, D., and Cameron, M. D. (2016). P450 3a-catalyzed o-dealkylation of lapatinib induces mitochondrial stress and activates Nrf2. *Chem. Res. Toxicol.* 29, 784–796. doi: 10.1021/acs.chemrestox.5b00524

Felser, A., Blum, K., Lindinger, P. W., Bouitbir, J., and Krahenbuhl, S. (2013). Mechanisms of hepatocellular toxicity associated with dronedarone–a comparison to amiodarone. *Toxicol. Sci.* 131, 480–490. doi: 10.1093/toxsci/kfs298

Felser, A., Stoller, A., Morand, R., Schnell, D., Donzelli, M., Terracciano, L., et al. (2014). Hepatic toxicity of dronedarone in mice: role of mitochondrial beta-oxidation. *Toxicology* 323, 1–9. doi: 10.1016/j.tox.2014.05.011

Feng, B., Xu, J. J., Bi, Y. A., Mireles, R., Davidson, R., Duignan, D. B., et al. (2009). Role of hepatic transporters in the disposition and hepatotoxicity of a HER2 tyrosine kinase inhibitor CP-724,714. *Toxicol. Sci.* 108, 492–500. doi: 10.1093/toxsci/kfp033

Fernandez-Checa, J. C., and Kaplowitz, N. (2005). Hepatic mitochondrial glutathione: transport and role in disease and toxicity. *Toxicol. Appl. Pharmacol.* 204, 263–273. doi: 10.1016/j.taap.2004.10.001

Ghatalia, P., Je, Y., Mouallem, N. E., Nguyen, P. L., Trinh, Q., Sonpavde, G., et al. (2014). Hepatotoxicity with vascular endothelial growth factor receptor tyrosine kinase inhibitors: a meta-analysis of randomized clinical trials. *Crit. Rev. Oncol. Hematol.* 93, 257–276. doi: 10.1016/j.critrevonc.2014.11.006

Gore, M. E., Szczylik, C., Porta, C., Bracarda, S., Bjarnason, G. A., Oudard, S., et al. (2009). Safety and efficacy of sunitinib for metastatic renal-cell carcinoma: an expanded-access trial. *Lancet. Oncol.* 10, 757–763. doi: 10.1016/S1470-2045(09)70162-7

Green, D. R., and Reed, J. C. (1998). Mitochondria and apoptosis. *Science* 281, 1309–1312. doi: 10.1126/science.281.5381.1309

Gripon, P., Rumin, S., Urban, S., Le Seyec, J., Glaise, D., Cannie, I., et al. (2002). Infection of a human hepatoma cell line by hepatitis B virus. *Proc. Natl. Acad. Sci. U.S.A.* 99, 15655–15660. doi: 10.1073/pnas.232137699

Hoppel, C., DiMarco, J. P., and Tandler, B. (1979). Riboflavin and rat hepatic cell structure and function. Mitochondrial oxidative metabolism in deficiency states. *J. Biol. Chem.* 254, 4164–4170.

Huang, Y. S., An, S. J., Chen, Z. H., and Wu, Y. L. (2009). Three cases of severe hepatic impairment caused by erlotinib. *Br. J. Clin. Pharmacol.* 68, 464–467. doi: 10.1111/j.1365-2125.2009.03459.x

Huynh, H. H., Pressiat, C., Sauvageon, H., Madelaine, I., Maslanka, P., Lebbe, C., et al. (2017). Development and validation of a simultaneous quantification method of 14 tyrosine kinase inhibitors in human plasma using LC-MS/MS. *Ther. Drug Monit.* 39, 43–54. doi: 10.1097/FTD.0000000000000357

Iacovelli, R., Palazzo, A., Procopio, G., Santoni, M., Trenta, P., De Benedetto, A., et al. (2014). Incidence and relative risk of hepatic toxicity in patients treated with anti-angiogenic tyrosine kinase inhibitors for malignancy. *Br. J. Clin. Pharmacol.* 77, 929–938. doi: 10.1111/bcp.12231

Josephs, D. H., Fisher, D. S., Spicer, J., and Flanagan, R. J. (2013). Clinical pharmacokinetics of tyrosine kinase inhibitors: implications for therapeutic drug monitoring. *Ther. Drug Monit.* 35, 562–587. doi: 10.1097/FTD.0b013e318292b931

Kaufmann, P., Torok, M., Hanni, A., Roberts, P., Gasser, R., and Krahenbuhl, S. (2005). Mechanisms of benzarone and benzbromarone-induced hepatic toxicity. *Hepatology* 41, 925–935. doi: 10.1002/hep.20634

Klempner, S. J., Choueiri, T. K., Yee, E., Doyle, L. A., Schuppan, D., and Atkins, M. B. (2012). Severe pazopanib-induced hepatotoxicity: clinical and histologic course in two patients. *J. Clin. Oncol.* 30, e264–e268. doi: 10.1200/jco.2011.41.0332

Knapp, A. C., Todesco, L., Beier, K., Terracciano, L., Sagesser, H., Reichen, J., et al. (2008). Toxicity of valproic acid in mice with decreased plasma and tissue carnitine stores. *J. Pharmacol. Exp. Ther.* 324, 568–575. doi: 10.1124/jpet.107.131185

Krahenbuhl, S., Brandner, S., Kleinle, S., Liechti, S., and Straumann, D. (2000). Mitochondrial diseases represent a risk factor for valproate-induced fulminant liver failure. *Liver* 20, 346–348. doi: 10.1034/j.1600-0676.2000.020004346.x

Krause, D. S., and Van Etten, R. A. (2005). Tyrosine kinases as targets for cancer therapy. *N. Engl. J. Med.* 353, 172–187. doi: 10.1056/NEJMra044389

Lau, C. L., Chan, S. T., Selvaratanam, M., Khoo, H. W., Lim, A. Y., Modamio, P., et al. (2015). Sunitinib-ibuprofen drug interaction affects the pharmacokinetics and tissue distribution of sunitinib to brain, liver, and kidney in male and female mice differently. *Fundam. Clin. Pharmacol.* 29, 404–416. doi: 10.1111/fcp.12126

Lee, W. M. (2003). Drug-induced hepatotoxicity. *N. Engl. J. Med.* 349, 474–485. doi: 10.1056/NEJMra021844

Liu, S., and Kurzrock, R. (2014). Toxicity of targeted therapy: implications for response and impact of genetic polymorphisms. *Cancer Treat. Rev.* 40, 883–891. doi: 10.1016/j.ctrv.2014.05.003

Mealing, S., Barcena, L., Hawkins, N., Clark, J., Eaton, V., Hirji, I., et al. (2013). The relative efficacy of imatinib, dasatinib and nilotinib for newly diagnosed chronic myeloid leukemia: a systematic review and network meta-analysis. *Exp. Hematol. Oncol.* 2:5. doi: 10.1186/2162-3619-2-5

Mele, A., Camerino, G. M., Calzolaro, S., Cannone, M., Conte, D., and Tricarico, D. (2014). Dual response of the KATP channels to staurosporine: a novel role of SUR2B, SUR1 and Kir6.2 subunits in the regulation of the atrophy in different skeletal muscle phenotypes. *Biochem. Pharmacol.* 91, 266–275. doi: 10.1016/j.bcp.2014.06.023

Mironova, G. D., Grigoriev, S. M., Skarga, Y., Negoda, A. E., and Kolomytkin, O. V. (1997). ATP-dependent potassium channel from rat liver mitochondria: inhibitory analysis, channel clusterization. *Membr. Cell Biol.* 10, 583–591.

Ong, M. M., Wang, A. S., Leow, K. Y., Khoo, Y. M., and Boelsterli, U. A. (2006). Nimesulide-induced hepatic mitochondrial injury in heterozygous Sod2(+/-) mice. *Free Radic. Biol. Med.* 40, 420–429. doi: 10.1016/j.freeradbiomed.2005.08.038

Pesta, D., and Gnaiger, E. (2012). High-resolution respirometry: OXPHOS protocols for human cells and permeabilized fibers from small biopsies of human muscle. *Methods Mol. Biol.* 810, 25–58. doi: 10.1007/978-1-61779-382-0_3

Price, K. E., Saleem, N., Lee, G., and Steinberg, M. (2013). Potential of ponatinib to treat chronic myeloid leukemia and acute lymphoblastic leukemia. *Onco Targets Ther.* 6, 1111–1118. doi: 10.2147/OTT.S36980

Ridruejo, E., Cacchione, R., Villamil, A. G., Marciano, S., Gadano, A. C., and Mando, O. G. (2007). Imatinib-induced fatal acute liver failure. *World J. Gastroenterol.* 13, 6608–6111.

Sato, Y., Fujimoto, D., Shibata, Y., Seo, R., Suginoshita, Y., Imai, Y., et al. (2014). Fulminant hepatitis following crizotinib administration for ALK-positive non-small-cell lung carcinoma. *Jpn. J. Clin. Oncol.* 44, 872–875. doi: 10.1093/jjco/hyu086

Schafer, F. Q., and Buettner, G. R. (2001). Redox environment of the cell as viewed through the redox state of the glutathione disulfide/glutathione couple. *Free Radic. Biol. Med.* 30, 1191–1212. doi: 10.1016/S0891-5849(01)00480-4

Seino, S., and Miki, T. (2003). Physiological and pathophysiological roles of ATP-sensitive K^+ channels. *Prog. Biophys. Mol. Biol.* 81, 133–176. doi: 10.1016/S0079-6107(02)00053-6

Shah, R. R., Morganroth, J., and Shah, D. R. (2013). Hepatotoxicity of tyrosine kinase inhibitors: clinical and regulatory perspectives. *Drug Saf.* 36, 491–503. doi: 10.1007/s40264-013-0048-4

Spector, N. L., Robertson, F. C., Bacus, S., Blackwell, K., Smith, D. A., Glenn, K., et al. (2015). Lapatinib plasma and tumor concentrations and effects on HER receptor phosphorylation in tumor. *PLoS ONE* 10:e0142845. doi: 10.1371/journal.pone.0142845

Spraggs, C. F., Budde, L. R., Briley, L. P., Bing, N., Cox, C. J., King, K. S., et al. (2011). HLA-DQA1*02:01 is a major risk factor for lapatinib-induced hepatotoxicity in women with advanced breast cancer. *J. Clin. Oncol.* 29, 667–673. doi: 10.1200/JCO.2010.31.3197

Spraggs, C. F., Parham, L. R., Hunt, C. M., and Dollery, C. T. (2012). Lapatinib-induced liver injury characterized by class II HLA and Gilbert's syndrome genotypes. *Clin. Pharmacol. Ther.* 91, 647–652. doi: 10.1038/clpt.2011.277

Spraggs, C. F., Xu, C. F., and Hunt, C. M. (2013). Genetic characterization to improve interpretation and clinical management of hepatotoxicity caused by tyrosine kinase inhibitors. *Pharmacogenomics* 14, 541–554. doi: 10.2217/pgs.13.24

Stewart, J. D., Horvath, R., Baruffini, E., Ferrero, I., Bulst, S., Watkins, P. B., et al. (2010). Polymerase gamma gene POLG determines the risk of sodium valproate-induced liver toxicity. *Hepatology* 52, 1791–1796. doi: 10.1002/hep.23891

Tan, S. Y., Kan, E., Lim, W. Y., Chay, G., Law, J. H., Soo, G. W., et al. (2011). Metronidazole leads to enhanced uptake of imatinib in brain, liver and kidney without affecting its plasma pharmacokinetics in mice. *J. Pharm. Pharmacol.* 63, 918–925. doi: 10.1111/j.2042-7158.2011.01296.x

Teng, W. C., Oh, J. W., New, L. S., Wahlin, M. D., Nelson, S. D., Ho, H. K., et al. (2010). Mechanism-based inactivation of cytochrome P450 3A4 by lapatinib. *Mol. Pharmacol.* 78, 693–703. doi: 10.1124/mol.110.065839

Teo, Y. L., Ho, H. K., and Chan, A. (2015). Formation of reactive metabolites and management of tyrosine kinase inhibitor-induced hepatotoxicity: a literature review. *Expert Opin. Drug Metab. Toxicol.* 11, 231–242. doi: 10.1517/17425255.2015.983075

Tujios, S., and Fontana, R. J. (2011). Mechanisms of drug-induced liver injury: from bedside to bench. *Nat. Rev. Gastroenterol. Hepatol.* 8, 202–211. doi: 10.1038/nrgastro.2011.22

Vander Heiden, M. G., Plas, D. R., Rathmell, J. C., Fox, C. J., Harris, M. H., and Thompson, C. B. (2001). Growth factors can influence cell growth and survival through effects on glucose metabolism. *Mol. Cell. Biol.* 21, 5899–5912. doi: 10.1128/MCB.21.17.5899-5912.2001

Weng, Z., Luo, Y., Yang, X., Greenhaw, J. J., Li, H., Xie, L., et al. (2015). Regorafenib impairs mitochondrial functions, activates AMP-activated protein kinase, induces autophagy, and causes rat hepatocyte necrosis. *Toxicology* 327, 10–21. doi: 10.1016/j.tox.2014.11.002

Xue, T., Luo, P., Zhu, H., Zhao, Y., Wu, H., Gai, R., et al. (2012). Oxidative stress is involved in Dasatinib-induced apoptosis in rat primary hepatocytes. *Toxicol. Appl. Pharmacol.* 261, 280–291. doi: 10.1016/j.taap.2012.04.010

Zahno, A., Brecht, K., Morand, R., Maseneni, S., Torok, M., Lindinger, P. W., et al. (2011). The role of CYP3A4 in amiodarone-associated toxicity on HepG2 cells. *Biochem. Pharmacol.* 81, 432–441. doi: 10.1016/j.bcp.2010.11.002

Conflict of Interest Statement: The authors declare that the research was conducted in the absence of any commercial or financial relationships that could be construed as a potential conflict of interest.

The reviewer JH declared a shared affiliation, though no other collaboration, with the authors to the handling Editor, who ensured that the process nevertheless met the standards of a fair and objective review.

Mechanisms of hepatocellular Toxicity associated with Tyrosine Kinase Inhibitors

Franziska Paech[1,2], Jamal Bouitbir, PhD[1,2,3], Stephan Krähenbühl, MD, PhD[1,2,3]

[1]Division of Clinical Pharmacology & Toxicology, University Hospital, Basel, Switzerland

[2]Department of Biomedicine, University of Basel, Switzerland

[3]Swiss Centre of Applied Human Toxicology

Corresponding author:

Stephan Krähenbühl, MD, PhD

Clinical Pharmacology & Toxicology

University Hospital

4031 Basel, Switzerland

Phone: +41 61 265 4715

Fax: +41 61 265 4560

e-mail: stephan.kraehenbuehl@usb.ch

Figures

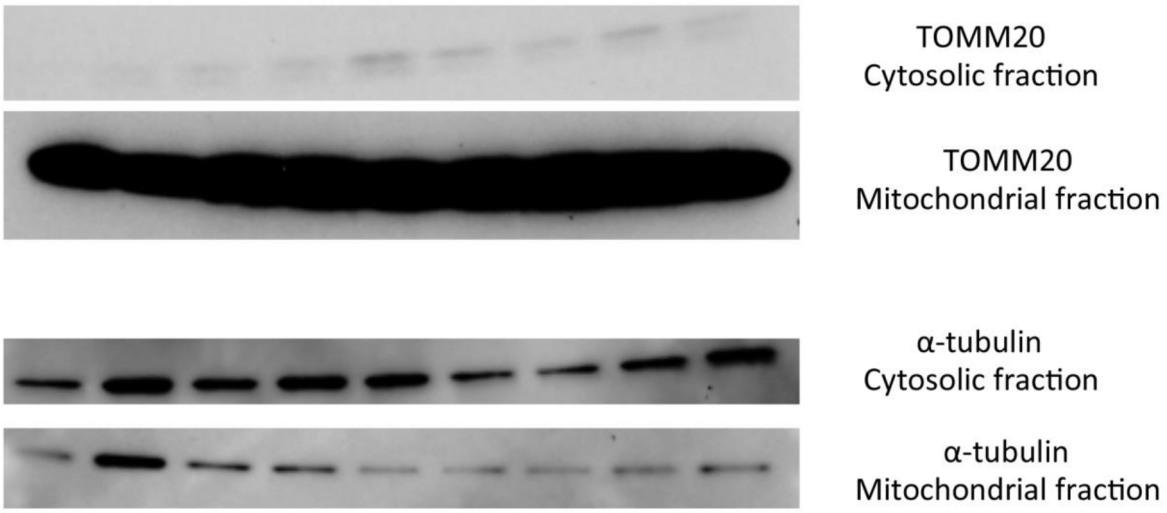

Supplementary Fig. S1. Western blot of TOMM20 and α-tubulin. Controls for the purity of the cytosolic and mitochondrial fraction of the experiment shown in Fig. 8A.

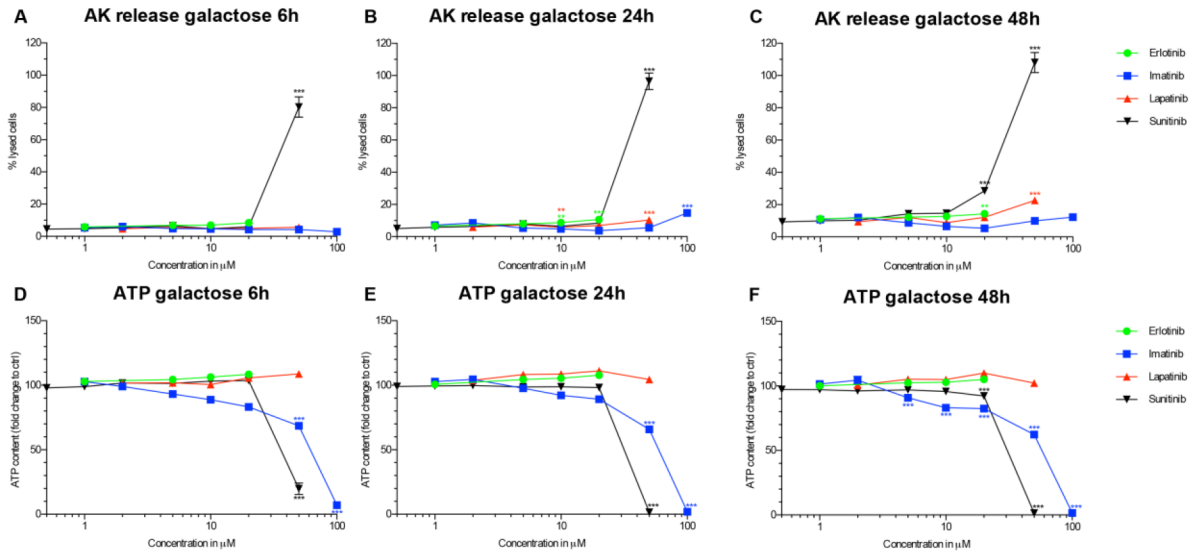

Supplementary Fig. S2. Cytotoxicity and effect on the intracellular ATP content in HepG2 cells with galactose. Cytotoxicity was assessed by the release of adenylate kinase. (A), (B), and (C) Cytotoxicity after drug exposure for 6h, 24h, and 48h. (D), (E), and (F) Intracellular ATP content after drug exposure for 6h, 24h, and 48h. Cytotoxicity data are expressed as % of positive control (0.5% Triton X) and ATP data are expressed as % of negative control (0.1% DMSO). Data represent the mean ± SEM of at least three independent experiments. *p < 0.05, **p < 0.01 or ***p < 0.001 versus DMSO control.

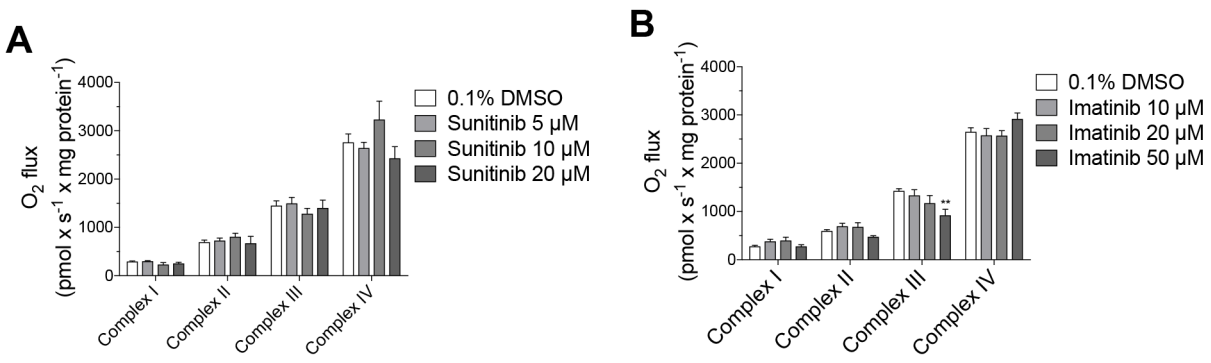

Supplementary Fig. S3. Effect on respiratory capacities through complexes I, II, III, and IV measured on the Oxygraph-2k-high-resolution respirometer. (A) and **(B)** Effect on HepG2 cells cultured with low glucose after sunitinib and imatinib exposure for 48 h. Data represent the mean±SEM of at least three independent experiments. **p < 0.01 versus DMSO control.

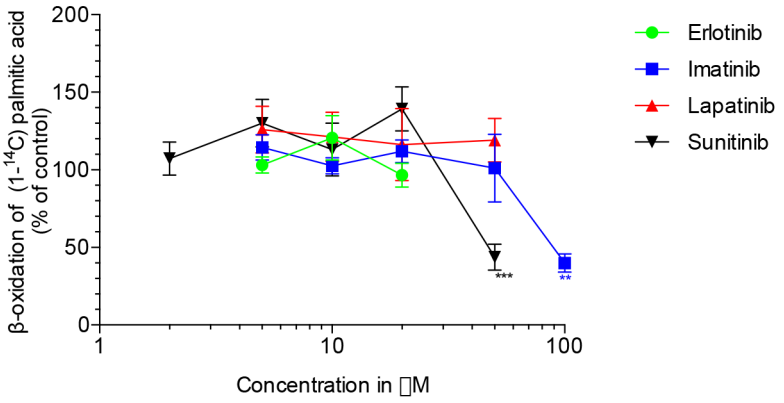

Supplementary Fig. S4. β-oxidation of [1-^{14}C] palmitic acid in HepG2 cells after drug exposure for 48 h. Basel β-oxidation activity of control incubations (0.1% DMSO) was 2.58 ± 1.35 nmol/min/mg. All data are expressed as percentage to control incubations containing 0.1% DMSO. Data represent the mean ± SEM of at least three independent experiments. **p < 0.01 or ***p < 0.001 versus DMSO control.

2 PAPER 2

MECHANISMS OF TOXICITY ASSOCIATED WITH SIX TYROSINE KINASE INHIBITORS IN HUMAN HEPATOCYTE CELL LINES

Within this article, we will investigate the mechanisms of hepatotoxicity for crizotinib, dastinib, pazopanib, ponatinib, regorafenib, and sorafenib *in vitro*.

Received: 14 August 2017 | Revised: 5 September 2017 | Accepted: 16 September 2017

DOI: 10.1002/jat.3551

WILEY Journal of Applied Toxicology

RESEARCH ARTICLE

Mechanisms of toxicity associated with six tyrosine kinase inhibitors in human hepatocyte cell lines

Cécile Mingard [1,2] | Franziska Paech [1,2] | Jamal Bouitbir [1,2,3] | Stephan Krähenbühl [1,2,3]

[1] Division of Clinical Pharmacology & Toxicology, University Hospital, Basel, Switzerland

[2] Department of Biomedicine, University of Basel, Switzerland

[3] Swiss Centre of Applied Human Toxicology, Switzerland

Correspondence
Stephan Krähenbühl, MD, PhD, Clinical Pharmacology & Toxicology, University Hospital, 4031 Basel, Switzerland.
Email: stephan.kraehenbuehl@usb.ch

Funding information
Schweizerischer Nationalfonds zur Förderung der Wissenschaftlichen Forschung, Grant/Award Number: SNF 31003A_156270

Abstract

Tyrosine kinase inhibitors have revolutionized the treatment of certain cancers. They are usually well tolerated, but can cause adverse reactions including liver injury. Currently, mechanisms of hepatotoxicity associated with tyrosine kinase inhibitors are only partially clarified. We therefore aimed at investigating the toxicity of regorafenib, sorafenib, ponatinib, crizotinib, dasatinib and pazopanib on HepG2 and partially on HepaRG cells. Regorafenib and sorafenib strongly inhibited oxidative metabolism (measured by the Seahorse -XF24 analyzer) and glycolysis, decreased the mitochondrial membrane potential and induced apoptosis and/or necrosis of HepG2 cells at concentrations similar to steady -state plasma concentrations in humans. In HepaRG cells, pretreatment with rifampicin decreased membrane toxicity (measured as adenylate kinase release) and dissipation of adenosine triphosphate stores, indicating that toxicity was associated mainly with the parent drugs. Ponatinib strongly impaired oxidative metabolism but only weakly glycolysis, and induced apoptosis of HepG2 cells at concentrations higher than steady -state plasma concentrations in humans. Crizotinib and dasatinib did not significantly affect mitochondrial functions and inhibited glycolysis only weakly, but induced apoptosis of HepG2 cells. Pazopanib was associated with a weak increase in mitochondrial reactive oxygen species accumulation and inhibition of glycolysis without being cytotoxic. In conclusion, regorafenib and sorafenib are strong mitochondrial toxicants and inhibitors of glycolysis at clinically relevant concentrations. Ponatinib affects mitochondria and glycolysis at higher concentrations than reached in plasma (but possibly in liver), whereas crizotinib, dasatinib and pazopanib showed no relevant toxicity. Mitochondrial toxicity and inhibition of glycolysis most likely explain hepatotoxicity associated with regorafenib, sorafenib and possibly pazopanib, but not for the other compounds investigated.

KEYWORDS

apoptosis, glycolysis, hepatocellular toxicity, mitochondrial toxicity, reactive oxygen species, Tyrosine kinase inhibitor

1 | INTRODUCTION

Tyrosine kinases (TK) are involved in regulating multiple cellular processes, including cellular proliferation, survival and differentiation (Shah, Morganroth, & Shah, 2013; Shchemelinin, Sefc, & Necas, 2006). Accordingly, deregulation of protein kinases is associated with many diseases such as autoimmune diseases and cancers (Levitzki & Gazit, 1995) and defective TKs are involved in tumor initiation and progression (Shchemelinin et al., 2006). Specific TKs have been linked to certain cancers, making TK inhibitors (TKIs) attractive targeted therapy for the treatment of cancer (Krause & Van Etten, 2005). The first approved TKI was imatinib in 2001 for chronic myeloid leukemia (Cohen, Johnson, & Pazdur, 2005). Since then, the Food and Drug Administration and the European Medicines Agency have approved more than 20 TKIs and many more are currently under development.

TKIs have a different toxicological profile than the classical cytotoxic agents. They are generally less toxic for hematopoiesis, but

Abbreviations: ATP, adenosine triphosphate; CYP, cytochrome P450 enzyme; DMSO, dimethyl sulfoxide; FCCP, carbonyl cyanide -4-(trifluoromethoxy) phenylhydrazone; GSH, glutathione (reduced form); PBS, phosphate -buffered saline; ROS, reactive oxygen species; SEM, standard error of the mean; tGSH, total GSH; TK, tyrosine kinase; TKI, tyrosine kinase inhibitor; TMRM, tetramethylrhodamine methyl ester; $\Delta\psi_m$, mitochondrial membrane potential

Cécile Mingard and Franziska Paech contributed equally to this work

there are concerns regarding toxicity of the skin, gastrointestinal tract, lungs, cardiovascular system, skeletal muscle and the liver (Breccia & Alimena, 2013). Hepatotoxicity has been reported for several TKIs, including regorafenib, sorafenib, ponatinib, crizotinib, dasatinib and pazopanib (Abou-Alfa et al., 2006; Bible et al., 2014; Camidge et al., 2012; Cortes et al., 2013; Di Lorenzo et al., 2009). In a recent review article, Shah et al. reported that 25 –30% of patients treated with TKIs in clinical trials showed a low-grade elevation in alanine aminotransferase (<5 times upper limit of normal) and approximately 2% of the patients developed an alanine aminotransferase increase ≥5 times upper limit of normal (Shah et al., 2013). A recent meta-analysis, which included more than 3000 patients, reported an approximately twofold increased risk for hepatotoxicity in patients treated with TKIs compared to control patients (Teo, Ho, & Chan, 2013). Liver failure and fatalities are rare, but have been reported for crizotinib (Sato et al., 2014; van Geel et al., 2016), pazopanib (Klempner et al., 2012), ponatinib (Price, Saleem, Lee, & Steinberg, 2013), regorafenib (Akamine et al., 2015; Raissouni et al., 2015; Sacre et al., 2016) and sorafenib (Brandi et al., 2015; Fairfax et al., 2012; Murad, Rabinowitz, & Lee, 2014; Rao et al., 2013; Yamasaki et al., 2016). The mechanisms of hepatotoxicity of TKIs are poorly understood, but are probably not related to kinase inhibition in hepatocytes (Shah et al., 2013). Recent publications reported mitochondrial toxicity for sorafenib, regorafenib and pazopanib (Weng et al., 2015; Zhang et al., 2017) as well as for dasatinib (Xue et al., 2012). Sorafenib, regorafenib and pazopanib impaired the function of the respiratory chain and decreased the mitochondrial membrane potential in isolated rat liver mitochondria (Xue et al., 2012) and in rat primary hepatocytes (Weng et al., 2015), whereas dasatanib uncoupled oxidative phosphorylation in isolated rat liver mitochondria (Xue et al., 2012). Furthermore, we showed recently that HepG2 cells exposed to imatinib or sunitinib had a reduced mitochondrial membrane potential, impaired oxygen consumption and increased mitochondrial oxidative stress, eventually leading to apoptosis and necrosis (Paech, Bouitbir, & Krahenbuhl, 2017). As most TKIs undergo intense hepatic metabolism by cytochrome P450 (CYP) 3A4 (Josephs, Fisher, Spicer, & Flanagan, 2013), TKI-associated hepatotoxicity may not only be due to the parent drug, but also due to metabolites (Teo, Ho, & Chan, 2015ab).

As the exact hepatotoxic mechanisms of TKIs are currently unclear and most data currently available were generated in hepatocytes or liver mitochondria from rats, we decided to investigate the toxicity of six TKIs associated with hepatotoxicity in human hepatocyte cell lines. Crizotinib is a specific inhibitor for the mutated anaplastic lymphoma kinase, dasatinib and ponatinib are multi-kinase inhibitors with a high specificity for the BCR-ABL TK receptor and pazopanib, regorafenib and sorafenib are multi-kinase inhibitors with a high specificity for the vascular endothelial growth factor receptors 1, 2 and 3. We focused on energy metabolism, as adenosine triphosphate (ATP) is essential for cell survival and as mitochondrial toxicity is an important mechanism of non-immunologic drug-associated liver injury (Han et al., 2013; Yuan & Kaplowitz, 2013). We used two human hepatoma cell lines, namely HepG2 cells grown either in the presence of glucose or of galactose, and HepaRG cells. HepG2 cells are well-suited for studying mitochondrial function (Felser, Blum, Lindinger, Bouitbir, & Krahenbuhl, 2013; Kamalian et al., 2015), but they have a low or lacking expression of CYP enzymes (Berger et al., 2016). In comparison, HepaRG cells have a conserved CYP expression, which can be induced by rifampicin (Berger et al., 2016), rendering them suitable for studying the potential role of CYP-associated metabolites. HepG2 cells were grown in the presence of glucose or of galactose, as cells grown in the presence of galactose are forced to generate most ATP by oxidative phosphorylation instead of glycolysis, rendering them sensitive to mitochondrial toxicants (Kamalian et al., 2015). The investigations revealed that regorafenib and sorafenib are strong mitochondrial toxicants and inhibitors of glycolysis, whereas the other TKIs investigated were less toxic.

2 | MATERIALS AND METHODS

2.1 | Chemicals

Crizotinib HCl, dasatinib, pazopanib, ponatinib, regorafenib and sorafenib were purchased from Sequoia research products (Pangbourne, Berks, UK). We prepared stock solutions in dimethyl sulfoxide (DMSO) and stored them at −20°C. All other chemicals were supplied by Sigma-Aldrich (Buchs, Switzerland), except where indicated.

Because of solubility reasons, we could treat with concentrations up to 100 μM for crizotinib and dasatinib, up to 50 μM for pazopanib, ponatinib and sorafenib and up to 20 μM for regorafenib.

2.2 | HepG2 cell culture

The human hepatocellular carcinoma cell line HepG2 was obtained from the American type culture collection (ATCC, Manassas, VA, USA). HepG2 cells were cultured under two different conditions, low glucose and galactose.

HepG2 cells under low glucose conditions were cultured in Dulbecco's modified Eagle medium (DMEM containing 5.55 mM [1 g l^{-1}] glucose, 4 mM L-glutamine and 1 mM pyruvate from Invitrogen, Basel, Switzerland) supplemented with 10% (v/v) heat-inactivated fetal bovine serum (FBS), 2 mM GlutaMax, 10 mM HEPES buffer, 10 mM non-essential amino acids, 100 units ml^{-1} penicillin and 100 μg ml^{-1} streptomycin.

HepG2 cells under galactose conditions were cultured for at least 3 weeks before used in the experiments in DMEM (no glucose, 4 mM L-glutamine) from Invitrogen supplemented with 10% (v/v) heat-inactivated FBS, 10 mM galactose, 2 mM L-glutamine, 10 mM HEPES buffer, 1 mM sodium pyruvate, 100 units ml^{-1} penicillin and 100 μg ml^{-1} streptomycin. The FBS was dialyzed through a Slide-A-Lyzer Dialysis Flask (Thermo Scientific, Rheinfach, Switzerland) to remove glucose according to the manufacturer's protocol.

2.3 | HepaRG cell culture

The HepaRG cell line was provided by Biopredic International (Saint-Gregoire, France). Cells were cultured and differentiated as described earlier (Gripon et al., 2002). HepaRG cells contain inducible CYPs, allowing to test the possible contribution of metabolites for toxicity (Berger et al., 2016). Induction of CYP3A4 and other CYPs was

achieved by preincubation of differentiated HepaRG cells with 20 μM rifampicin for 72 hours, with medium change every 24 hours.

All cells were kept at 37°C in a humidified 5% CO_2 cell culture incubator and passaged using trypsin. The cell number was determined using a Neubauer hemacytometer and viability was checked using the trypan blue exclusion method.

2.4 | Membrane toxicity

The integrity of the plasma membrane was assessed by using the ToxiLight assay from Lonza (Basel, Switzerland) according to the manufacturer's protocol. This assay measures the release of adenylate kinase in the extracellular space, which reflects the plasma membrane's integrity. HepG2 cells (glucose or galactose conditions) and HepaRG cells (glucose conditions) were grown in a 96-well plate (25 000 cells per well) and exposed to different concentrations of TKIs (2–100 μM) for 24 hours. The negative control was 0.1% DMSO and the positive control was 0.5% Triton-X. After incubation, 20 μl supernatant of each well was transferred to a new 96-well plate. Then, 50 μl of assay buffer was added to each well. After incubation in the dark for 5 minutes, the luminescence was measured using a Tecan M200 Pro Infinity plate reader (Männedorf, Switzerland). All data were normalized to positive control incubations containing 0.5% Triton X.

2.5 | Intracellular adenosine triphosphate content

The intracellular ATP content was measured using the CellTiter-Glo kit from Promega (Wallisellen, Switzerland) according to the manufacturer's protocol. HepG2 cells (glucose or galactose conditions) and HepaRG cells (glucose conditions) were grown in a 96-well plate (25 000 cells per well) and exposed to different concentrations of TKI (2–100 μM) for 24 hours. The negative control was 0.1% DMSO and the positive control was 0.5% Triton-X. After treatment, medium was removed to have 50 μl remaining in each well and afterwards 50 μl of assay buffer was added to each well. After incubation in the dark for 15 minutes, the luminescence was measured using a Tecan M200 Pro Infinity plate reader. All data were normalized to control incubations containing 0.1% DMSO.

2.6 | Mitochondrial membrane potential in HepG2 cells

Mitochondrial membrane potential ($\Delta\psi_m$) in HepG2 cells kept under low glucose conditions was determined using tetramethylrhodamine methyl ester (TMRM; Invitrogen). TMRM is a cationic fluorescent probe that accumulates within mitochondria depending on their $\Delta\psi_m$. HepG2 cells were seeded in 24-well plates (200 000 cells per well) and treated with different concentrations of TKIs (2–100 μM) for 24 hours. The negative control was 0.1% DMSO and the positive control was carbonyl cyanide-4-(trifluoromethoxy)phenylhydrazone (FCCP, 9 μM). FCCP is an uncoupler of mitochondrial oxidative phosphorylation and therefore decreases $\Delta\psi_m$. FCCP was added cells and 10 minutes later, cells were washed with phosphate-buffered saline (PBS) and suspended in PBS with 100 nM TMRM. After 15 minutes incubation in the dark, cells were centrifuged and resuspended in PBS for analyzing them with flow cytometry using a FACSCalibur (BD Bioscience, Allschwil, Switzerland). FlowJo software v10.0.8 (FlowJo; LCC, Ashland, OR, USA) was used to analyze the data.

2.7 | Cellular oxygen consumption

Cellular respiration in intact cells was measured with a Seahorse XF24 analyzer (Seahorse Biosciences, North Billerica, MA, USA) as described previously (Felser et al., 2013). HepG2 cells kept under low glucose conditions were seeded in Seahorse XF 24-well culture plates at 100 000 cells per well in DMEM growth medium and allow to adhere overnight. Cells were treated with the test compounds (1–50 μM) for 24 hours. Before the experiment, the medium was replaced with 750 μl unbuffered DMEM medium (4 mM L-glutamate, 1 mM pyruvate, 1 g l^{-1} glucose, 63.3 mM sodium chloride, pH 7.4) and equilibrated at 37°C in a CO_2-free incubator for at least 1 hour. Basal oxygen consumption rate was determined in the presence of glutamate and pyruvate (4 and 1 mM, respectively). The proton leak (a marker for uncoupling) was determined after inhibition of mitochondrial ATP production by 1 μM oligomycin (inhibitor of the F_0F_1-ATPase). Afterwards, the mitochondrial electron transport chain was stimulated maximally by the addition of the uncoupler FCCP (2 μM). Finally, the extramitochondrial respiration was estimated after the addition of complex I inhibitor rotenone (1 μM). For the determination of the basal respiration, the oxidative leak, and the maximum respiration, the estimate of the extra-mitochondrial respiration was subtracted (see Supporting information Figure S1). Respiration was expressed as oxygen consumption per minute normalized to the protein content of the incubations. For that, cells were fixed by adding 100 μl of 50% (w/v) trichloroacetic acid to each well and the plate was stored at 4°C for 1 hour. Trichloroacetic acid was then removed and the plate washed three times with MilliQ water. We added 50 μl sulfurhodamine (0.4% (w/v) in 1% (v/v) acetic acid) and incubated for 20 minutes at room temperature to stain the proteins. The plate was then washed with 1% acetic acid (v/v) and the incorporated dye was solubilized with 100 mM Tris base. The absorbance was determined at 490 nm using a Tecan M200 Pro Infinity plate reader. The protein concentration was calculated based on a calibration curve with bovine serum albumin.

2.8 | Mitochondrial superoxide accumulation

Mitochondrial superoxide accumulation was measured using the MitoSOX Red fluorophore probe from Invitrogen, according to the manufacturer's instructions. The MitoSOX Red mitochondrial superoxide indicator is a fluorogenic dye for highly selective detection of superoxide in the mitochondria ofliving cells. HepG2 cells kept under low glucose conditions were seeded in 96-well plates (25 000 cells per well) and treated with test compounds (5–100 μM) for 24 hours. The negative control was 0.1% DMSO and the positive control was 50 μM amiodarone. Afterwards, 100 μl PBS with 2.5 μM MitoSOX was added to each 96-well plate. After incubation at 37°C in the dark for 10 minutes, the fluorescence was measured using a Tecan M200 Pro Infinity plate reader with an excitation at 510 nm and an emission at 580 nm. We normalized the results to the protein content using a Pierce BCA Protein Assay Kit from Thermo Fisher Scientific (Waltham, MA, USA).

2.9 | Glutathione content

Total glutathione (reduced form) (tGSH) contents were measured using a previously described enzymatic recycling method (Rahman, Kode, & Biswas, 2006). The assay is based on the oxidation of GSH by 5,5-dithio-bis(2-nitrobenzoic acid) to the yellow derivative 5-thio-2-nitrobenzoic acid. HepG2 cells kept under low glucose conditions were seeded in six-well plates (600 000 cells per well) and treated with drugs (5–100 μM) for 24 hours. The negative control was 0.1% DMSO and the positive control was 100 μM buthionine sulfoximine, a substance known to reduce the level of tGSH. At the end, the absorbance at 412 nm was measured every 30 seconds for 2 minutes with a Tecan M200 Pro Infinity plate reader. The protein content of the cell extracts was determined with the Pierce Protein Assay Kit from Thermo Fisher Scientific (Waltham, MA, USA) and the tGSH content was adjusted to protein.

2.10 | Glycolysis

The glycolytic flux was determined via the conversion of [^{3}H]-glucose to ^3H_2O as described before (Vander Heiden et al., 2001). HepG2 cells kept under low glucose conditions were seeded in six-well plates (500 000 cells per well) and treated with drugs (1–100 μM) for 24 hours. The positive control was 20 mM 2-deoxy-D-glucose. After treatment, HepG2 cells were resuspended in 1 ml Krebs buffer (115 mM sodium chloride, 2 mM potassium chloride, 25 mM sodium bicarbonate, 1 mM magnesium chloride, 2 mM calcium chloride, 0.25% FBS, pH 7.4) and incubated for 30 minutes at 37°C. After centrifugation, cell pellets were resuspended in 0.5 ml Krebs buffer containing 10 mM glucose and 0.5 μl D-^{3}H(U) glucose (60 Ci mmol^{-1}, 0.5 μCi per assay; Perkin Elmer, Schwerzenbach, Switzerland) and incubated for 1 hour at 37°C. After centrifugation, 50 μl supernatant were transferred to tubes containing 50 μl 0.2 N HCl. Tubes were transferred to scintillation vials containing 0.5 ml water and sealed. ^3H_2O was allowed to evaporate from the tube and to condense in the 0.5 ml water for 1 week. Afterwards, the tube was removed and the radioactivity of the water was measured using a Packard (Palo Alto, CA, USA) 1900 TR liquid scintillation analyzer.

2.11 | Western blotting for markers of apoptosis

HepG2 cells kept under low glucose conditions were seeded in to a six-well plate (500 000 cells per well) and treated with different concentrations of TKIs (5–50 μM) for 24 hours. The negative control was 0.1% DMSO and the positive control was 200 nM staurosporin. Afterwards, HepG2 cells were lysed with RIPA buffer (150 mM sodium chloride, 1.0% NP-40, 0.5% sodium deoxycholate, 0.1% sodium dodecyl sulfate, 50 mM Tris, pH 8.0) containing complete Mini protease inhibitor cocktail (Roche Diagnostics, Mannheim, Germany). After centrifugation, the supernatant was collected and stored at −80°C. Proteins were resolved by sodium dodecyl sulfate–polyacrylamide gel electrophoresis using commercially available 4–12% NuPAGE Bis-Tris gels (Invitrogen) and transferred using the Trans-Blot Turbo Blotting System (Bio-Rad, Cressier, Switzerland). The membranes were incubated with poly ADP ribose polymerase (PARP; 46D11) rabbit monoclonal antibody (1:1000; Cell Signaling Technology, Danvers, MA, USA), anti-active caspase-3 antibody (1:1000, ab32042; Abcam, Cambridge, UK), and Anti-pro Caspase 3 antibody (1:1000, ab32150; Abcam, Cambridge, UK) antibodies. After washing, membranes were exposed to secondary antibodies (1:2000; Santa Cruz Biotechnology, Dallas, TX, USA). Immunoblots were developed using enhanced chemiluminescence (GE Healthcare, Little Chalfont, Bucks, UK). Band intensities of the scanned images were quantified using the National Institutes of Health Image J program, v1.47.

2.12 | Annexin V/propidium iodide

To study the mechanisms of cell death, we used the fluorescein isothiocyanate Annexin V/Dead Cell Apoptosis Kit from Invitrogen according to the manufacturer's protocol. HepG2 cells kept under low glucose conditions were seeded in 24-well plates (200 000 cells per well) and treated with different concentrations of TKIs (5–50 μM) for 24 hours. The negative control was 0.1% DMSO. Positive controls were 200 nM staurosporin for apoptosis and 50 μM amiodarone for necrosis. The cells were then analyzed with a FACSCalibur (BD Bioscience) channel FL-1 and FL-3. FlowJo software v10.0.8 was used to analyze the data.

2.13 | Statistical analysis

Data are given as the mean ± standard error of the mean (SEM) of at least three experiments in triplicates. Statistical analyses were performed using GraphPad Prism 6 (GraphPad Software, La Jolla, CA, USA). For the comparison of treatment groups to the 0.1% DMSO control group, one-way ANOVA was used followed by the Dunnett's post-test procedure. The CYP induction experiments in HepaRG cells were analyzed using two-way ANOVA followed by Bonferroni's post hoc test. $P < .05$ (*) was considered to be significant.

3 | RESULTS

3.1 | Membrane toxicity and adenosine triphosphate content in HepG2 cells

Adenylate kinase release was determined as a marker of the plasma membrane integrity, and the cellular ATP content as a marker of the energy metabolism. Plasma membrane integrity and ATP content were assessed using two different media: in one medium the nutrient was 5.5 mM glucose (glucose medium) and in the other one 10 mM galactose (galactose medium). In the presence of glucose, HepG2 cells can produce ATP not only via oxidative phosphorylation, but also via glycolysis. In the presence of galactose, cells are forced to produce ATP mainly via oxidative phosphorylation (Marroquin, Hynes, Dykens, Jamieson, & Will, 2007). In the presence of galactose, mitochondrial toxicants have been reported to deplete the cellular ATP content at lower concentrations than in the presence of glucose (Kamalian et al., 2015).

The effects of the six TKIs investigated on plasma membrane integrity and on the cellular ATP content of HepG2 cells exposed for 24 hours are shown in Figures 1(A–F) and in 2(A–F), respectively. Based on the curves displayed in these figures, the corresponding EC_{50} values were calculated (Table 1). With the exception of pazopanib, which was not membrane-toxic up to 50 μM, the TKIs

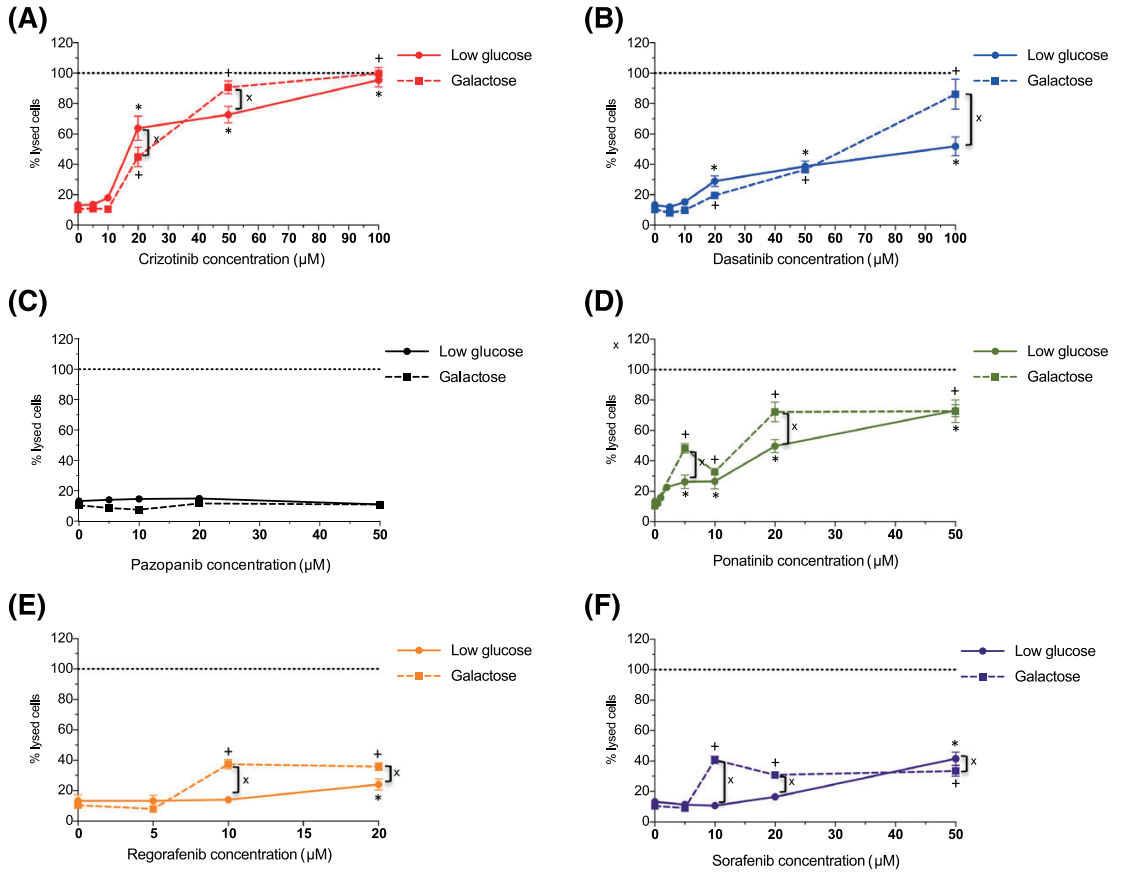

FIGURE 1 Membrane toxicity in HepG2 cells cultured in low glucose or galactose medium. Membrane toxicity was assessed by the release of adenylate kinase after exposure for 24 hours with crizotinib (A), dasatinib (B), pazopanib (C), ponatinib (D), regorafenib (E) and sorafenib (F). Data are expressed as the percentage oflysed cells with the values obtained for Triton X 0.1% set as 100%. Data represent the mean ± SEM of at least three independent experiments. * $P < .05$ vs. dimethyl sulfoxide control (glucose). $^{+}P < .05$ vs. dimethyl sulfoxide control (galactose). $^{x}P < .05$ galactose vs. glucose

TABLE 1 Quantification of membrane toxicity and ATP depletion by tyrosine kinase inhibitors in HepG2 cells

	EC_{50}-ATP (μM)		EC_{50}-MT (μM)		EC_{50}-ATP_{glu} / EC_{50}-ATP_{gal}	EC_{50}-MT_{glu} / EC_{50}-MT_{gal}
	Glucose	Galactose	Glucose	Galactose		
Crizotinib	12.2	19.9	16.9	21.7	0.61	0.78
Dasatinib	40.5	94.7	92.0	64.1	0.43	1.44
Pazopanib	>50	>50	>50	>50	ND	ND
Ponatinib	8.83	17.9	22.0	11.0	0.49	2.00
Regorafenib	>20	6.54	>20	>20	>3.06	ND
Sorafenib	16.7	5.51	>50	>50	3.04	ND

gal, galactose; glu, glucose; ND, not determinable.

We calculated the EC_{50} for the cellular decrease in the ATP content (EC_{50}-ATP; drug concentration that causes a 50% decrease in the ATP content compared to 0.1% DMSO control) and the EC_{50} for membrane toxicity (EC_{50}-MT; drug concentration that induces a 50% loss in membrane integrity compared to the positive control Triton -X) according to Swiss et al. (2013) based on the data shown in Figures 1 and 2. Ratios EC_{50}-ATP_{glu}/EC_{50}-ATP_{gal} > 2 can be considered as indicators of mitochondrial toxicity.

investigated were membrane-toxic and decreased the cellular ATP pool in a concentration-dependent fashion. As can be seen in the figures and as calculated in Table 1, regorafenib and sorafenib were generally more toxic in the presence of galactose as compared to glucose (Figures 1E,F and 2E,F). The EC_{50} regarding ATP depletion was for both drugs approximately three times lower in the presence of galactose than for glucose. Ponatonib was more membrane -toxic in the presence of galactose than for glucose (Figure 1D), ATP depletion was more accentuated in the presence of glucose (Figure 2D). Pazopanib was not membrane-toxic up to 50 μM (Figure 1C) and decreased the cellular ATP content only in the presence of galactose (Figure 2C). Crizotinib and dasatinib were both membrane -toxic and

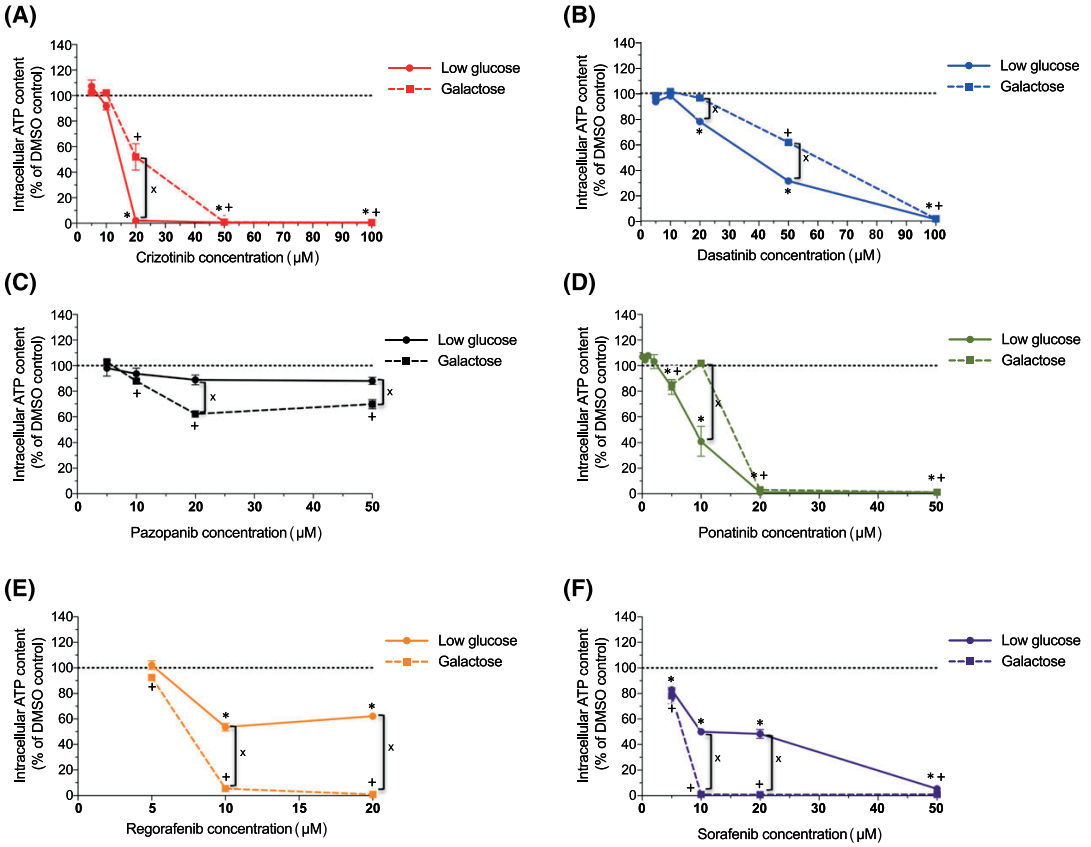

FIGURE 2 Intracellular ATP content in HepG2 cells cultured in low glucose or galactose medium. Intracellular ATP content was measured after exposure for 24 hours with crizotinib (A), dasatinib (B), pazopanib (C), ponatinib (D), regorafenib (E) and sorafenib (F). Data are expressed as decrease compared to control incubations containing 0.1% DMSO. ATP content for the control incubations was 13.4 ± 0.9 nmol mg $^{-1}$ protein (mean ± SEM, n = 4 incubations). Data represent the mean ± SEM of at least three independent experiments. * $P < .05$ vs. DMSO control (glucose). $^{+}P < .05$ vs. DMSO control (galactose). $^{x}P < .05$ galactose vs. glucose. DMSO, dimethyl sulfoxide

depleted the cellular ATP stores with a tendency for more accentuated toxicity in the presence of glucose (Figures 1A,B and 2A,B). Similar results for membrane toxicity and ATP content were obtained after exposure for 48 hours (data not shown).

A more pronounced toxicity in the presence of galactose as compared to glucose (Marroquin et al., 2007) has been proposed to reflect mitochondrial toxicity. Accordingly, regarding cellular ATP depletion, a ratio EC_{50}-ATP_{glu}/EC_{50}-ATP_{gal} > 2 can be considered as indicators of mitochondrial toxicity (Swiss, Niles, Cali, Nadanaciva, & Will, 2013). Based on the ratios shown in Table 1, we could assume mitochondrial toxicity at least for regorafenib and sorafenib, but not for crizotinib, dasatinib and pazopanib. Ponatinib showed a ratio of 2 for membrane toxicity (EC_{50}-MT_{glu}/EC_{50}-MT_{gal}) but <2 for cellular ATP depletion.

3.2 | Membrane toxicity and adenosine triphosphate content in HepaRG cells

Membrane toxicity and ATP content were also investigated in HepaRG cells (Figure 3A,B). These incubations were conducted in the glucose medium, as we wanted to assess the effect on glycolysis. After 24 hours of treatment, crizotinib and dasatinib were membrane -toxic and decreased the ATP content starting at 20 and 50 μM, respectively. Ponatinib was membrane -toxic starting at 10 μM but a decrease in ATP content was already observed at 5 μM. Regorafenib and sorafenib were membrane -toxic and decreased the ATP content starting at 5 μM. Pazopanib did not show any membrane toxicity or decrease in ATP content at the tested concentrations (up to 50 μM). CYP induction did not either affect membrane toxicity or depletion of the cellular ATP pool or reduced membrane toxicity (by approximately 40% for 5 μM regorafenib and 5 μM sorafenib) or cellular ATP depletion (by 19% to 45% for 20 μM crizotinib, 50 μM dasatinib, 5 μM regorafenib and 5 μM sorafenib). These findings indicate that the toxicity of the TKIs investigated is associated mainly with the parent compounds and less with CYP -associated metabolites. Based on these results we decided to pursue our experiment with the parent compounds using HepG2 cells, which represent a well -characterized human cell system suitable for investigating mitochondrial toxicity of drugs (Felser et al., 2013; Kamalian et al., 2015). We decided to conduct these experiments in glucose medium, as the physiological substrate is glucose and not galactose.

3.3 | Effect on mitochondrial membrane potential

To investigate the potential role of mitochondria in the observed reduction of the cellular ATP content, we first determined the effect

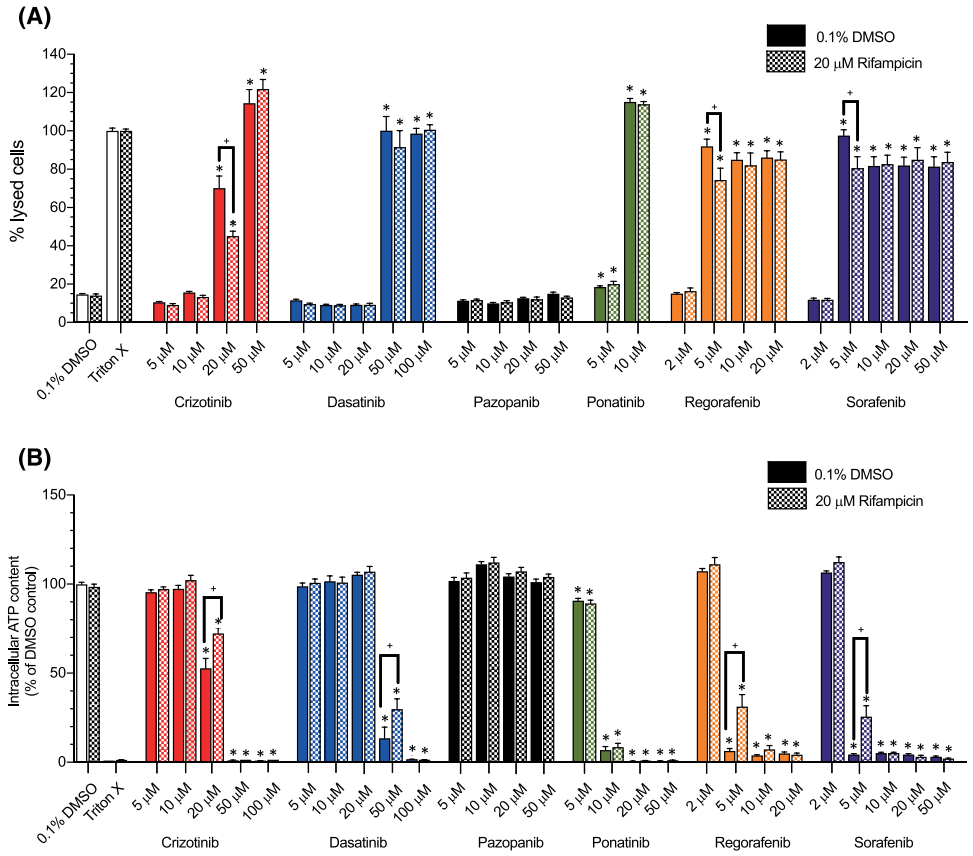

FIGURE 3 Effect of pretreatment with rifampicin on membrane toxicity and intracellular ATP content in HepaRG cells. HepaRG cells (cultured in low glucose medium) were pretreated for 72 hours with rifampicin and then exposed to drugs for 24 hours. (A) Membrane toxicity, assessed by the release of adenylate kinase. (B) Intracellular ATP content. Data are expressed as the percentage oflysed cells with the values obtained for Triton X 0.1% set as 100% or as decrease in the cellular ATP content in percentages compared to control incubations containing 0.1% DMSO. Data represent the mean ± SEM of at least three independent experiments. * $P < .05$ vs. DMSO control. $^{+}P < .05$ vs. pretreatment with rifampicin. DMSO, dimethyl sulfoxide

of TKIs on the mitochondrial membrane potential ($\Delta\psi_m$) in HepG2 cells. The mitochondrial membrane potential can be considered a marker for mitochondrial function and integrity (Kaufmann et al., 2005). We observed a dissipation in $\Delta\psi_m$ starting at 100 μM for dasatinib (Figure 4A), at 50 μM for crizotinib and ponatinib (Figure 4 A,B), and at 10 μM for regorafenib and sorafenib (Figure 4B). Pazopanib did not change the $\Delta\Psi_m$, which is consistent with the observation that it did not decrease the cellular ATP content.

3.4 | Effect on oxidative metabolism

The observed decrease in the cellular ATP content and in the mitochondrial membrane potential could be caused by inhibition and/or uncoupling of the respiratory chain (Felser et al., 2013; Kaufmann et al., 2005). Therefore, we assessed the oxygen consumption of cells treated with TKIs to study oxidative mitochondrial metabolism. Crizotinib and pazopanib did not significantly affect mitochondrial oxygen consumption (Figure 5A,C, respectively). Dasatinib increased oxygen consumption in the presence of oligomycin in a concentration -dependent way starting at 20 μM (Figure 5B), compatible with uncoupling of oxidative phosphorylation. Ponatinib reduced the basal and maximal respiration rate starting at 2 μM (Figure 5D). Regorafenib decreased the maximal and the ATP -linked respiration rate in a concentration -dependent manner and increased oxygen consumption in the presence of oligomycin starting at 2 μM (Figure 5E). Sorafenib decreased the maximal and ATP -linked respiration rate in a concentration -dependent way starting at 1 μM, and increased the oxygen consumption in the presence of oligomycin and decreased basal respiration starting at 5 μM (Figure 5F).

These results suggest inhibition of the mitochondrial electron transport chain by ponatinib, regorafenib and sorafenib, and possibly uncoupling of oxidative phosphorylation by dasatinib, regorafenib and sorafenib.

3.5 | Effect on mitochondrial reactive oxygen species accumulation, cellular glutathione and superoxide dismutase expression

Toxicants inhibiting the function of the mitochondrial electron transport chain can increase mitochondrial production of superoxide (Drose & Brandt, 2012). Accordingly, we observed an increased mitochondrial superoxide content starting at 5 μM for ponatinib (Figure 6B), at 10 μM

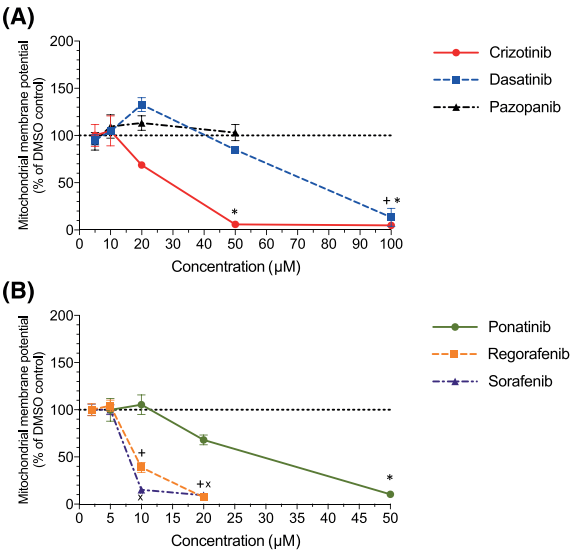

FIGURE 4 Effect on mitochondrial membrane potential. Membrane potential was assessed in HepG2 cells cultured in low glucose medium by tetramethylrhodamine methyl ester fluorescent staining after drug exposure for 24 hours. All data are expressed as percentage of control incubations containing 0.1% DMSO. Data represent the mean ± SEM of at least three independent experiments. * $P < .05$ vs. DMSO control (crizotinib, ponatinib), $^{+}P < .05$ vs. DMSO control (dasatinib, regorafenib), $^{x}P < .05$ vs. DMSO control (pazopanib, sorafenib). DMSO, dimethyl sulfoxide

for pazopanib, regorafenib and sorafenib (Figure 6A,B) and at 20 μM for crizotinib and dasatinib (Figure 6A) after 24 hours incubation. The effect on the mitochondrial superoxide content by pazopanib was clearly lower as compared to the other TKIs (Figure 6A).

Accumulating reactive oxygen species (ROS) can be degraded by the glutathione antioxidant system, which is a scavenger offree radicals (Fernandez-Checa & Kaplowitz, 2005; Schafer & Buettner, 2001). Accordingly, we observed GSH depletion starting at 10 μM for dasatinib and sorafenib (Figure 6C,D), at 20 μM for ponatinib and regorafenib (Figure 6D) and at 50 μM for crizotinib (Figure 6C). Pazopanib did not reduce total GSH content at the concentrations tested in the experiment (Figure 6C).

3.6 | Glycolysis in HepG2 cells

In the presence of glucose, HepG2 cells can produce ATP also by glycolysis. To investigate the effect of the TKIs on glycolysis, we determined the glycolytic flux via quantification of the conversion of [^{3}H]glucose to $^{3}H_2O$ (Figure 7). Glycolysis was inhibited starting at 2 μM with regorafenib, at 10 μM with sorafenib, at 50 μM with ponatinib (Figure 7B) and starting at 50 μM with dasatinib (Figure 7A). Pazopanib inhibited glycolysis at 20 μM, but not at 50 μM and crizotinib did not affect the glycolytic flux at the concentrations tested in the experiment (Figure 7A).

3.7 | Mechanisms of cell death in HepG2 cells

Impairment of mitochondrial function can be associated with cell destruction by apoptosis and/or necrosis (Green & Reed, 1998). Activation of caspase 3 is a key event in apoptosis and, together with cleavage of PARP, a reliable indicator of apoptosis (Bonifacio et al., 2016). Sorafenib and pazopanib were associated with a concentration-dependent increase in caspase 3 activation and in cleavage of PARP but without reaching statistical significance (Figures 8A,B). Crizotinib was associated with a significant increase in caspase 3 activation and PARP cleavage starting at 20 μM and dasatinib at 50 μM (Figure 8A,B). Ponatinib was associated with a strong increase in caspase 3 activation and PARP cleavage starting at 5 μM and regorafenib with caspase 3 activation starting at 5 μM.

In addition, the annexin V/propidium iodide assay was used to differentiate between apoptosis and necrosis (Figure 8C). Crizotinib induced apoptosis starting at 10 μM and dasatinib and pazopanib starting at 20 μM. Ponatinib and regorafenib showed apoptosis starting at 5 μM. Sorafenib caused apoptosis starting at 5 μM and necrosis starting at 10 μM.

4 | DISCUSSION

We investigated hepatocellular toxicity of six TKIs, which have been reported to cause liver injury in patients. In HepG2 cells, regorafenib and sorafenib strongly inhibited mitochondrial oxidative metabolism and glycolysis, and induced apoptosis and/or necrosis of HepG2 cells. Ponatinib inhibited mitochondrial oxidative metabolism as potently as regorafenib but only weakly glycolysis and induced apoptosis of HepG2 cells. Crizotinib and dasatinib did not affect mitochondrial respiration and only weakly glycolysis but induced apoptosis of HepG2 cells. Pazopanib did not affect mitochondrial respiration, inhibited glycolysis only weakly and was not cytotoxic.

Regorafenib and sorafenib were overall the most potent mitochondrial toxicants of the compounds investigated, which is in agreement with the recent study of Zhang et al. (2017). Both compounds were membrane-toxic and decreased the cellular ATP content at clearly lower concentrations in the presence of galactose than with glucose. This has been proposed to be an important marker for mitochondrial toxicity (Kamalian et al., 2015; Marroquin et al., 2007). Interestingly, ponatinib inhibited mitochondrial respiration as potently as regorafenib, but depleted the cellular ATP content less potently under galactose than under glucose conditions. On the other hand, also crizotinib, dasatinib and pazopanib depleted the cellular ATP content less potently under galactose than under glucose conditions, but did not significantly affect mitochondrial respiration. These results suggest that more potent ATP depletion under galactose than under glucose conditions is a good parameter for confirming mitochondrial toxicity of a compound, but may be less well suited for excluding mitochondrial toxicity. This is an important point that should be studied with a larger set of well characterized compounds. If true, it would lower the value of the cellular ATP pool under galactose and glucose conditions as a screening tool for mitochondrial toxicity.

In agreement with increased toxicity in the presence of galactose compared to glucose, regorafenib and sorafenib inhibited oxygen consumption of HepG2 cells in the presence of glutamate/pyruvate and after the addition of the uncoupler FCCP, compatible with a decreased function of enzyme complexes I, III and/or IV of the electron transport

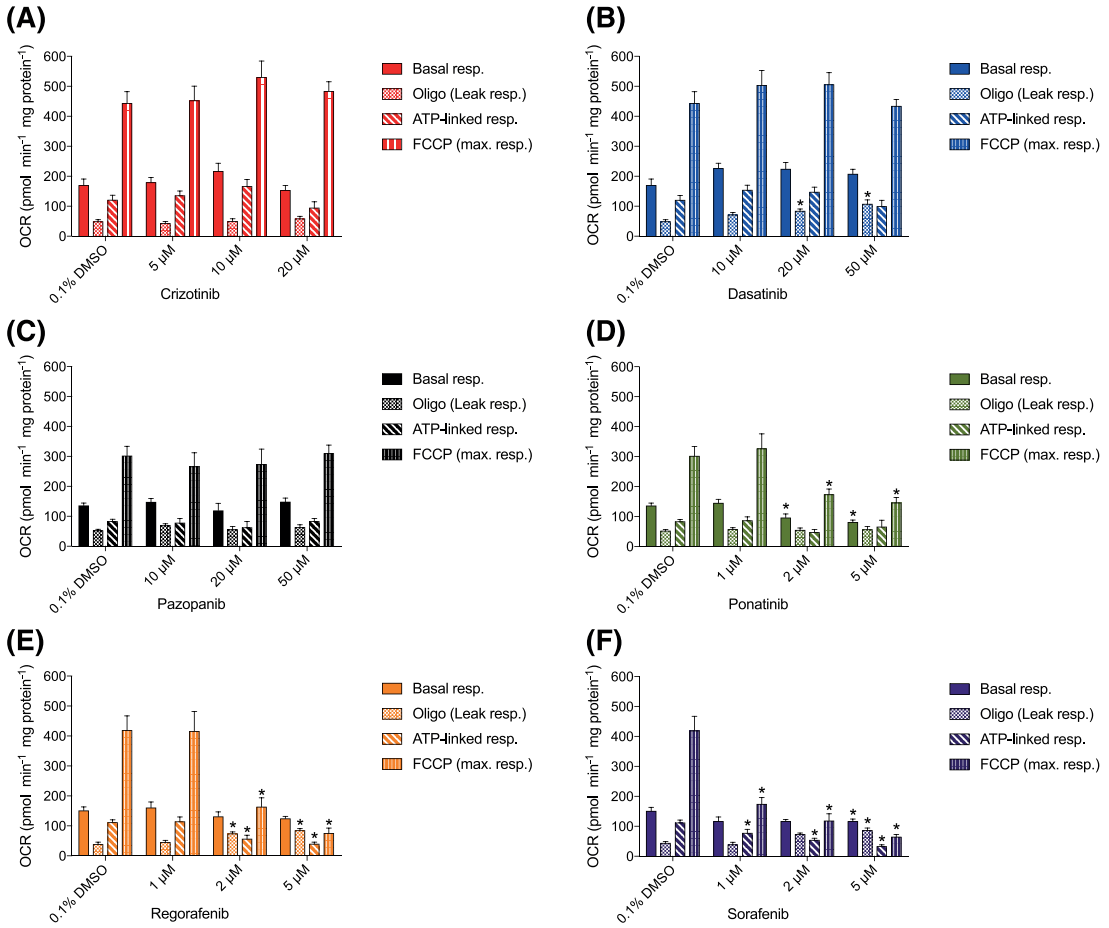

FIGURE 5 Mitochondrial respiration in HepG2 cells. HepG2 cells were cultured in low glucose medium. Basal, leak, ATP -linked and maximal respiration after exposure to crizotinib (A), dasatinib (B), pazopanib (C), ponatinib (D), regorafenib (E) and sorafenib (F) for 24 hours. Data represent the mean ± SEM of at least three independent experiments. * $P < .05$ vs. DMSO control. DMSO, dimethyl sulfoxide; FCCP, carbonyl cyanide-4-(trifluoromethoxy)phenylhydrazone; OCR, oxygen consumption rate; resp., respiration

chain. As the difference in basal respiration to oligomycin respiration was reduced in the presence of TKIs compared to control incubations, they possibly also uncoupled oxidative phosphorylation. Consequently, they were associated with a decrease in mitochondrial membrane potential, an increase in the mitochondrial ROS and a decrease in the cellular GSH content. The effects on mitochondria were all detectable at concentrations starting between 1 and 10 µM (Table 2), with inhibition of the electron transport chain starting at 1 −2 µM. The initial events appear therefore to be inhibition of the electron transport chain and uncoupling of oxidative phosphorylation, which are followed by a drop in the mitochondrial membrane potential, increased mitochondrial production of ROS (associated with inhibition of enzyme complexes I and/or III of the electron transport chain; Balaban, Nemoto, & Finkel, 2005), and a drop in the cellular GSH content. A consequence of these events is the opening of the mitochondrial permeability transition pore with the release of cytochrome c from the intermembrane space into the cytosol, which activates the apoptosis pathway. In the current study, we showed cleavage of caspase 3 and/or PARP, which are distal events in the apoptosis pathway, for all compounds except pazopanib and sorafenib and stimulation of apoptosis for all compounds investigated (Figure 8). Sorafenib and regorafenib inhibited also glycolysis at low concentrations (Table 2). This dual inhibition of ATP synthesis, mitochondrial toxicity and inhibition of glycolysis, is a likely explanation for the strong effect on the ATP pool in HepG2 cells by these two compounds.

For sorafenib, it was already known that it could induce ROS accumulation and GSH depletion in HepG2 cells (Chiou et al., 2009). The reason for the increased mitochondrial ROS concentrations was so far not known. The current study suggests that the increased ROS concentrations are associated with impairment of the activity of the mitochondrial electron transport chain (Balaban et al., 2005). Zhang et al. reported inhibition of mitochondrial respiration in the presence of succinate, inhibition of complex V and uncoupling of oxidative phosphorylation (Zhang et al., 2017), which is in agreement with our findings. In clinical studies, sorafenib reached maximal concentrations of approximately 6.5 µM (Herbrink et al., 2016), which is in the range where we started to observe mitochondrial toxicity. As liver concentrations may even be higher for TKIs than plasma concentrations (He et al., 2008; Lau et al., 2015; Spector et al., 2015), patients treated with sorafenib may be at risk for liver injury.

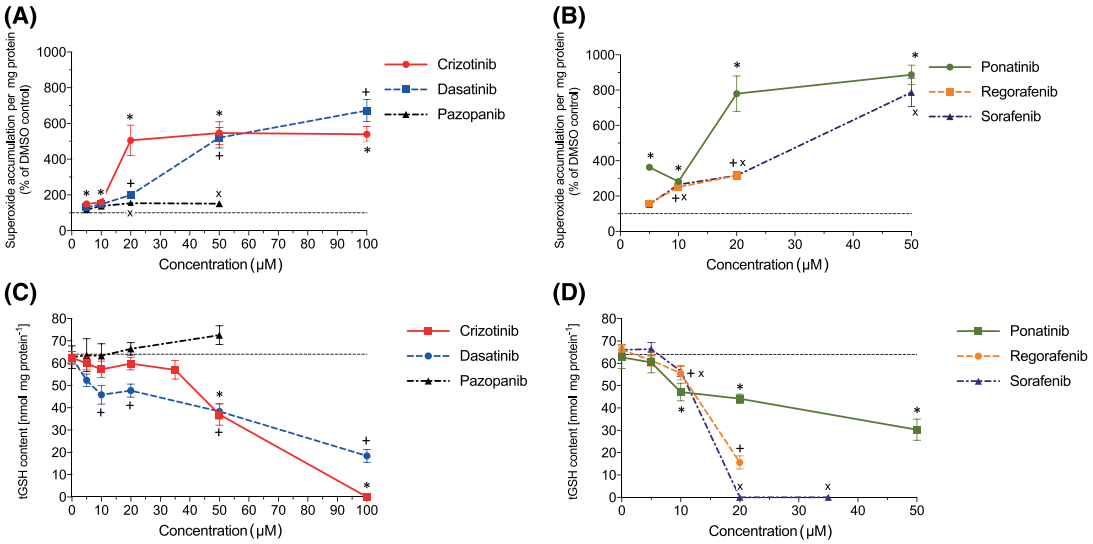

FIGURE 6 Mitochondrial reactive oxygen species concentration and cellular GSH content. (A,B) Mitochondrial reactive oxygen species concentration in HepG2 cells cultured in low glucose medium after drug exposure for 24 hours. (C, D) tGSH content in HepG2 cells with low glucose medium after drug exposure for 24 hours. All data are expressed as fold change to control incubations containing 0.1% DMSO. Data represent the mean ± SEM of at least three independent experiments. * $P < .05$ vs. DMSO control (crizotinib, ponatinib), $^{+}P < .05$ vs. DMSO control (dasatinib, regorafenib), $^{x}P < .05$ vs. DMSO control (pazopanib, sorafenib). DMSO, dimethyl sulfoxide; tGSH, total glutathione

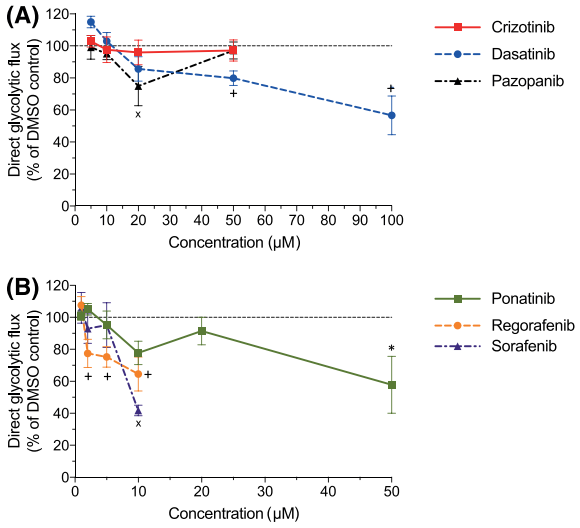

FIGURE 7 Glycolysis in HepG2 cells cultured in low glucose medium after drug exposure for 24 hours. All data are expressed as percentage of control incubations containing 0.1% DMSO. Rate of glycolysis for the control incubations was 24.5 ± 1.7 nmol h^{-1} 10^{-6} cells (mean ± SEM, n = 35 control incubations). Data represent the mean ± SEM of at least three independent experiments. * $P < .05$ vs. DMSO control (crizotinib, ponatinib), $^{+}P < .05$ vs. DMSO control (dasatinib, regorafenib), $^{x}P < .05$ vs. DMSO control (pazopanib, sorafenib). DMSO, dimethyl sulfoxide

Regarding regorafenib, toxic effects have been described in isolated rat liver mitochondria and in primary rat hepatocytes. In these studies, regorafenib inhibited mitochondrial respiration in the presence of malate/glutamate, uncoupled oxidative phosphorylation ofisolated mitochondria and induced mitochondrial swelling by mitochondrial permeability transition (Weng et al., 2015; Zhang et al., 2017). In primary rat hepatocytes, regorafenib uncoupled oxidative phosphorylation, reduced the mitochondrial membrane potential, decreased the cellular ATP and induced necrosis at concentrations between 2.5 and 15 μM (Weng et al., 2015). These data are in close agreement with the findings obtained by us, with the exception that we observed apoptosis and not necrosis. This difference may be related to the different models used. As apoptosis is dependent on ATP (Green & Reed, 1998), it is possible that the cellular ATP content dropped more rapidly in primary rat hepatocytes than in the HepG2 cells used by us.

In clinical studies, regorafenib reached plasma concentrations in the range of 5 μM after a single oral therapeutic dose and approximately 10 μM under steady-state conditions (Shirley & Keating, 2015). These are the concentrations where we started to observe hepatocellular toxicity. Similar to sorafenib, patients treated with regorafenib may be at risk for liver injury. Taking into account that CYP3A4 is the most important CYP for the metabolism of TKIs (Table 2) and that hepatocellular toxicity of TKIs was concentration -dependent, patients treated with sorafenib or regorafenib that have a low CYP3A4 activity, e.g., due to co -medication with CYP3A4 inhibitors (Teo et al., 2015), may be at increased risk for hepatotoxicity. In addition, regarding the mitochondrial toxicity of sorafenib and regorafenib, patients with pre -existing mitochondrial dysfunction may also be at an increased risk for toxicity. This has, for instance, been described for valproate (Krahenbuhl, Brandner, Kleinle, Liechti, & Straumann, 2000), in whom an impaired activity of the mitochondrial DNA polymerase gamma (POLG) is a risk factor for liver failure (Stewart et al., 2010).

Ponatinib depleted the cellular ATP stores at lower concentrations in the presence of glucose than galactose, but was membrane -toxic at lower concentrations in the presence of galactose compared to

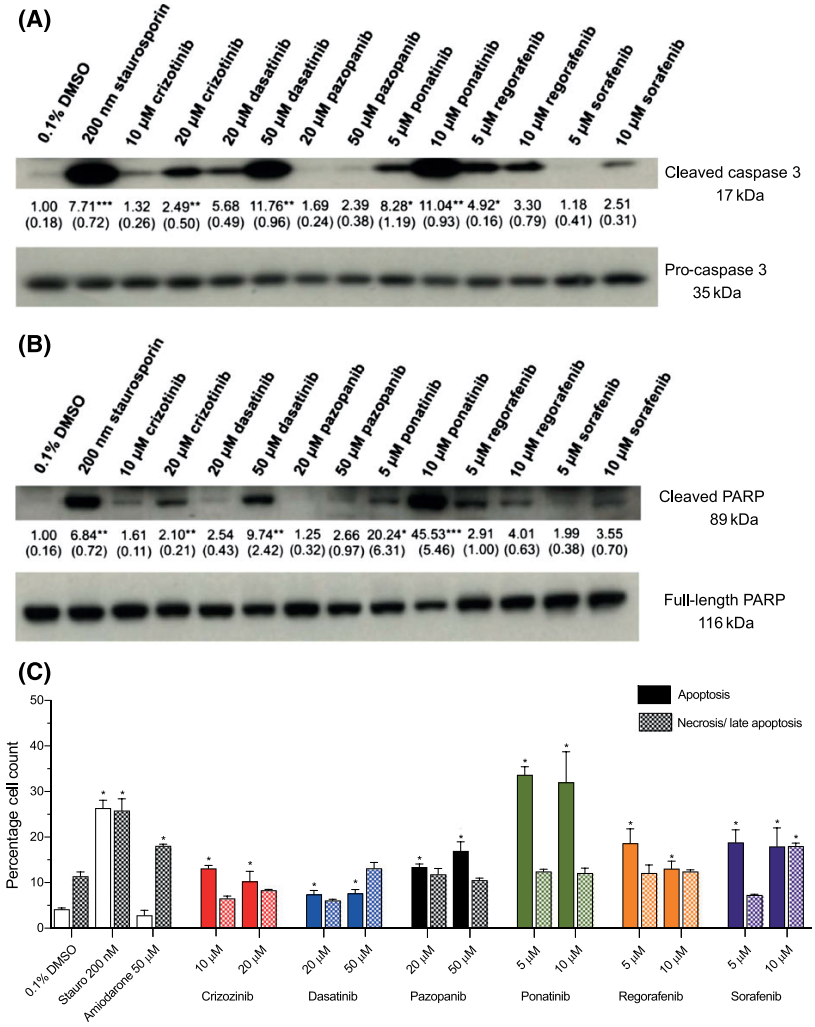

FIGURE 8 Assessment of apoptosis in HepG2 cells with low glucose medium. (A) Western blot analysis of the expression of active (cleaved) to pro-caspase 3. (B) Western blot analysis of the expression offull length to cleaved PARP. (C) Apoptosis and necrosis in HepG2 cells after drug exposure for 24 hours assessed by annexin V/propidium iodide. All data are expressed as fold change to control incubations containing 0.1% DMSO. Data represent the mean ± SEM of at least three independent experiments. * $P < .05$ vs. DMSO control. DMSO, dimethyl sulfoxide; PARP, poly ADP ribose polymerase

glucose (Table 1). Inhibition of glycolysis occurred at clearly higher concentrations (starting at 50 µM) than ATP depletion and may therefore not be relevant for hepatic toxicity of this compound. In the current study, ponatinib impaired mitochondrial oxidative metabolism starting at 2 µM. This finding contrasts with the report of Zhang et al. (2017), who found no mitochondrial toxicity in isolated rat liver mitochondria. This discrepancy may be explained by the species difference (human vs. rat) and/or by the different mitochondrial preparations (permeabilized cells vs. isolated mitochondria). Typical plasma steady -state concentrations reached with ponatinib are around 0.1 µM (Huynh et al., 2017), which is approximately 20 times lower than the lowest concentration associated with inhibition of mitochondrial respiration in HepG2 cells. Taking into account the findings in animals that the concentration of TKIs in the liver can be 10 –20 times higher than in blood (He et al., 2008), it appears nevertheless possible that toxic concentrations can be reached in livers of certain patients.

For crizotinib and desatinib, membrane toxicity and ATP depletion were not accentuated when glucose was replaced by galactose, suggesting primarily a non-mitochondrial mechanism of toxicity. Both compounds started to induce apoptosis at concentrations in the range 10–20 µM, which, based on our data, was probably not associated with a mitochondrial mechanism. Typical plasma steady -state concentrations reached are 1.9 µM for crizotinib (Kurata et al., 2015) and 0.2 µM for dasatinib (Huynh et al., 2017), which is clearly below the concentrations where we started to observe cytotoxicity. This suggests a non-mitochondrial mechanism of hepatotoxicity for these compounds.

Pazopanib was not associated with relevant membrane toxicity or ATP depletion and did not impair mitochondrial respiration in HepG2 cells up to 50 µM, suggesting a non-mitochondrial mechanism of hepatotoxicity. It has to be taken into account, however, that very high exposures can be reached with this compound in humans

TABLE 2 Pharmacokinetic and toxicity data of the six tyrosine kinase inhibitors investigated. Plasma concentrations were obtained from the literature (Abou-Alfa et al., 2006; Herbrink et al., 2016; Huynh et al., 2017; Kurata et al., 2015; Sunakawa et al., 2014) and are typical concentrations (C_{max}) obtained at steady state. Ranges indicate trough and C_{max} plasma concentrations at steady state. Pharmacokinetic data were obtained from the database of the Swiss drug authority Swissmedic (http://www.swissmedicinfo.ch/). Concentrations provided for the toxicological measurements represent the lowest concentrations at which toxicity was observed in the current study

	Crizotinib	Dasatinib	Pazopanib	Ponatinib	Regorafenib	Sorafenib
Steady-state concentration (μM)	1.2	0.05–0.15	93	0.08	2.5	5.0–10.6
Typical daily dose (mg)	500	100	800	45	160	800
V_d steady state (l)	1800	2500	NA	1000	NA	NA
Half-life (h)	42	6	31	24	30	48
Hepatic metabolism	CYP3A4/A5	CYP3A4	CYP3A4	CYP3A4	CYP3A4	CYP3A4
Membrane toxicity (glucose) (μM)	20	20	>50	5	20	50
Membrane toxicity (galactose) (μM)	20	20	>50	5	10	10
ATP depletion (glucose) (μM)	20	20	>50	5	10	5
ATP depletion (glucose) (μM)	20	50	10	5	5	5
Mitochondrial membrane potential (μM)	50	100	>50	50	10	10
Maximal oxygen consumption (μM)	>20	>50	>50	2	2	1
ROS accumulation (μM)	20	20	5	5	10	10
GSH depletion (μM)	50	10	>50	10	10	10
Inhibition of glycolysis (μM)	>50	50	20	50	2.5	10
Annexin V-positive cells (μM)	10	20	20	5	5	5
Propidium iodide-positive cells (μM)	>20	>50	>50	>10	>10	10

GSH, glutathione; NA, not applicable; ROS, reactive oxygen species.

(maximal plasma concentrations up to 100 μM; Herbrink et al., 2016), for which reason exposure-dependent toxicity cannot be completely excluded.

As reported in a review article (Shah et al., 2013) and in a meta-analysis (Teo et al., 2013), all TKIs investigated in the current study are associated with liver injury, which is asymptomatic in most patients. Liver failure is rare, but most case reports can be found for regorafenib and sorafenib, the most accentuated mitochondrial toxicants and inhibitors of glycolysis in the current study. It is possible that the accentuated ATP depletion observed in vitro with these drugs is also clinically relevant in susceptible patients. We did not find a clear relationship between the dominant TK inhibited and hepatocellular toxicity of the compounds tested. Although regorafenib and sorafenib, the most toxic of the TKIs investigated, are both vascular endothelial growth factor-specific multi-kinase inhibitors, this is also the case for pazopanib, which was almost not toxic. We therefore postulate off-target effects unrelated to the pharmacological activity of the drugs investigated.

Mitochondrial toxicity associated with TKIs is not limited to the liver, but can affect also other organs. For instance, different TKIs have been shown to be toxic on isolated rat heart mitochondria (Will et al., 2008) and mitochondrial toxicity was observed in humans and mice treated with imatinib (Kerkela et al., 2006). Many of the toxicities observed in patients treated with these drugs may therefore result from mitochondrial dysfunction.

In conclusion, regorafenib and sorafenib were strong mitochondrial toxicants at concentrations that can be reached in the plasma and liver of patients treated with these drugs. In addition, they also inhibited glycolysis, which may enhance their hepatotoxicity. Ponatinib impaired mitochondrial functions and glycolysis at higher concentrations than reached in plasma in patients but such concentrations may be reached in the liver. In comparison, crizotinib, dasatinib and pazotinib showed no relevant mitochondrial toxicity or inhibition of glycolysis in the concentration range investigated. For these drugs, so far undefined, non-mitochondrial mechanisms have to be postulated.

FINANCIAL SUPPORT

The study was supported by a grant from the Swiss National Science foundation to SK (SNF 31003A_156270).

CONFLICT OF INTEREST

The authors did not report any conflict ofinterest.

ORCID

Stephan Krähenbühl http://orcid.org/0000-0001-8347-4145

REFERENCES

Abou-Alfa, G. K., Schwartz, L., Ricci, S., Amadori, D., Santoro, A., Figer, A., … Saltz, L. B. (2006). Phase II study of sorafenib in patients with advanced hepatocellular carcinoma. Journal of Clinical Oncology 24, 4293–4300. https://doi.org/10.1200/jco.2005.01.3441

Akamine, T., Ando, K., Oki, E., Saeki, H., Nakashima, Y., Imamura, Y. U., … Maehara, Y. (2015). Acute liver failure due to regorafenib may be caused by impaired liver blood flow: A case report. Anticancer Research, 35, 4037–4041.

Balaban, R. S., Nemoto, S., & Finkel, T. (2005). Mitochondria, oxidants, and aging. Cell, 120, 483–495. https://doi.org/10.1016/j.cell.2005.02.001

Berger, B., Donzelli, M., Maseneni, S., Boess, F., Roth, A., Krahenbuhl, S., & Haschke, M. (2016). Comparison ofliver cell models using the Basel phenotyping cocktail. Frontiers in Pharmacology 7, 443. https://doi.org/10.3389

Bible, K. C., Suman, V. J., Molina, J. R., Smallridge, R. C., Maples, W. J., Menefee, M. E., …Erlichman, C. (2014). A multicenter phase 2 trial of pazopanib in metastatic and progressive medullary thyroid carcinoma:

MC057H. Journal of Clinical Endocrinology and Metabolism, 99, 1687–1693. https://doi.org/10.1210/jc.2013-3713

Bonifacio, A., Mullen, P. J., Mityko, I. S., Navegantes, L. C., Bouitbir, J., & Krahenbuhl, S. (2016). Simvastatin induces mitochondrial dysfunction and increased atrogin-1 expression in H9c2 cardiomyocytes and mice in vivo. Archives of Toxicology, 90, 203–215. https://doi.org/10.1007/s00204-014-1378-4

Brandi, G., De Lorenzo, S., Di Girolamo, S., Bellentani, S., Saccoccio, G., & Biasco, G. (2015). Fulminant hepatitis in a patient with hepatocellular carcinoma related to nonalcoholic steatohepatitis treated with sorafenib. Tumori, 101, e46–e48. https://doi.org/10.5301/je.5000247

Breccia, M., & Alimena, G. (2013). Occurrence and current management of side effects in chronic myeloid leukemia patients treated frontline with tyrosine kinase inhibitors. Leukemia Research, 37, 713–720. https://doi.org/10.1016/j.leukres.2013.01.021

Camidge, D. R., Bang, Y. J., Kwak, E. L., Iafrate, A. J., Varella-Garcia, M., Fox, S. B., …Shaw, A. T. (2012). Activity and safety of crizotinib in patients with ALK-positive non-small-cell lung cancer: Updated results from a phase 1 study. Lancet Oncology, 13, 1011–1019. https://doi.org/10.1016/s1470-2045(12)70344-3

Chiou, J. F., Tai, C. J., Wang, Y. H., Liu, T. Z., Jen, Y. M., & Shiau, C. Y. (2009). Sorafenib induces preferential apoptotic killing of a drug- and radio-resistant Hep G2 cells through a mitochondria-dependent oxidative stress mechanism. Cancer Biology & Therapy, 8, 1904–1913.

Cohen, M. H., Johnson, J. R., & Pazdur, R. (2005). U.S. Food and Drug Administration drug approval summary: Conversion ofimatinib mesylate (STI571; Gleevec) tablets from accelerated approval to full approval. Clinical Cancer Research, 11, 12–19.

Cortes, J. E., Kim, D. W., Pinilla-Ibarz, J., le Coutre, P., Paquette, R., Chuah, C., …Kantarjian, H. (2013). A phase 2 trial of ponatinib in Philadelphia chromosome-positive leukemias. New England Journal of Medicine, 369, 1783–1796. https://doi.org/10.1056/NEJMoa1306494

Drose, S., & Brandt, U. (2012). Molecular mechanisms of superoxide production by the mitochondrial respiratory chain. Advances in Experimental Medicine and Biology, 748, 145–169. https://doi.org/10.1007/978-1-4614-3573-0_6

Fairfax, B. P., Pratap, S., Roberts, I. S., Collier, J., Kaplan, R., Meade, A. M., … Protheroe, A. (2012). Fatal case of sorafenib-associated idiosyncratic hepatotoxicity in the adjuvant treatment of a patient with renal cell carcinoma. BMC Cancer, 12, 590. https://doi.org/10.1186/1471-2407-12-590

Felser, A., Blum, K., Lindinger, P. W., Bouitbir, J., & Krahenbuhl, S. (2013). Mechanisms of hepatocellular toxicity associated with dronedarone—A comparison to amiodarone. Toxicological Sciences, 131, 480–490. https://doi.org/10.1093/toxsci/kfs298

Fernandez-Checa, J. C., & Kaplowitz, N. (2005). Hepatic mitochondrial glutathione: Transport and role in disease and toxicity. Toxicology and Applied Pharmacology 204, 263–273. https://doi.org/10.1016/j.taap.2004.10.001

van Geel, R. M., Hendrikx, J. J., Vahl, J. E., van Leerdam, M. E., van den Broek, D., Huitema, A. D., …Burgers, S. A. (2016). Crizotinib-induced fatal fulminant liver failure. Lung Cancer (Amsterdam, Netherlands), 93, 17–19. https://doi.org/10.1016/j.lungcan.2015.12.010

Green, D. R., & Reed, J. C. (1998). Mitochondria and apoptosis. Science, 281, 1309–1312.

Gripon, P., Rumin, S., Urban, S., Le Seyec, J., Glaise, D., Cannie, I., …Guguen-Guillouzo, C. (2002). Infection of a human hepatoma cell line by hepatitis B virus. Proceedings of the National Academy of Sciences of the United States of America, 99, 15655–15660. https://doi.org/10.1073/pnas.232137699

Han, D., Dara, L., Win, S., Than, T. A., Yuan, L., Abbasi, S. Q., …Kaplowitz, N. (2013). Regulation of drug-induced liver injury by signal transduction pathways: Critical role of mitochondria. Trends in Pharmacological Sciences, 34, 243–253. https://doi.org/10.1016/j.tips.2013.01.009

He, K., Lago, M. W., Iyer, R. A., Shyu, W. C., Humphreys, W. G., & Christopher, L. J. (2008). Lacteal secretion, fetal and maternal tissue distribution of dasatinib in rats. Drug Metabolism and Disposition, 36, 2564–2570. https://doi.org/10.1124/dmd.108.022764

Herbrink, M., de Vries, N., Rosing, H., Huitema, A. D., Nuijen, B., Schellens, J. H., & Beijnen, J. H. (2016). Quantification of 11 therapeutic kinase inhibitors in human plasma for therapeutic drug monitoring using liquid chromatography coupled with tandem mass spectrometry. Therapeutic Drug Monitoring, 38, 649–656. https://doi.org/10.1097/ftd.0000000000000349

Huynh, H. H., Pressiat, C., Sauvageon, H., Madelaine, I., Maslanka, P., Lebbe, C., …Mourah, S. (2017). Development and validation of a simultaneous quantification method of 14 tyrosine kinase inhibitors in human plasma using LC-MS/MS. Therapeutic Drug Monitoring, 39, 43–54. https://doi.org/10.1097/ftd.0000000000000357

Josephs, D. H., Fisher, D. S., Spicer, J., & Flanagan, R. J. (2013). Clinical pharmacokinetics of tyrosine kinase inhibitors: Implications for therapeutic drug monitoring. Therapeutic Drug Monitoring, 35, 562–587. https://doi.org/10.1097/FTD.0b013e318292b931

Kamalian, L., Chadwick, A. E., Bayliss, M., French, N. S., Monshouwer, M., Snoeys, J., & Park, B. K. (2015). The utility of HepG2 cells to identify direct mitochondrial dysfunction in the absence of cell death. Toxicology In Vitro, 29, 732–740. https://doi.org/10.1016/j.tiv.2015.02.011

Kaufmann, P., Torok, M., Hanni, A., Roberts, P., Gasser, R., & Krahenbuhl, S. (2005). Mechanisms of benzarone and benzbromarone-induced hepatic toxicity. Hepatology, 41, 925–935. https://doi.org/10.1002/hep.20634

Kerkela, R., Grazette, L., Yacobi, R., Iliescu, C., Patten, R., Beahm, C., … Force, T. (2006). Cardiotoxicity of the cancer therapeutic agent imatinib mesylate. Nature Medicine, 12, 908–916. https://doi.org/10.1038/nm1446

Klempner, S. J., Choueiri, T. K., Yee, E., Doyle, L. A., Schuppan, D., & Atkins, M. B. (2012). Severe pazopanib-induced hepatotoxicity: Clinical and histologic course in two patients. Journal of Clinical Oncology, 30, e264–e268. https://doi.org/10.1200/JCO.2011.41.0332

Krahenbuhl, S., Brandner, S., Kleinle, S., Liechti, S., & Straumann, D. (2000). Mitochondrial diseases represent a risk factor for valproate-induced fulminant liver failure. Liver, 20, 346–348.

Krause, D. S., & Van Etten, R. A. (2005). Tyrosine kinases as targets for cancer therapy. New England Journal of Medicine, 353, 172–187. https://doi.org/10.1056/NEJMra044389

Kurata, Y., Miyauchi, N., Suno, M., Ito, T., Sendo, T., & Kiura, K. (2015). Correlation of plasma crizotinib trough concentration with adverse events in patients with anaplastic lymphoma kinase positive non-small-cell lung cancer. Journal of Pharmaceutical Health Care and Sciences, 1, 8. https://doi.org/10.1186/s40780-014-0008-x

Lau, C. L., Chan, S. T., Selvaratanam, M., Khoo, H. W., Lim, A. Y., Modamio, P., …Segarra, I. (2015). Sunitinib-ibuprofen drug interaction affects the pharmacokinetics and tissue distribution of sunitinib to brain, liver, and kidney in male and female mice differently. Fundamental & Clinical Pharmacology, 29, 404–416. https://doi.org/10.1111/fcp.12126

Levitzki, A., & Gazit, A. (1995). Tyrosine kinase inhibition: An approach to drug development. Science, 267, 1782–1788.

Di Lorenzo, G., Carteni, G., Autorino, R., Bruni, G., Tudini, M., Rizzo, M., … De Placido, S. (2009). Phase II study of sorafenib in patients with sunitinib-refractory metastatic renal cell cancer. Journal of Clinical Oncology, 27, 4469–4474. https://doi.org/10.1200/jco.2009.22.6480

Marroquin, L. D., Hynes, J., Dykens, J. A., Jamieson, J. D., & Will, Y. (2007). Circumventing the Crabtree effect: Replacing media glucose with galactose increases susceptibility of HepG2 cells to mitochondrial toxicants. Toxicological Sciences, 97, 539–547. https://doi.org/10.1093/toxsci/kfm052

Murad, W., Rabinowitz, I., & Lee, F. C. (2014). Sorafenib-induced grade four hepatotoxicity in a patient with recurrent gastrointestinal stromal tumor (GIST): A case report and review ofliterature. ACG Case Reports Journal, 1, 115–117. https://doi.org/10.14309/crj.2014.19

Paech, F., Bouitbir, J., & Krahenbuhl, S. (2017). Hepatocellular toxicity associated with tyrosine kinase inhibitors: Mitochondrial damage and

inhibition of glycolysis. Frontiers in Pharmacology, 8, 367. https://doi.org/10.3389/fphar.2017.00367

Price, K. E., Saleem, N., Lee, G., & Steinberg, M. (2013). Potential of ponatinib to treat chronic myeloid leukemia and acute lymphoblastic leukemia. OncoTargets and Therapy, 6, 1111–1118. https://doi.org/10.2147/OTT.S36980

Rahman, I., Kode, A., & Biswas, S. K. (2006). Assay for quantitative determination of glutathione and glutathione disulfide levels using enzymatic recycling method. Nature Protocols, 1, 3159–3165. https://doi.org/10.1038/nprot.2006.378

Raissouni, S., Quraishi, Z., Al-Ghamdi, M., Monzon, J., Tang, P., & Vickers, M. M. (2015). Acute liver failure and seizures as a consequence of regorafenib exposure in advanced rectal cancer. BMC Research Notes, 8, 538. https://doi.org/10.1186/s13104-015-1502-4

Rao, J., Feng, M., Qian, X., Li, G., Wang, X., Zhang, F., & Lu, L. (2013). Liver transplantation treating the patient with hepatic failure associated with sorafenib treatment: Report of a case. Hepato-Gastroenterology, 60, 1317–1319. https://doi.org/10.5754/hge13185

Sacre, A., Lanthier, N., Dano, H., Aydin, S., Leggenhager, D., Weber, A., … Van den Eynde, M. (2016). Regorafenib induced severe toxic hepatitis: Characterization and discussion. Liver International, 36, 1590–1594. https://doi.org/10.1111/liv.13217

Sato, Y., Fujimoto, D., Shibata, Y., Seo, R., Suginoshita, Y., Imai, Y., & Tomii, K. (2014). Fulminant hepatitis following crizotinib administration for ALK-positive non-small-cell lung carcinoma. Japanese Journal of Clinical Oncology, 44, 872–875. https://doi.org/10.1093/jjco/hyu086

Schafer, F. Q., & Buettner, G. R. (2001). Redox environment of the cell as viewed through the redox state of the glutathione disulfide/glutathione couple. Free Radical Biology & Medicine, 30, 1191–1212.

Shah, R. R., Morganroth, J., & Shah, D. R. (2013). Hepatotoxicity of tyrosine kinase inhibitors: Clinical and regulatory perspectives. Drug Safety, 36, 491–503. https://doi.org/10.1007/s40264-013-0048-4

Shchemelinin, I., Sefc, L., & Necas, E. (2006). Protein kinases, their function and implication in cancer and other diseases. Folia Biologica (Praha), 52, 81–100.

Shirley, M., & Keating, G. M. (2015). Regorafenib: A review ofits use in patients with advanced gastrointestinal stromal tumours. Drugs, 75, 1009–1017. https://doi.org/10.1007/s40265-015-0406-x

Spector, N. L., Robertson, F. C., Bacus, S., Blackwell, K., Smith, D. A., Glenn, K., …Koch, K. M. (2015). Lapatinib plasma and tumor concentrations and effects on HER receptor phosphorylation in tumor. PLoS One, 10, e0142845. https://doi.org/10.1371/journal.pone.0142845

Stewart, J. D., Horvath, R., Baruffini, E., Ferrero, I., Bulst, S., Watkins, P. B., …Chinnery, P. F. (2010). Polymerase gamma gene POLG determines the risk of sodium valproate-induced liver toxicity. Hepatology, 52, 1791–1796. https://doi.org/10.1002/hep.23891

Sunakawa, Y., Furuse, J., Okusaka, T., Ikeda, M., Nagashima, F., Ueno, H., … Sasaki, Y. (2014). Regorafenib in Japanese patients with solid tumors: Phase I study of safety, efficacy, and pharmacokinetics. Investigational New Drugs, 32, 104–112. https://doi.org/10.1007/s10637-013-9953-8

Swiss, R., Niles, A., Cali, J. J., Nadanaciva, S., & Will, Y. (2013). Validation of a HTS-amenable assay to detect drug-induced mitochondrial toxicity in the absence and presence of cell death. Toxicology In Vitro, 27, 1789–1797. https://doi.org/10.1016/j.tiv.2013.05.007

Teo, Y. L., Ho, H. K., & Chan, A. (2013). Risk of tyrosine kinase inhibitors-induced hepatotoxicity in cancer patients: A meta-analysis. Cancer Treatment Reviews, 39, 199–206. https://doi.org/10.1016/j.ctrv.2012.09.004

Teo, Y. L., Ho, H. K., & Chan, A. (2015a). Formation of reactive metabolites and management of tyrosine kinase inhibitor-induced hepatotoxicity: A literature review. Expert Opinion on Drug Metabolism & Toxicology, 11, 231–242. https://doi.org/10.1517/17425255.2015.983075

Teo, Y. L., Ho, H. K., & Chan, A. (2015b). Metabolism-related pharmacokinetic drug-drug interactions with tyrosine kinase inhibitors: Current understanding, challenges and recommendations. British Journal of Clinical Pharmacology, 79, 241–253. https://doi.org/10.1111/bcp.12496

Vander Heiden, M. G., Plas, D. R., Rathmell, J. C., Fox, C. J., Harris, M. H., & Thompson, C. B. (2001). Growth factors can influence cell growth and survival through effects on glucose metabolism. Molecular and Cellular Biology, 21, 5899–5912.

Weng, Z., Luo, Y., Yang, X., Greenhaw, J. J., Li, H., Xie, L., …Shi, Q. (2015). Regorafenib impairs mitochondrial functions, activates AMP-activated protein kinase, induces autophagy, and causes rat hepatocyte necrosis. Toxicology, 327, 10–21. https://doi.org/10.1016/j.tox.2014.11.002

Will, Y., Dykens, J. A., Nadanaciva, S., Hirakawa, B., Jamieson, J., Marroquin, L. D., …Jessen, B. A. (2008). Effect of the multitargeted tyrosine kinase inhibitors imatinib, dasatinib, sunitinib, and sorafenib on mitochondrial function in isolated rat heart mitochondria and H9c2 cells. Toxicological Sciences, 106, 153–161. https://doi.org/10.1093/toxsci/kfn157

Xue, T., Luo, P., Zhu, H., Zhao, Y., Wu, H., Gai, R., …He, Q. (2012). Oxidative stress is involved in Dasatinib-induced apoptosis in rat primary hepatocytes. Toxicology and Applied Pharmacology, 261, 280–291. https://doi.org/10.1016/j.taap.2012.04.010

Yamasaki, A., Umeno, N., Harada, S., Tanaka, K., Kato, M., & Kotoh, K. (2016). Deteriorated portal flow may cause liver failure in patients with hepatocellular carcinoma being treated with sorafenib. Journal of Gastrointestinal Oncology, 7, E36–E40. https://doi.org/10.21037/jgo.2015.10.07

Yuan, L., & Kaplowitz, N. (2013). Mechanisms of drug-induced liver injury. Clinics in Liver Disease, 17(507–518), vii. https://doi.org/10.1016/j.cld.2013.07.002

Zhang, J., Salminen, A., Yang, X., Luo, Y., Wu, Q., White, M., … Shi, Q. (2017). Effects of 31 FDA approved small-molecule kinase inhibitors on isolated rat liver mitochondria. Archives of Toxicology, 91, 2921–2938. https://doi.org/10.1007/s00204-016-1918-1

SUPPORTING INFORMATION

Additional Supporting Information may be found online in the supporting information tab for this article.

How to cite this article: Mingard C, Paech F, Bouitbir J, Krähenbühl S. Mechanisms of toxicity associated with six tyrosine kinase inhibitors in human hepatocyte cell lines. J Appl Toxicol. 2017;1–14. https://doi.org/10.1002/jat.3551

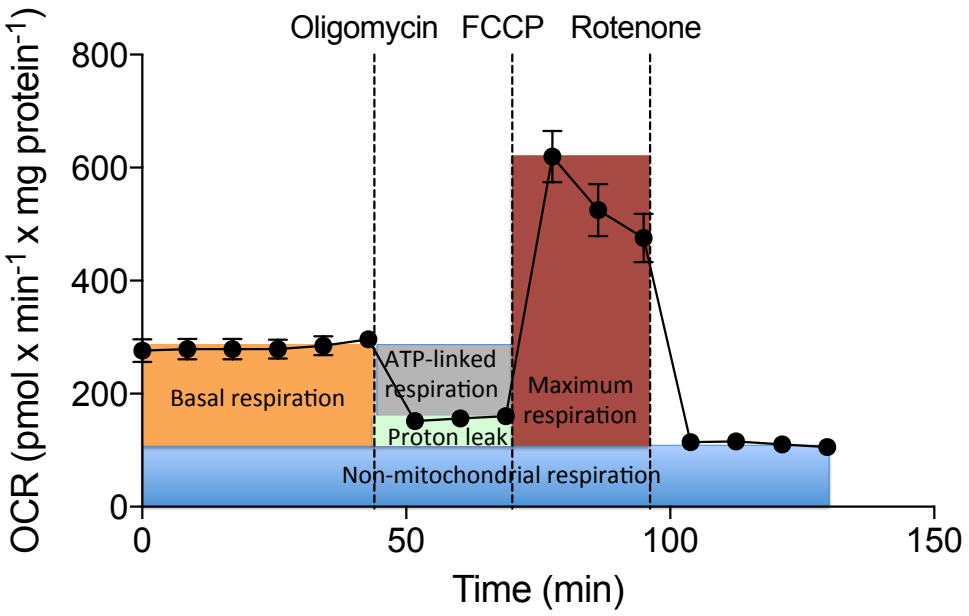

Supplementary Fig. S1. Representative scheme of the Seahorse XF24 Analyzer experiment. HepG2 cells (100 000 cells/well) in DMEM growth medium were allowed to adhere overnight and then treated with the test compounds for 24 h. Before the experiment, the medium was replaced with 750 µl unbuffered DMEM medium (4mM L-glutamate, 1 mM pyruvate, 1 g/l glucose, 63.3 mM sodium chloride, pH 7.4). After determination of the basal oxygen consumption (OCR), 1 µM oligomycin (inhibitor of the F0F1-ATPase) was added for the determination of the proton leak and the ATP-linked respiration. Afterwards, 2 µM FCCP (mitochondrial uncoupler) was added for maximal stimulation of the mitochondrial electron transport chain. Finally, the extramitochondrial respiration was estimated after the addition of complex I inhibitor rotenone (1 µM). For the determination of the basal respiration, the oxidative leak, and the maximum respiration, the extramitochondrial respiration was subtracted.

3 PAPER 3

MECHANISMS OF MITOCHONDRIAL TOXICITY OF THE KINASE INHIBITORS PONATINIB, REGORAFENIB AND SORAFENIB IN HUMAN HEPATIC HEPG2 CELLS

Within this article, we will better characterize the mechanisms underlying the mitochondrial impairement observed with pozopanib, regorafenib, and sorafenib in more detail *in vitro*.

Toxicology 395 (2018) 34–44

Contents lists available at ScienceDirect

Toxicology

journal homepage: www.elsevier.com/locate/toxicol

Mechanisms of mitochondrial toxicity of the kinase inhibitors ponatinib, regorafenib and sorafenib in human hepatic HepG2 cells

Franziska Paech[a,b], Cécile Mingard[a,b], David Grünig[a,b], Vanessa F. Abegg[a,b], Jamal Bouitbir[a,b,c], Stephan Krähenbühl[a,b,c,*]

[a] Division of Clinical Pharmacology & Toxicology, University Hospital, Basel, Switzerland
[b] Department of Biomedicine, University of Basel, Switzerland
[c] Swiss Centre for Applied Human Toxicology, Switzerland

ARTICLE INFO

Keywords:
Kinase inhibitor
Hepatotoxicity
Mitochondrial toxicity
Reactive oxygen species (ROS)
Mitochondrial fission & mitophagy
Apoptosis

ABSTRACT

Previous studies have shown that certain kinase inhibitors are mitochondrial toxicants. In the current investigation, we determined the mechanisms of mitochondrial impairment by the kinase inhibitors ponatinib, regorafenib, and sorafenib in more detail. In HepG2 cells cultured in galactose and exposed for 24 h, all three kinase inhibitors investigated depleted the cellular ATP pools at lower concentrations than cytotoxicity occurred, compatible with mitochondrial toxicity. The kinase inhibitors impaired the activity of different complexes of the respiratory chain in HepG2 cells exposed to the toxicants for 24 h and in isolated mouse liver mitochondria exposed acutely. As a consequence, they increased mitochondrial production of ROS in HepG2 cells in a time- and concentration-dependent fashion and decreased the mitochondrial membrane potential concentration-dependently. In HepG2 cells exposed for 24 h, they induced mitochondrial fragmentation, lysosome content and mitophagy as well as mitochondrial release of cytochrome c, leading to apoptosis and/or necrosis. In conclusion, the kinase inhibitors ponatinib, regorafenib, and sorafenib impaired the function of the respiratory chain, which was associated with increased ROS production and a drop in the mitochondrial membrane potential. Despite activation of defense measures such as mitochondrial fission and mitophagy, some cells were liquidated concentration-dependently by apoptosis or necrosis. Mitochondrial dysfunction may represent a toxicological mechanism of hepatotoxicity associated with certain kinase inhibitors.

1. Introduction

Tyrosine kinases are important enzymes involved in a variety of biological processes, including cell proliferation, survival, and differentiation (Shah et al., 2013; Shchemelinin et al., 2006). Due to their role in cell proliferation, expression of defective tyrosine kinases is involved in tumor initiation and progression (Shchemelinin et al., 2006) and dysregulation of tyrosine kinase expression can be associated with cancer development (Levitzki and Gazit, 1995). This role of tyrosine kinases in cancerogenesis has led to the development of a new class of anticancer drugs, the tyrosine kinase inhibitors (Krause and Van Etten, 2005). Most of them inhibit more than one kinase and are called multikinase inhibitors (MKIs).

Compared to classical cytotoxic agents, the hepatotoxicity of MKIs is generally less pronounced, but MKIs are associated for instance with toxicity of the skin, the intestine, the heart, and the liver (Breccia and Alimena, 2013). Hepatotoxicity has been reported for several MKIs, including ponatinib, regorafenib, and sorafenib (Josephs et al., 2013; Shah et al., 2013; Spraggs et al., 2013). Clinical trials indicated a low grade elevation in alanine aminotransferase (ALT) and/or aspartate aminotransferase (AST) in 25–30% and a high grade elevation (> 5 times upper limit of normal) in approximately 2% of patients treated with MKIs (Shah et al., 2013). A recent meta-analysis including more than 18,000 patients demonstrated an elevated risk of hepatotoxicity associated with tyrosine kinase inhibitors (Ghatalia et al., 2015) with an incidence of hepatic failure of 0.8%. Fatalities are fortunately rare, but have been reported for several MKIs including pazopanib (Klempner et al., 2012) and regorafenib (Mir et al., 2016).

The exact mechanism of MKI-induced hepatotoxicity has not been completely elucidated; however, it may be related to mitochondrial

Abbreviations: MKI, multikinase inhibitor; ALT, alanine aminotransferase; AST, aspartate aminotransferase; DRP1, dynamin-related protein 1; FIS1, mitochondrial fission 1; ROS, reactive oxygen species; DMSO, dimethylsulfoxide; AK, adenylate kinase; PBS, phosphate buffered saline; $\Delta\psi_m$, mitochondrial membrane potential; TMRM, tetramethylrhodamine methyl ester; FCCP, carbonyl cyanide-4-(trifluoromethoxy)phenylhydrazone; SEM, standard error of the mean; SOD, superoxide dismutase; LC3, Microtubule-associated protein light chain 3

* Corresponding author at: Clinical Pharmacology & Toxicology, University Hospital, 4031 Basel, Switzerland.
E-mail address: stephan.kraehenbuehl@usb.ch (S. Krähenbühl).

https://doi.org/10.1016/j.tox.2018.01.005
Received 19 October 2017; Received in revised form 23 December 2017; Accepted 12 January 2018
Available online 16 January 2018
0300-483X/

damage. Recent publications suggest hepatic mitochondrial toxicity for dasatinib (Xue et al., 2012), lapatenib (Eno et al., 2016), and regorafenib (Weng et al., 2015; Zhang et al., 2017), and sorafenib and pazopanib (Zhang et al., 2017). Our group has shown recently in HepG2 cells that exposure to imatinib or sunitinib reduced the mitochondrial membrane potential, and was associated with impaired oxygen consumption and mitochondrial oxidative stress (Paech et al., 2017a). In a second recent publication, we reported that regorafenib, ponatinib and sorafenib inhibited mitochondrial oxidative metabolism and glycolysis, and induced apoptosis and/or necrosis of HepG2 cells at concentrations reachable in humans (Mingard et al., 2017). Importantly, MKIs cannot only damage hepatic mitochondria, but have also been described to be toxic for cardiac mitochondria, supporting the notion that MKIs are mitochondrial toxicants (Kerkela et al., 2006; Will et al., 2008).

Mitochondria are dynamic organelles, which have different possibilities to react after a toxic insult. A decrease in the mitochondrial membrane potential is associated with mitochondrial fission, with the aim to separate the defective and the functioning parts of the mitochondria (Westermann, 2010). Fission is initiated by recruitment of the dynamin-related protein 1 (DRP1) to the outer mitochondrial membrane by mitochondrial fission 1 (FIS1) (Palmer et al., 2011). After fission, the mitochondrial network has a fragmented appearance and the defective mitochondrial fragments can undergo mitophagy, which can be regarded as a protective process to remove damaged mitochondria (Ding and Yin, 2012). If the toxic insult is too pronounced, mitochondrial repair by fission and mitophagy is impossible and cells either undergo necrosis when the cellular ATP level is low or apoptosis, which is ATP-dependent. The induction of cell death can be initiated by release of cytochrome *c* out of damaged mitochondria into the cytoplasm (Green and Reed, 1998).

Based on these considerations, the aim of the current study was to investigate in more detail the mechanisms underlying the mitochondrial toxicity of ponatinib, regorafenib, and sorafenib in HepG2 cells. We determined the cellular ATP content and mitochondrial reactive oxygen species (ROS) production using a medium containing galactose, since HepG2 cells grown in galactose generate ATP mainly in mitochondria and are sensitive to mitochondrial toxicants (Brecht et al., 2017; Kamalian et al., 2015). In addition, we also determined the effects of the toxicants on the activity of the individual enzyme complexes of the mitochondrial electron transport chain and on the consequences resulting from impaired activity of these enzyme complexes, in particular on mitochondrial fission, mitophagy, and cell death.

2. Materials and methods

2.1. Chemicals

Ponatinib, regorafenib, and sorafenib were purchased from Sequoia research products (Pangbourne, UK). We prepared stock solutions in dimethylsulfoxide (DMSO) and stored them at −20 °C. All other chemicals were supplied by Sigma-Aldrich (Buchs, Switzerland), except where indicated.

2.2. HepG2 cell culture

The human hepatocellular carcinoma cell line HepG2 was obtained from the American type culture collection (ATCC, Manassas, VA, USA). HepG2 cells were cultured under two different conditions, low glucose and galactose.

HepG2 cells under low glucose conditions were cultured in Dulbecco's Modified Eagle Medium (DMEM containing 5.55 mM (1 g/l) glucose, 4 mM L-glutamine, and 1 mM pyruvate from Invitrogen, Basel, Switzerland) supplemented with 10% (v/v) heat-inactivated fetal bovine serum (FBS), 2 mM GlutaMax, 10 mM HEPES buffer, 10 mM non-essential amino acids, 100 units/ml penicillin, and 100 µg/ml streptomycin.

HepG2 cells under galactose conditions were first cultured in low glucose medium. On the day of the experiment, HepG2 cells were centrifuged, the supernatant was removed and cells were resuspended in galactose medium (Dulbecco's Modified Eagle Medium (DMEM, no glucose, 4 mM L-glutamine) from Invitrogen (Basel, Switzerland) supplemented with 10% (v/v) heat-inactivated FBS, 10 mM galactose, 2 mM L-glutamine, 10 mM HEPES buffer, 1 mM sodium pyruvate, 100 units/ml penicillin, and 100 µg/ml streptomycin) for 4 h or 24 h before starting the treatment (Swiss and Will, 2011). The FBS was dialyzed through a Slide-A-Lyzer Dialysis Flask (Thermo Scientific, Reinach, Switzerland) to remove glucose according to the manufacturer's protocol. All experiments were performed under glucose medium except the release of adenylate kinase, the intracellular ATP content and the mitochondrial superoxide accumulation, which were performed under galactose medium.

All cells were kept at 37 °C in a humidified 5% CO_2 cell culture incubator and passaged using trypsin. The cell number was determined using a Neubauer hemacytometer and viability was checked using the trypan blue exclusion method.

2.3. Isolation of mouse liver mitochondria

The experiments were performed in accordance with the institutional guidelines for the care and use of laboratory animals. Male C57BL/6J mice (n = 3, age 7–10 weeks) were purchased from Charles River Laboratories (Sutzfeld, Germany) and housed in a standard facility with 12 h light–dark cycles and controlled temperature (21–22 °C). The mice were fed a standard pellet chow and water *ad libitum*.

Liver mitochondria were isolated by differential centrifugation as described before (Hoppel et al., 1979). The mitochondrial protein content was determined using the Pierce BCA protein assay kit from Merck (Zug, Switzerland).

2.4. Membrane toxicity

Membrane toxicity was assessed by using the ToxiLight assay from Lonza (Basel, Switzerland) according to the manufacturer's protocol. This assay measures the release of adenylate kinase (AK) in the medium, which reflects the plasma membrane's integrity. HepG2 cells in galactose conditions were grown in a 96-well plate (25′000 cells/well) and exposed to different concentrations of MKIs (5–50 µM) for 24 h. The plasma concentrations of ponatinib, regorafenib and sorafenib are in the range of 0.1, 2.5 and 5 to 10 µM, respectively (Herbrink et al., 2016; Huynh et al., 2017; Sunakawa et al., 2014). Since the liver concentration of MKIs can be considerably higher than the plasma concentrations (Lau et al., 2015), it can be assumed that at least the lowest concentrations used can be reached in the liver *in vivo*. The negative control was 0.1% DMSO and the positive control was 0.5% Triton-X. After incubation, 20 µL supernatant of each well was transferred to a new 96-well plate. Then, 50 µL of assay buffer was added to each well. After incubation in the dark for 5 min, the luminescence was measured using a Tecan M200 Pro Infinity plate reader (Männedorf, Switzerland). All data were normalized to positive control incubations containing 0.5% Triton X (set at 100% cell lysis).

2.5. Intracellular ATP content

The intracellular ATP content was measured using the CellTiter-Glo kit from Promega (Wallisellen, Switzerland) according to the manufacturer's protocol. HepG2 cells in galactose conditions were grown in a 96-well plate (25,000 cells/well) and exposed to different concentrations of MKI (5–50 µM) for 24 h. The negative control was 0.1% DMSO and the positive control was 0.5% Triton-X. After treatment, medium was removed in order to have 50 µL remaining in each well and afterwards 50 µL of assay buffer was added to each well. After incubation in

the dark for 15 min, the luminescence was measured using a Tecan M200 Pro Infinity plate reader (Männedorf, Switzerland). All data were normalized to control incubations containing 0.1% DMSO.

2.6. Activity of specific enzyme complexes of the mitochondrial electron transport chain

The activity of specific enzyme complexes of the respiratory chain was analyzed using an Oxygraph-2k high-resolution respirometer equipped with DataLab software (Oroboros instruments, Innsbruck, Austria) as described previously (Paech et al., 2017b). HepG2 cells under low glucose conditions were treated with test compounds (1–10 µM) for 24 h. Afterwards, they were suspended in MiR05 (mitochondrial respiration medium containing 0.5 mM EGTA, 3 mM magnesium chloride, 20 mM taurine, 10 mM potassium dihydrogen phosphate, 20 mM HEPES, 110 mM sucrose, 1 g/l fatty-acid free bovine serum albumin, and 60 mM lactobionic acid, pH 7.1) and transferred to the pre-calibrated Oxygraph chamber (Pesta and Gnaiger, 2012).

Respiratory capacities through complexes I, II, III, and IV were assessed in HepG2 cells permeabilized with digitonin (10 µg/1 million cells). Complexes I and III were analyzed using L-glutamate/malate (10 and 2 mM, respectively) as substrates followed by the addition of adenosine-diphosphate (ADP; 2.5 mM). Then, the oxidative leak, a marker for uncoupling, was identified by the assessment of the residual oxygen consumption after addition of oligomycin (1 µM). After that, we determined the maximal oxidative capacity in the presence of L-glutamate/malate with the addition of FCCP (1 µM) followed by inhibition of complex I with rotenone (0.5 µM). Afterwards, duroquinol (500 µM) was added to investigate complex III activity.

Complexes II and IV were analyzed using succinate/rotenone (10 mM and 0.5 µM, respectively) as substrates followed by the addition of ADP (2.5 mM). The oxidative leak was identified by the assessment of the residual oxygen consumption after addition of oligomycin (1 µM), followed by the addition of FCCP (1 µM) in order to evaluate the uncoupling capacity. After this, the inhibitor antimycin A (2.5 µM) was added to block complex III. Subsequently, N,N,N',*N*'-tetramethyl-1,4-phenylendiamine/ascorbate (0.5 and 2 mM, respectively) were added to investigate complex IV.

The integrity of the outer mitochondrial membrane was confirmed by the absence of a stimulatory effect of exogenous cytochrome *c* (10 µM) on respiration. Respiration was expressed as pmol O_2 per second per mg protein. Protein concentrations were determined using the Pierce BCA protein assay kit from Merck (Zug, Switzerland).

2.7. Activity of enzyme complexes of the electron transport chain in isolated mitochondria

The individual activities of mitochondrial enzyme complexes (I–IV) were assessed by well-established spectrophotometric methods (Krahenbuhl et al., 1991; Krahenbuhl et al., 1994) in isolated mouse liver mitochondria, which had been kept frozen at −80 °C.

Briefly, for complex I, we used the conversion of NADH to NAD using decylubiquinone as an electron acceptor monitoring at 340 nm. The activity of complex II was based on the conversion of oxidized dichloroindophenol to its reduced form at 600 nm using succinate as substrate. For complex III, we used decylubiquinol as a substrate and determined the conversion of ferricytochrome *c* to ferrocytochrome *c* at 550 nm. For complex IV, we followed the conversion of ferrocytochrome *c* to ferricytochrome *c* at 550 nm using ubiquinole as substrate. The activity of the respective enzyme complexes was determined as the difference in the presence of specific inhibitors (rotenone for complex I, thenoyltrifluroacetone for complex II, antimycin A for complex III, and sodium azide for complex IV).

The activitiy of mitochondrial enzyme complex V was assessed in freshly-isolated mouse liver mitochondria using an Oxygraph-2k high-resolution respirometer equipped with DataLab software (Oroboros instruments, Innsbruck, Austria). Freshly-isolated mouse liver mitochondria were suspended in MiR06 (mitochondrial respiration medium containing 0.5 mM EGTA, 3 mM magnesium chloride, 20 mM taurine, 10 mM potassium dihydrogen phosphate, 20 mM HEPES, 110 mM sucrose, 1 g/L fatty-acid free bovine serum albumin, 60 mM lactobionic acid, and 280 units/ml catalase, pH 7.1) and 250 µg mitochondria were transferred to the pre-calibrated Oxygraph chamber and treated for 15 min with drugs. The respiratory capacity through complex V was analyzed using adenosine-diphosphate (ADP; 2.5 mM) followed by N,N,N',*N*'-tetramethyl-1,4-phenylendiamine/ascorbate (0.5 and 2 mM, respectively). Afterwards, complex V was inhibited by addition of oligomycin (2 µg/ml). Activity of complex V was calculated by the difference of both states. The activity of each complex was expressed as nmol per minute per mg protein.

2.8. Mitochondrial superoxide accumulation

Mitochondrial superoxide accumulation was measured using the MitoSOX Red fluorophore probe from Invitrogen (Basel, Switzerland), according to the manufacturer's manual. The MitoSOX Red mitochondrial superoxide indicator is a fluorogenic dye for highly selective detection of superoxide in the mitochondria of living cells. HepG2 cells kept under galactose condition were seeded in 96-well plates (25,000 cells/well) and treated with test compounds (5–50 µM) for 24 h. The negative control was 0.1% DMSO and the positive control was 50 µM amiodarone. Afterwards, 100 µL phosphate buffered saline (PBS) with 2.5 µM MitoSOX was added to each 96-well. After incubation at 37 °C in the dark for 10 min, the fluorescence was measured using a Tecan M200 Pro Infinity plate reader (Männedorf, Switzerland) with an excitation at 510 nm and an emission at 580 nm. We normalized the results to the protein content using Pierce BCA Protein Assay Kit from Thermo Fisher Scientific (Waltham, MA, USA).

2.9. Western blotting

HepG2 cells kept under low glucose condition were seeded in 6 well-plate (500'000 cells/well) and treated with different concentrations of MKIs (2–20 µM) for 24 h. The negative control was 0.1% DMSO. Afterwards, HepG2 cells were lysed with RIPA buffer (150 mM sodium chloride, 1.0% NP-40, 0.5% sodium deoxycholate, 0.1% sodium dodecyl sulphate, 50 mM Tris, pH 8.0) containing complete Mini protease inhibitor cocktail (Roche Diagnostics, Mannheim, Germany). After centrifugation, the supernatant was collected and stored at −80 °C. Proteins were resolved by SDS-PAGE using commercially available 4–12% NuPAGE Bis-Tris gels (Invitrogen, Basel, Switzerland) and transferred using the Trans-Blot Turbo Blotting System (Bio-Rad, Cressier, Switzerland). The membranes were incubated with Anti-SOD2 antibody (ab16956, Abcam, Cambridge, UK), Anti-OPA1 antibody (ab157457, Abcam, Cambridge, UK), Anti-TTC11 antibody (ab71498, Abcam, Cambridge, UK), Anti-MAP1LC3A antibody (ab168803, Abcam, Cambridge, UK), Anti-Bcl2 antibody (ab692, Abcam, Cambridge, UK), Caspase-3 antibody (8G10, Cell Signaling Technology, Danvers, USA), and GAPDH (sc-365062, Santa Cruz Biotechnology, Dallas, USA) antibodies. After washing, membranes were exposed to secondary antibodies (Santa Cruz Biotechnology, Dallas, USA). Immunoblots were developed using Clarity Western ECL Substrate (Bio-Rad Laboratories, Hercules, USA). Protein expression was quantified using the Fusion Pulse TS device (Vilber Lourmat, Oberschwaben, Germany).

2.10. Mitochondrial membrane potential

Mitochondrial membrane potential ($\Delta\psi_m$) in HepG2 cells kept under low glucose conditions was determined using tetramethylrhodamine methyl ester (TMRM, Invitrogen, Basel, Switzerland). TMRM is a cationic fluorescent probe that accumulates within mitochondria depending on their $\Delta\psi_m$. HepG2 cells were seeded in 24-well plates

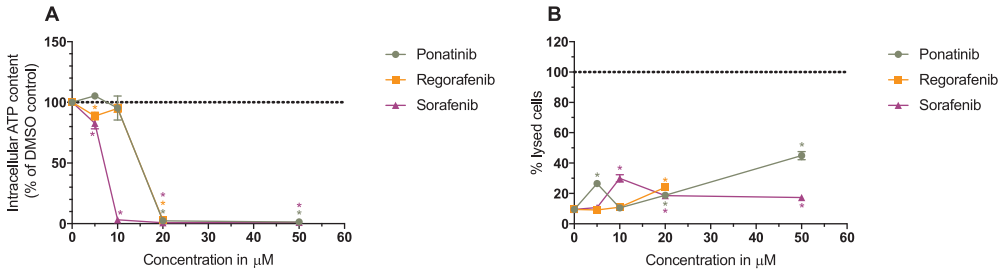

Fig. 1. Intracellular ATP content and cytotoxicity in HepG2 cells with galactose medium. Intracellular ATP content (A) and cytotoxicity (B) were measured after exposure for 24 h with ponatinib, regorafenib, and sorafenib. HepG2 cells were switched to 10 mM galactose medium 4 h before starting the treatment. Data are expressed as the decrease compared to control incubations containing 0.1% DMSO. The ATP content for the control incubations was 13.4 ± 0.9 nmol/mg protein (mean ± SEM, n = 4 control incubations). Cytotoxicity data are expressed as the percentage of lysed cells with the values obtained for Triton X 0.1% set as 100%. Data represent the mean ± SEM of at least three independent experiments. *p < 0.05 versus DMSO 0.1% control.

(200,000 cells/well) and treated with different concentrations of MKIs (2–50 µM) for 24 h. The negative control was 0.1% DMSO and the positive control carbonyl cyanide-4-(trifluoromethoxy)phenylhydrazone (FCCP, 9 µM). FCCP is an uncoupler of mitochondrial oxidative phosphorylation and therefore decreases $\Delta\psi_m$. FCCP was added to the cells and ten minutes later, cells were washed with PBS and suspended in PBS with 100 nM TMRM. After 15 min incubation in the dark, cells were centrifuged and resuspended in PBS for analyzing them with flow cytometry using a FACSCalibur (BD Bioscience, Allschwil, Switzerland). FlowJo software v10.0.8 (FlowJo, LCC, Ashland, OR, USA) was used to analyze the data.

2.11. Fission, mitophagy and apoptosis determined by microscopy

HepG2 cells under low glucose conditions were seeded in 8 well µ-Slide (ibidi, Martinsried, Germany) and treated with MKIs for 24 h at the concentrations indicated in the respective figures. Afterwards, cells were stained with 75 nM mitotracker (Thermo Fisher Scientific, Waltham, MA, USA), 50 nM lysotracker (Thermo Fisher Scientific, Waltham, MA, USA) and 1.8 µM Hoechst 33258 for 1 h. After staining, cells were washed twice with PBS and mounted with antifade-mounting medium (Thermo Fisher Scientific, Waltham, MA, USA). Cells were imaged on an Olympus IX83 microscope with a magnification of 100× (Olympus, Shinjuku, Japan).

2.12. Quantification of cytochrome c in cytoplasm

For the quantification of cytochrome *c*, cytoplasm and mitochondria were separated using a Mitochondrial/Cytosol Fractionation Kit (ab65320, Abcam, Cambridge, UK). Afterwards, the cytochrome *c* content in the cytosolic fraction was quantified by western blotting using Anti-cytochrome C antibody (ab133504, Abcam, Cambridge, UK).

2.13. Annexin V/Propidium iodide

To study the mechanisms of cell death, we used the FITC Annexin V/Dead Cell Apoptosis Kit from Invitrogen (Basel, Switzerland) according to the manufacturer's protocol. HepG2 cells kept under low glucose conditions were seeded in 24-well plates (200,000 cells/well) and treated with different concentrations of MKIs (5–10 µM) for 24 h. The negative control was 0.1% DMSO. Positive controls were 200 nM staurosporin for apoptosis and 50 µM amiodarone for necrosis. The cells were then analyzed with a FACSCalibur (BD Bioscience, Allschwill, Switzerland) channel FL-1 and FL-3. FlowJo software v10.0.8 was used to analyze the data.

2.14. Statistical analysis

Data are given as the mean ± standard error of the mean (SEM) of at least three experiments in triplicates. Statistical analyses were performed using GraphPad Prism 6 (GraphPad Software, La Jolla, CA, USA). For the comparison of treatment groups to the 0.1% DMSO control group, one-way ANOVA was used followed by the Dunnett's posttest procedure. *P*-values < 0.05 (*) were considered significant.

3. Results

3.1. Cytotoxicity and ATP content in HepG2 cells

AK release was determined as a marker of membrane toxicity, and the cellular ATP content as an estimate for mitochondrial function. For that, HepG2 cells were switched to 10 mM galactose medium at least 4 h before starting the treatment (Kamalian et al., 2015). In the presence of glucose, HepG2 cells can produce ATP not only via oxidative phosphorylation, but also via glycolysis. By using galactose, cells are forced to produce ATP mainly via oxidative phosphorylation (Marroquin et al., 2007). In the presence of galactose, mitochondrial toxicants deplete therefore the cellular ATP content at lower concentrations (Brecht et al., 2017; Kamalian et al., 2015).

The effects of ponatinib, regorafenib, and sorefenib on the intracellular ATP content and on membrane toxicity in HepG2 cells 4 h after replacement of glucose by galactose are shown in Fig. 1A and B. All three MKIs investigated decreased the intracellular ATP content and were membrane toxic in a concentration-dependent manner. In the presence of ponatinib, almost no ATP was left at 20 µM, while only 20% of the cells were lysed at this concentration, suggesting that mitochondrial toxicity precedes membrane toxicity. Regorafenib decreased the ATP content and was membrane toxic starting (the term starting reflects the lowest concentration at which a significant difference to control incubations was observed) at 5 µM and 20 µM, respectively. Sorafenib was starting to decrease the cellular ATP content at 5 µM and to be membrane toxic at 10 µM. Similar results were obtained when the medium was changed from glucose to galactose 24 h before starting the treatment with the toxicants (Supplementary Fig. S1).

These results suggested that ponatinib, regorafenib, and sorafenib were mitochondrial toxicants. The results are compatible with previous observations by us in the presence of a low glucose medium (Mingard et al., 2017).

3.2. Effect on enzyme complexes of the electron transport chain

In order to analyze the mechanism of mitochondrial toxicity in more detail, we first determined the effect of these compounds on the respiratory capacity of HepG2 cells using a high-resolution respirometry

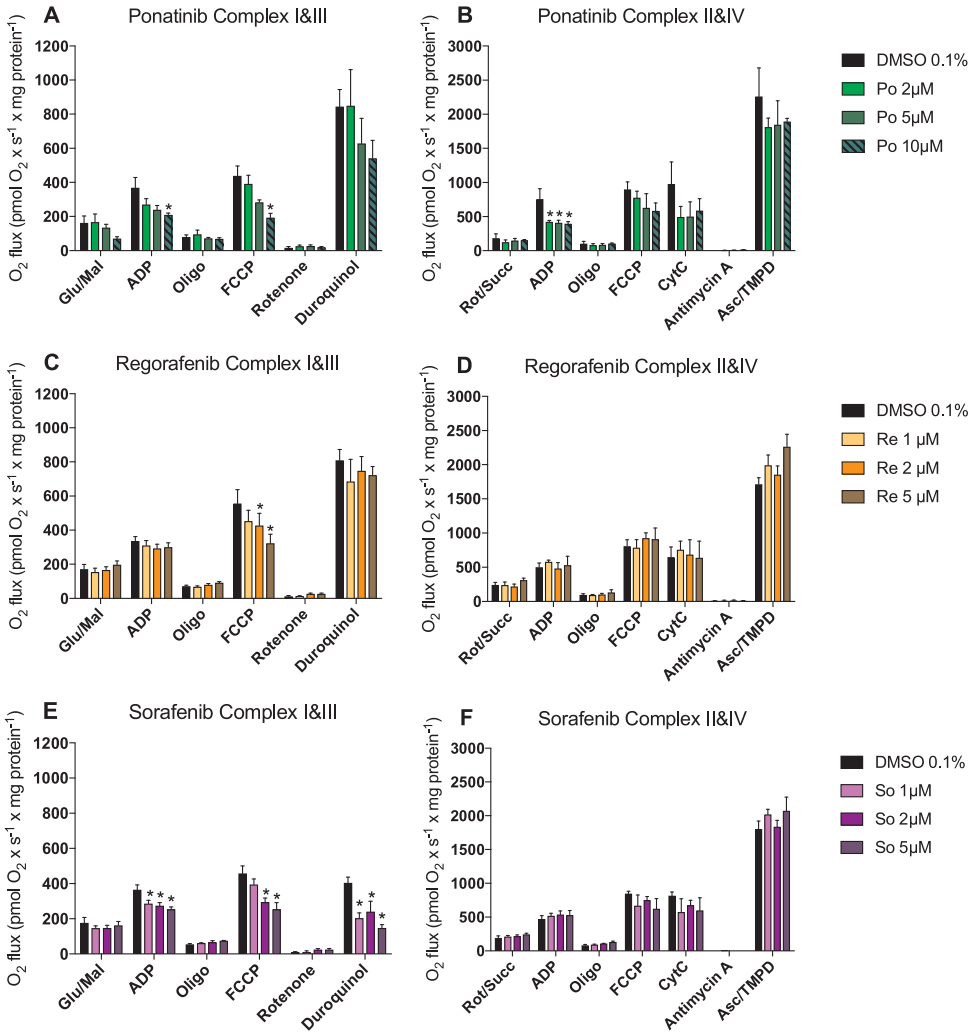

Fig. 2. Effect on respiratory capacities through complexes I, II, III, and IV measured on the Oxygraph-2k-high-resolution respirometer in HepG2 cells. Activity of complex I and III (A) and of complex II and III (B) on HepG2 cells cultured with low glucose after ponatinib exposure for 24 h. Activity of complex I and III (C) and of complex II and III (D) on HepG2 cells cultured with low glucose after regorafenib exposure for 24 h. Activity of complex I and III (E) and of complex II and III (F) on HepG2 cells cultured with low glucose after sorafenib exposure for 24 h. Data represent the mean ± SEM of at least three independent experiments. *$p < 0.05$ versus DMSO 0.1% control.

system.

Ponatinib inhibited the enzyme complexes I and II starting at 10 µM and 2 µM, respectively (Fig. 2A and B), and regorafenib started to inhibit the maximal capacity of complex I starting at 2 µM (Fig. 2C and D). Sorafenib started to inhibit complex I and complex III already at 1 µM (Fig. 2E and F).

3.3. Effect on activity of enzyme complexes of the electron transport chain in isolated mitochondria

The activity of individual complexes I–IV of the electron transport chain (ETC) was determined using frozen mouse liver mitochondria; for complex V, freshly isolated mitochondria were used.

Ponatinib inhibited the activity of complexes I, III, and V of the ETC starting at 20 µM (Fig. 3A, C, and E). Regorafenib inhibited the activity of complexes II, III, and V in a dose-dependent fashion starting at 5 µM, 10 µM, and 5 µM, respectively (Fig. 3B, C, and E). The activity of complexes II, III, IV, and V was decreased with sorafenib starting at 5 µM (Fig. 3B–E).

3.4. Effect on mitochondrial ROS accumulation and SOD2 expression

Toxicants inhibiting the function of the mitochondrial electron transport chain, especially complexes I and III, can increase mitochondrial production of superoxide (Drose and Brandt, 2012). In the current study, in HepG2 cells under galactose conditions, we found a dose- and time-dependent mitochondrial superoxide accumulation for all three toxicants investigated (Fig. 4A–C). After incubation for 24 h, mitochondrial ROS accumulation started at 5 µM for ponatinib and at 10 µM for regorafenib and sorafenib. Compared to previous findings in low glucose medium and after an incubation for 24 h, mitochondrial ROS accumulation started at the identical concentration for ponatinib, but at lower concentrations for regorafenib and sorafenib (10 µM vs. 20 µM) (Mingard et al., 2017).

Accumulating ROS can be degraded by superoxide dismutase (SOD). SOD2 is located in the mitochondrial matrix (Bresciani et al., 2015).

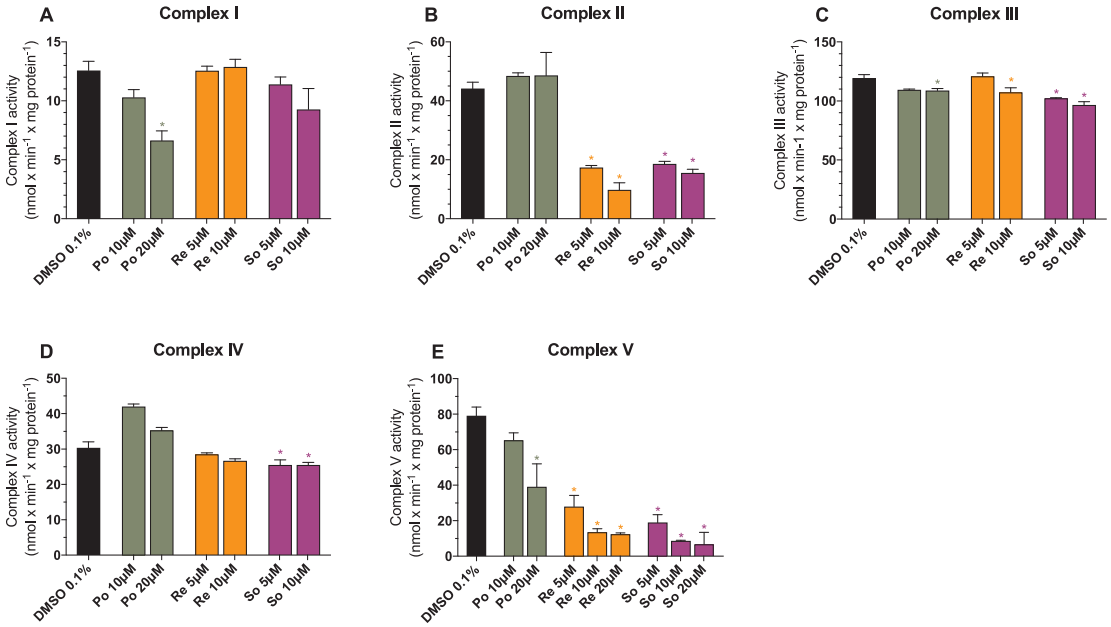

Fig. 3. Effect on the individual activity of the enzyme complexes of the electron transport chain in isolated mouse liver mitochondria. Activity of Complex I (A), complex II (B), complex III (C), complex IV (D), and complex V (E) of the respiratory chain after exposure with ponatinib, regorafenib, and sorafenib for 15 min. Data represent the mean ± SEM of at least three independent experiments. *p < 0.05 versus DMSO 0.1% controls.

Despite the increase in mitochondrial ROS production, the protein expression of SOD2 showed no significant increase (Fig. 4D and E). It is possible that the exposure to the toxicants and to mitochondrial ROS was too short for induction of SOD2.

Another potential consequence of the inhibition of the respiratory chain is a decrease in the mitochondrial membrane potential. As shown in Fig. 4F, after incubation for 24 h, this decrease started at 20 µM for ponatinib, and at 10 µM for regorafenib and sorafenib.

3.5. Fission and fusion in HepG2 cells

In reality, mitochondria build a network and continually fuse and divide (Westermann, 2010) (Fig. 5, Supplementary Fig. 2). Several studies have shown that these processes have important consequences for the morphology and function of mitochondria (Detmer and Chan, 2007a,b) and that they can be influenced by mitochondrial toxicants, which decrease the mitochondrial membrane potential (Westermann,

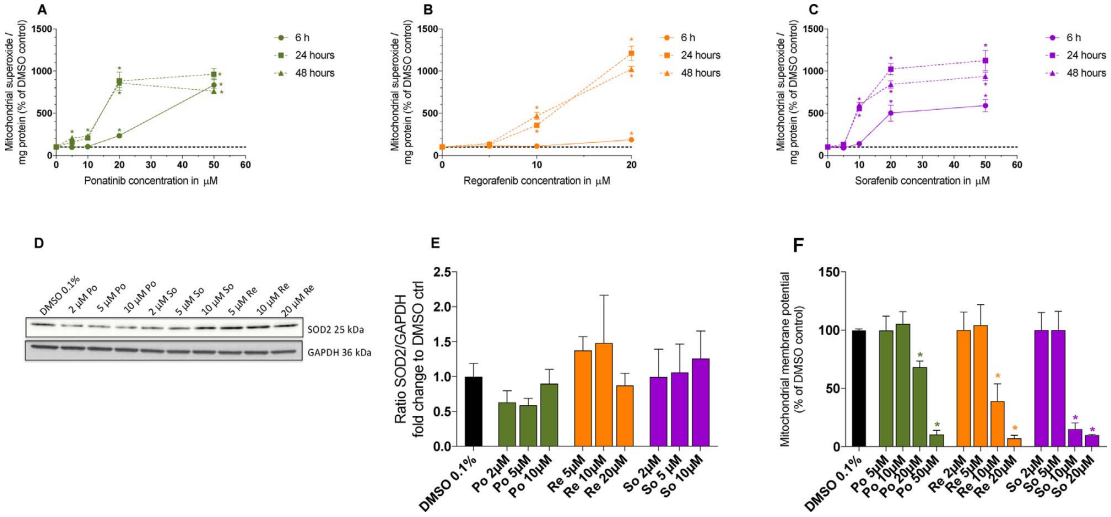

Fig. 4. Mitochondrial ROS accumulation and SOD2 expression. Mitochondrial ROS production by HepG2 cells cultured with galactose medium during exposure to ponatinib (A), regorafenib (B), and sorafenib (C) for 6 to 48 h. (D) and (E) SOD2 protein expression and (F) mitochondrial membrane potential in HepG2 cells cultured with low glucose medium exposed to different concentrations of the toxicants for 24 h. ROS data are expressed as the increase in percent relative to control incubations set at 100%. SOD2 protein expression is shown as fold change to control incubations. The mitochondrial membrane potential is expressed as the percentage relative to control incubations set at 100%. All data represent the mean ± SEM of at least three independent experiments. *p < 0.05 versus respective DMSO 0.1% control incubations.

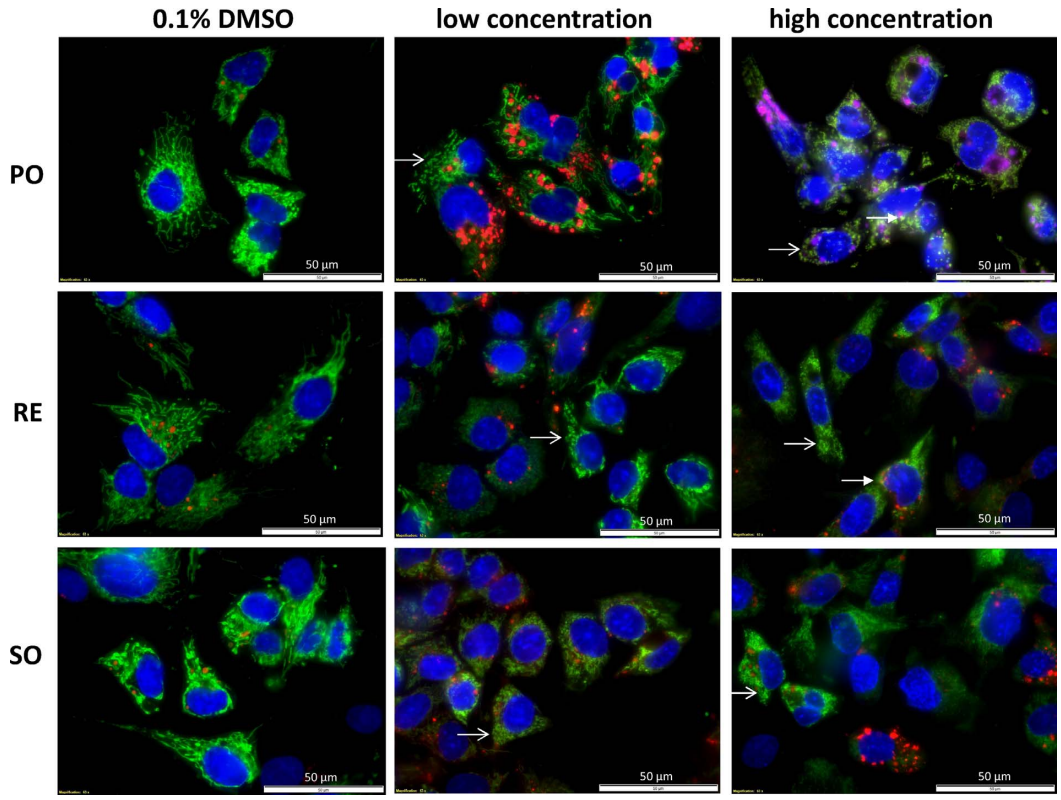

Fig. 5. Morphology of HepG2 cells under control conditions (DMSO 0.1%) and after exposure to toxicants for 24 h. HepG2 cells were exposed to 0.5 µM (low concentration) or 5 µM (high concentration) ponatinib, or 1 µM (low concentration) or 10 µM (high concentration) regorafenib or sorafenib for 24 h. Cells were stained with mitotracker (mitochondria, green), Hoechst 33258 (nuclei, blue) and lysotracker (lysosomes, red) as described in Methods. Open arrows indicate mitochondrial fission and closed arrows mitophagy (lysosomes containing mitochondria become yellow). Purple lysosomes indicate apoptosis. (For interpretation of the references to colour in this figure legend, the reader is referred to the web version of this article.)

2010). Opa1 is an important protein involved in mitochondrial fusion (Chen et al., 2016) and Fis1 in mitochondrial fission (Zungu et al., 2011).

As shown in Fig. 5 and supplementary Figs. 3–8, the morphology of the mitochondrial network changed with increasing concentrations of the toxicants. Under control conditions (DMSO 0.1%), mitochondria formed a dense network and almost no fragmentation was detectable (Supplementary Fig. 2). With increasing concentrations of the toxicants and with increasing exposure time, this network became more and more fragmented for all toxicants investigated.

The protein expression of Opa1 was reduced numerically without reaching statistical significance by regorafenib, but was not affected by ponatinib and sorafenib (Fig. 6A). Fis1 protein expression was increased numerically without reaching statistical significance by ponatinib but remained unaffected by regorafenib and sorafenib (Fig. 6B).

As described above, the morphological findings suggested a shift from fusion to fission in HepG2 cells treated with the MKI inhibitors (Fig. 5 and Supplementary Figs. 2–8). This shift can be regarded as a consequence of the impaired activity of the mitochondrial respiratory chain with mitochondrial accumulation of ROS and decrease in the mitochondrial membrane potential in the presence of the MKI inhibitors.

3.6. Mitophagy in HepG2 cells

Mitophagy represents the selective removal of mitochondria (or parts of mitochondria) by autophagy. Damaged mitochondria recruit parkin to the outer membrane which ubiquitinates mitochondrial outer membrane proteins and thereby induces the formation of the autophagosome (Youle and van der Bliek, 2012). During this process, the cytosolic microtubule-associated protein light chain 3 (LC3)-I is conjugated with phosphatidylethanolamine to form lipidated LC3-II, which is an integral membrane component of the autophagosome. Lipidation of LC3-I to LC3-II is a key process in the formation of the phagophore (Hamacher-Brady and Brady, 2016) and the ratio LC3II/LC3I is considered to be a marker of autophagy.

First, we evaluated mitophagy in HepG2 cells exposed to MKIs (ponatinib at 0.5 and 5 µM; regorafenib and sorafenib at 1 and 10 µM) for 1, 3, 6 and 24 h. Ponatinib was associated with an increased number of lysosomes already starting after one hour of exposure at both concentrations (Supplementary Figs. 3 and 4). At both concentrations, there were lysosomes containing mitochondria (starting at 24 h at 0.5 µM and at 3 h at 5 µM), indicating mitophagy (Fig. 5 and Supplementary Figs. 3 and 4). In support of these findings, as shown in Fig. 6C and D, ponatinib was associated with a significant increase in the LC3II/LC3I ratio, demonstrating the formation of autophagosomes.

Compared to control incubations, also regorafenib was associated with an increased number of lysosomes staring 1 h after exposure (Supplementary Figs. 5 and 6). As shown in Fig. 5 and in Supplementary Figs. 5 and 6, regorafenib was associated with mitophagy, which was visbile starting at 3 h after exposure at both concentrations. In contrast to these microscopic findings, regorafenib did not affect the LC3II/LC3I ratio (Fig. 6C and D).

Exposure of HepG2 cells to sorafenib was associated with an

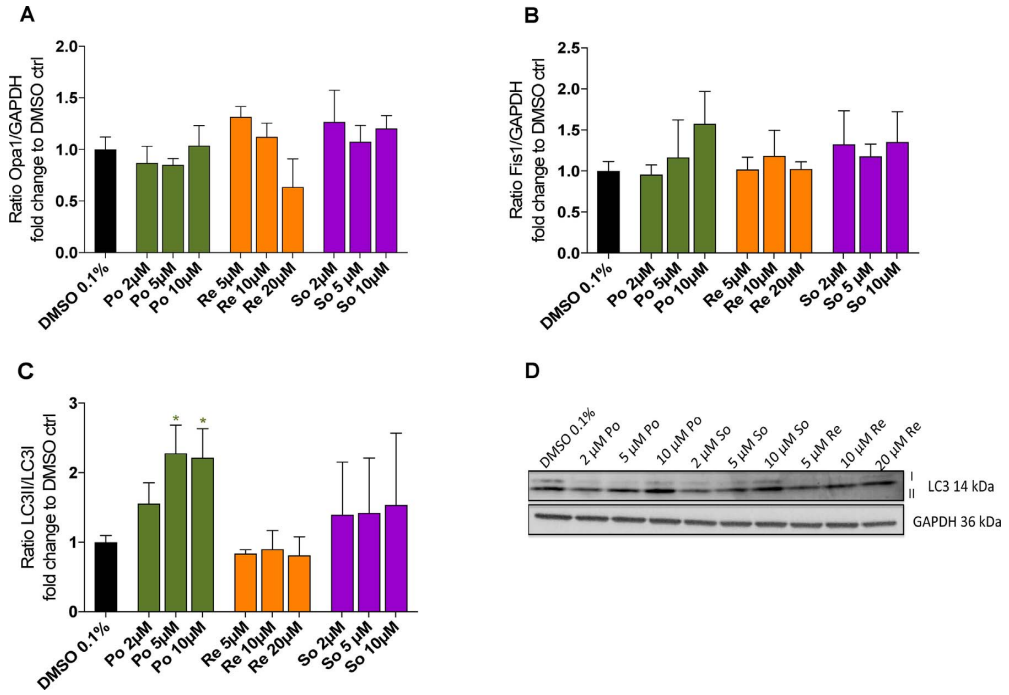

Fig. 6. Protein expression of Opa1, Fis1 and LC3 in HepG2 cells. HepG2 cells were treated with the toxicants for 24 h and western blots were performed as described in Methods. (A) Opa1 protein expression. (B) Fis1 protein expression. (C) Expression of LC3II and LC3I given as the ratio LC3II/LC3I. (D) Western blot of LC3I and LC3II. Protein expression data are shown relative to control incubations. Data represent the mean ± SEM of at least three independent experiments. *p < 0.05 versus DMSO 0.1% control.

increase in the number of lysosomes starting 1 h after exposure (supplementary Figs. 7 and 8). Furthermore, sorafenib induced mitophagy at both concentrations, starting at 3 h (1 µM) or at 1 h (10 µM) after exposure. Sorafenib numerically increased the LC3II/LC3I ratio, but this increase did not reach statistical significance (Fig. 6C and D).

These findings indicate that the three MKIs investigated induce mitochondrial fission and mitophagy in a time and concentration dependent fashion, but, concerning mitophagy, possibly with different mechanisms.

3.7. Mechanisms of cell death in HepG2 cells

When the damage to the mitochondria is too extensive, repair by mitochondrial fission and mitophagy is impossible and the cells undergo apoptosis or necrosis (Youle and van der Bliek, 2012). As shown in Fig. 7A, all MKIs investigated induced creased early apoptosis of HepG2 cells at 5 µM and 10 µM to a different extent. Sorafenib also increased cell necrosis at 10 µM. Release of cytochrome *c* from damaged mitochondria into the cytoplasm is an initial trigger for cell death (Green and Reed, 1998). As shown in Fig. 7B, ponatinib, regorafenib, and sorafenib were all associated with an increase of cytochrome *c* in the cytoplasm starting at 5 µM, 10 µM, and 2 µM, respectively.

Apoptosis can be associated with a decrease of the anti-apoptotic protein Bcl2. As shown in Fig. 7C, the MKIs investigated did not significantly affect the protein expression of Bcl2. We also determined activation of caspase 3 as a marker of apoptosis. As shown in Fig. 7D, ponatinib and regorafenib significantly increased the activation of caspase 3, whereas sorafenib did not affect activation of caspase 3. Moreover, the exposure with ponatinib, regorafenib and, to lesser extent, also sorafenib were associated with an increase in the number of lysosomes containing nuclei at different time points after exposure to the toxicants (purple color in lysosomes in Fig. 5 and Supplementary Figs. 3–8), supporting described in Fig. 7.

These results show that both apoptosis (for all MKIs investigated) and necrosis (for sorafenib) are mechanisms for cell death associated with the MKIs investigated.

4. Discussion

The current study showed that ponatinib, regorafenib, and sorafenib are mitochondrial toxicants that impair the activity of the respiratory chain. In HepG2 cells exposed for 24 h, the main effects were observed on complex I (all three compounds), complex II (ponatinib), and complex III (sorafenib), and in isolated mouse liver mitochondria exposed acutely on complex I (ponatinib), complex II (sorafenib), complex III (all compounds), complex IV (regorafenib), and complex V (all compounds) of the respiratory chain. Moreover, we showed that the impairment of mitochondrial respiration by MKIs in HepG2 cells was associated with an increase in mitochondrial fission and mitophagy and in some cells with mitochondrial release of cytochrome c leading to apoptosis and/or necrosis.

The observation that the three MKIs ponatinib, regorafenib, and sorafenib impair mitochondrial function is not new. We have published recently that these three MKIs inhibit mitochondrial respiration in permeabilized HepG2 cells exposed for 24 h in the presence of glutamate, which is a complex I-linked substrate (Mingard et al., 2017). In their recent publication, Zhang et al. have shown that, after acute exposure, regorafenib and sorafenib impaired the function of isolated rat liver mitochondria at concentrations reached in humans, whereas ponatinib showed no mitochondrial toxicity (Zhang et al., 2017). Regorafenib and sorafenib both stimulated state 4 respiration in the presence of glutamate and succinate, suggesting uncoupling of oxidative phosphorylation. In addition, regorafenib inhibited complex II and sorafenib complex V of the respiratory chain. Regarding sorafenib, mitochondrial toxicity has also been described in human neuroblastoma cells (Bull et al., 2012), in H9c2 myoblastic cells (Will et al., 2008) and in HepG2

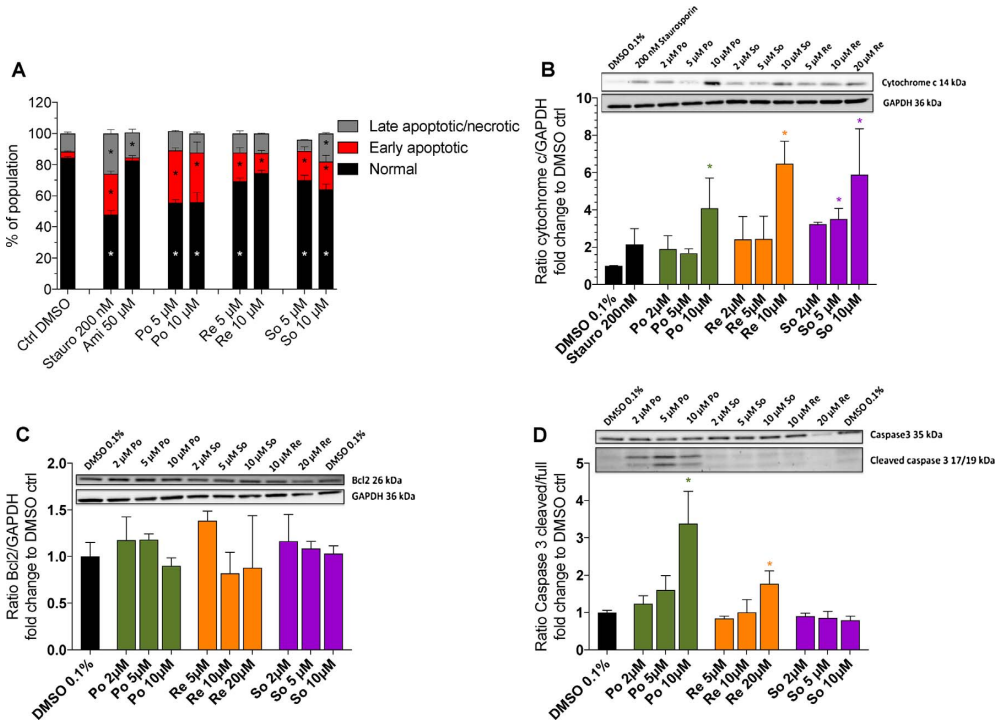

Fig. 7. Cell death associated with multikinase inhibitors. (A) Induction of apoptosis and necrosis of HepG2 cells treated with the toxicants for 24 h as determined by staining with annexin V/propidium iodide. (B) Quantification of cytochrome *c* in the cytosol of HepG2 cells (C) Protein expression of Bcl2. (D) Protein expression of caspase 3 and cleaved caspase 3. Cell populations are displayed as the percentage of healthy, apoptotic, and necrotic cells of the respective cell population. Protein expression is shown relative to control incubations. Data represent the mean ± SEM of at least three independent experiments. *p < 0.05 versus DMSO 0.1% control.

cells (Chiou et al., 2009). In the studies of Will et al. and Zhang et al., acute exposure of isolated mitochondria to sorafenib was associated with uncoupling of the respiratory chain and inhibition of complex II, III, and IV of the respiratory chain (Will et al., 2008; Zhang et al., 2017), which agrees well with the results of the current study. After long-term exposure of human neuroblastoma cells to sorafenib, complex I has been reported to be damaged and to have a decreased activity (Bull et al., 2012), which agrees with the data obtained in the current study in HepG2 cells exposed for 24 h. Regarding regorafenib, mitochondrial toxicity on acutely exposed isolated rat liver mitochondria has not only been shown by Zhang et al. (Zhang et al., 2017), but also by Weng et al. (Weng et al., 2015). In both studies, regorafenib uncoupled oxidative phosphorylation, and Weng et al. showed also mitochondrial swelling and a decrease in the mitochondrial membrane potential. The current study revealed inhibition of complex II, III, and V of the respiratory chain of acutely exposed mouse liver mitochondria, which at least partially agrees with the study of Zhang et al. who showed inhibition of complex II (Zhang et al., 2017). Importantly, similar to sorafenib, long-term exposure of HepG2 cells resulted in a different pattern, since, in the current study mainly complex I was affected. For ponatinib, Zhang et al. reported no mitochondrial toxicity after acute exposure of rat liver mitochondria (Zhang et al., 2017), which contrasts with the findings of the current study, showing inhibition of complex I, III, and V. This difference may be due to different susceptibility of rat and mouse liver mitochondria to this compound. Importantly, long-term exposure of HepG2 cells was associated with a decreased function of complex I and II, again showing that acute exposure and long-term exposure can yield different results. The results for long-term exposure are compatible those reported by Talbert et al. in human induced pluripotent stem cell-derived cardiomyocytes, where 5–10 µM ponatinib was associated with increased mitochondrial ROS production and lipid accumulation (Talbert et al., 2015), suggesting mitochondrial toxicity.

As mentioned above, the current study showed that acute and long-term exposure can affect mitochondrial functions differently. Beside the longer treatment, the actual exposure to the toxicants at the time point of the assays may also have been different. Before the determination of mitochondrial function, we removed the cell supernatant and replaced it with buffer containing no toxicant and permeabilized the HepG2 cells. The actual concentration of the toxicants in mitochondria of HepG2 cells may therefore have been considerably lower than in the acutely exposed isolated mitochondria. Experiments in suitable models for acute exposure, e.g. in isolated mitochondria, and for long-term exposure, e.g. in suitable cell models, are therefore necessary to obtain a more complete picture of mitochondrial toxicity associated with kinase inhibitors.

A consequence of the inhibition of complex I and III of the electron transport chain is an increase in mitochondrial ROS production (Drose and Brandt, 2012), which was observed in the current study in time- and concentration-dependent fashion. Mitochondrial ROS production in HepG2 cells exposed for 24 h and 48 h started at similar concentrations than inhibition of the electron transport chain, supporting the notion that ROS production is a consequence of the inhibition of the electron transport. Another consequence of the inhibition of the respiratory chain is a drop in the mitochondrial membrane potential, since fewer protons are pumped from the mitochondrial matrix into the intermembrane space. Increased mitochondrial ROS and decreased mitochondrial membrane potential are triggers for mitochondrial fission (Palmer et al., 2011; Westermann, 2010; Youle and van der Bliek, 2012), which was observed for the three MKIs investigated. Mitochondrial fission can be accompanied by mitophagy, since damaged

mitochondria are potentially dangerous for cells and should be removed (Ding and Yin, 2012; Hamacher-Brady and Brady, 2016). Indeed, mitophagy was also increased in the presence the three MKIs investigated in a time and concentration dependent fashion. In agreement with the current study, an increase in mitophagy has also been described in primary rat hepatocytes exposed for 7 h to regorafenib by Weng et al. (Weng et al., 2015). In contrast to Weng et al., we observed an increase in LC3-II, a marker of autophagy (Ding and Yin, 2012) only for ponatinib and sorafenib (for sorafenib only numerically), but not for regorafenib. In their review, Ding and Yin also described direct lysosomal removal of mitochondria without formation of an autophagosome (Ding and Yin, 2012), which may explain this finding.

Mitophagy is a protective mechanism of cells to avoid apoptosis or necrosis (Ding and Yin, 2012; Hamacher-Brady and Brady, 2016; Palikaras and Tavernarakis, 2014). When the toxic insult is too intense, however, the protective mechanisms including mitophagy are overwhelmed and cells are liquidated. As our study showed, these events can be observed concomitantly; some cells were going to recover while others sustained apoptosis (for all MKIs) and necrosis (for 10 µM sorafenib). In their recent article, Zhang et al. described that inhibition of complex III and V by sorafenib was associated with the stabilization of the protein kinase PINK1 on the outer mitochondrial membrane (Lang et al., 2002). PINK1 attracted and activated (phosphorylated) Parkin, which triggered apoptosis (and not mitophagy) due to ubiquitination and proteolytic degradation of Mcl-1. In the current study, in HepG2 cells, sorafenib did not affect Mcl-1 expression and we observed both, mitophagy and apoptosis. It therefore seems that the actions of sorafenib on mitophagy and apoptosis are cell specific.

In conclusion, the MKIs sorafenib, regorafenib, and ponatinib decreased the activity of the enzyme complexes of the respiratory chain in acutely exposed mouse liver mitochondria and in mitochondria of HepG2 cells exposed for 24 h. Impairment of the activity of the respiratory chain was associated with cellular ATP depletion, mitochondrial ROS production, and a drop in the mitochondrial membrane potential. This triggered mitochondrial fission and mitophagy as protective mechanisms. Despite these protective measures, some cells progressed to apoptosis or necrosis in concentration-dependent fashion. Mitochondrial dysfunction may represent a cause for hepatotoxicity associated with these compounds.

Conflict of interest

None of the authors has a conflict of interest regarding this study.

Financial support

The study was supported by a grant from the Swiss National Science foundation to SK (SNF 31003A_156270)

Appendix A. Supplementary data

Supplementary data associated with this article can be found, in the online version, at https://doi.org/10.1016/j.tox.2018.01.005.

References

Breccia, M., Alimena, G., 2013. Occurrence and current management of side effects in chronic myeloid leukemia patients treated frontline with tyrosine kinase inhibitors. Leuk. Res. 37, 713–720.

Brecht, K., Riebel, V., Couttet, P., Paech, F., Wolf, A., Chibout, S.D., Pognan, F., Krahenbuhl, S., Uteng, M., 2017. Mechanistic insights into selective killing of OXPHOS-dependent cancer cells by arctigenin. Toxicol. In Vitro 40, 55–65.

Bresciani, G., da Cruz, I.B., Gonzalez-Gallego, J., 2015. Manganese superoxide dismutase and oxidative stress modulation. Adv. Clin. Chem. 68, 87–130.

Bull, V.H., Rajalingam, K., Thiede, B., 2012. Sorafenib-induced mitochondrial complex I inactivation and cell death in human neuroblastoma cells. J. Proteome Res. 11, 1609–1620.

Chen, M., Chen, Z., Wang, Y., Tan, Z., Zhu, C., Li, Y., Han, Z., Chen, L., Gao, R., Liu, L., Chen, Q., 2016. Mitophagy receptor FUNDC1 regulates mitochondrial dynamics and mitophagy. Autophagy 12, 689–702.

Chiou, J.F., Tai, C.J., Wang, Y.H., Liu, T.Z., Jen, Y.M., Shiau, C.Y., 2009. Sorafenib induces preferential apoptotic killing of a drug- and radio-resistant Hep G2 cells through a mitochondria-dependent oxidative stress mechanism. Cancer Biol. Ther. 8, 1904–1913.

Detmer, S.A., Chan, D.C., 2007a. Complementation between mouse Mfn1 and Mfn2 protects mitochondrial fusion defects caused by CMT2A disease mutations. J. Cell Biol. 176, 405–414.

Detmer, S.A., Chan, D.C., 2007b. Functions and dysfunctions of mitochondrial dynamics. Nat. Rev. Mol. Cell Biol. 8, 870–879.

Ding, W.X., Yin, X.M., 2012. Mitophagy: mechanisms, pathophysiological roles, and analysis. Biol. Chem. 393, 547–564.

Drose, S., Brandt, U., 2012. Molecular mechanisms of superoxide production by the mitochondrial respiratory chain. Adv. Exp. Med. Biol. 748, 145–169.

Eno, M.R., El-Gendy Bel, D., Cameron, M.D., 2016. P450 3A-catalyzed O-dealkylation of lapatinib induces mitochondrial stress and activates nrf2. Chem. Res. Toxicol. 29, 784–796.

Ghatalia, P., Je, Y., Mouallem, N.E., Nguyen, P.L., Trinh, Q.D., Sonpavde, G., Choueiri, T.K., 2015. Hepatotoxicity with vascular endothelial growth factor receptor tyrosine kinase inhibitors: a meta-analysis of randomized clinical trials. Crit. Rev. Oncol. Hematol. 93, 257–276.

Green, D.R., Reed, J.C., 1998. Mitochondria and apoptosis. Science 281, 1309–1312.

Hamacher-Brady, A., Brady, N.R., 2016. Mitophagy programs: mechanisms and physiological implications of mitochondrial targeting by autophagy. Cell Mol. Life Sci. 73, 775–795.

Herbrink, M., de Vries, N., Rosing, H., Huitema, A.D., Nuijen, B., Schellens, J.H., Beijnen, J.H., 2016. Quantification of 11 therapeutic kinase inhibitors in human plasma for therapeutic drug monitoring using liquid chromatography coupled with tandem mass spectrometry. Ther. Drug Monit. 38, 649–656.

Hoppel, C., DiMarco, J.P., Tandler, B., 1979. Riboflavin and rat hepatic cell structure and function. Mitochondrial oxidative metabolism in deficiency states. J. Biol. Chem. 254, 4164–4170.

Huynh, H.H., Pressiat, C., Sauvageon, H., Madelaine, I., Maslanka, P., Lebbe, C., Thieblemont, C., Goldwirt, L., Mourah, S., 2017. Development and validation of a simultaneous quantification method of 14 tyrosine kinase inhibitors in human plasma using LC-MS/MS. Ther. Drug Monit. 39, 43–54.

Josephs, D.H., Fisher, D.S., Spicer, J., Flanagan, R.J., 2013. Clinical pharmacokinetics of tyrosine kinase inhibitors: implications for therapeutic drug monitoring. Ther. Drug Monit. 35, 562–587.

Kamalian, L., Chadwick, A.E., Bayliss, M., French, N.S., Monshouwer, M., Snoeys, J., Park, B.K., 2015. The utility of HepG2 cells to identify direct mitochondrial dysfunction in the absence of cell death. Toxicol. In Vitro 29, 732–740.

Kerkela, R., Grazette, L., Yacobi, R., Iliescu, C., Patten, R., Beahm, C., Walters, B., Shevtsov, S., Pesant, S., Clubb, F.J., Rosenzweig, A., Salomon, R.N., Van Etten, R.A., Alroy, J., Durand, J.B., Force, T., 2006. Cardiotoxicity of the cancer therapeutic agent imatinib mesylate. Nat. Med. 12, 908–916.

Klempner, S.J., Choueiri, T.K., Yee, E., Doyle, L.A., Schuppan, D., Atkins, M.B., 2012. Severe pazopanib-induced hepatotoxicity: clinical and histologic course in two patients. J. Clin. Oncol. 30, e264–e268.

Krahenbuhl, S., Chang, M., Brass, E.P., Hoppel, C.L., 1991. Decreased activities of ubiquinol:ferricytochrome c oxidoreductase (complex III) and ferrocytochrome c:oxygen oxidoreductase (complex IV) in liver mitochondria from rats with hydroxycobalamin [c-lactam]-induced methylmalonic aciduria. J. Biol. Chem. 266, 20998–21003.

Krahenbuhl, S., Talos, C., Wiesmann, U., Hoppel, C.L., 1994. Development and evaluation of a spectrophotometric assay for complex III in isolated mitochondria, tissues and fibroblasts from rats and humans. Clin. Chim. Acta 230, 177–187.

Lang, C., Schafer, M., Varga, L., Zimmermann, A., Krahenbuhl, S., Krahenbuhl, L., 2002. Hepatic and skeletal muscle glycogen metabolism in rats with short-term cholestasis. J. Hepatol. 36, 22–29.

Lau, C.L., Chan, S.T., Selvaratanam, M., Khoo, H.W., Lim, A.Y., Modamio, P., Marino, E.L., Segarra, I., 2015. Sunitinib-ibuprofen drug interaction affects the pharmacokinetics and tissue distribution of sunitinib to brain, liver, and kidney in male and female mice differently. Fundam. Clin. Pharmacol. 29, 404–416.

Levitzki, A., Gazit, A., 1995. Tyrosine kinase inhibition: an approach to drug development. Science 267, 1782–1788.

Marroquin, L.D., Hynes, J., Dykens, J.A., Jamieson, J.D., Will, Y., 2007. Circumventing the Crabtree effect: replacing media glucose with galactose increases susceptibility of HepG2 cells to mitochondrial toxicants. Toxicol. Sci. 97, 539–547.

Mingard, C., Paech, F., Bouitbir, J., Krähenbühl, S., 2017. Mechanisms of toxicity associated with six tyrosine kinase inhibitors in human hepatocyte cell lines. J. Appl. Toxicol.(october). http://dx.doi.org/10.1002/jat.3551. [Epub ahead of print].

Mir, O., Brodowicz, T., Italiano, A., Wallet, J., Blay, J.Y., Bertucci, F., Chevreau, C., Piperno-Neumann, S., Bompas, E., Salas, S., Perrin, C., Delcambre, C., Liegl-Atzwanger, B., Toulmonde, M., Dumont, S., Ray-Coquard, I., Clisant, S., Taieb, S., Guillemet, C., Rios, M., Collard, O., Bozec, L., Cupissol, D., Saada-Bouzid, E., Lemaignan, C., Eisterer, W., Isambert, N., Chaigneau, L., Cesne, A.L., Penel, N., 2016. Safety and efficacy of regorafenib in patients with advanced soft tissue sarcoma (REGOSARC): a randomised, double-blind, placebo-controlled, phase 2 trial. Lancet Oncol. 17, 1732–1742.

Paech, F., Bouitbir, J., Krahenbuhl, S., 2017a. Hepatocellular toxicity associated with tyrosine kinase inhibitors: mitochondrial damage and inhibition of glycolysis. Front. Pharmacol. 8, 367.

Paech, F., Messner, S., Spickermann, J., Wind, M., Schmitt-Hoffmann, A.H., Witschi, A.T., Howell, B.A., Church, R.J., Woodhead, J., Engelhardt, M., Krahenbuhl, S., Maurer, M., 2017b. Mechanisms of hepatotoxicity associated with the monocyclic beta-lactam

antibiotic BAL30072. Arch. Toxicol. 91 (11), 3647–3662.
Palikaras, K., Tavernarakis, N., 2014. Mitochondrial homeostasis: the interplay between mitophagy and mitochondrial biogenesis. Exp. Gerontol. 56, 182–188.
Palmer, C.S., Osellame, L.D., Stojanovski, D., Ryan, M.T., 2011. The regulation of mitochondrial morphology: intricate mechanisms and dynamic machinery. Cell. Signal. 23, 1534–1545.
Pesta, D., Gnaiger, E., 2012. High-resolution respirometry: OXPHOS protocols for human cells and permeabilized fibers from small biopsies of human muscle. Methods Mol. Biol. (Clifton N.J.) 810, 25–58.
Shah, R.R., Morganroth, J., Shah, D.R., 2013. Hepatotoxicity of tyrosine kinase inhibitors: clinical and regulatory perspectives. Drug Saf. 36, 491–503.
Shchemelinin, I., Sefc, L., Necas, E., 2006. Protein kinases, their function and implication in cancer and other diseases. Folia Biol. (Praha) 52, 81–100.
Spraggs, C.F., Xu, C.F., Hunt, C.M., 2013. Genetic characterization to improve interpretation and clinical management of hepatotoxicity caused by tyrosine kinase inhibitors. Pharmacogenomics 14, 541–554.
Sunakawa, Y., Furuse, J., Okusaka, T., Ikeda, M., Nagashima, F., Ueno, H., Mitsunaga, S., Hashizume, K., Ito, Y., Sasaki, Y., 2014. Regorafenib in Japanese patients with solid tumors: phase I study of safety, efficacy, and pharmacokinetics. Invest. New Drugs 32, 104–112.
Swiss, R., Will, Y., 2011. Assessment of mitochondrial toxicity in HepG2 cells cultured in high-glucose- or galactose-containing media. Curr. Protoc. Toxicol (Chapter 2, Unit2 20).
Talbert, D.R., Doherty, K.R., Trusk, P.B., Moran, D.M., Shell, S.A., Bacus, S., 2015. A multi-parameter in vitro screen in human stem cell-derived cardiomyocytes identifies ponatinib-induced structural and functional cardiac toxicity. Toxicol. Sci. 143, 147–155.
Weng, Z., Luo, Y., Yang, X., Greenhaw, J.J., Li, H., Xie, L., Mattes, W.B., Shi, Q., 2015. Regorafenib impairs mitochondrial functions, activates AMP-activated protein kinase, induces autophagy, and causes rat hepatocyte necrosis. Toxicology 327, 10–21.
Westermann, B., 2010. Mitochondrial fusion and fission in cell life and death. Nat. Rev. Mol. Cell Biol. 11, 872–884.
Will, Y., Dykens, J.A., Nadanaciva, S., Hirakawa, B., Jamieson, J., Marroquin, L.D., Hynes, J., Patyna, S., Jessen, B.A., 2008. Effect of the multitargeted tyrosine kinase inhibitors imatinib, dasatinib, sunitinib, and sorafenib on mitochondrial function in isolated rat heart mitochondria and H9c2 cells. Toxicol. Sci. 106, 153–161.
Xue, T., Luo, P., Zhu, H., Zhao, Y., Wu, H., Gai, R., Wu, Y., Yang, B., Yang, X., He, Q., 2012. Oxidative stress is involved in Dasatinib-induced apoptosis in rat primary hepatocytes. Toxicol. Appl. Pharmacol. 261, 280–291.
Youle, R.J., van der Bliek, A.M., 2012. Mitochondrial fission, fusion, and stress. Science 337, 1062–1065.
Zhang, J., Salminen, A., Yang, X., Luo, Y., Wu, Q., White, M., Greenhaw, J., Ren, L., Bryant, M., Salminen, W., Papoian, T., Mattes, W., Shi, Q., 2017. Effects of 31 FDA approved small-molecule kinase inhibitors on isolated rat liver mitochondria. Arch. Toxicol. 91, 2921–2938.
Zungu, M., Schisler, J., Willis, M.S., 2011. All the little pieces -regulation of mitochondrial fusion and fission by ubiquitin and small ubiquitin-like modifer and their potential relevance in the heart. Circ. J. 75, 2513–2521.

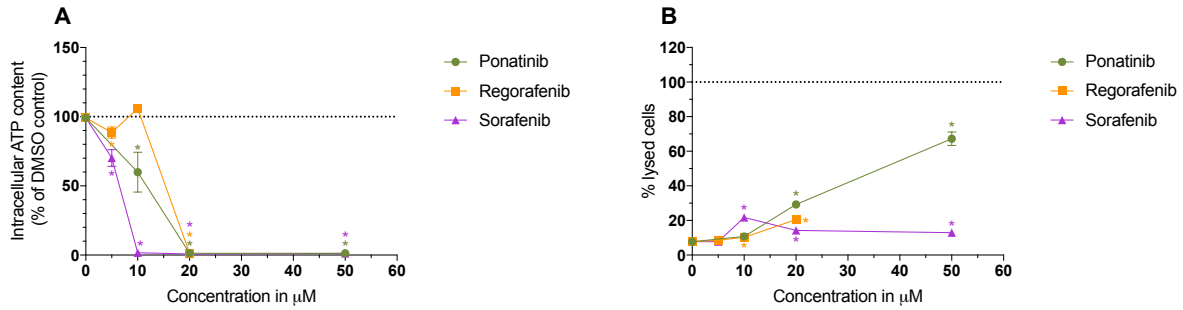

Supplementary Fig. S1. Intracellular ATP content and cytotoxicity in HepG2 cells with galactose medium. Cytotoxicity was assessed by the release of adenylate kinase. Intracellular ATP content (A) and cytotoxicity (B) were measured after exposure for 24 hours with ponatinib, regorafenib, and sorafenib. HepG2 cells were switched to 10 mM galactose medium 24 h before starting the treatment. Data are expressed as the decrease compared to control incubations containing 0.1% DMSO. Cytotoxicity data are expressed as the percentage of lysed cells with the values obtained for Triton X 0.1% set as 100%. Data represent the mean±SEM of at least three independent experiments. *p < 0.05 versus DMSO 0.1% control.

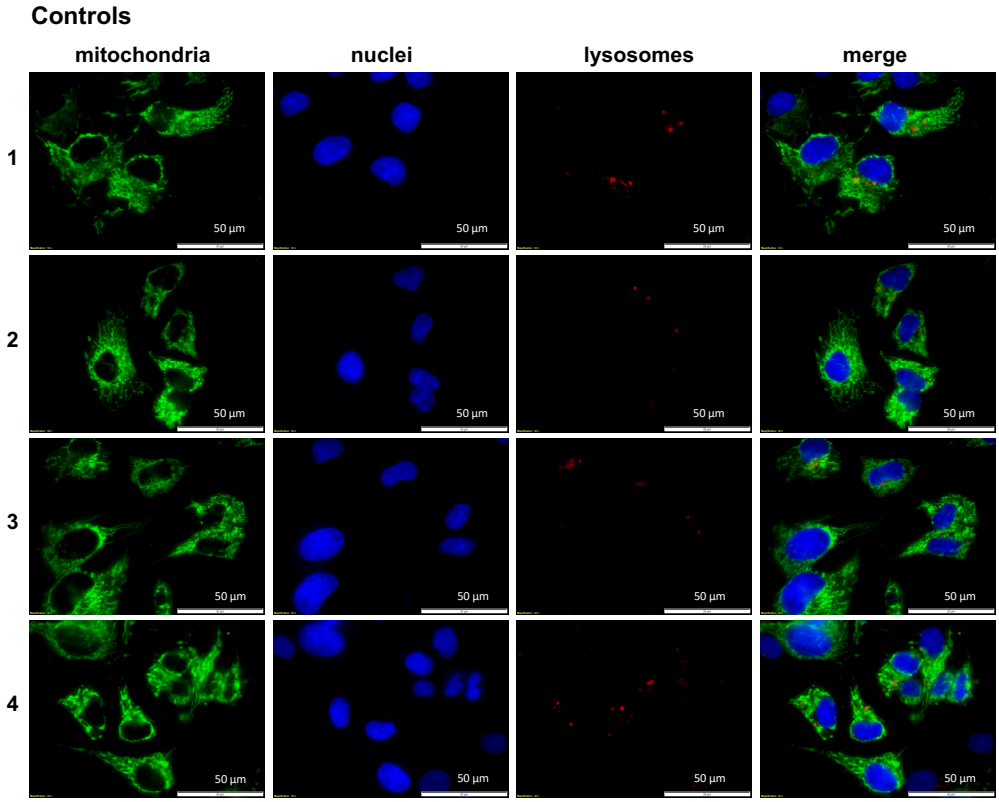

Supplementary Fig. S2. Morphology of HepG2 cells. HepG2 cells were cultured in the presence of 0.1% DMSO and stained with mitotracker (mitochondria), Hoechst 33258 (nuclei) and lysotracker (lysosomes) as described in Methods. Mitochondria form a network and there are only few lysosomes. Mitophagy (mitochondria in lysosomes rendering lysosomes yellow in merge) is absent. There is also no apoptosis (lysosomes digesting nuclear fragments are purple in merge).

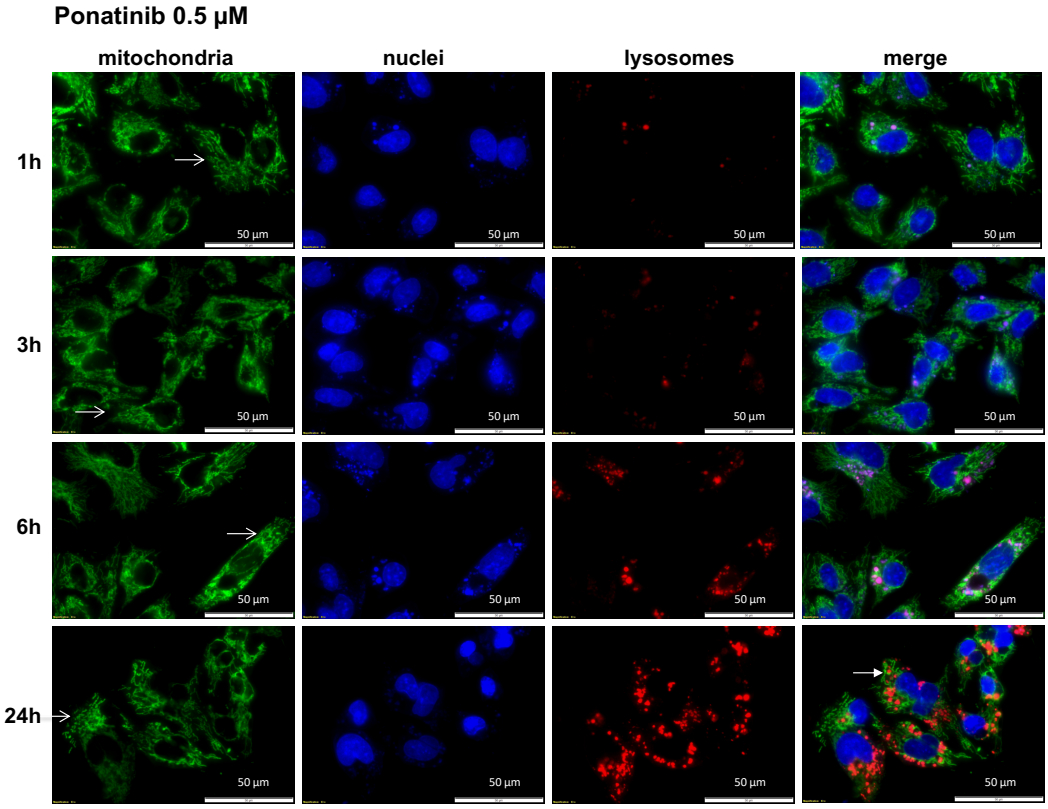

Supplementary Fig. S3. Effect of ponatinib 0.5 µM on the morphology of HepG2 cells. HepG2 cells were exposed to 0.5 µM ponatinib for 1h, 3h, 6h or 24h. Cells were stained with mitotracker (mitochondria), Hoechst 33258 (nuclei) and lysotracker (lysosomes) as described in Methods. Open arrows indicate mitochondrial fission and closed arrows mitophagy (lysosomes containing mitochondria are yellow in merge). Purple lysosomes in merge indicate apoptosis.

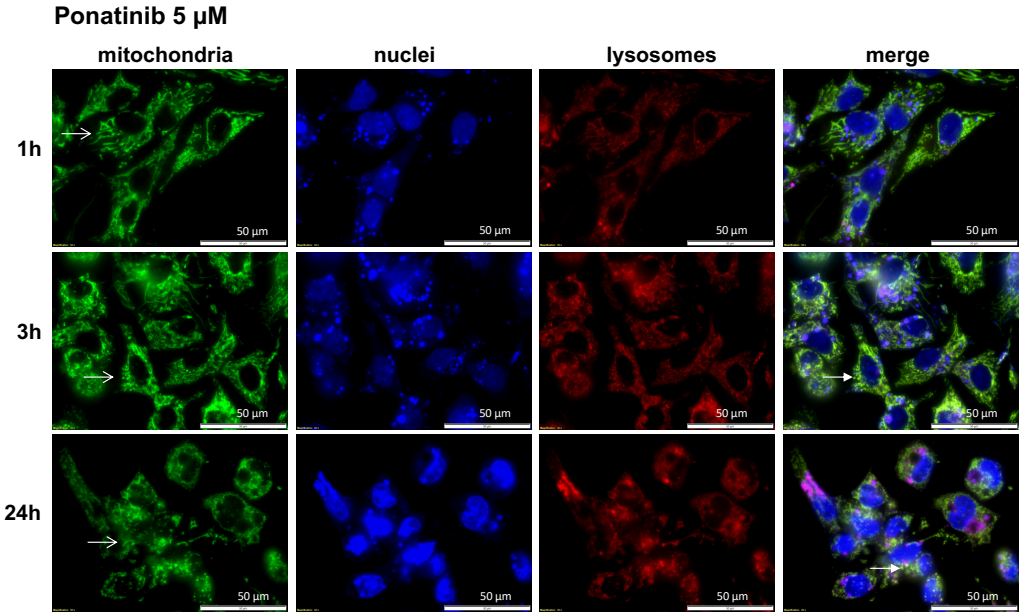

Supplementary Fig. S4. Effect of ponatinib 5 µM on the morphology of HepG2 cells. HepG2 cells were exposed to 5 µM ponatinib for 1h, 3h or 24h. Cells were stained with mitotracker (mitochondria), Hoechst 33258 (nuclei) and lysotracker (lysosomes) as described in Methods. Open arrows indicate mitochondrial fission and closed arrows mitophagy (lysosomes containing mitochondria are yellow in merge). Purple lysosomes in merge indicate apoptosis (lysosomes digesting nuclear debris appear purple).

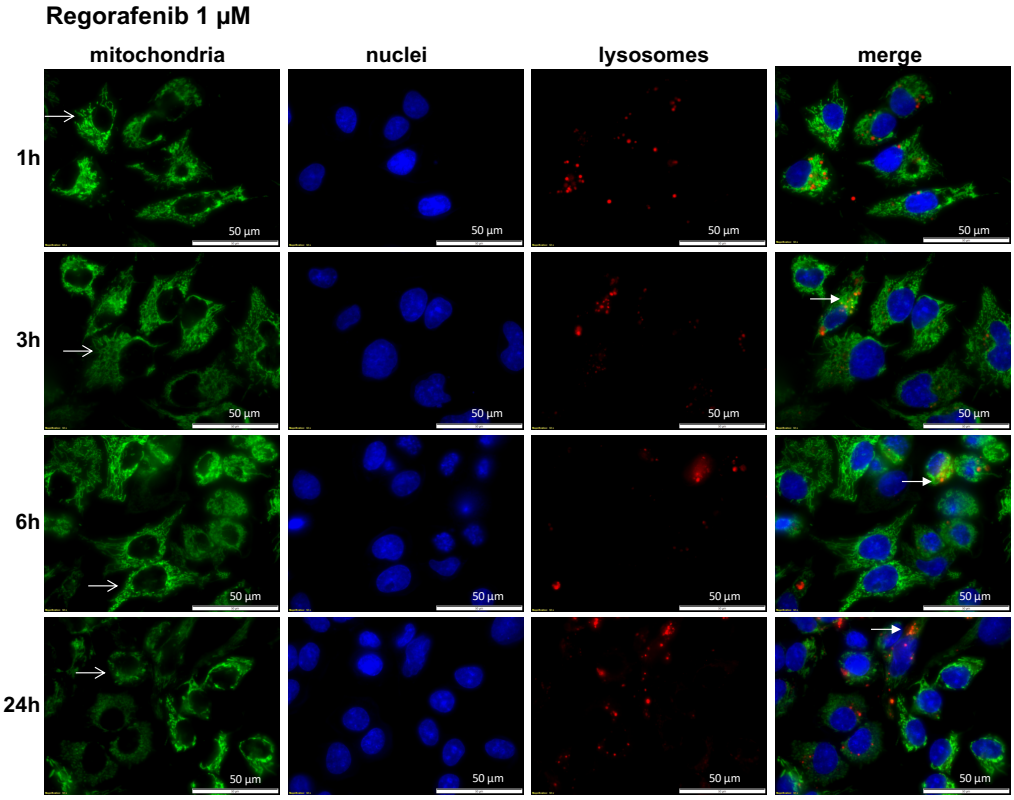

Supplementary Fig. S5. Effect of regorafenib 1 µM on the morphology of HepG2 cells. HepG2 cells were exposed to 1 µM regorafenib for 1h, 3h, 6h or 24h. Cells were stained with mitotracker (mitochondria), Hoechst 33258 (nuclei) and lysotracker (lysosomes) as described in Methods. Open arrows indicate mitochondrial fission and closed arrows mitophagy (lysosomes containing mitochondria are yellow in merge). Purple lysosomes in merge indicate apoptosis (lysosomes digesting nuclear debris appear purple).

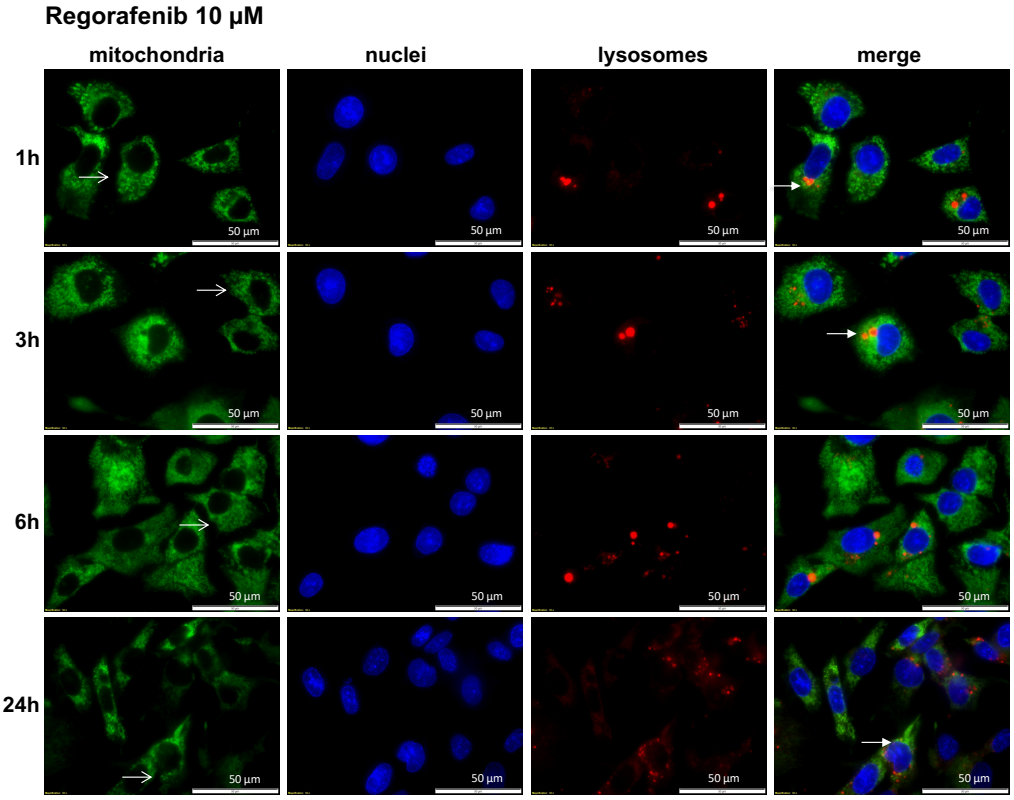

Supplementary Fig. S6. Effect of regorafenib 10 µM on the morphology of HepG2 cells. HepG2 cells were exposed to 10 µM regorafenib for 1h, 3h, 6h or 24h. Cells were stained with mitotracker (mitochondria), Hoechst 33258 (nuclei) and lysotracker (lysosomes) as described in Methods. Open arrows indicate mitochondrial fission and closed arrows mitophagy (lysosomes containing mitochondria are yellow in merge). Purple lysosomes in merge indicate apoptosis (lysosomes digesting nuclear debris appear purple).

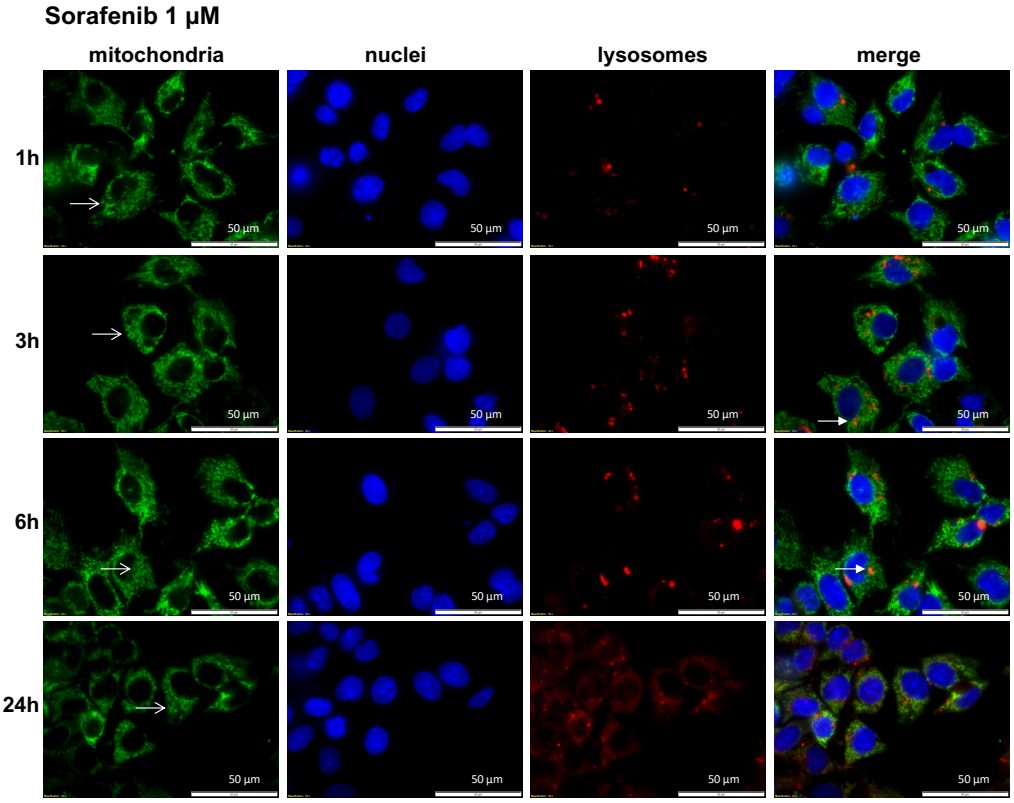

Supplementary Fig. S7. Effect of sorafenib 1 µM on the morphology of HepG2 cells. HepG2 cells were exposed to 1 µM sorafenib for 1h, 3h, 6h or 24h. Cells were stained with mitotracker (mitochondria), Hoechst 33258 (nuclei) and lysotracker (lysosomes) as described in Methods. Open arrows indicate mitochondrial fission and closed arrows mitophagy (lysosomes containing mitochondria are yellow in merge). Purple lysosomes in merge indicate apoptosis (lysosomes digesting nuclear debris appear purple).

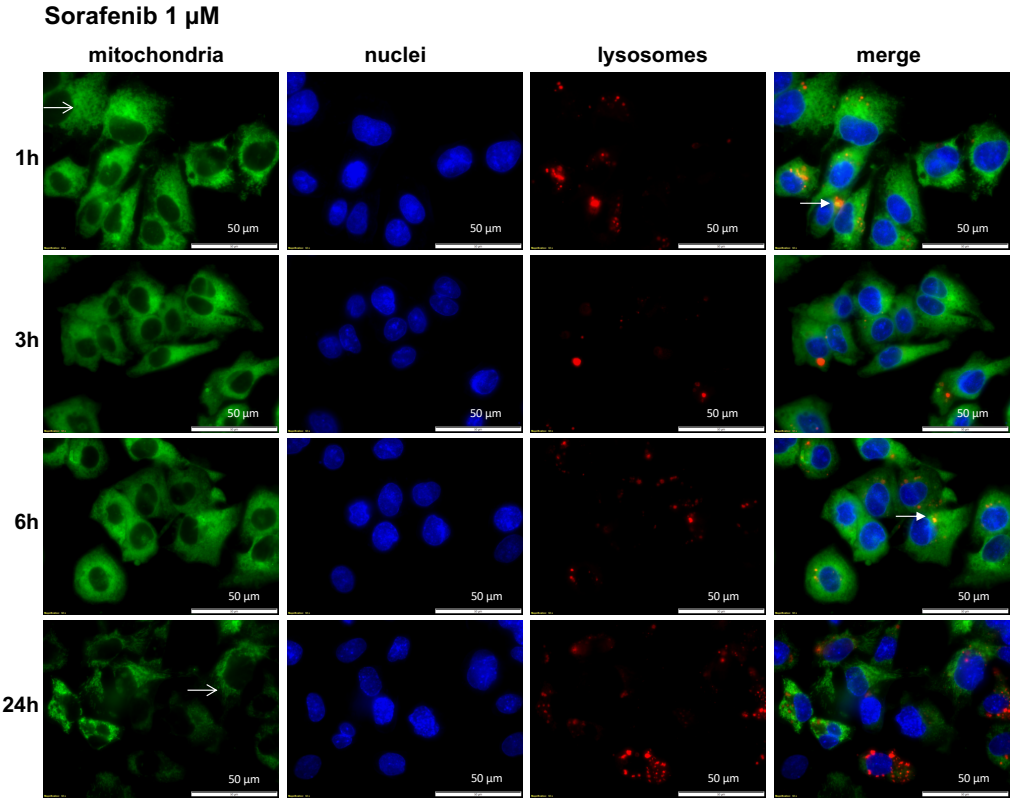

Supplementary Fig. S8. Effect of sorafenib 10 µM on the morphology of HepG2 cells. HepG2 cells were exposed to 10 µM sorafenib for 1h, 3h, 6h or 24h. Cells were stained with mitotracker (mitochondria), Hoechst 33258 (nuclei) and lysotracker (lysosomes) as described in Methods. Open arrows indicate mitochondrial fission and closed arrows mitophagy (lysosomes containing mitochondria are yellow in merge). Purple lysosomes in merge indicate apoptosis (lysosomes digesting nuclear debris appear purple).

4 PAPER 4

SUNITINIB INDUCES HEPATOCYTE MITOCHONDRIAL DAMAGE AND APOPTOSIS IN MICE

Within this article, we switched to the *in vivo* situation and will investigate the mechanisms of hepatotoxicity for sunitinib in mice.

Toxicology 409 (2018) 13–23

Contents lists available at ScienceDirect

Toxicology

journal homepage: www.elsevier.com/locate/toxicol

Sunitinib induces hepatocyte mitochondrial damage and apoptosis in mice

Franziska Paech[a,b], Vanessa F. Abegg[a,b], Urs Duthaler[a,b], Luigi Terracciano[c,d], Jamal Bouitbir[a,b,c], Stephan Krähenbühl[a,b,c,*]

[a] Division of Clinical Pharmacology & Toxicology, University Hospital, Basel, Switzerland
[b] Department of Biomedicine, University of Basel, Switzerland
[c] Swiss Centre for Applied Human Toxicology, Switzerland
[d] Department of Molecular Pathology, Institute for Pathology, University Hospital Basel, Switzerland

ARTICLE INFO

Keywords:
Sunitinib
Hepatotoxicity
Mitochondrial toxicity
Reactive oxygen species (ROS)
Apoptosis
PGC-1α

ABSTRACT

Reports concerning hepatic mitochondrial toxicity of sunitinib are conflicting. We therefore decided to conduct a toxicological study in mice. After having determined the highest dose that did not affect nutrient ingestion and body weight, we treated mice orally with sunitinib (7.5 mg/kg/day) for 2 weeks. At the end of treatment, peak sunitinib plasma concentrations were comparable to those achieved in humans and liver concentrations were approximately 25-fold higher than in plasma. Sunitinib did not affect body weight, but increased plasma ALT activity 6-fold. The activity of enzyme complexes of the electron transport chain (ETC) was decreased numerically in freshly isolated and complex III activity significantly in previously frozen liver mitochondria. In previously frozen mitochondria, sunitinib decreased NADH oxidase activity concentration-dependently in both treatment groups. The hepatic mitochondrial reactive oxygen species (ROS) content and superoxide dismutase 2 expression were increased in sunitinib-treated mice. Protein and mRNA expression of several subunits of mitochondrial enzyme complexes were decreased in mitochondria from sunitinib-treated mice. Protein expression of PGC-1α, citrate synthase activity and mtDNA copy number were all decreased in livers of sunitinib-treated mice, indicating impaired mitochondrial proliferation. Caspase 3 activation and TUNEL-positive hepatocytes were increased in livers of sunitinib-treated mice, indicating hepatocyte apoptosis. In conclusion, sunitinib caused concentration-dependent toxicity in isolated mitochondria at concentrations reached in livers in vivo and inhibited hepatic mitochondrial proliferation. Daily mitochondrial insults and impaired mitochondrial proliferation most likely explain hepatocellular injury observed in mice treated with sunitinib.

1. Introduction

Sunitinib is a multikinase inhibitor that was approved by the Food and Drug Administration (FDA) in 2006 for the treatment of patients with advanced renal cell carcinoma, and later for patients with gastrointestinal stromal tumor and patients with chronic myeloid leukemia with disease progression on imatinib or intolerance to imatinib (Goodman et al., 2007; Motzer et al., 2009). Sunitinib inhibits various receptor-associated kinases, for example the kinase of the vascular endothelial growth factor receptors (VEGFR) 1–3 (Mendel et al., 2003), of the platelet-derived growth factor receptors (PDGFR) α and β (Roskoski, 2007), of the fetal liver tyrosine kinase receptor 3 (FLT3) (O'Farrell et al., 2003), of the stem cell factor receptor (c-kit) (Abrams et al., 2003), and of the colony stimulating factor 1 receptor (CSF1R) (Murray et al., 2003). Accordingly, sunitinib inhibits angiogenesis, tumor growth and metastasis formation (Faivre et al., 2006).

Although the use of sunitinib is quite safe, the drug is associated with potentially severe adverse reactions including fatigue (Bello et al., 2006), hypertension (Motzer et al., 2009), hematotoxicity (Motzer et al., 2009), and, less frequently, posterior encephalopathy (Cumurciuc et al., 2008), cardiotoxicity (Demetri et al., 2006) and hepatotoxicity (Mueller et al., 2008). In clinical trials, the frequency of elevated serum transaminases in patients treated with sunitinib was 40–60% for all grades and 2–5% for grade 3 and 4 (≥5 times upper limit of normal) (Shah et al., 2013). Sunitinib-associated liver failure was observed in 0.3% of the patients and fatalities have been reported (Guillen et al., 2016).

The underlying mechanisms of the hepatotoxicity associated with sunitinib and with other kinase inhibitors are currently not fully elucidated. In HepG2 cells, we showed previously that sunitinib impaired oxygen consumption, reduced the mitochondrial membrane potential and increased mitochondrial reactive oxygen species (ROS) production

* Corresponding author at: Clinical Pharmacology & Toxicology, University Hospital, 4031 Basel, Switzerland.
E-mail address: stephan.kraehenbuehl@usb.ch (S. Krähenbühl).

https://doi.org/10.1016/j.tox.2018.07.009
Received 13 May 2018; Received in revised form 13 July 2018; Accepted 16 July 2018
Available online 18 July 2018
0300-483X/

(Paech et al., 2017a). These findings occurred at concentrations that can be reached in patients, suggesting that hepatotoxicity associated with sunitinib can be caused by mitochondrial dysfunction. This interpretation is supported by similar findings with other kinase inhibitors, e.g. dasatinib (Xue et al., 2012) and regorafenib (Weng et al., 2015). In addition, in a recent study, the kinase inhibitors sorafenib, regorafenib and pazopanib impaired oxidative phosphorylation of rat liver mitochondria (Zhang et al., 2017). In the study of Zhang et al. sunitinib was, however, not toxic for isolated rat liver mitochondria.

Considering hepatic mitochondrial toxicity of sunitinib, so far only studies with isolated rat liver mitochondria (Zhang et al., 2017) and HepG2 cells (Paech et al., 2017a) have been published, whereas *in vivo* studies are lacking. For this reason, we decided to investigate the hepatotoxic potential of sunitinib in mice in vivo. In addition, we planned to isolate and characterize liver mitochondria and to test direct effects of sunitinib on these mitochondria. The current investigation could help to resolve the discrepancy between the study in isolated rat liver mitochondria (no toxicity) (Zhang et al., 2017) and in HepG2 cells (mitochondrial toxicity) (Paech et al., 2017a). In order to reach our aims, we first performed a dose-finding study aiming at finding a sunitinib dose that did not interfere with food intake and body weight of the animals. After that, we investigated the effect of sunitinib on liver morphology and composition as well as on the function of the mitochondrial respiratory chain and on mechanism of cell death in mice treated with this compound.

2. Materials and methods

2.1. Chemicals

Sunitinib was purchased from Carbosynth (San Diego, CA, USA). All other chemicals used in this study were purchased from Sigma-Aldrich (Buchs, Switzerland), if not indicated differently.

2.2. Animals

Male C57BL/6NRj mice (n = 32, age 7–10 weeks) were purchased from Elevage Janvier (Le Genest-Saint-Isle, France) and were acclimatized one week prior to the start of the study. The animals were housed in a standard facility with 12 h light-dark cycles and controlled temperature (21–22 °C). The mice were fed a standard pellet chow and water *ad libitum*. Experiments were reviewed and accepted by the cantonal veterinary authority of Basel, Switzerland (License 2873) and were performed in agreement with the guidelines for care and use of laboratory animals.

2.3. Study design and sunitinib administration

This study was performed in two steps. For the dose finding study (Part 1), 12 mice were randomly assigned to one of the 4 groups after one week of acclimatization: (1) animals treated with water for 14 days (n = 3); (2) animals treated with 5 mg/kg/day sunitinib for 14 days (n = 3); (3) animals treated with 10 mg/kg/day sunitinib for 7 days (n = 3); (4) animals treated with 20 mg/kg/day sunitinib for 7 days (n = 3).

For the part 2, 20 mice were randomly divided into two groups after one week of acclimatization: (1) animals treated with water for 14 days (n = 10); (2) animals treated with sunitinib (7.5 mg/kg/day for 14 days; n = 10). This dose of sunitinib was determined according to the results of the part 1.

Sunitinib was dissolved in water and the animals were treated once daily by oral gavage. Food and water consumption and changes in body weight were examined every day.

2.4. Sample collection

After the treatment for 7 or 14 days, the mice were anesthetized with an intraperitoneal application of ketamine (100 mg/kg) and xylazine (10 mg/kg). Then, blood was collected into heparin-coated tubes by intracardiac puncture. Plasma was separated by centrifugation at 3000 g for 15 min. The liver was immediately collected, weighed, and a part of the tissue was immediately frozen in isopentane cooled by liquid nitrogen and stored at −80 °C for later biochemical or histological analysis. The rest of the liver was used to isolate mitochondria. Plasma samples were kept at −80 °C until analysis.

2.5. Plasma and liver parameters

Mouse plasma was analyzed for the activity of alanine aminotransferase using the Alanine Aminotransferase Activity Assay Kit (Buchs, Switzerland). The liver glycogen content was determined after enzymatic digestion as glucose as described previously (Lang et al., 2002).

Plasma and liver concentrations of sunitinib (Toronto Research Chemicals, Ontario, Canada) were determined by liquid chromatography tandem mass spectrometry (LC–MS/MS). The LC–MS/MS system consisted of a Nexera SIL-30AC autosampler, a column-oven (CTO-20AC), four HPLC pumps (LC30AD), and a system controller (CBM-20 A), all acquired from Shimadzu (Kyoto, Japan). The UPLC system was coupled to a 5500 Q-Trap triple quadrupole mass spectrometer from AB Sciex (Concord, Canada), equipped with a turbo electrospray ionization source.

Plasma samples were precipitated with internal standard solution (5 ng/ml sunitinib-d10 [Toronto Research Chemicals, Ontario, Canada] in methanol) in a ratio of 1:20 (v/v). The suspension was centrifuged at 3220 × g for 30 min (Eppendorf Centrifuge 5810R) before 5 µL of the sample was injected into the system. Approximately 10 mg of liver was homogenized with a vibrating microbead homogenizer (Mikro-Dismembrator, Sartorius, Palaiseau, France) during 1 min at 2000 rpm. The liver tissue was extracted with 1 mL of methanol:water (1:1 v/v), containing 2.5 ng/ml sunitinib-d10. The samples were centrifuged at 3220 x g for 30 min and 5 µL supernatant were applied into the LC–MS/MS system. The samples were separated on a Kinetex F5 analytical column (50 × 2.1 mm, 2.6 µm 100 A, Phenomenex, Torrance, CA, USA) at 50 °C. The mobile phase A was water and mobile phase B methanol, both supplemented with 0.1% formic acid. Samples were loaded onto the analytical column using 20% mobile phase B. After 0.25 min the gradient was linearly increased within 1.5 min, reaching 95% mobile phase B. The column was washed for 0.5 min at 95% and thereafter reconditioned for another 0.3 min at 20% mobile phase B. The retention time of sunitinib was 1.6 min.

Sunitinib (399.1 → 283.1 *m/z*) and sunitinib-d10 (409.2 → 283.1 *m/z*) were analyzed in the positive mode by multiple reaction monitoring (MRM). The ion spray voltage was 5500 eV, the probe temperature was 500 °C, and the dwell time was 150 ms for each analyte.

2.6. Histological analysis of liver tissue

Cross sections (10 µm) with a cryostat microtome (CM1950, Leica, Wetzlar, Germany) were fixed with paraformaldehyde 4%. All sections were stained with hematoxylin eosin for a coarse assessment of tissue damage.

The glycogen content was investigated using periodic acid Schiff staining on paraformaldehyde fixed sections. For that, sections were incubated in 0.5% periodic acid for 8 min, washed in running water for 5 min and in distilled water twice for several seconds. Afterwards, they were incubated in Schiff' s solution for 10 min, followed by 0.5% sodium metabisulfite 3 times for 3 min each. Finally, cover slips were placed on glass slides with a mounting medium and observed under a light microscope.

Lipid accumulation was investigated by Oil red O staining of frozen liver sections. Oil red O was freshly diluted (3:2 in distilled water) from a stock solution in isopropanol (0.5 g in 100 ml) and sections were incubated for 15 min. After incubation, the slides were rinsed with 60% isopropanol, counterstained with haematoxylin and coverslipped in aqueous mountant. Collagen for fibrosis was detected by staining sections with 0.1% Sirius Red.

Pictures were captured on an Olympus IX83 microscope (60x objective; Olympus, Volketswil, Switzerland). The stained sections were investigated for pathological changes in the liver with the examiner blinded regarding the treatment of the animals.

2.7. Isolation of mouse liver mitochondria

Liver mitochondria were isolated by differential centrifugation as described before (Hoppel et al., 1979). The mitochondrial protein content was determined using the Pierce BCA protein assay kit from Merck (Zug, Switzerland).

2.8. Mitochondrial membrane potential

The mitochondrial membrane potential ($\Delta\Psi_m$) was determined using the [phenyl-^{3}H]-tetraphenylphosphonium bromide uptake assay. Freshly isolated mouse-liver mitochondria (100 µg protein/ml) were washed with incubation buffer (137.3 mM sodium chloride, 4.74 mM potassium chloride, 2.56 mM calcium chloride, 1.18 mM potassium phosphate, 1.18 mM magnesium chloride, 10 mM HEPES, 1 g/l glucose, pH 7.4). Mitochondria were then incubated at 37 °C in buffer containing 0.5 µl/ml [phenyl-^{3}H]-tetraphenylphosphonium bromide (40 Ci/mmol, Anawa trading SA, Wangen, Switzerland). After 15 min, the suspension was centrifuged and the mitochondrial pellet resuspended twice in fresh non-radioactive incubation buffer. The radioactivity of the pellet was measured on a Packard 1900 TR liquid scintillation analyzer. For the interpretation, we set the total count ([^{3}H]-TPP (0.5 µl/ml)) as 100%.

2.9. Activity of specific enzyme complexes of the mitochondrial electron transport chain in freshly isolated mouse liver mitochondria

The activity of specific enzyme complexes of the respiratory chain was analyzed using an Oxygraph-2k high-resolution respirometer equipped with DataLab software (Oroboros instruments, Innsbruck, Austria) as described previously (Paech et al., 2017b). Freshly isolated liver mitochondria (250 µg protein/chamber) were suspended in mitochondrial respiration medium MiR06 (mitochondrial respiration medium containing 0.5 mM EGTA, 3 mM magnesium chloride, 20 mM taurine, 10 mM potassium dihydrogen phosphate, 20 mM HEPES, 110 mM sucrose, 1 g/l fatty-acid free bovine serum albumin, 60 mM lactobionic acid, and 280 U/ml catalase, pH 7.1) and transferred to the pre-calibrated Oxygraph chamber (Pesta and Gnaiger, 2012).

Complexes I and III were analyzed using L-glutamate and malate (10 and 2 mM, respectively) as substrates followed by the addition of adenosine-diphosphate (ADP; 2.5 mM). Then, we added oligomycin (2.5 µM) for the determination of the leak-state respiration. This was followed by the addition of FCCP (1 µM) to reach a full stimulation of the electron transport chain. After that, we added rotenone (0.5 µM) as an inhibitor of complex I. Afterwards, duroquinol (500 µM) was added to investigate complex III activity, followed by the complex III inhibitor antimycin A (2.5 µM).

Complexes II and IV were analyzed using succinate and rotenone (10 mM and 0.5 µM, respectively) as substrates followed by the addition of ADP (2.5 mM). Then, we added oligomycin (2.5 µM) for the determination of the leak-state respiration. This was followed by the addition of FCCP (1 µM) to reach a full stimulation of the electron transport chain.

Then, we added the complex III inhibitor antimycin A (2.5 µM). *N*,*N*,*N*',*N*'-tetramethyl-1,4-phenylendiamine and ascorbate (0.5 and 2 mM, respectively) were then added to investigate complex IV, followed by the complex IV inhibitor KCN (1 mM). The integrity of the outer mitochondrial membrane was confirmed by the absence of a stimulatory effect of exogenous cytochrome *c* (10 µM) on respiration.

2.10. Activity of enzyme complexes of the electron transport chain in previously frozen liver mitochondria

The individual activities of mitochondrial enzyme complexes (I-IV) were assessed by well-established spectrophotometric methods (Krahenbuhl et al., 1991, 1994) in isolated frozen mouse liver mitochondria.

Briefly, for complex I, we used the conversion of NADH to NAD using decylubiquinone as an electron acceptor and monitoring at 340 nm. The activity of complex II was based on the conversion of oxidized dichloroindophenol to its reduced form at 600 nm using succinate as substrate. For complex III, we used decylubiquinol as a substrate and determined the conversion of ferricytochrome *c* to ferrocytochrome *c* at 550 nm. For complex IV, we followed the conversion of ferrocytochrome *c* to ferricytochrome *c* at 550 nm using ubiquinol as substrate. The activity of the respective enzyme complexes was determined as the difference in the presence of specific inhibitors (rotenone for complex I, thenoyltrifluroacetone for complex II, antimycin A for complex III and sodium azide for complex IV).

2.11. Activity of the mitochondrial NADH oxidase

The activity of the NADH oxidase was determined with previously frozen mitochondria using a Oxygraph-2k high-resolution respirometer equipped with DataLab software (Oroboros instruments, Innsbruck, Austria) as described previously (Krahenbuhl et al., 1991).

2.12. Levels of mRNA expression

Total RNA was extracted and purified from liver using the Qiagen Rneasy mini extraction kit (Qiagen, Hombrechtikon, Switzerland) and RNA quality was evaluated with the NanoDrop 2000 (Thermo Scientific, Wohlen, Switzerland). The Qiagen omniscript system was used to synthesize cDNA from 1 µg RNA. The expression of mRNA was assessed using SYBR Green real-time PCR (Roche Diagnostics, Rotkreuz, Switzerland). Quantification was performed using the comperative-threshold cycle method. We used GAPDH as an endogenous reference after evaluation. The Ct values observed for mRNA form livers of control and sunitinib-treated mice were 19.57 and 19.70, respectively. The primers used were purchased from Mycrosynth (Balgach, Switzerland) and are listed in Table S1.

2.13. Western blotting

Liver samples (20 mg) were homogenized with a vibrating microbead homogenizer (Mikro-Dismembrator, Sartorius, Palaiseau, France) during 1 min at 2000 rpm. The resulting tissue samples were suspended in RIPA (150 mM sodium chloride, 1.0% NP-40, 0.5% sodium deoxycholate, 0.1% sodium dodecyl sulphate, 50 mM Tris, pH 8.0) buffer, centrifuged and the supernatant was collected. Proteins (10 µg) were resolved by SDS-PAGE using commercially available 4–12% NuPAGE Bis-Tris gels (Invitrogen, Basel, Switzerland) and transferred using the Trans-Blot Turbo Blotting System (Bio-Rad, Cressier, Switzerland). The membranes were incubated with Total OXPHOS Rodent WB Antibody Cocktail (1:500, ab110413, Abcam, Cambridge, UK), Anti-SOD2 antibody (1:2000, ab16956, Abcam, Cambridge, UK), Caspase-3 Rabbit antibody (1:1000, 8G10, Cell Signaling Technology, Cambridge, UK), and Anti-PCG1 alpha (1:1000, ab106814, Abcam, Cambridge, UK) antibodies. After washing, membranes were exposed to secondary antibodies (Santa Cruz

Biotechnology, Dallas, USA). Immunoblots were developed using Clarity Western ECL Substrate (Bio-Rad Laboratories, Hercules, USA). Protein expression was quantified using the Fusion Pulse TS device (Vilber Lourmat, Oberschwaben, Germany).

2.14. Mitochondrial superoxide content

Mitochondrial superoxide was determined using the MitoSOX Red fluorophore probe from Invitrogen (Basel, Switzerland), according to the manufacturer's manual. The MitoSOX Red mitochondrial superoxide indicator is a fluorogenic dye for selective detection of superoxide in the mitochondria of living cells. Mitochondria (200 µg protein) were incubated for 10 min at 37 °C with 2.5 µM MitoSOX together with L-glutamate (10 mM) and L-malic acid (2 mM). Afterwards, the fluorescence was measured using a Tecan M200 Pro Infinity plate reader (Männerdorf, Switzerland) with an excitation at 510 nm and an emission at 580 nm. The superoxide concentration increased linearly over 10 min. The MitoSOX signal was adjusted to the citrate synthase activity.

2.15. GSH content

Glutathione (GSH) levels in mouse liver were determined by LC−MS/MS. A 10 mM stock solution of GSH was prepared in water supplemented with 2% formic acid. GSH-d5 was used as internal standards (1 mM in DMSO). The thiol group of GSH was derivatized with *N*-ethylmaleimide (NEM) in order to inhibit autoxidation to GSSG (Lang et al., 2002). GSH and GSH-d5 were incubated for 1 h in the derivatization solution to form GSH-NEM and GSH-NEM-d5. Calibration line of GSH-NEM (250 µM–0.25 µM) was prepared in the derivatization solution. Internal standard solution of GSH-NEM-d5 was made in 2% formic acid (1 µM).

Approximately 10 mg of liver was homogenized with a vibrating microbead homogenizer (Mikro-Dismembrator, Sartorius, Palaiseau, France) during 1 min at 2000 rpm. The liver tissue was extracted with 1 ml per 10 mg tissue of the derivatization solution. Samples were vortex-mixed and incubated for 1 h in order to derivatize GSH. Mouse liver homogenate samples were centrifuged at 16,100 g for 10 min (Eppendorf 5415 R centrifuge, Hamburg, Germany) and the supernatant was transferred in another tube. Calibrators and mouse liver homogenate samples were diluted with internal standard solution in a ratio of 1:3 (v/v) and 2.5 µl were injected into the LC–MS/MS system. A Shimadzu HPLC (Kyoto, Japan) which was coupled to an API 4000 QTrap tandem mass spectrometer (ABSciex, Concord, Canada) was used to determine the GSH-NEM levels in mouse liver. The analytes were positively charged by electro spray ionization and analyzed with scheduled multiple reaction monitoring. The ion spray voltage was 5500 eV and the probe temperature was 700 °C. The following masses were used: 433.1 → 304.0 *m/z* for GSH-NEM and 438.1 → 304.1 *m/z* for GSH-NEM-d5.

GSH-NEM was separated on a Luna omega polar C18 analytical column (50 mm × 2.1 mm, 1.6 µm, Phenomenex, Torrance, CA, USA) at 45 °C and a flow rate of 0.4 mL/min. Water (mobile phase A) and acetonitrile (mobile phase B) both supplemented with 0.1% acetic acid were used as mobile phases. Samples were loaded onto the analytical column using 0% mobile phase B and were inline diluted via a T union with mobile phase A during the first 0.5 min of each run. After 0.5 min the gradient was linearly increased within 1.25 min, reaching 95% mobile phase B. The column was washed for 0.5 min at 95% mobile phase B and thereafter reconditioned for another 0.75 min at 0% mobile phase B. The retention time of GSH-NEM was 1.62 min. The limits of quantification for sunitinib were 0.63 nmol/L (0.25 mg/mL) in plasma and 31.4 nmol/kg (12.5 ng/g) in liver.

2.16. Citrate synthase

Liver samples (20 mg) were homogenized with a vibrating microbead homogenizer (Mikro-Dismembrator, Sartorius, Palaiseau, France) in RIPA (150 mM sodium chloride, 1.0% NP-40, 0.5% sodium deoxycholate, 0.1% sodium dodecyl sulphate, 50 mM Tris, pH 8.0) buffer. Citrate synthase activity was determined in the supernatant by spectrophotometry (Tecan M200 Pro Infinity plate reader, Männedorf, Switzerland) using a 96-well plate as described earlier (Srere, 1969).

2.17. Mitochondrial DNA copy number

Total DNA was extracted using the DNeasy Blood and Tissue Kit (Qiagen, Hombrechtikon, Switzerland) following the manufacturer's instructions. The concentration of the extracted DNA was measured spectrophotometrically at 260 nm with the NanoDrop 2000 (Thermo Scientific, Wohlen, Switzerland). Afterwards, DNA was diluted in RNase free water to a final concentration of 10 ng/µL. The expression of the mitochondrial COX2 and nuclear hexokinase 2 genes (see Suppl. Table 1 for primers) was evaluated using SYBR Green real-time PCR (Roche Diagnostics, Rotkreuz, Basel) and was performed on an ABI PRISM 7700 sequence detector (PE Biosystems, Rotkreuz, Switzerland). Quantification was performed using the comparative-threshold cycle method (Quiros et al., 2017)

2.18. TUNEL assessment of apoptosis

TUNEL staining of nuclei positive for DNA strand breaks was performed using the Click-iT TUNEL Alexa Fluor 647 Imaging Assay (Invitrogen, Basel, Switzerland) on randomly selected slides with sections (10 µm) of frozen liver samples. Sections were prepared using a cryostat microtome (CM1950, Leica, Wetzlar, Germany) according to the manufacturer's manual. After staining, the sections were embedded with ProLong diamond antifade mountant with DAPI (Life Technologies, Wohlen, Switzerland) and were investigated with a fluorescence microscope (×20 objective; Olympus IX83, Volketswil, Switzerland). TUNEL positive cells were calculated by counting the number of TUNEL-stained nuclei. This number was divided by the total number of nuclei and multiplied by 100 in order to obtain the percentage of TUNEL positive cells.

2.19. Statistical analysis

Data are given as the mean ± standard error of the mean (SEM). Statistical analyses were performed by unpaired Student t-tests using GraphPad Prism 7 (GraphPad Software, La Jolla, CA, USA). *P*-values < 0.05 (*) were considered to be significant.

3. Results

3.1. Dose finding study

The goal of the first part of this project was to determine the optimal dose of sunitinib for the second part of the project. For that, we treated mice with 5, 10 or 20 mg/kg per day. In comparison to control mice, mice treated with 10 mg/kg/day or 20 mg/kg/day consumed less food and water, and showed a decrease in body weight already after three or one day, respectively (Fig. 1A–C). In addition, they appeared to be less mobile than control mice. Therefore, we stopped the treatment with these dosages already after 7 days and sacrificed these mice. In contrast, we did not observe changes in water and food intake, body weight or mobility in mice treated 5 mg/kg/day compared to control mice (Fig. 1A–C). Of note, mice treated with sunitinib showed a non-significant, dose-dependent decrease in liver weight (Fig. 1D). Based on these data, we performed the second part of this animal study with 7.5 mg/kg/day sunitinib for 14 days.

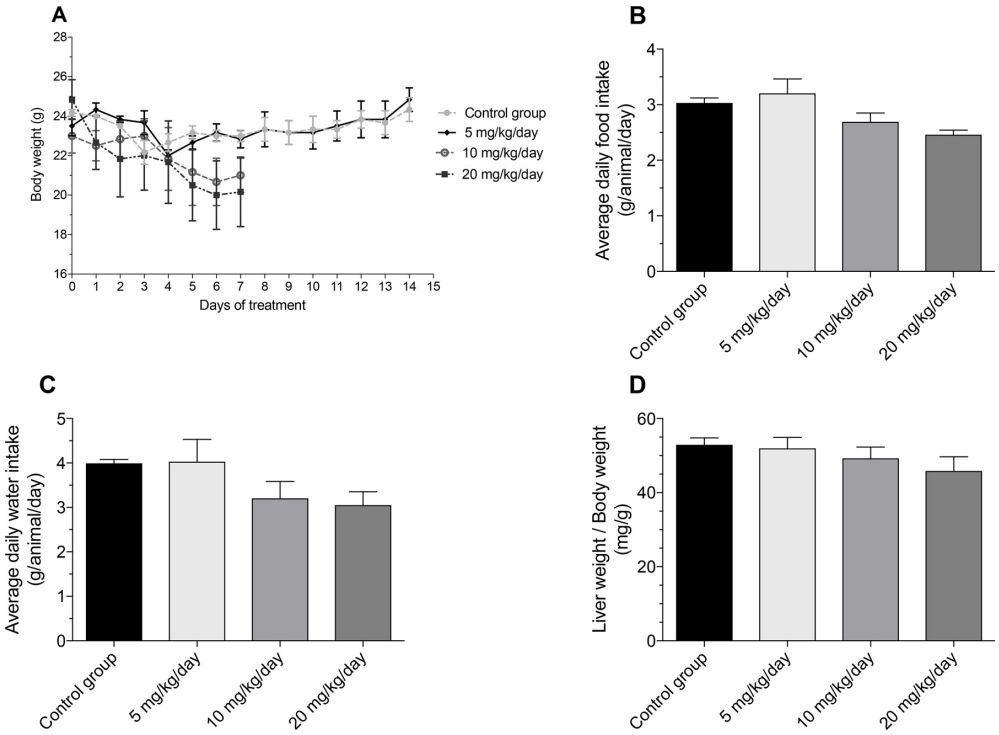

Fig. 1. Dose finding study.
(A) Body weight of sunitinib-treated and control mice. (B) Average daily food intake of sunitinib-treated and control mice. (C) Average daily water intake of sunitinib-treated and control mice. (D) Liver weight/body weight ratio. Data are expressed as mean ± SEM.

3.2. Principle study

3.2.1. Characterization of the animals

A daily dose of 7.5 mg/kg sunitinib for 14 days had no significant effect on food and water intake and on body weight compared to vehicle-treated control mice (Table 1). Liver, heart and kidney weight were also not affected by the treatment with sunitinib. However, the weight of the gastrocnemius muscle was significantly reduced. After 14 days, sunitinib-treated mice had a 5.8-fold increase in plasma levels of alanine aminotransferase (ALT) compared to control mice, indicating hepatocyte damage. At this time point, the sunitinib plasma trough concentration was 3.19 ± 1.38 nmol/L (1.27 ± 0.55 ng/mL) and the corresponding liver concentration 92.2 ± 48.4 nmol/kg (36.7 ± 19.3 ng/g) in sunitinib-treated mice. In control mice, sunitinib was not detected in plasma or liver.

Table 1
Characterization of the animals. Mice were treated with sunitinib 7.5 mg/kg for 14 days. Body weight and intake of food and water of the animals were determined daily. The organ weights were normalized to the body weight at study end. ALT activity in plasma was determined by a spectrophotometric assay. Data are presented as mean ± SEM.

	Control (n = 10)	Sunitinib (n = 10)
Body weight, start of study (g)	24.8 ± 0.6	25.0 ± 0.5
Body weight, end of study (g)	25.0 ± 0.6	25.4 ± 0.4
Change in body weight (%)	1.1 ± 1.4	1.5 ± 1.0
Food intake (g/animal/day)	3.96 ± 0.23	3.83 ± 0.11
Average water intake (g/animal/day)	4.66 ± 0.30	4.89 ± 0.20
Liver weight (mg/g bw)	45.8 ± 0.6	44.7 ± 1.1
Heart weight (mg/g bw)	4.29 ± 0.07	4.07 ± 0.07
Kidney weight (mg/g bw)	6.65 ± 0.10	6.50 ± 0.09
Gastrocnemius (mg/g bw)	6.15 ± 0.20	5.56 ± 0.10*
ALT (U/L) in plasma	1.8 ± 0.8	10.6 ± 4.9*

* $p < 0.05$ vs. control group.

3.2.2. Liver histology

As shown in supplementary Fig. S1, hematoxylin-eosin stained liver sections showed no pathological changes in liver architecture and no inflammatory infiltrates or hepatocyte necrosis in sunitinib-treated and control livers. Furthermore, we did not observe any change in the liver content of fat or glycogen and of fibrosis between control and sunitinib-treated mice. In agreement with the histological analysis, the hepatic glycogen content was not significantly different between control and sunitinib-treated animals (1.87 ± 0.51 vs. 2.31 ± 0.81 µmol/mg protein in control vs. sunitinib-treated mice; mean ± SEM, n = 10 per group).

3.2.3. Metabolic function of isolated liver mitochondria

Since sunitinib is a known mitochondrial toxicant in HepG2 cells (sunitinib reduced the mitochondrial membrane potential and inhibited complex I of the respiratory chain (Paech et al., 2017a)), we assessed the impact of sunitinib on oxidative metabolic function in isolated mouse liver mitochondria. Treatment with sunitinib for 14 days did not significantly impair the mitochondrial membrane potential of isolated liver mitochondria (Fig. 2A), whereas the activity of the complexes III and IV of the respiratory chain was reduced by 23% and 19%, respectively, but without reaching statistical significance (Fig. 2B).

In order to investigate these results further, we determined the activities of the individual mitochondrial enzyme complexes (I–IV) using spectrophotometric methods (Krahenbuhl et al., 1991, 1994) in freeze/thawed mouse liver mitochondria. Treatment with sunitinib was

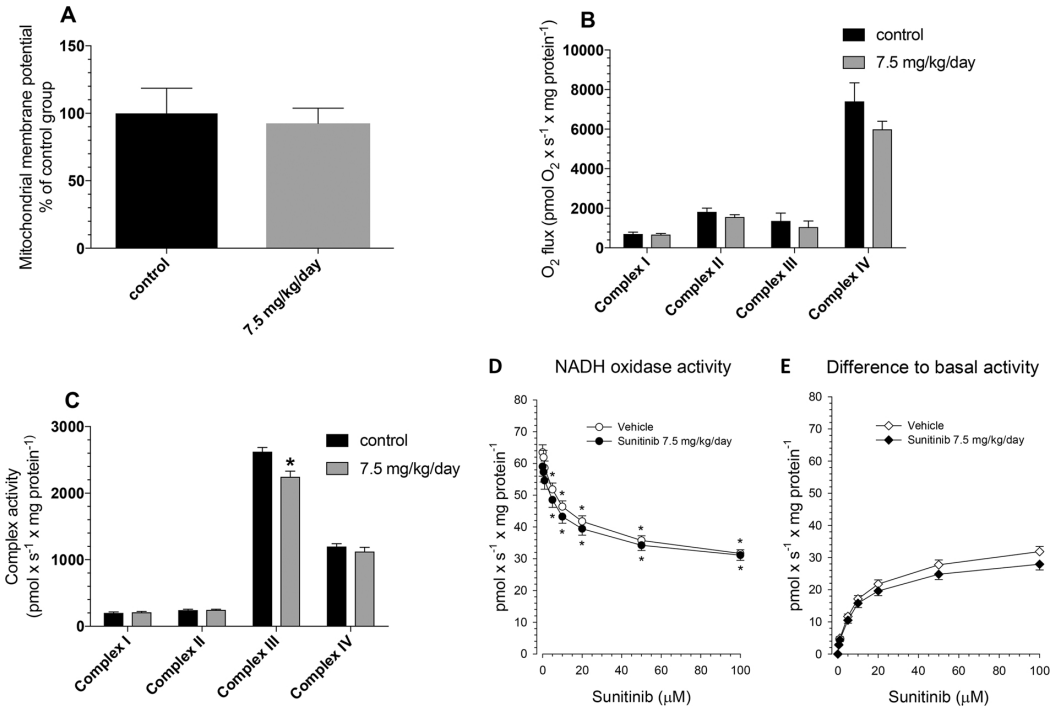

Fig. 2. Liver mitochondrial function.
(A) Mitochondrial membrane potential was measured with the [phenyl-^{3}H]-tetra-phenylphosphonium bromide uptake assay in freshly isolated liver mitochondria of sunitinib-treated and control mice. (B) Electron transport chain activities in freshly isolated liver mitochondria of sunitinib-treated and control mice measured with an Oxygraph-2k high-resolution respirometer. (C) Activity of the enzyme complexes of the electron transport chain in previously frozen liver mitochondria of sunitinib-treated and control mice. Complex activities were determined using established spectrophotometric methods in frozen and re-thawed liver mitochondria. *$p < 0.05$ vs. control. (D) Activity of NADH oxidase in previously frozen mitochondria in the presence of exogenous sunitinib. *$p < 0.05$ vs. respective basal activity (absence of sunitinib). (E) Difference between basal NADH oxidase activities (in the absence of sunitinib) and activities obtained in the presence of sunitinib in previously frozen liver mitochondria. There were no significant differences between the two groups. Data are expressed as mean ± SEM. N = 10 independent experiments performed with samples from 10 different animals in each group.

associated with a significant reduction of the complex III activity ($p < 0.05$), whereas the activity of complexes I, II and IV was not significantly affected (Fig. 2C).

In order to investigate the acute effect of sunitinib on mitochondria and to answer the question whether liver mitochondria isolated from sunitinib-treated mice were more susceptible to exogenous sunitinib than mitochondria from control mice, we determined the activity of the NADH oxidase under basal conditions and in the presence of increasing concentrations of exogenous sunitinib using freeze/thawed mitochondria (Fig. 2D). Under basal conditions (absence of exogenous sunitinib), mitochondria from sunitinib-treated mice showed an 8% decrease in the NADH oxidase activity compared to mitochondria from control mice ($p = 0.261$). In both mitochondria from control and from sunitinib-treated mice, exogenous sunitinib decreased NADH oxidase activity compared to basal values, reaching statistical significance at 5 μM. This decrease reached 50% and 47% at 100 μM sunitinib in mitochondria from control and sunitinib-treated mice, respectively. In order to answer the question, whether mitochondria from sunitinib-treated mice are more susceptible to exogenous sunitinib than control mitochondria, we calculated the difference between basal activities and activities in the presence of sunitinib for both mitochondria from sunitinib-treated and control mice (Fig. 2E). Since the difference between the two curves did not reach statistical significance at any concentration studied, we concluded that mitochondria from sunitinib-treated mice were not more susceptible to exogenous sunitinib than mitochondria from control mice.

3.2.4. Composition of mitochondrial enzyme complexes

In order to find out potential reasons for the observed decrease in the activity of the enzyme complexes of the electron transport chain with sunitinib long-term treatment, we analyzed mRNA and protein expression of subunits of these enzyme complexes. As shown in Fig. 3A, the mRNA expression of SDHA (subunit of complex II) was significantly reduced ($p = 0.03$). In addition, the mRNA expression of nuclear subunits of complex I, III, and V, and of a mitochondrial subunit of complex I, were reduced numerically without reaching statistical significance (Fig. 3A and B). Similarly, western blot analysis of the enzyme complexes of the respiratory chain showed a reduced protein content of protein subunits of complexes III–V by 29%, 32%, and 27%, respectively, in mitochondria from sunitinib-treated vs. control mice. In comparison, the protein content of subunits of complex I and II was not affected by treatment with sunitinib (Fig. 3C and supplementary Fig. S2).

3.2.5. Mitochondrial superoxide content and antioxidative defense

Toxicants inhibiting complex I and/or III of the electron transport chain can stimulate mitochondrial production of superoxide (Drose and Brandt, 2012). To assess the mitochondrial superoxide content, we stimulated the respiration of isolated liver mitochondria with glutamate and malate. The superoxide anion content increased by 36% in liver mitochondria from sunitinib-treated mice in the presence of glutamate and malate as substrates (Fig. 4A).

Long-term increase in the mitochondrial and cellular ROS content

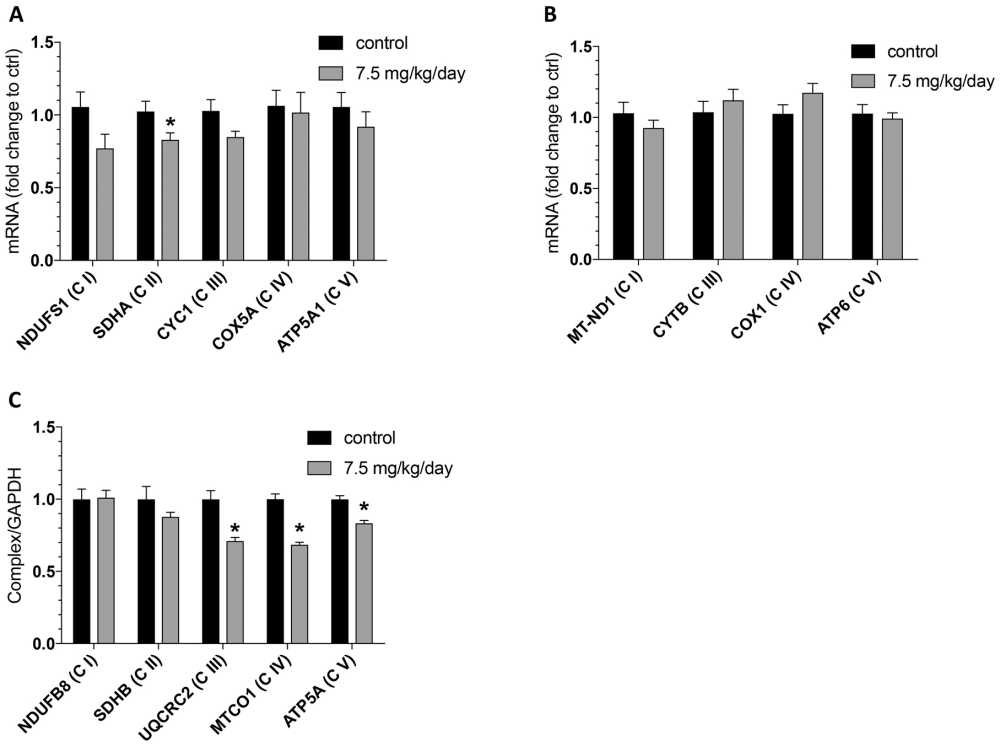

Fig. 3. mRNA and protein expression of subunits of enzyme complexes of the respiratory chain in liver tissue.
(A) mRNA expression of nuclear subunits of complexes I–V. (B) mRNA expression of mitochondrial subunits of complexes I–V. (C) Western blot analysis of the expression of subunits of complexes I–V. Data are expressed as mean ± SEM. N = 10 independent experiments performed with samples from 10 different animals in each group. *$p < 0.05$ vs. control group.

can lead to induction of the antioxidative defense system. SOD2 is an enzyme in the mitochondrial matrix which degrades superoxide anions and which can be upregulated under conditions of increased mitochondrial ROS content (Felser et al., 2013). Indeed, sunitinib-treatment was associated with an increase in the protein expression of the mitochondrial superoxide dismutase (SOD2) by 40% ($p < 0.05$, Fig. 4B and C), suggesting also an increase in SOD2 activity.

Glutathione is an important antioxidative substance which is involved in the degradation of ROS (Fernandez-Checa and Kaplowitz, 2005). As shown in Fig. 4D, the hepatic glutathione content was decreased by 14% in sunitinib-treated compared to control mice, which was close to statistical significance ($p = 0.0531$). Interestingly, the mRNA expression of glutathione synthetase was increased 1.5-fold in livers of mice treated with sunitinib compared to the control group, possibly representing a compensatory reaction regarding the increase in the cellular ROS content and the continuous consumption of glutathione for ROS degradation (Fig. 4E) (Mari and Cederbaum, 2000).

3.2.6. Markers of mitochondrial proliferation

Hepatic mitochondrial insults can be associated with proliferation of mitochondria (Krahenbuhl et al., 1992, 1990). Citrate synthase, a marker of the mitochondrial content, was reduced by 16% ($p < 0.05$) in sunitinib-treated mice compared to control mice (Fig. 5A). Moreover, mitochondrial DNA copy number was also decreased by 30% with the sunitinib treatment (Fig. 5B). Assuming impaired mitochondrial proliferation, we also determined the protein expression of PGC-1α, which is a master regulator of mitochondrial biosynthesis (Palikaras and Tavernarakis, 2014). PGC-1α protein expression was reduced by 32% with sunitinib treatment ($p < 0.05$, Fig. 5C and D). These findings indicated that sunitinib suppressed mitochondrial proliferation and thereby blocked the compensation of the sunitinib-associated mitochondrial toxicity by mitochondrial proliferation.

3.2.7. Mechanism of cell death

Mitochondrial damage can lead to leakage of cytochrome c from the intermembrane space into the cytoplasm, which can induce hepatocyte apoptosis and/or necrosis. Cleavage and activation of caspase 3 is a key event in apoptosis (Bonifacio et al., 2016). The determination of full-length (pro)caspase 3 revealed two bands; the upper band at 35 kD was used for the determination of the protein concentration (Fig. 6A). The lower band was different from the band for cleaved caspase 3, which was detected at 19 kD. The ratio of the hepatic protein content of cleaved caspase 3 to procaspase 3 was increased after treatment with sunitinib ($p < 0.05$, Fig. 6A and B). In agreement, TUNEL staining showed that the proportion of nuclei positive for DNA strand breaks doubled with sunitinib treatment, reaching statistical significance (Fig. 6C and D). Augmented hepatocyte damage is compatible with the observed increase in the activity of ALT in plasma of mice treated with sunitinib.

4. Discussion

The study demonstrates that mice treated with 7.5 mg sunitinib per kg body weight for 14 days developed hepatocellular injury (increased activity of ALT in plasma), which was most likely caused by direct liver mitochondrial toxicity of sunitinib. In addition, sunitinib inhibited the proliferation of liver mitochondria.

The first part of the study revealed that doses of ≥10 mg/kg

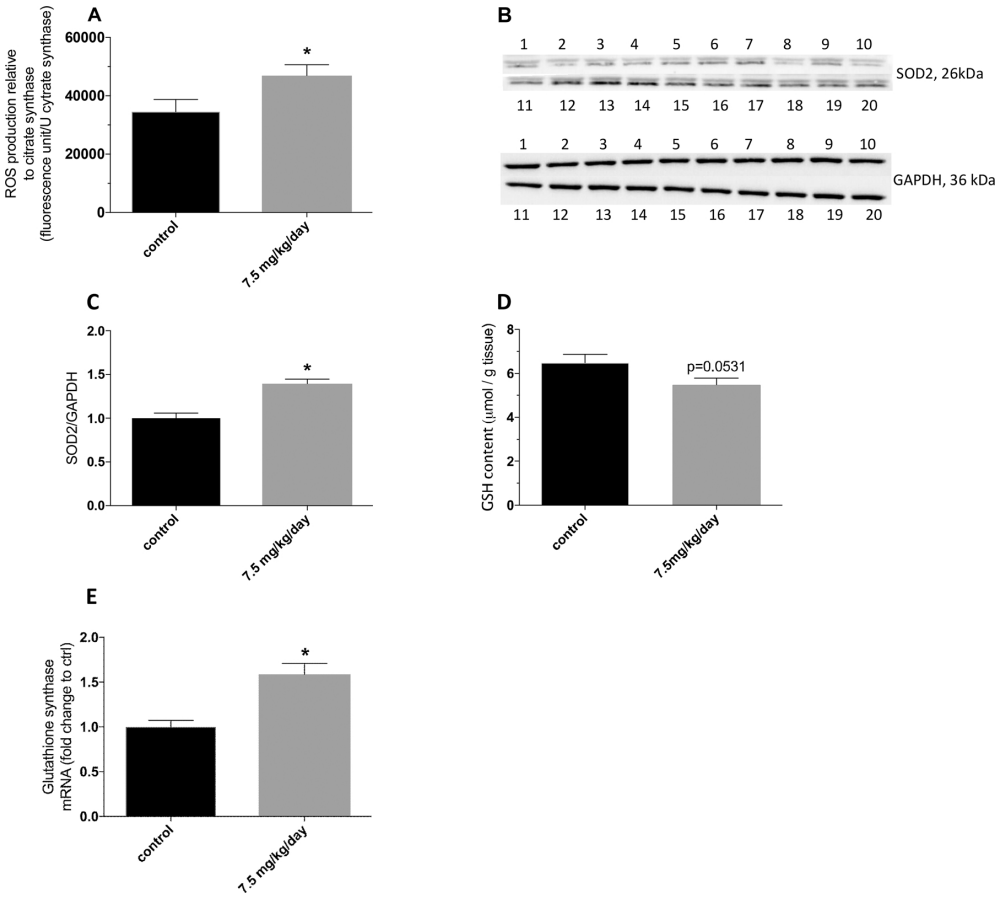

Fig. 4. Hepatic mitochondrial superoxide content and anti-oxidative systems.
(A) The mitochondrial superoxide content was measured with MitoSOX Red reagent in freshly isolated liver mitochondria of sunitinib-treated and control mice incubated with malate/glutamate over 10 min and was related to citrate synthase. (B) Western blots showing the expression levels of SOD2 and GAPDH. Numbers indicate individual mice (1–10 = control mice, 11–20 sunitinib-treated mice) (C) Quantification of SOD2 protein expression normalized against GAPDH. (D) mRNA expression levels of glutathione synthetase. Data are expressed as mean ± SEM. N = 10 independent experiments performed with samples from 10 different animals in each group. *p < 0.05 vs. control group.

impaired food and water intake and led to a decrease in body weight of the animals treated. Since it would have been difficult to differentiate between direct drug effects on the liver and secondary effects related to impaired food and water intake, we decided to study a dose which did not affect food and water consumption. The observation that a dose of ≥10 mg/kg was toxic was surprising, since studies have been published with much higher doses in mice where no adverse effects on food and water consumption and on body weight have been reported (Haznedar et al., 2009). Based on the results in the pilot study, we decided to treat the mice with 7.5 mg sunitinib per kg body weight for 14 days.

We have shown previously that sunitinib directly impairs the function of mitochondria in HepG2 cells and in HepaRG cells (Paech et al., 2017a). Sunitinib depleted the ATP content of HepG2 and HepaRG cells at lower concentrations than membrane toxicity occurred, and reduced cellular oxygen consumption, impaired the activity of complex I of the electron transport chain, increased mitochondrial ROS production and induced apoptosis in HepG2 cells. In contrast, in a recent study in isolated rat liver mitochondria, sunitinib showed no toxicity at clinically relevant concentrations (Zhang et al., 2017). This difference may be explained by the diverse experimental models used – human cell lines in the study of Paech et al. and isolated rat liver mitochondria in the study of Zhang et al. – and by the different experimental settings. While Zhang et al. studied acute effects on freshly isolated mitochondria (Zhang et al., 2017), the cell lines used in the study of Paech et al. were exposed for 6–48 h (Paech et al., 2017a). These observations suggest that for the assessment of mitochondrial toxicity associated with sunitinib both the experimental model used and the experimental settings are important factors.

In the current study, the investigation of the NADH oxidase activity revealed that sunitinib was directly toxic on previously frozen mouse liver mitochondria and that mitochondria from mice treated with sunitinib were not more susceptible to exogenous sunitinib than mitochondria from control mice. As mentioned above, the detection of direct mitochondrial toxicity of sunitinib disagrees with the findings of Zhang et al. (Zhang et al., 2017), but is in accordance with our previous findings (Paech et al., 2017a). Based on the determined hepatic sunitinib concentrations and pharmacokinetic calculations (see below), we can assume that the maximal hepatic concentrations after oral ingestion of sunitinib exceeded the concentrations needed for mitochondrial toxicity. It is therefore likely that mitochondrial damage occurred after every ingestion of sunitinib, leading to death of susceptible hepatocytes with a concomitant increase in the plasma ALT activity (see Fig. 6E).

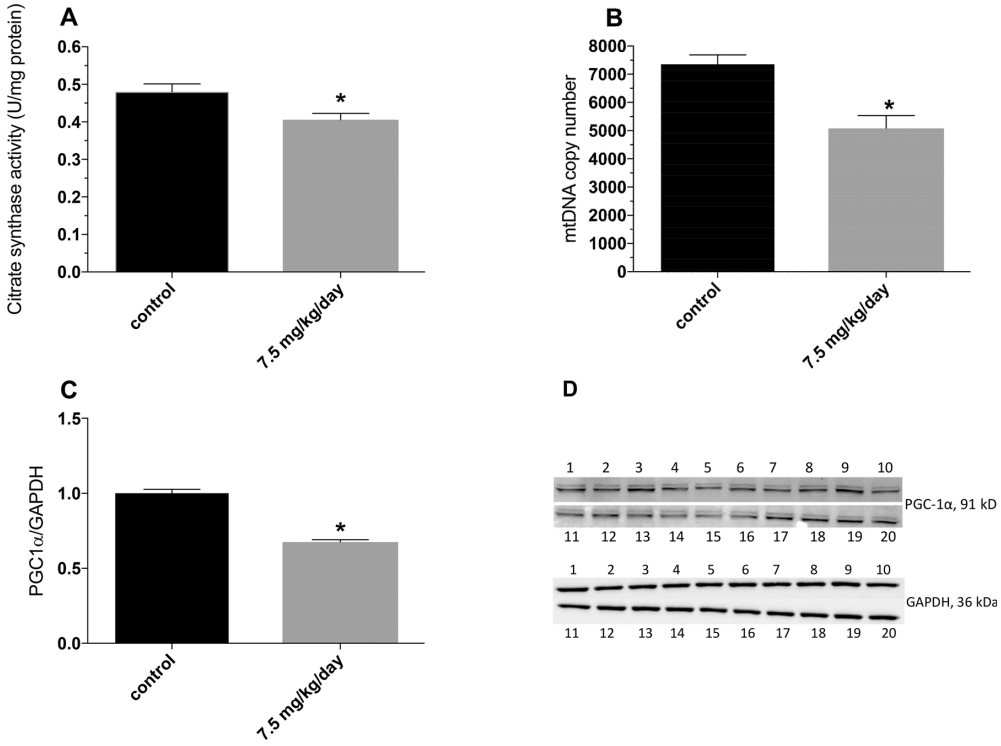

Fig. 5. Hepatic mitochondrial proliferation.
(A) Activity of the citrate synthase of sunitinib-treated and control mice. (B) Mitochondrial DNA copy number. (C) Western blots showing the expression levels of PGC-1α and GAPDH. Numbers indicate individual mice (1–10 = control mice, 11–20 sunitinib-treated mice) (D) Quantification of PGC-1α protein expression normalized against GAPDH. Data are expressed as mean ± SEM. N = 10 independent experiments performed with samples from 10 different animals in each group. *$p < 0.05$ vs. control group.

The observations that the NADH oxidase activity was not significantly impaired in mitochondria from sunitinib-treated mice in the absence of exogenous sunitinib and that mitochondria from sunitinib-treated mice were not more susceptible to exogenous sunitinib than mitochondria from control mice suggest that the mitochondria could recover almost completely between the individual sunitinib doses. In agreement with these findings, the mitochondrial membrane potential, a sensitive marker of mitochondrial damage (Felser et al., 2013), was not significantly decreased in liver mitochondria of sunitinib-treated mice. In addition, the activity of the electron transport chain enzyme complexes determined in freshly isolated liver mitochondria were also not significantly decreased in sunitinib-treated mice, again suggesting an almost complete recovery after the acute mitochondrial insults. On the other hand, complex III activity was decreased in isolated, freeze-thawed mitochondria and ROS production by mitochondria from sunitinib-treated mice was significantly increased, suggesting an incomplete recovery from the acute mitochondrial insults by sunitinib. Even if a permanent damage in liver mitochondria from sunitinib-treated mice existed after stopping treatment with sunitinib, the mitochondrial impairment would hardly be strong enough to be of toxicological relevance. As discussed above and as illustrated in Fig. 6E, the data of the current study suggest that the repetitive mitochondrial insults after every ingestion are responsible for liver injury in mice treated with sunitinib.

Interestingly, we observed decreases in citrate synthase activity, in the mitochondrial DNA copy number and in the protein expression of PGC-1α, a key regulator of energy metabolism and mitochondrial biogenesis (Liang and Ward, 2006; Scarpulla, 2011), in livers of mice treated with sunitinib. These findings were compatible with impaired hepatic mitochondrial proliferation, possibly explaining reduced mRNA and protein expression as well as impaired activity of complex III of the electron transport chain in the liver of sunitinib-treated mice. In agreement and support of this hypothesis, hepatocytes isolated from PGC-1α knock-out mice had impaired oxygen consumption, suggesting impaired mitochondrial function (Leone et al., 2005). Impaired activity of complex I and III of the mitochondrial electron transport chain is a likely reason for increased mitochondrial superoxide production (Drose and Brandt, 2012; Felser et al., 2013), which we observed in liver mitochondria from sunitinib-treated mice. Since mitochondrial stress such as increased mitochondrial ROS content and decreased cellular ATP content are established stimulators of PGC-1α expression (Liang and Ward, 2006; Scarpulla, 2011), the observed decrease in the hepatic expression of PGC-1α in mice treated with sunitinib was not expected. The most likely explanation for these findings is that the multikinase inhibitor sunitinib itself suppressed the expression of PGC-1α. How exactly sunitinib could impair protein expression of PGC-1α is, to the best of our knowledge, not directly deducible from its pharmacological properties has to be assessed in future studies.

As mentioned above, decreases in the activity of the mitochondrial enzyme complexes I and III can be associated with increased mitochondrial superoxide production (Drose and Brandt, 2012; Felser et al., 2013). Mitochondria can degrade superoxide anion by SOD2, which is expressed in the mitochondrial matrix (Bresciani et al., 2015). If mitochondrial superoxide production exceeds the capacity of SOD2, oxidative damage to lipids, proteins and DNA is possible. As shown in the current and in preceding investigations (Felser et al., 2013), SOD2

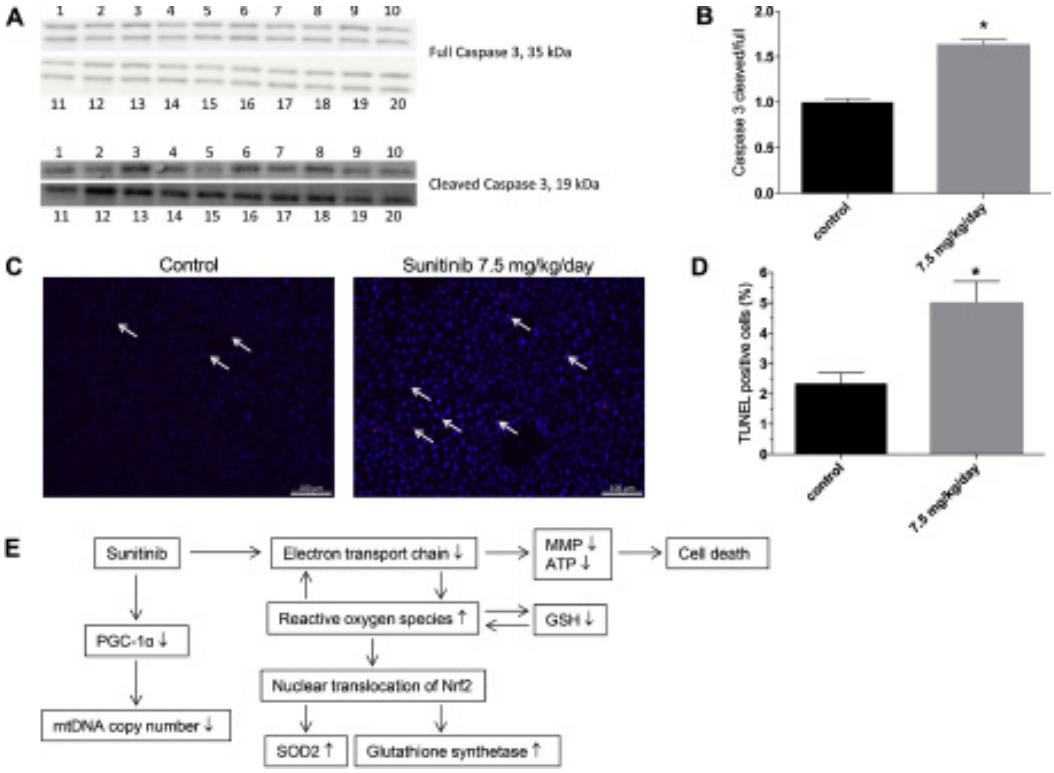

Fig. 6. Assessment of cell death and overall effect of sunitinib.
(A) Western blots showing the protein content of full-length and cleaved caspase 3. Full-length caspase was quantified using the upper band at 35 kD. Numbers indicate individual mice (1–10 = control mice, 11–20 sunitinib-treated mice) (B) Quantification of active (cleaved) to full-length caspase 3 protein expression. (C) Nuclei were stained with DAPI shown in blue and TUNEL nuclei were visualized with magenta fluorescein in liver of sunitinib-treated and control mice. (D) The percentage of TUNEL positive cells was calculated by counting the number of TUNEL-stained nuclei divided by the total number of nuclei multiplied by 100. At least 5 randomly chosen sections from every animal were investigated. (E). Schematic representation of the effects of sunitinib on mouse livers. Sunitinib inhibits complex I and III activity of the electron transport chain, which decreases the mitochondrial membrane potential (MMP) and cellular ATP content, and increases the cellular ROS content. Decreases in the MMP and cellular ATP content are associated with apoptosis and necrosis. An increase in cellular ROS induces nuclear translocation of Nrf2, increasing the transcription of SOD2 and glutathione synthetase. Sunitinib reduces the expression of PGC-1α, which impairs mitochondrial proliferation. The reduction of the MMP and the cellular ATP content by sunitinib has been shown in a previous publication (Paech et al., 2017a). Data are expressed as mean ± SEM. N = 10 independent experiments performed with samples from 10 different animals in each group. *$p < 0.05$ vs. control group. (For interpretation of the references to colour in this figure legend, the reader is referred to the web version of this article.)

can be upregulated in order to counteract increased mitochondrial production of ROS. A further consequence of an increased mitochondrial ROS content is induction of the mitochondrial permeability transition, eventually leading to rupture of the outer mitochondrial membrane with leakage of cytochrome c and other pro-apoptotic factors into the cytoplasm and induction of apoptosis and/or necrosis (Carraro and Bernardi, 2016; Jaeschke et al., 2012). In the current study, we could demonstrate an increase in the activation of caspase 3 and of TUNEL-positive hepatocytes, indicating stimulation of hepatocyte apoptosis in mice treated with sunitinib. The observed increase in the serum ALT activity in mice treated with sunitinib suggests that a small portion of hepatocytes was also eliminated by necrosis. Increased mitochondrial production of ROS, which is most likely a consequence of the inhibition of the electron transport chain, appears therefore to be an important factor for liver toxicity of sunitinib (see Fig. 6E).

In the current study, we determined a sunitinib plasma concentration of 3.18 nmol/L. This concentration is lower than typical plasma concentrations in humans treated with sunitinib, which are in a range of 0.1 to 0.2 µmol/L (Herbrink et al., 2016; Huynh et al., 2017). It has to be taken into account, however, that we determined trough values and that we administered a single dose every 24 h. Assuming a plasma half-life of approximately 4 h after oral administration in mice (Haznedar et al., 2009), the calculated maximal plasma concentration is in the range of 0.2 µmol/L, which agrees well with the plasma concentrations observed in humans. In comparison, the liver concentration was approximately 25 times higher, which is in agreement with previous studies showing much higher liver than plasma concentrations (Chen et al., 2015; Lau et al., 2015). Similar to plasma, the half-life of the hepatic elimination of sunitinib reported by Lau et al (Lau et al., 2015) was also in the range of 4 h. The calculated maximal concentration in the liver is therefore in the range of 5–10 nmol/g liver. At concentrations in this range (5–10 µmol/L), we started to observe mitochondrial dysfunction in HepG2 cells exposed to sunitinib for 24 h (Paech et al., 2017a) and impairment of mitochondrial NADH oxidase in the current study (Fig. 2D). This comparison shows that sunitinib could reach potentially toxic concentrations in the livers of the mice treated in the current study. If the tissue distribution of sunitinib is similar between mice and humans, this would also be the case for humans.

In conclusion, mice treated daily with 7.5 mg/kg sunitinib for 14 days exhibited hepatocellular liver injury caused most likely by direct, concentration-dependent toxicity of sunitinib. These repetitive mitochondrial insults were associated with an increase in the

mitochondrial ROS content, leading to hepatocyte injury. In addition, sunitinib impaired hepatic mitochondrial proliferation, which may have contributed to hepatic mitochondrial toxicity.

Financial support

The study was supported by a grant from the Swiss National Science foundation to SK (SNF 31003A_156270)

Conflict of interest

None of the authors has a conflict of interest regarding this study.

Appendix A. Supplementary data

Supplementary material related to this article can be found, in the online version, at doi:https://doi.org/10.1016/j.tox.2018.07.009.

References

Abrams, T.J., Lee, L.B., Murray, L.J., Pryer, N.K., Cherrington, J.M., 2003. SU11248 inhibits KIT and platelet-derived growth factor receptor beta in preclinical models of human small cell lung cancer. Mol. Cancer Ther. 2, 471–478.

Bello, C.L., Sherman, L., Zhou, J., Verkh, L., Smeraglia, J., Mount, J., Klamerus, K.J., 2006. Effect of food on the pharmacokinetics of sunitinib malate (SU11248), a multi-targeted receptor tyrosine kinase inhibitor: results from a phase I study in healthy subjects. Anticancer Drugs 17, 353–358.

Bonifacio, A., Mullen, P.J., Mityko, I.S., Navegantes, L.C., Bouitbir, J., Krahenbuhl, S., 2016. Simvastatin induces mitochondrial dysfunction and increased atrogin-1 expression in H9c2 cardiomyocytes and mice in vivo. Arch. Toxicol. 90, 203–215.

Bresciani, G., da Cruz, I.B., Gonzalez-Gallego, J., 2015. Manganese superoxide dismutase and oxidative stress modulation. Adv. Clin. Chem. 68, 87–130.

Carraro, M., Bernardi, P., 2016. Calcium and reactive oxygen species in regulation of the mitochondrial permeability transition and of programmed cell death in yeast. Cell Calcium 60, 102–107.

Chen, X., Wang, Z., Liu, M., Liao, M., Wang, X., Du, H., Chen, J., Yao, M., Li, Q., 2015. Determination of sunitinib and its active metabolite, N-desethyl sunitinib in mouse plasma and tissues by UPLC-MS/MS: assay development and application to pharmacokinetic and tissue distribution studies. Biomed. Chromatogr. 29, 679–688.

Cumurciuc, R., Martinez-Almoyna, L., Henry, C., Husson, H., de Broucker, T., 2008. Posterior reversible encephalopathy syndrome during sunitinib therapy. Rev. Neurol. (Paris) 164, 605–607.

Demetri, G.D., van Oosterom, A.T., Garrett, C.R., Blackstein, M.E., Shah, M.H., Verweij, J., McArthur, G., Judson, I.R., Heinrich, M.C., Morgan, J.A., Desai, J., Fletcher, C.D., George, S., Bello, C.L., Huang, X., Baum, C.M., Casali, P.G., 2006. Efficacy and safety of sunitinib in patients with advanced gastrointestinal stromal tumour after failure of imatinib: a randomised controlled trial. Lancet 368, 1329–1338.

Drose, S., Brandt, U., 2012. Molecular mechanisms of superoxide production by the mitochondrial respiratory chain. Adv. Exp. Med. Biol. 748, 145–169.

Faivre, S., Delbaldo, C., Vera, K., Robert, C., Lozahic, S., Lassau, N., Bello, C., Deprimo, S., Brega, N., Massimini, G., Armand, J.P., Scigalla, P., Raymond, E., 2006. Safety, pharmacokinetic, and antitumor activity of SU11248, a novel oral multitarget tyrosine kinase inhibitor, in patients with cancer. J. Clin. Oncol. 24, 25–35.

Felser, A., Blum, K., Lindinger, P.W., Bouitbir, J., Krahenbuhl, S., 2013. Mechanisms of hepatocellular toxicity associated with dronedarone–a comparison to amiodarone. Toxicol. Sci. 131, 480–490.

Fernandez-Checa, J.C., Kaplowitz, N., 2005. Hepatic mitochondrial glutathione: transport and role in disease and toxicity. Toxicol. Appl. Pharmacol. 204, 263–273.

Goodman, V.L., Rock, E.P., Dagher, R., Ramchandani, R.P., Abraham, S., Gobburu, J.V., Booth, B.P., Verbois, S.L., Morse, D.E., Liang, C.Y., Chidambaram, N., Jiang, J.X., Tang, S., Mahjoob, K., Justice, R., Pazdur, R., 2007. Approval summary: sunitinib for the treatment of imatinib refractory or intolerant gastrointestinal stromal tumors and advanced renal cell carcinoma. Clin. Cancer Res. 13, 1367–1373.

Guillen, S.S., Meijer, M., de Jongh, F.E., 2016. Lethal acute liver failure in a patient treated with sunitinib. BMJ Case Rep. 2016.

Haznedar, J.O., Patyna, S., Bello, C.L., Peng, G.W., Speed, W., Yu, X., Zhang, Q., Sukbuntherng, J., Sweeny, D.J., Antonian, L., Wu, E.Y., 2009. Single- and multiple-dose disposition kinetics of sunitinib malate, a multitargeted receptor tyrosine kinase inhibitor: comparative plasma kinetics in non-clinical species. Cancer Chemother. Pharmacol. 64, 691–706.

Herbrink, M., de Vries, N., Rosing, H., Huitema, A.D., Nuijen, B., Schellens, J.H., Beijnen, J.H., 2016. Quantification of 11 therapeutic kinase inhibitors in human plasma for therapeutic drug monitoring using liquid chromatography coupled with tandem mass spectrometry. Ther. Drug Monit. 38, 649–656.

Hoppel, C., DiMarco, J.P., Tandler, B., 1979. Riboflavin and rat hepatic cell structure and function. Mitochondrial oxidative metabolism in deficiency states. J. Biol. Chem. 254, 4164–4170.

Huynh, H.H., Pressiat, C., Sauvageon, H., Madelaine, I., Maslanka, P., Lebbe, C., Thieblemont, C., Goldwirt, L., Mourah, S., 2017. Development and validation of a simultaneous quantification method of 14 tyrosine kinase inhibitors in human plasma using LC-MS/MS. Ther. Drug Monit. 39, 43–54.

Jaeschke, H., McGill, M.R., Ramachandran, A., 2012. Oxidant stress, mitochondria, and cell death mechanisms in drug-induced liver injury: lessons learned from acetaminophen hepatotoxicity. Drug Metab. Rev. 44, 88–106.

Krahenbuhl, S., Ray, D.B., Stabler, S.P., Allen, R.H., Brass, E.P., 1990. Increased hepatic mitochondrial capacity in rats with hydroxy-cobalamin[c-lactam]-induced methylmalonic aciduria. J. Clin. Invest. 86, 2054–2061.

Krahenbuhl, S., Chang, M., Brass, E.P., Hoppel, C.L., 1991. Decreased activities of ubiquinol:ferricytochrome c oxidoreductase (complex III) and ferrocytochrome c:oxygen oxidoreductase (complex IV) in liver mitochondria from rats with hydroxycobalamin [c-lactam]-induced methylmalonic aciduria. J. Biol. Chem. 266, 20998–21003.

Krahenbuhl, S., Krahenbuhl-Glauser, S., Stucki, J., Gehr, P., Reichen, J., 1992. Stereological and functional analysis of liver mitochondria from rats with secondary biliary cirrhosis: impaired mitochondrial metabolism and increased mitochondrial content per hepatocyte. Hepatology 15, 1167–1172.

Krahenbuhl, S., Talos, C., Wiesmann, U., Hoppel, C.L., 1994. Development and evaluation of a spectrophotometric assay for complex III in isolated mitochondria, tissues and fibroblasts from rats and humans. Clin. Chim. Acta 230, 177–187.

Lang, C., Schafer, M., Varga, L., Zimmermann, A., Krahenbuhl, S., Krahenbuhl, L., 2002. Hepatic and skeletal muscle glycogen metabolism in rats with short-term cholestasis. J. Hepatol. 36, 22–29.

Lau, C.L., Chan, S.T., Selvaratanam, M., Khoo, H.W., Lim, A.Y., Modamio, P., Marino, E.L., Segarra, I., 2015. Sunitinib-ibuprofen drug interaction affects the pharmacokinetics and tissue distribution of sunitinib to brain, liver, and kidney in male and female mice differently. Fundam. Clin. Pharmacol. 29, 404–416.

Leone, T.C., Lehman, J.J., Finck, B.N., Schaeffer, P.J., Wende, A.R., Boudina, S., Courtois, M., Wozniak, D.F., Sambandam, N., Bernal-Mizrachi, C., Chen, Z., Holloszy, J.O., Medeiros, D.M., Schmidt, R.E., Saffitz, J.E., Abel, E.D., Semenkovich, C.F., Kelly, D.P., 2005. PGC-1alpha deficiency causes multi-system energy metabolic derangements: muscle dysfunction, abnormal weight control and hepatic steatosis. PLoS Biol. 3, e101.

Liang, H., Ward, W.F., 2006. PGC-1alpha: a key regulator of energy metabolism. Adv. Physiol. Educ. 30, 145–151.

Mari, M., Cederbaum, A.I., 2000. CYP2E1 overexpression in HepG2 cells induces glutathione synthesis by transcriptional activation of gamma-glutamylcysteine synthetase. J. Biol. Chem. 275, 15563–15571.

Mendel, D.B., Laird, A.D., Xin, X., Louie, S.G., Christensen, J.G., Li, G., Schreck, R.E., Abrams, T.J., Ngai, T.J., Lee, L.B., Murray, L.J., Carver, J., Chan, E., Moss, K.G., Haznedar, J.O., Sukbuntherng, J., Blake, R.A., Sun, L., Tang, C., Miller, T., Shirazian, S., McMahon, G., Cherrington, J.M., 2003. In vivo antitumor activity of SU11248, a novel tyrosine kinase inhibitor targeting vascular endothelial growth factor and platelet-derived growth factor receptors: determination of a pharmacokinetic/pharmacodynamic relationship. Clin. Cancer Res. 9, 327–337.

Motzer, R.J., Hutson, T.E., Tomczak, P., Michaelson, M.D., Bukowski, R.M., Oudard, S., Negrier, S., Szczylik, C., Pili, R., Bjarnason, G.A., Garcia-del-Muro, X., Sosman, J.A., Solska, E., Wilding, G., Thompson, J.A., Kim, S.T., Chen, I., Huang, X., Figlin, R.A., 2009. Overall survival and updated results for sunitinib compared with interferon alfa in patients with metastatic renal cell carcinoma. J. Clin. Oncol. 27, 3584–3590.

Mueller, E.W., Rockey, M.L., Rashkin, M.C., 2008. Sunitinib-related fulminant hepatic failure: case report and review of the literature. Pharmacotherapy 28, 1066–1070.

Murray, L.J., Abrams, T.J., Long, K.R., Ngai, T.J., Olson, L.M., Hong, W., Keast, P.K., Brassard, J.A., O'Farrell, A.M., Cherrington, J.M., Pryer, N.K., 2003. SU11248 inhibits tumor growth and CSF-1R-dependent osteolysis in an experimental breast cancer bone metastasis model. Clin. Exp. Metastasis 20, 757–766.

O'Farrell, A.M., Abrams, T.J., Yuen, H.A., Ngai, T.J., Louie, S.G., Yee, K.W., Wong, L.M., Hong, W., Lee, L.B., Town, A., Smolich, B.D., Manning, W.C., Murray, L.J., Heinrich, M.C., Cherrington, J.M., 2003. SU11248 is a novel FLT3 tyrosine kinase inhibitor with potent activity in vitro and in vivo. Blood 101, 3597–3605.

Paech, F., Bouitbir, J., Krahenbuhl, S., 2017a. Hepatocellular toxicity associated with tyrosine kinase inhibitors: mitochondrial damage and inhibition of glycolysis. Front. Pharmacol. 8, 367.

Paech, F., Messner, S., Spickermann, J., Wind, M., Schmitt-Hoffmann, A.H., Witschi, A.T., Howell, B.A., Church, R.J., Woodhead, J., Engelhardt, M., Krahenbuhl, S., Maurer, M., 2017b. Mechanisms of hepatotoxicity associated with the monocyclic beta-lactam antibiotic BAL30072. Arch. Toxicol. 91, 3647–3662.

Palikaras, K., Tavernarakis, N., 2014. Mitochondrial homeostasis: the interplay between mitophagy and mitochondrial biogenesis. Exp. Gerontol. 56, 182–188.

Pesta, D., Gnaiger, E., 2012. High-resolution respirometry: OXPHOS protocols for human cells and permeabilized fibers from small biopsies of human muscle. Methods Mol. Biol. 810, 25–58.

Quiros, P.M., Goyal, A., Jha, P., Auwerx, J., 2017. Analysis of mtDNA/nDNA ratio in mice. Curr. Protoc. Mouse Biol. 7, 47–54.

Roskoski Jr., R., 2007. Sunitinib: a VEGF and PDGF receptor protein kinase and angiogenesis inhibitor. Biochem. Biophys. Res. Commun. 356, 323–328.

Scarpulla, R.C., 2011. Metabolic control of mitochondrial biogenesis through the PGC-1 family regulatory network. Biochim. Biophys. Acta 1813, 1269–1278.

Shah, R.R., Morganroth, J., Shah, D.R., 2013. Hepatotoxicity of tyrosine kinase inhibitors: clinical and regulatory perspectives. Drug Saf. 36, 491–503.

Srere, P.A., 1969. [1] Citrate synthase. Methods Enzymol. 13, 3–11.

Weng, Z., Luo, Y., Yang, X., Greenhaw, J.J., Li, H., Xie, L., Mattes, W.B., Shi, Q., 2015. Regorafenib impairs mitochondrial functions, activates AMP-activated protein kinase, induces autophagy, and causes rat hepatocyte necrosis. Toxicology 327, 10–21.

Xue, T., Luo, P., Zhu, H., Zhao, Y., Wu, H., Gai, R., Wu, Y., Yang, B., Yang, X., He, Q., 2012. Oxidative stress is involved in Dasatinib-induced apoptosis in rat primary hepatocytes. Toxicol. Appl. Pharmacol. 261, 280–291.

Zhang, J., Salminen, A., Yang, X., Luo, Y., Wu, Q., White, M., Greenhaw, J., Ren, L., Bryant, M., Salminen, W., Papoian, T., Mattes, W., Shi, Q., 2017. Effects of 31 FDA approved small-molecule kinase inhibitors on isolated rat liver mitochondria. Arch. Toxicol. 91, 2921–2938.

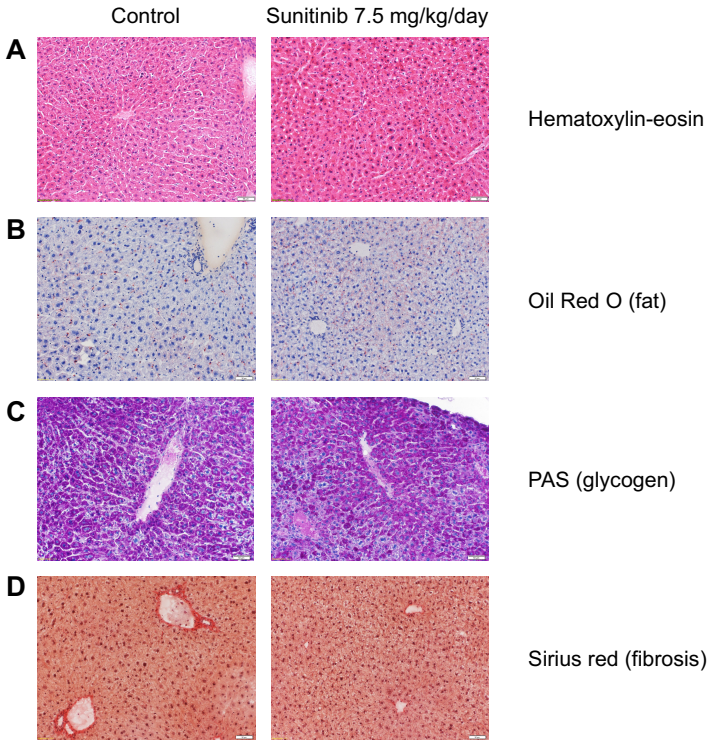

Supplementary Fig. S1. Histological analysis of liver sections. Cross sections (10 µm) were fixed and stained as described below. Staining with hematoxylin eosin was performed paraformaldehyde 4% fixed sections for a coarse assessment of tissue damage. Lipid accumulation was investigated by Oil red O staining from sections of frozen liver. The glycogen content was investigated using periodic acid Schiff staining on paraformaldehyde 4% fixed sections. Collagen for fibrosis was detected by staining paraformaldehyde 4% fixed sections with 0.1% Sirius Red. No differences were detectable between sections from control and sunitinib-treated animals.

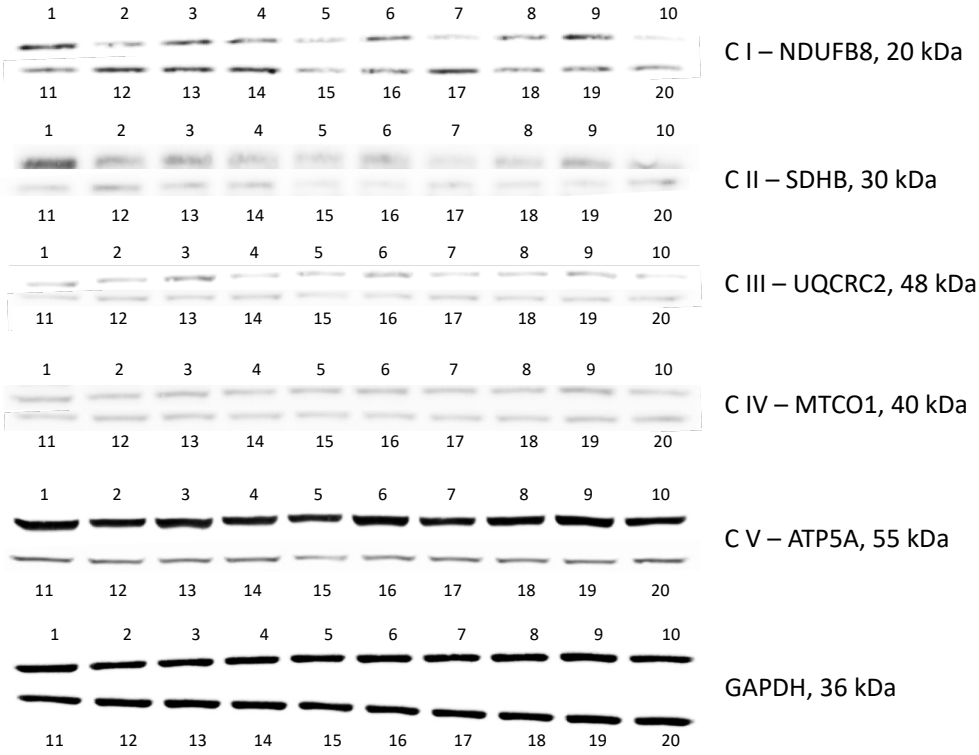

Supplementary Fig. S2. Western blot of subunits of the mitochondrial enzyme complexes I-V. Western blots were performed as described in Methods. Numbers indicate individual mice (1-10 = control mice, 11-20 sunitinib-treated mice).

DISCUSSION

Tyrosine kinase inhibitors are a new class of anticancer drugs that have revolutionized the treatment of certain cancers. They are usually well tolerated with lower toxicity than classical chemotherapeutic agents but still with a narrow therapeutic window. While hepatotoxicity is known for most TKIs, underlying mechanisms are only partially clarified. We therefore aimed to investigate the detailed *in vitro* and *in vivo* mechanisms of hepatotoxicity of ten TKIs, which have been reported to cause liver injury in patients.

We found that regorafenib and sorafenib were strong mitochondrial toxicants at concentrations that can be reached in plasma and liver of patients treated with these drugs. They inhibited mitochondrial oxidative metabolism, uncoupled mitochondrial oxidative phosphorylation, increased mitochondrial formation of ROS, and induced apoptosis and/or necrosis in HepG2 cells. In addition, they also inhibited glycolysis, which may enhance their hepatotoxicity. Imatinib, lapatinib, ponatinib, and sunitinib impaired mitochondrial function and glycolysis at higher concentrations than reached in plasma in patients but such concentrations may be reached in the liver. Imatinib, lapatinib, and sunitinib reduce the mitochondrial membrane potential, are associated with ROS formation, induce apoptosis, and impair glycolysis in HepG2 cells. In addition, imatinib and sunitinib were associated with impaired mitochondrial oxidative metabolism and reduced cellular GSH levels. Ponatinib strongly inhibited mitochondrial oxidative metabolism and increased mitochondrial ROS formation but only weakly glycolysis and induced apoptosis of HepG2 cells. In comparison, crizotinib, dasatinib, erlotinib, and pazopanib showed no relevant mitochondrial toxicity or inhibition of glycolysis in the concentration range investigated. For these drugs, so far undefined, non-mitochondrial mechanisms of hepatotoxicity have to be postulated. In addition, mice treated with 7.5 mg/kg sunitinib for 14 days had increased transaminase levels, inhibited mitochondrial oxidative metabolism, increased ROS formation, reduced mitochondrial biogenesis, and induced apoptosis.

1 REGORAFENIB AND SORAFENIB

Regorafenib and sorafenib were the most potent mitochondrial toxicants *in vitro* in our study, which is in agreement with the recent study of Zhang et al. (Zhang et al. 2017b). Regorafenib and sorafenib decreased the intracellular ATP content and were cytotoxic at lower

concentrations in the presence of galactose medium, which has been suggested to be an important marker for mitochondrial toxicity (Kamalian et al. 2015; Marroquin et al. 2007). Regorafenib and sorafenib inhibited mitochondrial oxidative metabolism by inhibiting complex I and/or III of the ETC in HepG2 cells and complex II (sorafenib), complex III (both), complex IV (regorafenib), and complex V (both) in isolated mitochondria exposed acutely. It is known that inhibition of complex I and complex III of the electron transport chain is related to an increased mitochondrial ROS formation (Drose and Brandt 2012). This ROS formation is associated with reduction of cellular GSH stores and induction of mitochondrial membrane permeability transition (Green and Reed 1998; Kaufmann et al. 2005). Increased mitochondrial ROS formation was shown for regorafenib and sorafenib. Mitochondrial ROS formation started at similar concentrations as the inhibition of ETC, supporting that ROS formation is a consequence of ETC inhibition. In addition, at the same concentrations we showed decreases in the GSH content and in the mitochondrial membrane potential.

Increased mitochondrial ROS and decreased mitochondrial membrane potential could activate mitochondrial fission (Palmer et al. 2011; Westermann 2010; Youle and van der Bliek 2012), which we showed for regorafenib and sorafenib. Fission creates smaller mitochondria which may be eliminated by mitophagy to remove damaged and potentially dangerous mitochondria (Archer 2013). Actually, we could observe an increased mitophagy after treatment with regorafenib and sorafenib. As mitophagy is used to remove damaged mitochondria, it is a protective mechanism of cells to avoid apoptosis or necrosis (Ding and Yin 2012; Hamacher-Brady and Brady 2016; Palikaras and Tavernarakis 2014). However, when the mitochondria are too damaged, mitophagy is overwhelmed and cells are eliminated. Indeed, we could observe apoptosis for regorafenib and sorafenib and necrosis for sorafenib.

Furthermore, both compounds inhibited glycolysis at similar concentrations as observed for mitochondrial inhibition. The dual inhibition of ATP synthesis by ETC inhibition and inhibition of glycolysis is a likely explanation for the strong effects of regorafenib and sorafenib on the ATP pool.

Our findings for regorafenib and sorafenib are for the most part consistent with previous observations. Regarding regorafenib, Zhang et al. and Weng et al. have shown that regorafenib impaired the mitochondrial function at concentrations that are reached in humans (Weng et al. 2015; Zhang et al. 2017b). In both studies, regorafenib uncoupled oxidative phosphorylation, showed mitochondrial swelling, and a decreased mitochondrial membrane

potential, which is in agreement with our findings. Regorafenib inhibited complex II in isolated rat liver mitochondria (Zhang et al. 2017b), which is in partial agreement with our findings of complex II, III, and V inhibition in acutely exposed isolated mice liver mitochondria. In agreement with our study, increased mitophagy has been described in primary rat hepatocytes exposed with regorafenib (Weng et al. 2015). Regorafenib has been associated with induction of necrosis in rat hepatocytes (Weng et al. 2015), whereas we observed apoptosis. This may be explained be the different cell models that were used. Apoptosis is dependent on ATP (Wang and Youle 2009) while necrosis does not need ATP. It is therefore possible that the intracellular ATP content dropped more rapidly in rat hepatocytes than in the HepG2 cells we used.

Regarding regorafenib, Weng et al. postulated that uncoupling of OXPHOS is the initial event leading to downstream effects (Fig. 33) (Weng et al. 2015). Mitochondrial membrane potential, ATP shortage, and triggered mitochondrial permeability transition were following events at later time points. The ATP shortage was associated with AMPK and autophagy activation. Regorafenib-induced hepatocyte death was predominantly due to necrosis and not apoptosis, very likely because of the lack of sufficient ATP.
In our study, we observed uncoupling of OXPHOS starting at 2 µM after 24 h treatment with regorafenib. Mitochondrial membrane potential decrease and ATP shortage started at 10 µM after 24 h treatment and thus at higher concentration as uncoupling of OXPHOS. Unfortunately, we did not investigate time dependency of these events. But concerning concentrations, we could confirm that uncoupling of OXPHOS and eventually complex inhibition of the ETC are the initial events leading afterwards to ATP shortage, decreased mitochondrial membrane potential, ROS formation, mitophagy, and apoptosis.

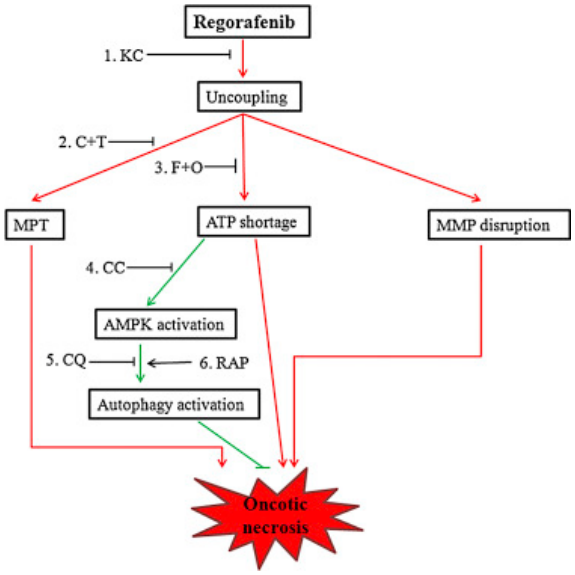

Figure 33: Postulated mechanism for regorafenib toxicity according to (Weng et al. 2015). Uncoupling of OXPHOS is the initial event leading to the downstream effects ATP shortage, mitochondrial membrane disruption, and mitochondrial permeability transition.

Sorafenib-associated toxicity has been studied by several groups and mitochondrial toxicity has been described in human neuroblastoma cells (Bull et al. 2012), in H9c2 myoblastic cells (Will et al. 2008), HepG2 cells (Chiou et al. 2009), and isolated rat liver mitochondria (Zhang et al. 2017b). Zhang et al. have shown that sorafenib impaired the mitochondrial function after acute exposure in concentrations that are reached in humans (Zhang et al. 2017b). Sorafenib showed uncoupling of the respiratory chain and inhibition of complex II/III and IV in acutely exposed mitochondria (Will et al. 2008; Zhang et al. 2017b), which agrees with our observations. Bull et al. showed complex I inhibition after long-term exposure of human neuroblastoma cells with sorafenib (Bull et al. 2012). These data are in agreement with our long-term data after 24 hours exposure. In addition, sorafenib induced ROS accumulation and GSH depletion in HepG2 cells at concentrations below patient plasma concentrations (Chiou et al. 2009), which agree with our findings.

In their recent article, Zhang et al. suggested the model that sorafenib inhibits both receptor tyrosine kinases signaling and mitochondrial quality control pathways to cause tumor suppression (Figure 34) (Zhang et al. 2017a). Sorafenib shuts down both PI3K/AKT and MEK pathways, both of which are known to regulate transcription of Bcl-2 and Mcl-1. In addition, sorafenib inhibits the activity of complex II/III and complex V of the ETC, followed by depolarization of the mitochondrial membrane potential and stabilization of the protein kinase PINK1 in the outer mitochondrial membrane, which leads to Parkin phosphorylation.

Parkin ubiquitylates numerous substrates on mitochondria, including Mcl-1, and lowers the overall levels of the anti-apoptotic Bcl-2 proteins triggering apoptosis and not mitophagy (Zhang et al. 2017a). In our study, sorafenib was also associated with inhibited complexes of the ETC and depolarized mitochondrial membrane potential. But sorafenib did not affect Mcl-1 expression in HepG2 cells and we detected both, mitophagy and apoptosis. It therefore seems that the activation of sorafenib on mitophagy and apoptosis are cell specific.

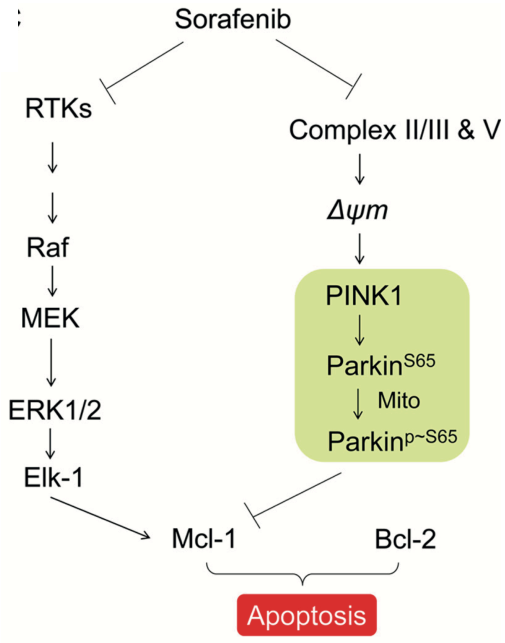

Figure 34: Proposed model for sorafenib induced cellular response via kinase-dependent or mitochondrion-dependent pathways (Zhang et al. 2017a).

It is known that sorafenib (Figure 35) induces apoptosis through a caspase-independent mechanism, activates the pro-apoptotic Bak and Bax proteins, reduces the mitochondrial membrane potential, down-regulates the levels of the anti-apoptotic Bcl-2 and Bcl-xL proteins, and releases cytochrome *c* from mitochondria in malignant cells (Panka et al. 2006). In addition, apoptosis was related to the induction of stress of the endoplasmic reticulum, down-regulation of the anti-apoptotic protein Mcl-1, and pronounced ROS generation (Rahmani et al. 2007). It is possible that the mitochondrial toxicity in hepatocytes follows a similar pathway as we also observed depolarization of the mitochondrial membrane potential, ROS formation, and release of cytochrome *c* into the cytoplasm.

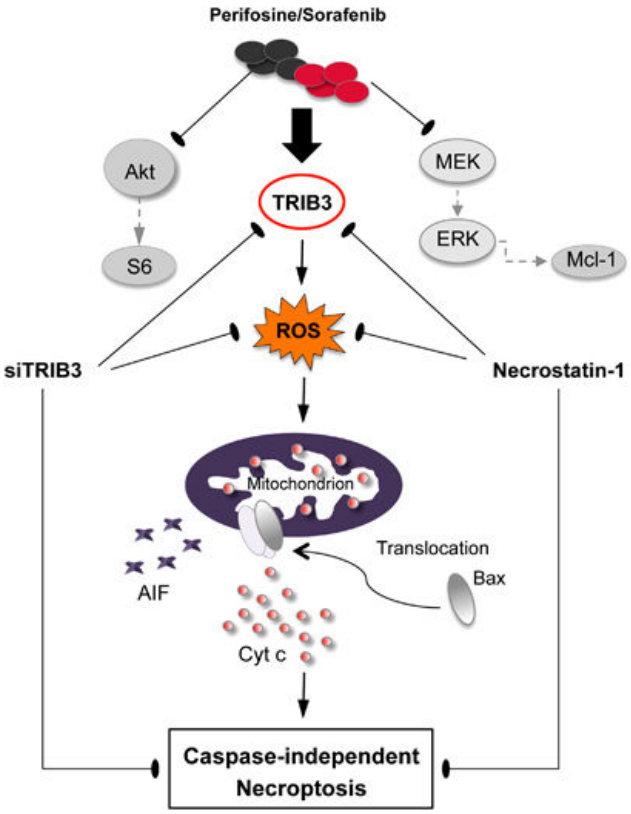

Figure 35: Proposed model of perifosine/sorafenib mechanism of action (Locatelli et al. 2013). Perifosine/sorafenib treatment triggers necroptotic cell death that is mediated by ROS production. Upregulation of TRIB3 leads to activation of Bax, mitochondrial outer membrane permeabilization, release of cytochrome *c*, and apoptosis-inducing factor (AIF), ultimately leading to caspase-independent necroptosis.

2 PONATINIB

Ponatinib impaired mitochondrial function and glycolysis at higher concentrations than reached in patient plasma, but such concentrations may be reached in the liver. Ponatinib depleted intracellular ATP stores at lower concentrations than cytotoxicity occurred and was more cytotoxic under galactose conditions compared to glucose conditions. Both are markers of mitochondrial toxicity (Kamalian et al. 2015; Marroquin et al. 2007). Ponatinib inhibited the mitochondrial oxidative metabolism by inhibiting complexes I and II in HepG2 cells and complexes I, III, and V in isolated mitochondria and consequently increased mitochondrial ROS formation at the same concentrations as ETC inhibition as ROS formation is associated with complex I and III inhibition (Drose and Brandt 2012). Increased ROS formation is also

related to reduced GSH stores and induction of mitochondrial membrane permeability transition, which is further associated with mitochondrial swelling, rupture of the outer mitochondrial membrane, and release of cytochrome *c* into the cytoplasm, which induces cell death through apoptosis and/or necrosis (Antico Arciuch et al. 2012; Green and Reed 1998; Kaufmann et al. 2005). We could demonstrate a decrease in GSH content and in mitochondrial membrane potential and a release of cytochrome *c* into the cytoplasm for ponatinib. In addition, impairment of mitochondria was associated with increased mitochondrial fission and mitophagy as increased mitochondrial ROS and decreased mitochondrial membrane potential are associated with mitochondrial fission (Palmer et al. 2011; Westermann 2010; Youle and van der Bliek 2012). Mitophagy is a protective mechanism for the cells to avoid apoptosis or necrosis. But at higher concentrations, ponatinib induced apoptosis, suggesting that mitophagy is overwhelmed and damaged cells are eliminated. Furthermore, inhibition of glycolysis occurred at 10-times higher concentrations than ATP depletion, suggesting that inhibition of glycolysis is not the main mechanism of ponatinib-induced hepatotoxicity.

Another study in acutely exposed isolated rat liver mitochondria did not find mitochondrial toxicity for ponatinib (Zhang et al. 2017b). These findings are in contrast to our observations but these results were obtained in different cell systems and species compared to our study, which perhaps explains the different findings. Talbert et al. reported that ponatinib is associated with ROS formation and lipid accumulation in human induced pluripotent stem cell-derived cardiomyocytes (Talbert et al. 2015), suggesting mitochondrial toxicity.

3 SUNITINIB

Sunitinib also impaired mitochondrial function and glycolysis at higher concentrations than reached in plasma in patients, but such concentrations may be reached in the liver. Sunitinib impaired the mitochondrial function by inhibiting complex I. As a consequence sunitinib induced oxidative stress, GSH depletion, and mitochondrial membrane potential decrease. This is associated with the release of cytochrome *c* and finally with induction of apoptosis. All these effects occurred in a concentration range between 1 µM and 20 µM of sunitinib. Moreover, sunitinib inhibited glycolysis at 20 µM. The plasma concentrations that are reached

in patients are between 0.1 µM and 0.3 µM (Di Gion et al. 2011) and therefore 10-100 times lower than the concentrations where mitochondrial effects occurred.

Our *in vitro* investigations are in agreement with another study in mouse liver mitochondria where sunitinib induced loss in mitochondrial membrane potential and inhibited complex II (Porceddu et al. 2012). In contrast, a study in isolated rat liver mitochondria did not show any mitochondrial toxicity due to sunitinib (Zhang et al. 2017b). This may reflect species differences (human versus rat) or that the duration of exposure is important for the mitochondrial impairment as this study treated the rat mitochondria for 5 to 30 minutes whereas we treated the HepG2 cells for 48 hours. In addition, our study showed that ATP depletion and cytotoxicity were time dependent.

A daily dose of 7.5 mg/kg/day sunitinib for 14 days induced hepatocellular injury, which was related to mitochondrial damage and hepatocyte apoptosis. Treatment with 7.5 mg/kg/day sunitinib for 14 days had no effects on the food and water intake, body weight or liver weight. But our investigations showed a decreased activity of all complexes of the electron transport chain with a significant decrease for complex III activity. In addition, the protein content of subunits of complexes III, IV, and V were decreased, maybe explaining the decreased complex III activity. Moreover, the citrate synthase activity, which is a marker for the mitochondrial content, was significantly decreased due to sunitinib-treatment. Furthermore, the key regulator of energy metabolism and mitochondrial biogenesis PGC-1α (Lynch et al. 2017) was decreased. Impaired mRNA expression of subunits of complexes of the respiratory chain is in agreement with impaired mitochondrial biogenesis in sunitinib-treated mice. As previously mentioned, inhibition of complex I and complex III of the electron transport chain is related to increased mitochondrial ROS formation (Drose and Brandt 2012). Indeed, we observed an increased mitochondrial ROS formation in mice treated with sunitinib. Mitochondrial superoxide can be degraded by SOD2, an important member of the antioxidant system, and SOD2 can be upregulated as a response to increased mitochondrial ROS (Felser et al. 2013) which was shown in our *in vivo* study. Further consequences of complex inhibition and increased ROS formation are the mitochondrial permeability transition induction (Antico Arciuch et al. 2012), leading to outer mitochondrial membrane rupture, release of cytochrome *c*, and finally apoptosis. Indeed, we could show increased caspase 3 activation, increased TUNEL-positive hepatocytes and increased ALT levels, indicating hepatocyte apoptosis in mice treated with sunitinib.

The sunitinib plasma concentration in mice was 3.18 nmol/l, whereas the liver concentration was 92 nmol/kg. Typical C_{max} concentration of patients treated with sunitinib are between 0.1 µM and 0.3 µM (Di Gion et al. 2011). However, we determined trough values 24 hours after the last sunitinib administration. Therefore, the calculated maximal plasma concentration in mice is around 0.2 µmol/l, if we assume a plasma half-life of 4 hours in mice (Haznedar et al. 2009). This concentration agrees well with the plasma concentrations observed in humans. Importantly, the liver concentration in mice was 26-fold higher than in plasma, which is in agreement with previous studies also showing higher liver than plasma concentrations (He et al. 2008; Lau et al. 2015; Spector et al. 2015).
Taking the 26-fold higher liver concentrations into consideration, concentrations between 0.1 µM and 0.3 µM in plasma of patients would give concentrations between 2.6 µM and 7.8 µM in the liver of patients. In our *in vitro* study, we could see a decreased membrane potential and ROS formation already at 1 µM and 2 µM, respectively, whereas ATP depletion occurred at 5 µM, demonstrating that mitochondrial impairment occurs at concentrations relevant for patients.

At the moment, there are no *in vivo* studies regarding hepatotoxicity of sunitinib *in vivo*. Maayah et al. investigated the effects of 25, 50, and 100 mg/kg sunitinib treatment for 15 and 30 days in Wistar albino rats on cardiotoxicity (Maayah et al. 2014). Sunitinib treatment caused increase in cardiac enzymes in plasma, changes in histopathology, and induction in several hypertrophic markers. Chu et al. treated mice for 12 days with 40 mg/kg/day sunitinib and investigated abnormalities of cardiomyocytes on transmission electron microscopy with mitochondrial swelling and degenerative changes including membrane whorls, effaced cristae, and induction of apoptosis (Chu et al. 2007). These findings are going in the same direction as our observations of hepatocyte injury with impaired mitochondria and induction of apoptosis.

Abdel-Aziz et al. proposed a mechanism for sunitinib-induced cognitive defects (Abdel-Aziz et al. 2016). Sunitinib is interfering with VEGF/VEGFR2/mTOR signaling. In addition, sunitinib induced chromatin fragmentation and distortion of mitochondrial cristae architecture *via* increasing p53 and caspase 3 while reducing Bcl-2 and nuclear factor kappa B (NFκB) levels eventually resulting in apoptotic cell death. Furthermore, sunitinib switched off autophagic recycling machinery through decreasing beclin-1, Atg-5 and increasing SQTSM1/p62, resulting in accumulation of dysfunctional autophagosomes. Therefore,

increased apoptosis and decreased autophagy leading to the sunitinib-induced effects. In our study, we could show increased caspase 3 cleavage and induction of apoptosis, but we did not investigate the other mentioned pathways.

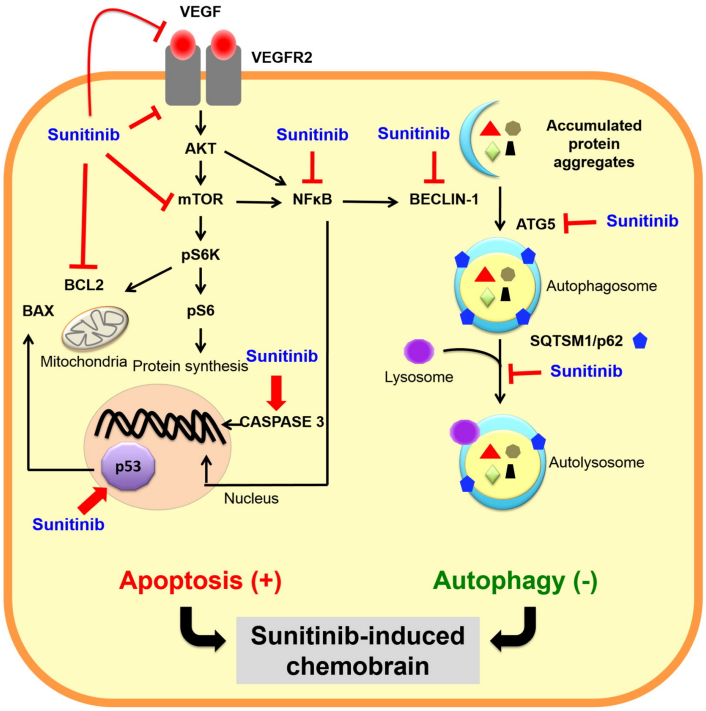

Figure 36: Mechanistic insights into sunitinib-induced cognitive deficits (Abdel-Aziz et al. 2016). Sunitinib interfered with VEGF/VEGFR2/mTOR signaling. Furthermore, sunitinib induced chromatin fragmentation and distortion of mitochondrial cristae architecture via increasing p53 and caspase 3 while reducing Bcl-2 and nuclear factor kappa B (NFκB) levels eventually ensuing apoptotic cell death. In addition, sunitinib switched off autophagic recycling machinery through decreasing beclin-1, Atg-5 and increasing SQTSM1/p62, resulting in accumulation of dysfunctional autophagosomes.

4 IMATINIB

Imatinib impaired the mitochondrial function by inhibiting complex III, inducing oxidative stress, and GSH depletion, reducing the mitochondrial membrane potential, releasing cytochrome *c*, and finally inducing apoptosis through caspase 3 and PARP cleavage at a concentration range between 5 µM and 50 µM. In addition, imatinib inhibited glycolysis at 50 µM. The plasma concentration for imatinib reached in patients is 3.2 µM (Bolton et al.

2004). The mitochondrial impairment and inhibition of glycolysis started at higher concentrations than reached in plasma in patients. However, several studies showed that liver concentrations of TKIs are 8, 35, and 10 fold increased compared to plasma concentrations (He et al. 2008; Lau et al. 2015; Spector et al. 2015). Therefore, such concentrations where mitochondrial impairment takes place may be reached in the liver of patients treated with imatinib. A study in isolated rat liver mitochondria showed decreased mitochondrial oxidative metabolism and release of cytochrome *c* at 60 µM and 100 µM (Zhang et al. 2017b). These findings are in agreement with our observations.

In isolated cardiomyocytes, imatinib (Figure 37) resulted in increased endoplasmic reticulum stress due to Abl kinase inhibition, leading to TIM23 degradation. TIM23 is essential for protein import into the mitochondrial matrix, and thus unfolded proteins accumulate in the mitochondrial intermembrane space leading to a collapse of the mitochondrial membrane potential and mitochondrial death pathways. In addition, impaired protein import will negatively affect major mitochondrial metabolic pathway such as mitochondrial DNA synthesis, TCA, β-oxidation, and heme synthesis (Varga et al. 2015). Another study showed that imatinib induces mitochondrial transmembrane permeability dissipation and activation of caspase 3 and 9, demonstrating that the effect of imatinib is at the mitochondrial level (Jacquel et al. 2003). In addition, imatinib decreased the expression of the anti-apoptotic proteins Bcl-2, Bcl-xL, and Mcl-1 and increased the expression of the pro-apoptotic Bim (Jacquel et al. 2003). Kerkela et al. also showed endoplasmic reticulum stress, collapse of the mitochondrial membrane potential, release of cytochrome *c* into the cytosol, reduced cellular ATP content, and cell death in cardiomyocytes (Kerkela et al. 2006). In our studies, we found ATP depletion, release of cytochrome *c*, and apoptosis at 5 µM or 10 µM, whereas complex III inhibition, oxidative stress, and GSH depletion started at 50 µM. We can therefore hypothesize that imatinib-induced hepatotoxicity could be in a similar pathway as in cardiomyocytes. Unfortunately, we did not measure endoplasmic reticulum stress in our study.

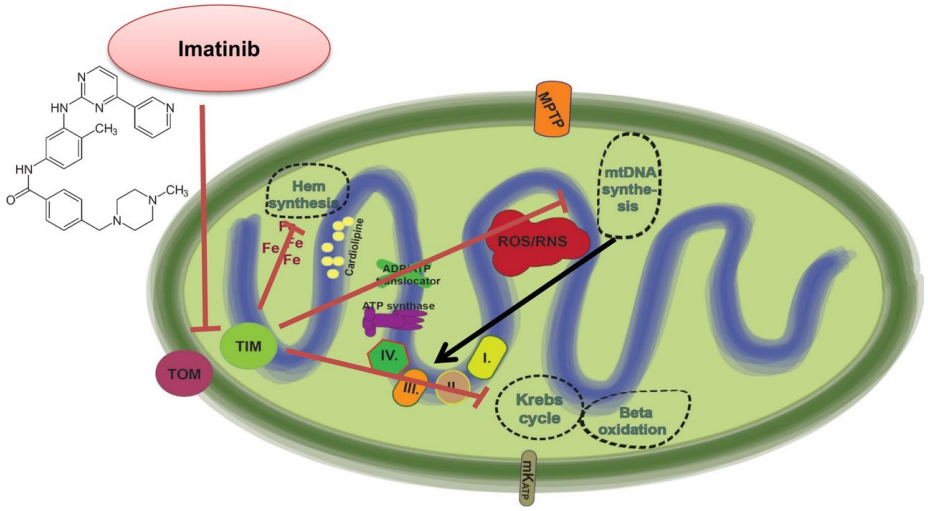

Figure 37: Mechanisms of imatinib cardiotoxicity (Varga et al. 2015). Inhibition of Abl kinase by imatinib induces mitochondrial dysfunction due to endoplasmic reticulum stress, leading to TIM23 degradation. Consequently, unfolded proteins accumulate in the mitochondrial intermembrane space leading to a collapse of the mitochondrial membrane potential and mitochondrial death pathways. Moreover, impaired protein import will negatively affect major mitochondrial metabolic pathway such as mitochondrial DNA synthesis, TCA, β-oxidation, and heme synthesis. TIM: translocase of the inner membrane, TOM: translocase of the outer membrane

5 LAPATINIB

Lapatinib impaired mitochondrial function and glycolysis at higher concentrations than reached in plasma in patients but such concentrations may be reached in the liver. Lapatinib decreased the mitochondrial membrane potential, induced oxidative stress, induced apoptosis, and decreased glycolysis in HepG2 cells at 20 µM, which is above the 4.8 µM plasma concentration in patients. Lapatinib showed a more pronounced cytotoxicity and intracellular ATP reduction in the presence of glucose medium, which favors glycolysis, compared to galactose medium, which favors mitochondrial ATP production. This supports the hypothesis that the mechanism of hepatotoxicity of lapatinib partially involved mitochondria and, possibly to a larger extent, inhibition of glycolysis and other non-mitochondrial-toxicity pathways. Lapatinib did not impair the oxidative metabolism, but decreased the mitochondrial membrane potential, increased mitochondrial oxidative stress, and was associated with the release of cytochrome *c* into the cytoplasm and induction of apoptosis. CYP induction

increased the toxicity of lapatinib, suggesting the formation of toxic metabolites. This is in agreement with two other studies where CYP3A4 induction in HepaRG cells was involved in lapatinib-induced hepatotoxicity (Hardy et al. 2014) and where the O-dealkylated lapatinib metabolite induced oxidative stress, reduced oxygen consumption, and decreased GSH levels (Eno et al. 2016). Another study in isolated rat liver mitochondria showed that lapatinib released cytochrome *c* at 10-fold Cmax, but did not impair the oxidative metabolism, did not reduce the mitochondrial membrane potential, did not affect mitochondrial swelling and did not increase oxidative stress (Zhang et al. 2017b). These findings are in agreement with our observations that mitochondrial impairment is not the main mechanism of hepatotoxicity of lapatinib.

Castellino et al. proposed several lapatinib-induced hepatotoxicity mechanisms (Figure 38) (Castellino et al. 2012). First, several lapatinib metabolites by CYP3A4 in the liver could form reactive electrophilic intermediates that could contribute to hepatotoxicity. These metabolites could form glutathione and cysteinglycine conjugates (Teng et al. 2010). In addition, lapatinib is a mechanism-based inactivator of CYP3A4 (Teng et al. 2010). Secondly, a pharmacogenetic analysis of patients with metastatic breast cancer experiencing liver injury with lapatinib exposure reported a significant association with the HLA-DQA1*02:01 and ALT elevation suggesting adaptive immune system activation (Spraggs et al. 2011). Furthermore, the interaction with drug transporters is involved either directly or indirectly in the underlying mechanism of hepatotoxicity (Polli et al. 2008). In addition, inhibition of bile salt efflux pump by lapatinib has been investigated leading to interruption of bile salt export and causing cholestatic liver damage (Castellino et al. 2012). Feng et al. suggested a combination of direct cytotoxicity to mitochondria and inhibition of bile salt efflux to explain the clinical hepatotoxicity observed in a structural similar TKI (Feng et al. 2009). Regarding our results, we observed cytotoxicity in hepatocytes at 10 µM whereas other mitochondrial impairment started at higher concentrations. We did not measure transporter or bile salt efflux in our study. It is therefore difficult to say if we have a similar pathway in HepG2 cells, but the fact that CYP induction by rifampicin in HepaRG cells increased the ATP reduction, suggests that lapatinib metabolites contribute to the lapatinib-induced hepatotoxicity.

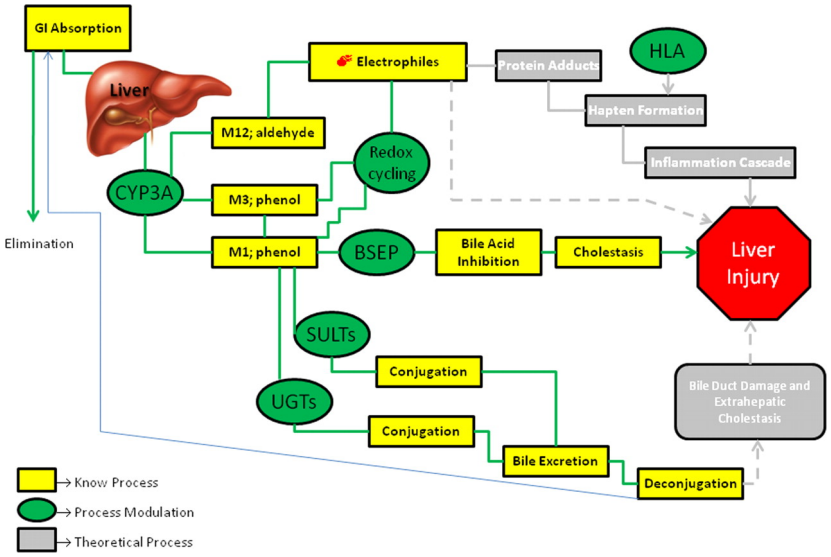

Figure 38: Possible lapatinib hepatotoxicity mechanisms (Castellino et al. 2012). GI: gastrointestinal, BSEP: bile salt exort pump, SULT: sulfotransferase, UGT: UDP-glucuronosyltransferase.

6 CRIZOTINIB AND DASATINIB

For crizotinib and dasatinib, cytotoxicity and ATP depletion were not enhanced under galactose conditions compared to glucose conditions suggesting a non-mitochondrial mechanism of hepatotoxicity. In addition, CYP-associated metabolites of crizotinib and dasatinib were less toxic compared to the parent compounds. Both compounds started to induce apoptosis at 10 µM and 20 µM, respectively, which was at lower concentrations than other investigated effects like ATP depletion, mitochondrial membrane potential, and ROS formation, which started at 20 µM, 50 µM, or 100 µM. Therefore, the induction of apoptosis is probably not associated with mitochondrial mechanisms. Crizotinib was not associated with inhibition of glycolysis, whereas dasatinib inhibited glycolysis at 50 µM. Typical plasma concentrations in patients are 1.9 µM for crizotinib (Kurata et al. 2015) and 0.6 µM for dasatinib (Haura et al. 2010). These concentrations are clearly below the concentrations where we observed toxicity. This proposes a non-mitochondrial mechanism of hepatotoxicity for crizotinib and dasatinib.

Our observations for crizotinib and dasatinib are for the most part consistent with previous findings. In isolated rat liver mitochondria, crizotinib induced mitochondrial effects at much

higher concentrations than Cmax concentration in patients and dasatinib did not cause mitochondrial toxicity (Zhang et al. 2017b). In another study in rat hepatocytes, dasatinib was associated with oxidative stress, decreased mitochondrial membrane potential, and induction of apoptosis starting at 7.5 µM or 15 µM (Xue et al. 2012) which is again higher than plasma concentration in patients. But a study after single oral dose of radio-labeled dasatinib administered to rats showed that the liver concentration was eight-times higher than dasatinib plasma concentration (He et al. 2008). Considering this, the observed effects may be starting at patients' liver concentrations.

7 ERLOTINIB AND PAZOPANIB

Erlotinib and pazopanib were the least toxic compounds of the 10 investigated TKIs in this study. Neither showed cytotoxicity or ATP depletion and did not disturb the mitochondrial membrane potential or mitochondrial oxygen consumption in HepG2 cells up to 20 µM and 50 µM, respectively. Higher concentrations could not be investigated due to solubility problems in the cell culture medium. Erlotinib was slightly cytotoxic and decreased the ATP in HepaRG cells and CYP induction decreased the toxicity of erlotinib, implying the formation of non-toxic metabolites. Because erlotinib did not affect oxidative metabolism or mitochondrial membrane potential, mitochondrial mechanism of hepatotoxicity could be excluded. Erlotinib did not impair glycolysis, but induced apoptosis at 20 µM. The induction of the apoptotic pathway is probably due to non-mitochondrial pathways. Our results are in relative agreement with another study in isolated rat liver mitochondria that showed no mitochondrial impairment of erlotinib except inhibition of complex V at 10-fold Cmax (Zhang et al. 2017b).

Deng et al. proposed a pathway for erlotinib-induced apoptosis (Fig. 39) (Deng et al. 2007). The key step is the induction of BIM, a pro-apoptotic protein, to the intrinsic apoptotic pathway. This pathway could be demonstrated in non-small cell lung cancer cells as wells as in a model hematopoietic cell line suggesting that this apoptosis-inducing pathway might be a general feature to be expected of inhibition of activated EGFR in many different cellular contexts. Among all tissues, EGFR is most highly expressed in hepatocytes of adult livers indicating the important role in liver repair and regeneration (Komposch and Sibilia 2015).

Therefore, it is possible that erlotinib-induced apoptosis in hepatocytes in due to the same pathway. Unfortunately, in our study we did not investigate the protein content of members of the Bcl2-family like BIM or Bcl-2. We could show an increased release of cytochrome *c* into the cytosol and cleavage of caspase 3.

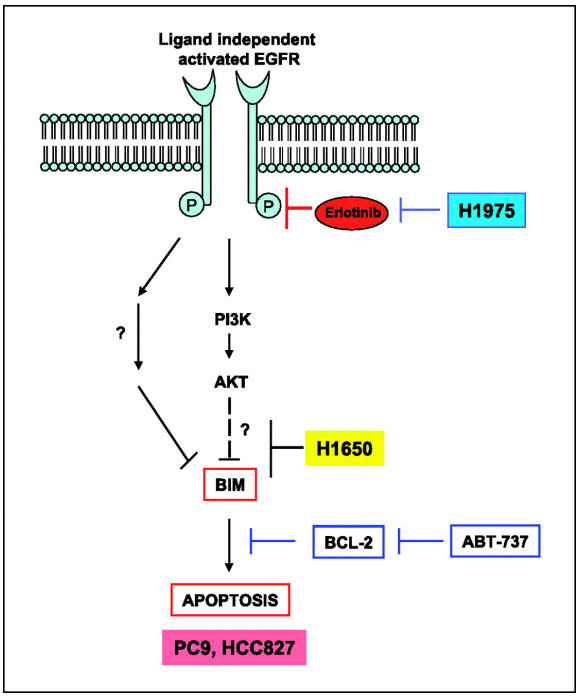

Figure 39: Model of erlotinib-induced apoptosis (Deng et al. 2007). Erlotinib inhibits activated EGFR. This result is up-regulation of BIM, a pro-apoptotic molecule. The downstream effect of BIM is induction of apoptosis.

Pazopanib had a slightly increased ROS accumulation, but to a much lower extent than all the other TKIs. In addition, it induced apoptosis at 20 µM and inhibited glycolysis at 20 µM. The induction of apoptosis is probably non-mitochondrial. It has to be considered, that pazopanib can reach plasma concentrations up to 100 µM in patients while we could investigate the effects only up to 50 µM. Therefore, exposure-dependent toxicity at higher concentration cannot be excluded completely. A study described pazopanib-mediated hepatotoxicity in patient-specific hepatocyte-like cells (HLCs) derived from induced pluripotent stem cells (Choudhury et al. 2017). In this study, pazopanib was more cytotoxic in HLCs derived from patients with pazopanib-induced clinically hepatotoxicity compared to HLCs derived from patients treated with pazopanib having no hepatic effects. In addition, pazopanib induced oxidative stress, depletion of GSH, and caused disruption of iron metabolism. Another study in isolated rat liver mitochondria showed impaired oxygen consumption and inhibition of

complex I at Cmax concentration (Zhang et al. 2017b). These results were obtained in different cell systems and species, perhaps explaining the different findings.

8 ARE THE OBSERVED HEPATOTOXICITY EVENTS ON- OR OFF-TARGET EFFECTS?

The fact that some approved TKIs show no liver injury (Shah et al. 2013), indicates that the TKI-induced hepatotoxicity is unlikely due to overall kinase inhibition. But the question arises whether the inhibition of a designated TK leads to hepatotoxicity. Table 4 shows the targets of the 10 investigated TKIs. The investigated TKIs inhibit a broad range of kinases with VEGFR, PDGFR, c-kit, and BCR-ABL1 as the most common targets. Most case reports for hepatotoxicity can be found for regorafenib and sorafenib, the most pronounced mitochondrial toxicants and inhibitors of glycolysis in our study. Regorafenib and sorafenib both inhibit VEGFR and PDGFR, but this is also the case for pazopanib, which was almost not toxic to HepG2 cells. We could therefore postulate that off-target effects unrelated to the pharmacological activity leading to hepatotoxicity.

Table 4: Targets of the investigated TKIs. The TKIs are listed according to their hepatotoxicity with erlotinib as the least toxic TKI. The main targets are marked in red.

	VEGFR	PDGFR	FGFR	RAF	c-kit	BCR-ABL1	Others
Regorafenib	x	x	x	x	x		
Sorafenib	x	x			x		
Ponatinib	x		x			x	
Sunitinib	x	x			x		FLT3, CSF1R
Imatinib		x			x	x	
Lapatinib							ErbB1, HER2, EGFR
Crizotinib							ALK, ROS1
Dasatinib					x	x	Src
Pazopanib	x	x			x		
Erlotinib							EGFR

In addition, there is no evidence that hepatotoxicity is related to a particular chemical class as lapatinib is an anilinoquinazoline, pazopanib is an aminopyrimidine, regorafenib is a pyridylcarboxamide, and sunitinib is a pyrrolylcarboxamide while all showing hepatotoxicity *in vitro* and in patients (Shah et al. 2013). But it has to be mentioned, that the chemical structures of regorafenib and sorafenib (compare Fig. 30 and Fig. 31) are quite similar with just a fluoro-group difference and both have a similar pathway of hepatotoxicity. Furthermore, patients who develop hepatotoxicity on gefitinib are able to tolerate erlotinib, although both have a 4-anilinoquinazoline structure and inhibit both EGFR-mediated pathways (Shah et al. 2013). For sunitinib-induced cardiotoxicity, an off-target inhibition of AMP-activated protein kinase was postulated (Kerkela et al. 2009). Taking all these points together, off-target toxicity of TKIs could be suggested.

9 LIVER CONCENTRATIONS

The hepatic exposure of drugs is primarily dependent on the administered dose, but may also be affected by interacting drugs. Since all TKIs are mainly metabolized by CYP3A4 (Josephs et al. 2013), concomitant treatment with CYP3A4 inhibitors, such as ketoconazole, may increase toxicity and the likelihood of developing fatal liver injury. For imatinib, lapatinib, and sunitinib, CYP3A4 inducers could also increase the risk for liver toxicity, since the metabolites formed may be more toxic than the corresponding parent compounds. Because of the involvement in the metabolism of the TKIs, differences in CYP3A4-mediated metabolism may have important consequences that influence the development of clinical hepatotoxicity, which could arise because of different genetic or environmental factors (Castellino et al. 2012).

In addition, as shown by data in mice, the TKI concentrations in liver may be higher than the plasma concentrations. The increase in liver to plasma concentration was eight-fold for dasatinib, 35-fold for sunitinib, and 10-fold for lapatinib (He et al. 2008; Lau et al. 2015; Spector et al. 2015). In our mice study, we could demonstrate a 26-fold increased liver concentration compared to plasma concentrations.

10 INTRINSIC VS. IDIOSYNCRATIC DILI

The finding of mitochondrial toxicity for regorafenib and sorafenib at *in vitro* concentrations similar or below clinically therapeutic blood concentrations raises the question why hepatotoxicity is not more frequently seen in patients treated with these drugs. Thus, the infrequent but profound hepatotoxicity seen in patients may reflect individual variations in regorafenib and sorafenib pharmacokinetics such that *in vivo* hepatocyte exposures indeed approach the hepatotoxic level observed in the current studies (Weng et al. 2015). In addition, the strong regeneration capacity of the liver has to take into consideration.

Considering the low incidence and occurrence at therapeutic dosage, TKI-induced liver injury can be regarded as an idiosyncratic (type B) adverse reaction, suggesting that affected patients have susceptibility factors (Tujios and Fontana 2011). However, as indicated by our studies and as observed in clinical practice, TKI-associated hepatotoxicity seems to be dose-related, favoring intrinsic (type A) toxicity as a mechanism. The data of our studies and clinical experience suggest that exposure is an important risk factor for TKI-associated toxicity. As discussed in the previous chapter, hepatic exposure is primarily dependent on the administered dose, but may also be affected by interacting drugs.

In addition to mitochondrial toxicity, patients with preexisting mitochondrial dysfunction such as an impaired ETC or an impaired antioxidative system, may also be at increased risk for toxicity.

CONCLUSION

In conclusion, our investigations demonstrate that regorafenib and sorafenib were strong mitochondrial inhibitors at concentrations that can be reached in plasma and liver of patients. The inhibition of the ETC is perhaps the initial event leading to downstream effects such as ATP depletion, ROS formation, mitophagy, and apoptosis. Moreover, they also inhibited glycolysis, which may further increase their toxic effects. Imatinib, lapatinib, ponatinib, and sunitinib were associated with mitochondrial dysfunctions and inhibition of glycolysis at concentration that may be reached in liver of affected patients, as liver concentrations could be multifold higher than plasma concentrations. In contrast, crizotinib, dasatinib, erlotinib, and pazopanib showed neither relevant mitochondrial impairment nor inhibition of glycolysis. For these drugs, undefined, non-mitochondrial mechanisms of hepatotoxicity have to be postulated.

As TKIs are used for cancer patients who have exhausted conventional treatment options, the possible liver risk should be carefully weighed against its clinical benefits.

OUTLOOK

Our studies demonstrated that inhibition of the electron transport chain and oxidative stress are two of the key factors for the toxicity of several TKIs.

A possibility to investigate whether an impaired antioxidant system is a susceptibility factor for TKI-associated hepatotoxicity is by knocking down SOD2 or NRF2 or depleting the GSH pool with buthionine-sulfoximine in HepG2 cells. SOD2 is an important enzyme for detoxifying ROS and protects cells against cell death. A lack of SOD2 leads to increased mitochondrial ROS formation, which leads to activation of apoptosis. NRF2 is a nuclear transcription factor which induces the antioxidant system after stimulation by ROS (Ma 2013). If an impaired antioxidant system would be a susceptibility factor, this should make cells more susceptible to TKIs.

We investigated the effects of sunitinib *in vivo* in C57BL/6 wild-type mice and could show induced hepatocellular injury, which was related to mitochondrial damage and hepatocyte apoptosis after treatment with 7.5 mg/kg/day sunitinib for 14 days. It would be interesting to do the same experiments in a mouse model with reduced antioxidant capacity to see whether this could be a risk factor for hepatotoxicity. Such mouse models could be the $SOD2^{+/-}$ mouse model or the NRF2 knock-out mouse model. $SOD2^{+/-}$ mice are more susceptible to nimesulide than wild-type mice (Ong et al. 2006). In agreement with the important role of NRF2 for the regulation of the antioxidant system, NRF2 knock-out mice have been shown to be more susceptible to paracetamol (Enomoto et al. 2001) and to 1-bromopropane (Liu et al. 2010). Thus, treatment of these mice with sunitinib should increase mitochondrial impairment, confirming that oxidative stress is a susceptibility factor in mice treated with sunitinib.

Furthermore, at the moment there is not enough known about the susceptibility factors of TKI-induced hepatotoxicity. Genome-wide association studies (GWAS) could be used to identify genetic susceptibility factors for TKI-associated hepatotoxicity.

Moreover, our data show that acute and long-term exposure can affect mitochondria differently. At the moment, it is not clear where the differences in the hepatotoxicity-mechanisms are. We suggest that the actual concentration of TKIs in the mitochondria might be lower in HepG2 cells after long-term exposure compared to acutely exposed isolated mitochondria. Therefore, it would be useful to investigate the difference of acute and long-term exposure and the time-dependency of TKI-induced hepatotoxicity in more detail to obtain a complete picture of mitochondrial toxicity of TKIs and their susceptibility factors.

BIBLIOGRAPHY

Abdel-Aziz AK, Mantawy EM, Said RS, Helwa R (2016) The tyrosine kinase inhibitor, sunitinib malate, induces cognitive impairment in vivo via dysregulating VEGFR signaling, apoptotic and autophagic machineries. Exp Neurol 283(Pt A):129-41 doi:10.1016/j.expneurol.2016.06.004

Abrams TJ, Lee LB, Murray LJ, Pryer NK, Cherrington JM (2003) SU11248 inhibits KIT and platelet-derived growth factor receptor beta in preclinical models of human small cell lung cancer. Molecular cancer therapeutics 2(5):471-8

Ademowo OS, Dias HKI, Burton DGA, Griffiths HR (2017) Lipid (per) oxidation in mitochondria: an emerging target in the ageing process? Biogerontology doi:10.1007/s10522-017-9710-z

Aguilera DG, Tsimberidou AM (2009) Dasatinib in chronic myeloid leukemia: a review. Ther Clin Risk Manag 5(2):281-9

Aithal GP, Watkins PB, Andrade RJ, et al. (2011) Case definition and phenotype standardization in drug-induced liver injury. Clinical pharmacology and therapeutics 89(6):806-15 doi:10.1038/clpt.2011.58

Amacher DE (2012) The primary role of hepatic metabolism in idiosyncratic drug-induced liver injury. Expert opinion on drug metabolism & toxicology 8(3):335-47 doi:10.1517/17425255.2012.658041

Amitay-Laish I, Stemmer SM, Lacouture ME (2011) Adverse cutaneous reactions secondary to tyrosine kinase inhibitors including imatinib mesylate, nilotinib, and dasatinib. Dermatologic therapy 24(4):386-95 doi:10.1111/j.1529-8019.2011.01431.x

Antherieu S, Chesne C, Li R, Guguen-Guillouzo C, Guillouzo A (2012) Optimization of the HepaRG cell model for drug metabolism and toxicity studies. Toxicology in vitro : an international journal published in association with BIBRA 26(8):1278-85 doi:10.1016/j.tiv.2012.05.008

Antico Arciuch VG, Elguero ME, Poderoso JJ, Carreras MC (2012) Mitochondrial regulation of cell cycle and proliferation. Antioxidants & redox signaling 16(10):1150-80 doi:10.1089/ars.2011.4085

Apel K, Hirt H (2004) Reactive oxygen species: metabolism, oxidative stress, and signal transduction. Annu Rev Plant Biol 55:373-99 doi:10.1146/annurev.arplant.55.031903.141701

Archer SL (2013) Mitochondrial dynamics--mitochondrial fission and fusion in human diseases. The New England journal of medicine 369(23):2236-51 doi:10.1056/NEJMra1215233

Baker MJ, Frazier AE, Gulbis JM, Ryan MT (2007) Mitochondrial protein-import machinery: correlating structure with function. Trends Cell Biol 17(9):456-64 doi:10.1016/j.tcb.2007.07.010

Balaban RS, Nemoto S, Finkel T (2005) Mitochondria, oxidants, and aging. Cell 120(4):483-95 doi:10.1016/j.cell.2005.02.001

Bird MJ, Thorburn DR, Frazier AE (2014) Modelling biochemical features of mitochondrial neuropathology. Biochimica et biophysica acta 1840(4):1380-92 doi:10.1016/j.bbagen.2013.10.017

Blachly-Dyson E, Forte M (2001) VDAC channels. IUBMB life 52(3-5):113-8 doi:10.1080/15216540152845902

Bolton AE, Peng B, Hubert M, et al. (2004) Effect of rifampicin on the pharmacokinetics of imatinib mesylate (Gleevec, STI571) in healthy subjects. Cancer chemotherapy and pharmacology 53(2):102-6 doi:10.1007/s00280-003-0722-9

Bonini MG, Miyamoto S, Mascio PD, Augusto O (2004) Production of the Carbonate Radical Anion during Xanthine Oxidase Turnover in the Presence of Bicarbonate. Journal of Biological Chemistry 279(50):51836-51843 doi:10.1074/jbc.M406929200

Bova MP, Tam D, McMahon G, Mattson MN (2005) Troglitazone induces a rapid drop of mitochondrial membrane potential in liver HepG2 cells. Toxicology letters 155(1):41-50 doi:10.1016/j.toxlet.2004.08.009

Brand MD (2010) The sites and topology of mitochondrial superoxide production. Experimental gerontology 45(7-8):466-72 doi:10.1016/j.exger.2010.01.003

Brand MD, Nicholls DG (2011) Assessing mitochondrial dysfunction in cells. The Biochemical journal 435(2):297-312 doi:10.1042/BJ20110162

Brave M, Goodman V, Kaminskas E, et al. (2008) Sprycel for chronic myeloid leukemia and Philadelphia chromosome-positive acute lymphoblastic leukemia resistant to or intolerant of imatinib mesylate. Clinical cancer research : an official journal of the American Association for Cancer Research 14(2):352-9 doi:10.1158/1078-0432.CCR-07-4175

Breccia M, Alimena G (2013) Occurrence and current management of side effects in chronic myeloid leukemia patients treated frontline with tyrosine kinase inhibitors. Leukemia research 37(6):713-20 doi:10.1016/j.leukres.2013.01.021

Brunmair B, Lest A, Staniek K, et al. (2004) Fenofibrate impairs rat mitochondrial function by inhibition of respiratory complex I. The Journal of pharmacology and experimental therapeutics 311(1):109-14 doi:10.1124/jpet.104.068312

Bull VH, Rajalingam K, Thiede B (2012) Sorafenib-induced mitochondrial complex I inactivation and cell death in human neuroblastoma cells. Journal of proteome research 11(3):1609-20 doi:10.1021/pr200790e

Burris HA, 3rd, Hurwitz HI, Dees EC, et al. (2005) Phase I safety, pharmacokinetics, and clinical activity study of lapatinib (GW572016), a reversible dual inhibitor of epidermal growth factor receptor tyrosine kinases, in heavily pretreated patients with metastatic carcinomas. Journal of clinical oncology : official journal of the American Society of Clinical Oncology 23(23):5305-13 doi:10.1200/JCO.2005.16.584

Camello-Almaraz C, Gomez-Pinilla PJ, Pozo MJ, Camello PJ (2006) Mitochondrial reactive oxygen species and Ca2+ signaling. American journal of physiology Cell physiology 291(5):C1082-8 doi:10.1152/ajpcell.00217.2006

Castell JV, Jover R, Martnez-Jimnez CP, Gmez-Lechn MJ (2006) Hepatocyte cell lines: their use, scope and limitations in drug metabolism studies. Expert opinion on drug metabolism & toxicology 2(2):183-212 doi:10.1517/17425255.2.2.183

Castellino S, O'Mara M, Koch K, Borts DJ, Bowers GD, MacLauchlin C (2012) Human metabolism of lapatinib, a dual kinase inhibitor: implications for hepatotoxicity. Drug metabolism and disposition: the biological fate of chemicals 40(1):139-50 doi:10.1124/dmd.111.040949

Chan DC (2012) Fusion and fission: interlinked processes critical for mitochondrial health. Annu Rev Genet 46:265-87 doi:10.1146/annurev-genet-110410-132529

Chan K, Truong D, Shangari N, O'Brien PJ (2005) Drug-induced mitochondrial toxicity. Expert opinion on drug metabolism & toxicology 1(4):655-69 doi:10.1517/17425255.1.4.655

Chan NC, Salazar AM, Pham AH, et al. (2011) Broad activation of the ubiquitin–proteasome system by Parkin is critical for mitophagy. Human molecular genetics 20(9):1726-1737 doi:10.1093/hmg/ddr048

Chen H, Chomyn A, Chan DC (2005) Disruption of fusion results in mitochondrial heterogeneity and dysfunction. The Journal of biological chemistry 280(28):26185-92 doi:10.1074/jbc.M503062200

Chiou JF, Tai CJ, Wang YH, Liu TZ, Jen YM, Shiau CY (2009) Sorafenib induces preferential apoptotic killing of a drug- and radio-resistant Hep G2 cells through a mitochondria-dependent oxidative stress mechanism. Cancer biology & therapy 8(20):1904-13

Choudhury Y, Toh YC, Xing J, et al. (2017) Patient-specific hepatocyte-like cells derived from induced pluripotent stem cells model pazopanib-mediated hepatotoxicity. Scientific reports 7:41238 doi:10.1038/srep41238

Chu TF, Rupnick MA, Kerkela R, et al. (2007) Cardiotoxicity associated with tyrosine kinase inhibitor sunitinib. Lancet 370(9604):2011-9 doi:10.1016/S0140-6736(07)61865-0

Cogliati S, Frezza C, Soriano ME, et al. (2013) Mitochondrial cristae shape determines respiratory chain supercomplexes assembly and respiratory efficiency. Cell 155(1):160-71 doi:10.1016/j.cell.2013.08.032

Cortes JE, Kantarjian H, Shah NP, et al. (2012) Ponatinib in refractory Philadelphia chromosome-positive leukemias. The New England journal of medicine 367(22):2075-88 doi:10.1056/NEJMoa1205127

Couto N, Malys N, Gaskell SJ, Barber J (2013) Partition and turnover of glutathione reductase from Saccharomyces cerevisiae: a proteomic approach. Journal of proteome research 12(6):2885-94 doi:10.1021/pr4001948

Cowan-Jacob SW, Guez V, Fendrich G, et al. (2004) Imatinib (STI571) resistance in chronic myelogenous leukemia: molecular basis of the underlying mechanisms and potential strategies for treatment. Mini Rev Med Chem 4(3):285-99

Dalle-Donne I, Rossi R, Colombo G, Giustarini D, Milzani A (2009) Protein S-glutathionylation: a regulatory device from bacteria to humans. Trends Biochem Sci 34(2):85-96 doi:10.1016/j.tibs.2008.11.002

Daly AK, Donaldson PT, Bhatnagar P, et al. (2009) HLA-B[ast]5701 genotype is a major determinant of drug-induced liver injury due to flucloxacillin. Nature genetics 41(7):816-819 doi:http://www.nature.com/ng/journal/v41/n7/suppinfo/ng.379_S1.html

Demirci U, Buyukberber S, Yilmaz G, et al. (2012) Hepatotoxicity associated with lapatinib in an experimental rat model. European journal of cancer 48(2):279-85 doi:10.1016/j.ejca.2011.10.011

Deng J, Shimamura T, Perera S, et al. (2007) Proapoptotic BH3-only BCL-2 family protein BIM connects death signaling from epidermal growth factor receptor inhibition to the mitochondrion. Cancer research 67(24):11867-75 doi:10.1158/0008-5472.CAN-07-1961

Devarbhavi H (2012) An Update on Drug-induced Liver Injury. J Clin Exp Hepatol 2(3):247-59 doi:10.1016/j.jceh.2012.05.002

Di Gion P, Kanefendt F, Lindauer A, et al. (2011) Clinical pharmacokinetics of tyrosine kinase inhibitors: focus on pyrimidines, pyridines and pyrroles. Clin Pharmacokinet 50(9):551-603 doi:10.2165/11593320-000000000-00000

Ding WX, Yin XM (2012) Mitophagy: mechanisms, pathophysiological roles, and analysis. Biological chemistry 393(7):547-64 doi:10.1515/hsz-2012-0119

Donato MT, Jover R, Gomez-Lechon MJ (2013) Hepatic cell lines for drug hepatotoxicity testing: limitations and strategies to upgrade their metabolic competence by gene engineering. Current drug metabolism 14(9):946-68

Drose S, Brandt U (2012) Molecular mechanisms of superoxide production by the mitochondrial respiratory chain. Advances in experimental medicine and biology 748:145-69 doi:10.1007/978-1-4614-3573-0_6

Dykens JA, Will Y (2007) The significance of mitochondrial toxicity testing in drug development. Drug Discov Today 12(17-18):777-85 doi:10.1016/j.drudis.2007.07.013

Elchuri S, Oberley TD, Qi W, et al. (2005) CuZnSOD deficiency leads to persistent and widespread oxidative damage and hepatocarcinogenesis later in life. Oncogene 24(3):367-80 doi:10.1038/sj.onc.1208207

Elshafie HS, Armentano MF, Carmosino M, Bufo SA, De Feo V, Camele I (2017) Cytotoxic Activity of Origanum Vulgare L. on Hepatocellular Carcinoma cell Line HepG2 and

Evaluation of its Biological Activity. Molecules 22(9) doi:10.3390/molecules22091435

Eno MR, El-Gendy Bel D, Cameron MD (2016) P450 3A-Catalyzed O-Dealkylation of Lapatinib Induces Mitochondrial Stress and Activates Nrf2. Chem Res Toxicol 29(5):784-96 doi:10.1021/acs.chemrestox.5b00524

Enomoto A, Itoh K, Nagayoshi E, et al. (2001) High sensitivity of Nrf2 knockout mice to acetaminophen hepatotoxicity associated with decreased expression of ARE-regulated drug metabolizing enzymes and antioxidant genes. Toxicological sciences : an official journal of the Society of Toxicology 59(1):169-77

Fairfax BP, Pratap S, Roberts IS, et al. (2012) Fatal case of sorafenib-associated idiosyncratic hepatotoxicity in the adjuvant treatment of a patient with renal cell carcinoma. BMC cancer 12:590 doi:10.1186/1471-2407-12-590

Faivre S, Delbaldo C, Vera K, et al. (2006) Safety, pharmacokinetic, and antitumor activity of SU11248, a novel oral multitarget tyrosine kinase inhibitor, in patients with cancer. Journal of clinical oncology : official journal of the American Society of Clinical Oncology 24(1):25-35 doi:10.1200/JCO.2005.02.2194

Favaloro B, Allocati N, Graziano V, Di Ilio C, De Laurenzi V (2012) Role of apoptosis in disease. Aging (Albany NY) 4(5):330-49 doi:10.18632/aging.100459

Felser A, Blum K, Lindinger PW, Bouitbir J, Krahenbuhl S (2013) Mechanisms of hepatocellular toxicity associated with dronedarone--a comparison to amiodarone. Toxicological sciences : an official journal of the Society of Toxicology 131(2):480-90 doi:10.1093/toxsci/kfs298

Feng B, Xu JJ, Bi YA, et al. (2009) Role of hepatic transporters in the disposition and hepatotoxicity of a HER2 tyrosine kinase inhibitor CP-724,714. Toxicological sciences : an official journal of the Society of Toxicology 108(2):492-500 doi:10.1093/toxsci/kfp033

Fischel-Ghodsian N (2005) Genetic factors in aminoglycoside toxicity. Pharmacogenomics 6(1):27-36 doi:10.1517/14622416.6.1.27

Fontana RJ (2014) Pathogenesis of idiosyncratic drug-induced liver injury and clinical perspectives. Gastroenterology 146(4):914-28 doi:10.1053/j.gastro.2013.12.032

Forman HJ, Zhang H, Rinna A (2009) Glutathione: overview of its protective roles, measurement, and biosynthesis. Mol Aspects Med 30(1-2):1-12 doi:10.1016/j.mam.2008.08.006

Fromenty B, Pessayre D (1995) Inhibition of mitochondrial beta-oxidation as a mechanism of hepatotoxicity. Pharmacology & Therapeutics 67(1):101-154 doi:http://dx.doi.org/10.1016/0163-7258(95)00012-6

Fruehauf JP, Meyskens FL, Jr. (2007) Reactive oxygen species: a breath of life or death? Clinical cancer research : an official journal of the American Association for Cancer Research 13(3):789-94 doi:10.1158/1078-0432.CCR-06-2082

Gambacorti-Passerini C, le Coutre P, Mologni L, et al. (1997) Inhibition of the ABL kinase activity blocks the proliferation of BCR/ABL+ leukemic cells and induces apoptosis. Blood cells, molecules & diseases 23(3):380-94 doi:10.1006/bcmd.1997.0155

Gao X, Wen X, Esser L, et al. (2003) Structural basis for the quinone reduction in the bc1 complex: a comparative analysis of crystal structures of mitochondrial cytochrome bc1 with bound substrate and inhibitors at the Qi site. Biochemistry 42(30):9067-80 doi:10.1021/bi0341814

Gems D, Partridge L (2008) Stress-response hormesis and aging: "that which does not kill us makes us stronger". Cell metabolism 7(3):200-3 doi:10.1016/j.cmet.2008.01.001

Gerber DE, Minna JD (2010) ALK inhibition for non-small cell lung cancer: from discovery to therapy in record time. Cancer cell 18(6):548-51 doi:10.1016/j.ccr.2010.11.033

Gomez-Lechon MJ, Tolosa L, Conde I, Donato MT (2014) Competency of different cell models to predict human hepatotoxic drugs. Expert opinion on drug metabolism & toxicology 10(11):1553-68 doi:10.1517/17425255.2014.967680

Gorman GS, Chinnery PF, DiMauro S, et al. (2016) Mitochondrial diseases. Nat Rev Dis Primers 2:16080 doi:10.1038/nrdp.2016.80

Gotink KJ, Verheul HM (2010) Anti-angiogenic tyrosine kinase inhibitors: what is their mechanism of action? Angiogenesis 13(1):1-14 doi:10.1007/s10456-009-9160-6

Gray JP, Mishin V, Heck DE, Laskin DL, Laskin JD (2010) Inhibition of NADPH cytochrome P450 reductase by the model sulfur mustard vesicant 2-chloroethyl ethyl sulfide is associated with increased production of reactive oxygen species. Toxicology and applied pharmacology 247(2):76-82 doi:10.1016/j.taap.2010.05.015

Green DR, Reed JC (1998) Mitochondria and apoptosis. Science 281(5381):1309-12

Guillouzo A, Corlu A, Aninat C, Glaise D, Morel F, Guguen-Guillouzo C (2007) The human hepatoma HepaRG cells: a highly differentiated model for studies of liver metabolism and toxicity of xenobiotics. Chemico-biological interactions 168(1):66-73 doi:10.1016/j.cbi.2006.12.003

Gunawan BK, Kaplowitz N (2007) Mechanisms of drug-induced liver disease. Clin Liver Dis 11(3):459-75, v doi:10.1016/j.cld.2007.06.001

Hamacher-Brady A, Brady NR (2016) Mitophagy programs: mechanisms and physiological implications of mitochondrial targeting by autophagy. Cellular and molecular life sciences : CMLS 73(4):775-95 doi:10.1007/s00018-015-2087-8

Han D, Dara L, Win S, et al. (2013) Regulation of drug-induced liver injury by signal transduction pathways: critical role of mitochondria. Trends Pharmacol Sci 34(4):243-53 doi:10.1016/j.tips.2013.01.009

Hardy KD, Wahlin MD, Papageorgiou I, Unadkat JD, Rettie AE, Nelson SD (2014) Studies on the role of metabolic activation in tyrosine kinase inhibitor-dependent hepatotoxicity: induction of CYP3A4 enhances the cytotoxicity of lapatinib in HepaRG cells. Drug metabolism and disposition: the biological fate of chemicals 42(1):162-71 doi:10.1124/dmd.113.054817

Hargreaves IP, Al Shahrani M, Wainwright L, Heales SJ (2016) Drug-Induced Mitochondrial Toxicity. Drug safety 39(7):661-74 doi:10.1007/s40264-016-0417-x

Haura EB, Tanvetyanon T, Chiappori A, et al. (2010) Phase I/II study of the Src inhibitor dasatinib in combination with erlotinib in advanced non-small-cell lung cancer. Journal of clinical oncology : official journal of the American Society of Clinical Oncology 28(8):1387-94 doi:10.1200/JCO.2009.25.4029

Hayyan M, Hashim MA, AlNashef IM (2016) Superoxide Ion: Generation and Chemical Implications. Chem Rev 116(5):3029-85 doi:10.1021/acs.chemrev.5b00407

Haznedar JO, Patyna S, Bello CL, et al. (2009) Single- and multiple-dose disposition kinetics of sunitinib malate, a multitargeted receptor tyrosine kinase inhibitor: comparative plasma kinetics in non-clinical species. Cancer chemotherapy and pharmacology 64(4):691-706 doi:10.1007/s00280-008-0917-1

He K, Lago MW, Iyer RA, Shyu WC, Humphreys WG, Christopher LJ (2008) Lacteal secretion, fetal and maternal tissue distribution of dasatinib in rats. Drug metabolism and disposition: the biological fate of chemicals 36(12):2564-70 doi:10.1124/dmd.108.022764

Herbrink M, de Vries N, Rosing H, et al. (2016) Quantification of 11 Therapeutic Kinase Inhibitors in Human Plasma for Therapeutic Drug Monitoring Using Liquid Chromatography Coupled With Tandem Mass Spectrometry. Therapeutic drug monitoring 38(6):649-656 doi:10.1097/FTD.0000000000000349

Higa GM, Abraham J (2007) Lapatinib in the treatment of breast cancer. Expert review of anticancer therapy 7(9):1183-92 doi:10.1586/14737140.7.9.1183

Hochhaus A, Kreil S, Corbin AS, et al. (2002) Molecular and chromosomal mechanisms of resistance to imatinib (STI571) therapy. Leukemia 16(11):2190-6 doi:10.1038/sj.leu.2402741

Houk BE, Bello CL, Kang D, Amantea M (2009) A population pharmacokinetic meta-analysis of sunitinib malate (SU11248) and its primary metabolite (SU12662) in healthy volunteers and oncology patients. Clinical cancer research : an official journal of the American Association for Cancer Research 15(7):2497-506 doi:10.1158/1078-0432.CCR-08-1893

Houten SM, Wanders RJ (2010) A general introduction to the biochemistry of mitochondrial fatty acid beta-oxidation. J Inherit Metab Dis 33(5):469-77 doi:10.1007/s10545-010-9061-2

Huang YS, An SJ, Chen ZH, Wu YL (2009) Three cases of severe hepatic impairment caused by erlotinib. British journal of clinical pharmacology 68(3):464-7 doi:10.1111/j.1365-2125.2009.03459.x

Hussaini SH, Farrington EA (2014) Idiosyncratic drug-induced liver injury: an update on the 2007 overview. Expert Opin Drug Saf 13(1):67-81 doi:10.1517/14740338.2013.828032

Ikon N, Ryan RO (2017) Cardiolipin and mitochondrial cristae organization. Biochimica et biophysica acta 1859(6):1156-1163 doi:10.1016/j.bbamem.2017.03.013

Imai K, Takaoka A (2006) Comparing antibody and small-molecule therapies for cancer. Nature reviews Cancer 6(9):714-27 doi:10.1038/nrc1913

Jacquel A, Herrant M, Legros L, et al. (2003) Imatinib induces mitochondria-dependent apoptosis of the Bcr-Abl-positive K562 cell line and its differentiation toward the erythroid lineage. FASEB journal : official publication of the Federation of American Societies for Experimental Biology 17(14):2160-2 doi:10.1096/fj.03-0322

Jaeschke H, Gores GJ, Cederbaum AI, Hinson JA, Pessayre D, Lemasters JJ (2002) Mechanisms of hepatotoxicity. Toxicological sciences : an official journal of the Society of Toxicology 65(2):166-76

Joe MK, Nakaya N, Abu-Asab M, Tomarev SI (2015) Mutated myocilin and heterozygous Sod2 deficiency act synergistically in a mouse model of open-angle glaucoma. Human molecular genetics 24(12):3322-34 doi:10.1093/hmg/ddv082

Jornayvaz FR, Shulman GI (2010) Regulation of mitochondrial biogenesis. Essays Biochem 47:69-84 doi:10.1042/bse0470069

Josephs DH, Fisher DS, Spicer J, Flanagan RJ (2013) Clinical pharmacokinetics of tyrosine kinase inhibitors: implications for therapeutic drug monitoring. Therapeutic drug monitoring 35(5):562-87 doi:10.1097/FTD.0b013e318292b931

Josse R, Aninat C, Glaise D, et al. (2008) Long-term functional stability of human HepaRG hepatocytes and use for chronic toxicity and genotoxicity studies. Drug metabolism and disposition: the biological fate of chemicals 36(6):1111-8 doi:10.1124/dmd.107.019901

Kamalian L, Chadwick AE, Bayliss M, et al. (2015) The utility of HepG2 cells to identify direct mitochondrial dysfunction in the absence of cell death. Toxicology in vitro : an international journal published in association with BIBRA 29(4):732-40 doi:10.1016/j.tiv.2015.02.011

Kapadia S, Hapani S, Choueiri TK, Wu S (2013) Risk of liver toxicity with the angiogenesis inhibitor pazopanib in cancer patients. Acta oncologica 52(6):1202-12 doi:10.3109/0284186X.2013.782103

Kaufmann P, Torok M, Hanni A, Roberts P, Gasser R, Krahenbuhl S (2005) Mechanisms of benzarone and benzbromarone-induced hepatic toxicity. Hepatology 41(4):925-35 doi:10.1002/hep.20634

Kaufmann P, Torok M, Zahno A, Waldhauser KM, Brecht K, Krahenbuhl S (2006) Toxicity of statins on rat skeletal muscle mitochondria. Cellular and molecular life sciences : CMLS 63(19-20):2415-25 doi:10.1007/s00018-006-6235-z

Keisner SV, Shah SR (2011) Pazopanib: the newest tyrosine kinase inhibitor for the treatment of advanced or metastatic renal cell carcinoma. Drugs 71(4):443-54 doi:10.2165/11588960-000000000-00000

Kerkela R, Grazette L, Yacobi R, et al. (2006) Cardiotoxicity of the cancer therapeutic agent imatinib mesylate. Nature medicine 12(8):908-16 doi:10.1038/nm1446

Kerkela R, Woulfe KC, Durand J-B, et al. (2009) Sunitinib-Induced Cardiotoxicity Is Mediated by Off-Target Inhibition of AMP-Activated Protein Kinase. Clinical and Translational Science 2(1):15-25 doi:10.1111/j.1752-8062.2008.00090.x

Kim SH, Naisbitt DJ (2016) Update on Advances in Research on Idiosyncratic Drug-Induced Liver Injury. Allergy Asthma Immunol Res 8(1):3-11 doi:10.4168/aair.2016.8.1.3

Klempner SJ, Choueiri TK, Yee E, Doyle LA, Schuppan D, Atkins MB (2012) Severe pazopanib-induced hepatotoxicity: clinical and histologic course in two patients. Journal of clinical oncology : official journal of the American Society of Clinical Oncology 30(27):e264-8 doi:10.1200/JCO.2011.41.0332

Komposch K, Sibilia M (2015) EGFR Signaling in Liver Diseases. Int J Mol Sci 17(1) doi:10.3390/ijms17010030

Konig H, Copland M, Chu S, Jove R, Holyoake TL, Bhatia R (2008) Effects of dasatinib on SRC kinase activity and downstream intracellular signaling in primitive chronic myelogenous leukemia hematopoietic cells. Cancer research 68(23):9624-33 doi:10.1158/0008-5472.CAN-08-1131

Kunutsor SK, Laukkanen JA (2017) Gamma-glutamyltransferase and risk of chronic kidney disease: A prospective cohort study. Clin Chim Acta 473:39-44 doi:10.1016/j.cca.2017.08.014

Kurata Y, Miyauchi N, Suno M, Ito T, Sendo T, Kiura K (2015) Correlation of plasma crizotinib trough concentration with adverse events in patients with anaplastic lymphoma kinase positive non-small-cell lung cancer. J Pharm Health Care Sci 1:8 doi:10.1186/s40780-014-0008-x

Kwak EL, Sordella R, Bell DW, et al. (2005) Irreversible inhibitors of the EGF receptor may circumvent acquired resistance to gefitinib. Proceedings of the National Academy of Sciences of the United States of America 102(21):7665-70 doi:10.1073/pnas.0502860102

Lai KK, Gang DL, Zawacki JK, Cooley TP (1991) Fulminant hepatic failure associated with 2',3'-dideoxyinosine (ddI). Ann Intern Med 115(4):283-4

Lammert C, Einarsson S, Saha C, Niklasson A, Bjornsson E, Chalasani N (2008) Relationship between daily dose of oral medications and idiosyncratic drug-induced liver injury: Search for signals. Hepatology 47(6):2003-2009 doi:10.1002/hep.22272

Lau CL, Chan ST, Selvaratanam M, et al. (2015) Sunitinib-ibuprofen drug interaction affects the pharmacokinetics and tissue distribution of sunitinib to brain, liver, and kidney in male and female mice differently. Fundam Clin Pharmacol 29(4):404-16 doi:10.1111/fcp.12126

Lee NR, Yhim HY, Yim CY, Kwak JY, Song EK (2011) Sunitinib-induced hyperammonemic encephalopathy in gastrointestinal stromal tumors. Ann Pharmacother 45(10):e56 doi:10.1345/aph.1Q038

Lee WM (2003) Drug-induced hepatotoxicity. The New England journal of medicine 349(5):474-85 doi:10.1056/NEJMra021844

Lee WM (2013) Drug-induced acute liver failure. Clin Liver Dis 17(4):575-86, viii doi:10.1016/j.cld.2013.07.001

Leung L, Kalgutkar AS, Obach RS (2012) Metabolic activation in drug-induced liver injury. Drug Metab Rev 44(1):18-33 doi:10.3109/03602532.2011.605791

Li J, Zhao M, He P, Hidalgo M, Baker SD (2007) Differential metabolism of gefitinib and erlotinib by human cytochrome P450 enzymes. Clinical cancer research : an official journal of the American Association for Cancer Research 13(12):3731-7 doi:10.1158/1078-0432.CCR-07-0088

Li X, Kamenecka TM, Cameron MD (2009) Bioactivation of the epidermal growth factor receptor inhibitor gefitinib: implications for pulmonary and hepatic toxicities. Chem Res Toxicol 22(10):1736-42 doi:10.1021/tx900256y

Li X, Kamenecka TM, Cameron MD (2010) Cytochrome P450-mediated bioactivation of the epidermal growth factor receptor inhibitor erlotinib to a reactive electrophile. Drug metabolism and disposition: the biological fate of chemicals 38(7):1238-45 doi:10.1124/dmd.109.030361

Licata A (2016) Adverse drug reactions and organ damage: The liver. Eur J Intern Med 28:9-16 doi:10.1016/j.ejim.2015.12.017

Liu F, Ichihara S, Valentine WM, et al. (2010) Increased susceptibility of Nrf2-null mice to 1-bromopropane-induced hepatotoxicity. Toxicological sciences : an official journal of the Society of Toxicology 115(2):596-606 doi:10.1093/toxsci/kfq075

Liu W, Makrauer FL, Qamar AA, Janne PA, Odze RD (2007) Fulminant hepatic failure secondary to erlotinib. Clinical gastroenterology and hepatology : the official clinical practice journal of the American Gastroenterological Association 5(8):917-20 doi:10.1016/j.cgh.2007.04.014

Llovet JM, Ricci S, Mazzaferro V, et al. (2008) Sorafenib in Advanced Hepatocellular Carcinoma. New England Journal of Medicine 359(4):378-390 doi:10.1056/NEJMoa0708857

Locatelli SL, Giacomini A, Guidetti A, et al. (2013) Perifosine and sorafenib combination induces mitochondrial cell death and antitumor effects in NOD/SCID mice with Hodgkin lymphoma cell line xenografts. Leukemia 27(8):1677-87 doi:10.1038/leu.2013.28

Los M, Mozoluk M, Ferrari D, et al. (2002) Activation and caspase-mediated inhibition of PARP: a molecular switch between fibroblast necrosis and apoptosis in death receptor signaling. Molecular biology of the cell 13(3):978-88 doi:10.1091/mbc.01-05-0272

Lu SC (2013) Glutathione synthesis. Biochimica et biophysica acta 1830(5):3143-53 doi:10.1016/j.bbagen.2012.09.008

Lucena MI, Garcia-Martin E, Andrade RJ, et al. (2010) Mitochondrial superoxide dismutase and glutathione peroxidase in idiosyncratic drug-induced liver injury. Hepatology 52(1):303-12 doi:10.1002/hep.23668

Lynch MR, Tran MT, Parikh SM (2017) PGC1alpha in the kidney. Am J Physiol Renal Physiol:ajprenal 00263 2017 doi:10.1152/ajprenal.00263.2017

Ma Q (2013) Role of nrf2 in oxidative stress and toxicity. Annu Rev Pharmacol Toxicol 53:401-26 doi:10.1146/annurev-pharmtox-011112-140320

Maayah ZH, Ansari MA, El Gendy MA, Al-Arifi MN, Korashy HM (2014) Development of cardiac hypertrophy by sunitinib in vivo and in vitro rat cardiomyocytes is influenced by the aryl hydrocarbon receptor signaling pathway. Archives of Toxicology 88(3):725-738 doi:10.1007/s00204-013-1159-5

Manning G, Whyte DB, Martinez R, Hunter T, Sudarsanam S (2002) The protein kinase complement of the human genome. Science 298(5600):1912-34 doi:10.1126/science.1075762

Marroquin LD, Hynes J, Dykens JA, Jamieson JD, Will Y (2007) Circumventing the Crabtree effect: replacing media glucose with galactose increases susceptibility of HepG2 cells

to mitochondrial toxicants. Toxicological sciences : an official journal of the Society of Toxicology 97(2):539-47 doi:10.1093/toxsci/kfm052

Mates JM, Perez-Gomez C, Nunez de Castro I (1999) Antioxidant enzymes and human diseases. Clin Biochem 32(8):595-603

Matsuda N, Sato S, Shiba K, et al. (2010) PINK1 stabilized by mitochondrial depolarization recruits Parkin to damaged mitochondria and activates latent Parkin for mitophagy. J Cell Biol 189(2):211-21 doi:10.1083/jcb.200910140

Mealing S, Barcena L, Hawkins N, et al. (2013) The relative efficacy of imatinib, dasatinib and nilotinib for newly diagnosed chronic myeloid leukemia: a systematic review and network meta-analysis. Experimental hematology & oncology 2(1):5 doi:10.1186/2162-3619-2-5

Mendel DB, Laird AD, Xin X, et al. (2003) In vivo antitumor activity of SU11248, a novel tyrosine kinase inhibitor targeting vascular endothelial growth factor and platelet-derived growth factor receptors: determination of a pharmacokinetic/pharmacodynamic relationship. Clinical cancer research : an official journal of the American Association for Cancer Research 9(1):327-37

Messner S, Agarkova I, Moritz W, Kelm JM (2013) Multi-cell type human liver microtissues for hepatotoxicity testing. Arch Toxicol 87(1):209-13 doi:10.1007/s00204-012-0968-2

Meyer JN, Leung MCK, Rooney JP, et al. (2013) Mitochondria as a Target of Environmental Toxicants. Toxicological Sciences 134(1):1-17 doi:10.1093/toxsci/kft102

Midgley RS, Kerr DJ, Flaherty KT, et al. (2007) A phase I and pharmacokinetic study of lapatinib in combination with infusional 5-fluorouracil, leucovorin and irinotecan. Annals of oncology : official journal of the European Society for Medical Oncology / ESMO 18(12):2025-9 doi:10.1093/annonc/mdm366

Mishin V, Gray JP, Heck DE, Laskin DL, Laskin JD (2010) Application of the Amplex Red/Horseradish Peroxidase Assay to Measure Hydrogen Peroxide Generation by Recombinant Microsomal Enzymes. Free radical biology & medicine 48(11):1485-1491 doi:10.1016/j.freeradbiomed.2010.02.030

Mishra P, Carelli V, Manfredi G, Chan DC (2014) Proteolytic cleavage of Opa1 stimulates mitochondrial inner membrane fusion and couples fusion to oxidative phosphorylation. Cell metabolism 19(4):630-41 doi:10.1016/j.cmet.2014.03.011

Mishra P, Chan DC (2016) Metabolic regulation of mitochondrial dynamics. J Cell Biol 212(4):379-87 doi:10.1083/jcb.201511036

Mol CD, Fabbro D, Hosfield DJ (2004) Structural insights into the conformational selectivity of STI-571 and related kinase inhibitors. Curr Opin Drug Discov Devel 7(5):639-48

Mourier A, Motori E, Brandt T, et al. (2015) Mitofusin 2 is required to maintain mitochondrial coenzyme Q levels. The Journal of Cell Biology 208(4):429-442 doi:10.1083/jcb.201411100

Mross K, Frost A, Steinbild S, et al. (2012) A phase I dose-escalation study of regorafenib (BAY 73-4506), an inhibitor of oncogenic, angiogenic, and stromal kinases, in patients with advanced solid tumors. Clinical cancer research : an official journal of the American Association for Cancer Research 18(9):2658-67 doi:10.1158/1078-0432.CCR-11-1900

Mueller SO, Guillouzo A, Hewitt PG, Richert L (2015) Drug biokinetic and toxicity assessments in rat and human primary hepatocytes and HepaRG cells within the EU-funded Predict-IV project. Toxicology in vitro : an international journal published in association with BIBRA 30(1 Pt A):19-26 doi:10.1016/j.tiv.2015.04.014

Muller FL, Song W, Liu Y, et al. (2006) Absence of CuZn superoxide dismutase leads to elevated oxidative stress and acceleration of age-dependent skeletal muscle atrophy. Free radical biology & medicine 40(11):1993-2004 doi:10.1016/j.freeradbiomed.2006.01.036

Murray LJ, Abrams TJ, Long KR, et al. (2003) SU11248 inhibits tumor growth and CSF-1R-dependent osteolysis in an experimental breast cancer bone metastasis model. Clin Exp Metastasis 20(8):757-66

Nguyen GT, Green ER, Mecsas J (2017) Neutrophils to the ROScue: Mechanisms of NADPH Oxidase Activation and Bacterial Resistance. Front Cell Infect Microbiol 7:373 doi:10.3389/fcimb.2017.00373

O'Farrell AM, Abrams TJ, Yuen HA, et al. (2003) SU11248 is a novel FLT3 tyrosine kinase inhibitor with potent activity in vitro and in vivo. Blood 101(9):3597-605 doi:10.1182/blood-2002-07-2307

O'Hare T, Eide CA, Deininger MW (2007) Bcr-Abl kinase domain mutations, drug resistance, and the road to a cure for chronic myeloid leukemia. Blood 110(7):2242-9 doi:10.1182/blood-2007-03-066936

Okatsu K, Koyano F, Kimura M, et al. (2015) Phosphorylated ubiquitin chain is the genuine Parkin receptor. The Journal of Cell Biology 209(1):111-128 doi:10.1083/jcb.201410050

Ong MM, Wang AS, Leow KY, Khoo YM, Boelsterli UA (2006) Nimesulide-induced hepatic mitochondrial injury in heterozygous Sod2(+/-) mice. Free radical biology & medicine 40(3):420-9 doi:10.1016/j.freeradbiomed.2005.08.038

Ott M, Gogvadze V, Orrenius S, Zhivotovsky B (2007) Mitochondria, oxidative stress and cell death. Apoptosis : an international journal on programmed cell death 12(5):913-22 doi:10.1007/s10495-007-0756-2

Palikaras K, Tavernarakis N (2014) Mitochondrial homeostasis: The interplay between mitophagy and mitochondrial biogenesis. Experimental gerontology 56(Supplement C):182-188 doi:https://doi.org/10.1016/j.exger.2014.01.021

Palmer CS, Osellame LD, Stojanovski D, Ryan MT (2011) The regulation of mitochondrial morphology: intricate mechanisms and dynamic machinery. Cellular signalling 23(10):1534-45 doi:10.1016/j.cellsig.2011.05.021

Panka DJ, Wang W, Atkins MB, Mier JW (2006) The Raf inhibitor BAY 43-9006 (Sorafenib) induces caspase-independent apoptosis in melanoma cells. Cancer research 66(3):1611-9 doi:10.1158/0008-5472.CAN-05-0808

Paul MK, Mukhopadhyay AK (2004) Tyrosine kinase - Role and significance in Cancer. Int J Med Sci 1(2):101-115

Pawson T (2004) Specificity in signal transduction: from phosphotyrosine-SH2 domain interactions to complex cellular systems. Cell 116(2):191-203

Pellegrinotti M, Fimognari FL, Franco A, Repetto L, Pastorelli R (2009) Erlotinib-induced hepatitis complicated by fatal lactic acidosis in an elderly man with lung cancer. Ann Pharmacother 43(3):542-5 doi:10.1345/aph.1L468

Pessayre D, Berson A, Fromenty B, Mansouri A (2001) Mitochondria in steatohepatitis. Semin Liver Dis 21(1):57-69

Pessayre D, Fromenty B, Berson A, et al. (2012) Central role of mitochondria in drug-induced liver injury. Drug Metab Rev 44(1):34-87 doi:10.3109/03602532.2011.604086

Pessayre D, Mansouri A, Berson A, Fromenty B (2010) Mitochondrial involvement in drug-induced liver injury. Handb Exp Pharmacol(196):311-65 doi:10.1007/978-3-642-00663-0_11

Pessayre D, Mansouri A, Haouzi D, Fromenty B (1999) Hepatotoxicity due to mitochondrial dysfunction. Cell Biology and Toxicology 15(6):367-373 doi:10.1023/a:1007649815992

Pinti M, Troiano L, Nasi M, Ferraresi R, Dobrucki J, Cossarizza A (2003) Hepatoma HepG2 cells as a model for in vitro studies on mitochondrial toxicity of antiviral drugs: which correlation with the patient? J Biol Regul Homeost Agents 17(2):166-171

Polli JW, Humphreys JE, Harmon KA, et al. (2008) The role of efflux and uptake transporters in [N-{3-chloro-4-[(3-fluorobenzyl)oxy]phenyl}-6-[5-({[2-(methylsulfonyl)ethyl]amino }methyl)-2-furyl]-4-quinazolinamine (GW572016, lapatinib) disposition and drug interactions. Drug metabolism and disposition: the biological fate of chemicals 36(4):695-701 doi:10.1124/dmd.107.018374

Porceddu M, Buron N, Roussel C, Labbe G, Fromenty B, Borgne-Sanchez A (2012) Prediction of liver injury induced by chemicals in human with a multiparametric assay on isolated mouse liver mitochondria. Toxicological sciences : an official journal of the Society of Toxicology 129(2):332-45 doi:10.1093/toxsci/kfs197

Prasad V, Mailankody S (2014) The accelerated approval of oncologic drugs: Lessons from ponatinib. Jama 311(4):353-354 doi:10.1001/jama.2013.284531

Price KE, Saleem N, Lee G, Steinberg M (2013) Potential of ponatinib to treat chronic myeloid leukemia and acute lymphoblastic leukemia. OncoTargets and therapy 6:1111-8 doi:10.2147/OTT.S36980

Proctor WR, Foster AJ, Vogt J, et al. (2017) Utility of spherical human liver microtissues for prediction of clinical drug-induced liver injury. Arch Toxicol 91(8):2849-2863 doi:10.1007/s00204-017-2002-1

Rahmani M, Davis EM, Crabtree TR, et al. (2007) The Kinase Inhibitor Sorafenib Induces Cell Death through a Process Involving Induction of Endoplasmic Reticulum Stress. Molecular and cellular biology 27(15):5499-5513 doi:10.1128/MCB.01080-06

Raissouni S, Quraishi Z, Al-Ghamdi M, Monzon J, Tang P, Vickers MM (2015) Acute liver failure and seizures as a consequence of regorafenib exposure in advanced rectal cancer. BMC research notes 8:538 doi:10.1186/s13104-015-1502-4

Raymond E, Faivre S, Armand JP (2000) Epidermal Growth Factor Receptor Tyrosine Kinase as a Target for Anticancer Therapy. Drugs 60(1):15-23 doi:10.2165/00003495-200060001-00002

Reed JC (2001) Apoptosis-regulating proteins as targets for drug discovery. Trends in molecular medicine 7(7):314-9

Regev A (2014) Drug-induced liver injury and drug development: industry perspective. Semin Liver Dis 34(2):227-39 doi:10.1055/s-0034-1375962

Ridruejo E, Cacchione R, Villamil AG, Marciano S, Gadano AC, Mando OG (2007) Imatinib-induced fatal acute liver failure. World journal of gastroenterology : WJG 13(48):6608-111

Roberts PG, Hirst J (2012) The deactive form of respiratory complex I from mammalian mitochondria is a Na+/H+ antiporter. The Journal of biological chemistry 287(41):34743-51 doi:10.1074/jbc.M112.384560

Robin MA, Le Roy M, Descatoire V, Pessayre D (1997) Plasma membrane cytochromes P450 as neoantigens and autoimmune targets in drug-induced hepatitis. Journal of hepatology 26 Suppl 1:23-30

Roskoski R, Jr. (2007) Sunitinib: a VEGF and PDGF receptor protein kinase and angiogenesis inhibitor. Biochemical and biophysical research communications 356(2):323-8 doi:10.1016/j.bbrc.2007.02.156

Roth RA, Ganey PE (2010) Intrinsic versus idiosyncratic drug-induced hepatotoxicity--two villains or one? The Journal of pharmacology and experimental therapeutics 332(3):692-7 doi:10.1124/jpet.109.162651

Sacre A, Lanthier N, Dano H, et al. (2016) Regorafenib induced severe toxic hepatitis: characterization and discussion. Liver international : official journal of the International Association for the Study of the Liver 36(11):1590-1594 doi:10.1111/liv.13217

Scagliotti G, Govindan R (2010) Targeting angiogenesis with multitargeted tyrosine kinase inhibitors in the treatment of non-small cell lung cancer. The oncologist 15(5):436-46 doi:10.1634/theoncologist.2009-0225

Schacher-Kaufmann S, Pless M (2010) Acute Fatal Liver Toxicity under Erlotinib. Case reports in oncology 3(2):182-188 doi:10.1159/000315366

Schlessinger J (2000) Cell signaling by receptor tyrosine kinases. Cell 103(2):211-25

Schon EA, Bonilla E, DiMauro S (1997) Mitochondrial DNA mutations and pathogenesis. Journal of bioenergetics and biomembranes 29(2):131-49

Schon EA, DiMauro S, Hirano M (2012) Human mitochondrial DNA: roles of inherited and somatic mutations. Nat Rev Genet 13(12):878-90 doi:10.1038/nrg3275

Shah NP, Sawyers CL (2003) Mechanisms of resistance to STI571 in Philadelphia chromosome-associated leukemias. Oncogene 22(47):7389-95 doi:10.1038/sj.onc.1206942

Shah RR, Morganroth J, Shah DR (2013) Hepatotoxicity of tyrosine kinase inhibitors: clinical and regulatory perspectives. Drug safety 36(7):491-503 doi:10.1007/s40264-013-0048-4

Shaw AT, Kim DW, Nakagawa K, et al. (2013) Crizotinib versus chemotherapy in advanced ALK-positive lung cancer. The New England journal of medicine 368(25):2385-94 doi:10.1056/NEJMoa1214886

Shutt T, Geoffrion M, Milne R, McBride HM (2012) The intracellular redox state is a core determinant of mitochondrial fusion. EMBO Reports 13(10):909-915 doi:10.1038/embor.2012.128

Smith J (2005) Erlotinib: small-molecule targeted therapy in the treatment of non-small-cell lung cancer. Clin Ther 27(10):1513-34 doi:10.1016/j.clinthera.2005.10.014

Spector NL, Robertson FC, Bacus S, et al. (2015) Lapatinib Plasma and Tumor Concentrations and Effects on HER Receptor Phosphorylation in Tumor. PloS one 10(11):e0142845 doi:10.1371/journal.pone.0142845

Spraggs CF, Budde LR, Briley LP, et al. (2011) HLA-DQA1*02:01 is a major risk factor for lapatinib-induced hepatotoxicity in women with advanced breast cancer. Journal of clinical oncology : official journal of the American Society of Clinical Oncology 29(6):667-73 doi:10.1200/JCO.2010.31.3197

Spraggs CF, Parham LR, Hunt CM, Dollery CT (2012) Lapatinib-induced liver injury characterized by class II HLA and Gilbert's syndrome genotypes. Clinical pharmacology and therapeutics 91(4):647-52 doi:10.1038/clpt.2011.277

Stephens C, Lucena MI, Andrade RJ (2012) Genetic variations in drug-induced liver injury (DILI): resolving the puzzle. Front Genet 3:253 doi:10.3389/fgene.2012.00253

Stewart MJ, Steenkamp V (2000) The biochemistry and toxicity of atractyloside: a review. Therapeutic drug monitoring 22(6):641-9

Strumberg D, Clark JW, Awada A, et al. (2007) Safety, pharmacokinetics, and preliminary antitumor activity of sorafenib: a review of four phase I trials in patients with advanced refractory solid tumors. The oncologist 12(4):426-37 doi:10.1634/theoncologist.12-4-426

Strumberg D, Scheulen ME, Schultheis B, et al. (2012) Regorafenib (BAY 73-4506) in advanced colorectal cancer: a phase I study. British journal of cancer 106(11):1722-7 doi:10.1038/bjc.2012.153

Suk KT, Kim DJ (2012) Drug-induced liver injury: present and future. Clin Mol Hepatol 18(3):249-57 doi:10.3350/cmh.2012.18.3.249

Swiss R, Will Y (2011) Assessment of mitochondrial toxicity in HepG2 cells cultured in high-glucose- or galactose-containing media. Curr Protoc Toxicol Chapter 2:Unit2 20 doi:10.1002/0471140856.tx0220s49

Talbert DR, Doherty KR, Trusk PB, Moran DM, Shell SA, Bacus S (2015) A multi-parameter in vitro screen in human stem cell-derived cardiomyocytes identifies ponatinib-induced structural and functional cardiac toxicity. Toxicological sciences : an official journal of the Society of Toxicology 143(1):147-55 doi:10.1093/toxsci/kfu215

Tao M, You CP, Zhao RR, et al. (2014) Animal mitochondria: evolution, function, and disease. Curr Mol Med 14(1):115-24

Teng WC, Oh JW, New LS, et al. (2010) Mechanism-based inactivation of cytochrome P450 3A4 by lapatinib. Molecular pharmacology 78(4):693-703 doi:10.1124/mol.110.065839

Teo YL, Ho HK, Chan A (2013) Risk of tyrosine kinase inhibitors-induced hepatotoxicity in cancer patients: a meta-analysis. Cancer treatment reviews 39(2):199-206 doi:10.1016/j.ctrv.2012.09.004

Teo YL, Ho HK, Chan A (2015) Metabolism-related pharmacokinetic drug-drug interactions with tyrosine kinase inhibitors: current understanding, challenges and recommendations. British journal of clinical pharmacology 79(2):241-53 doi:10.1111/bcp.12496

Togliatto G, Lombardo G, Brizzi MF (2017) The Future Challenge of Reactive Oxygen Species (ROS) in Hypertension: From Bench to Bed Side. Int J Mol Sci 18(9) doi:10.3390/ijms18091988

Trauner M, Meier PJ, Boyer JL (1998) Molecular pathogenesis of cholestasis. The New England journal of medicine 339(17):1217-27 doi:10.1056/NEJM199810223391707

Tujios S, Fontana RJ (2011) Mechanisms of drug-induced liver injury: from bedside to bench. Nat Rev Gastroenterol Hepatol 8(4):202-11 doi:10.1038/nrgastro.2011.22

Twig G, Elorza A, Molina AJ, et al. (2008) Fission and selective fusion govern mitochondrial segregation and elimination by autophagy. The EMBO journal 27(2):433-46 doi:10.1038/sj.emboj.7601963

van Geel RM, Hendrikx JJ, Vahl JE, et al. (2016) Crizotinib-induced fatal fulminant liver failure. Lung Cancer 93:17-9 doi:10.1016/j.lungcan.2015.12.010

Varga ZV, Ferdinandy P, Liaudet L, Pacher P (2015) Drug-induced mitochondrial dysfunction and cardiotoxicity. Am J Physiol Heart Circ Physiol 309(9):H1453-67 doi:10.1152/ajpheart.00554.2015

Waddell T, Cunningham D (2013) Evaluation of regorafenib in colorectal cancer and GIST. Lancet 381(9863):273-5 doi:10.1016/S0140-6736(12)62006-6

Walgren JL, Mitchell MD, Thompson DC (2005) Role of metabolism in drug-induced idiosyncratic hepatotoxicity. Crit Rev Toxicol 35(4):325-61

Wallace KB (2015) Multiple Targets for Drug-Induced Mitochondrial Toxicity. Curr Med Chem 22(20):2488-92

Wan PT, Garnett MJ, Roe SM, et al. (2004) Mechanism of activation of the RAF-ERK signaling pathway by oncogenic mutations of B-RAF. Cell 116(6):855-67

Wang C, Youle RJ (2009) The role of mitochondria in apoptosis*. Annu Rev Genet 43:95-118 doi:10.1146/annurev-genet-102108-134850

Weiler S, Merz M, Kullak-Ublick GA (2015) Drug-induced liver injury: the dawn of biomarkers? F1000Prime Rep 7:34 doi:10.12703/P7-34

Weise AM, Liu CY, Shields AF (2009) Fatal liver failure in a patient on acetaminophen treated with sunitinib malate and levothyroxine. Ann Pharmacother 43(4):761-6 doi:10.1345/aph.1L528

Weng Z, Luo Y, Yang X, et al. (2015) Regorafenib impairs mitochondrial functions, activates AMP-activated protein kinase, induces autophagy, and causes rat hepatocyte necrosis. Toxicology 327:10-21 doi:10.1016/j.tox.2014.11.002

Westermann B (2010) Mitochondrial fusion and fission in cell life and death. Nat Rev Mol Cell Biol 11(12):872-84 doi:10.1038/nrm3013

Wilhelm SM, Adnane L, Newell P, Villanueva A, Llovet JM, Lynch M (2008) Preclinical overview of sorafenib, a multikinase inhibitor that targets both Raf and VEGF and PDGF receptor tyrosine kinase signaling. Molecular cancer therapeutics 7(10):3129-3140 doi:10.1158/1535-7163.mct-08-0013

Will Y, Dykens JA, Nadanaciva S, et al. (2008) Effect of the multitargeted tyrosine kinase inhibitors imatinib, dasatinib, sunitinib, and sorafenib on mitochondrial function in isolated rat heart mitochondria and H9c2 cells. Toxicological sciences : an official journal of the Society of Toxicology 106(1):153-61 doi:10.1093/toxsci/kfn157

Williamson JR, Cooper RH (1980) Regulation of the citric acid cycle in mammalian systems. FEBS letters 117(Supplement 1):K73-K85 doi:https://doi.org/10.1016/0014-5793(80)80572-2

Wilson AJ, Gill EK, Abudalo RA, Edgar KS, Watson CJ, Grieve DJ (2017a) Reactive oxygen species signalling in the diabetic heart: emerging prospect for therapeutic targeting. Heart doi:10.1136/heartjnl-2017-311448

Wilson C, Munoz-Palma E, Gonzalez-Billault C (2017b) From birth to death: A role for reactive oxygen species in neuronal development. Seminars in cell & developmental biology doi:10.1016/j.semcdb.2017.09.012

Wirth C, Brandt U, Hunte C, Zickermann V (2016) Structure and function of mitochondrial complex I. Biochimica et biophysica acta 1857(7):902-14 doi:10.1016/j.bbabio.2016.02.013

Wood ER, Truesdale AT, McDonald OB, et al. (2004) A unique structure for epidermal growth factor receptor bound to GW572016 (Lapatinib): relationships among protein conformation, inhibitor off-rate, and receptor activity in tumor cells. Cancer research 64(18):6652-9 doi:10.1158/0008-5472.CAN-04-1168

Xie F, Ding X, Zhang QY (2016) An update on the role of intestinal cytochrome P450 enzymes in drug disposition. Acta Pharm Sin B 6(5):374-383 doi:10.1016/j.apsb.2016.07.012

Xu CF, Johnson T, Wang X, et al. (2016) HLA-B*57:01 Confers Susceptibility to Pazopanib-Associated Liver Injury in Patients with Cancer. Clinical cancer research : an official journal of the American Association for Cancer Research 22(6):1371-7 doi:10.1158/1078-0432.CCR-15-2044

Xue T, Luo P, Zhu H, et al. (2012) Oxidative stress is involved in Dasatinib-induced apoptosis in rat primary hepatocytes. Toxicology and applied pharmacology 261(3):280-91 doi:10.1016/j.taap.2012.04.010

Yang B, Papoian T (2012) Tyrosine kinase inhibitor (TKI)-induced cardiotoxicity: approaches to narrow the gaps between preclinical safety evaluation and clinical outcome. Journal of applied toxicology : JAT 32(12):945-51 doi:10.1002/jat.2813

Yang X, Wang J, Dai J, et al. (2015) Autophagy protects against dasatinib-induced hepatotoxicity via p38 signaling. Oncotarget 6(8):6203-17 doi:10.18632/oncotarget.3357

Youle RJ, van der Bliek AM (2012) Mitochondrial fission, fusion, and stress. Science 337(6098):1062-5 doi:10.1126/science.1219855

Yun CH, Okerholm RA, Guengerich FP (1993) Oxidation of the antihistaminic drug terfenadine in human liver microsomes. Role of cytochrome P-450 3A(4) in N-dealkylation and C-hydroxylation. Drug metabolism and disposition: the biological fate of chemicals 21(3):403-9

Yusoff AAMA, Farizan; Idris, Zamzuri;, Jaafar HA, Jafri Malin (2015) Understanding Mitochondrial DNA in Brain Tumorigenesis, Molecular Considerations and Evolving Surgical Management Issues in the Treatment of Patients with a Brain Tumor,

Zamek-Gliszczynski MJ, Hoffmaster KA, Nezasa K, Tallman MN, Brouwer KL (2006) Integration of hepatic drug transporters and phase II metabolizing enzymes:

mechanisms of hepatic excretion of sulfate, glucuronide, and glutathione metabolites. Eur J Pharm Sci 27(5):447-86 doi:10.1016/j.ejps.2005.12.007

Zeilinger K, Freyer N, Damm G, Seehofer D, Knospel F (2016) Cell sources for in vitro human liver cell culture models. Experimental biology and medicine 241(15):1684-98 doi:10.1177/1535370216657448

Zhang C, Liu Z, Bunker E, et al. (2017a) Sorafenib Targets the Mitochondrial Electron Transport Chain Complexes and ATP Synthase to Activate the PINK1-Parkin Pathway and Modulate Cellular Drug Response. The Journal of biological chemistry doi:10.1074/jbc.M117.783175

Zhang J, Salminen A, Yang X, et al. (2017b) Effects of 31 FDA approved small-molecule kinase inhibitors on isolated rat liver mitochondria. Arch Toxicol 91(8):2921-2938 doi:10.1007/s00204-016-1918-1

Zhang J, Yang PL, Gray NS (2009) Targeting cancer with small molecule kinase inhibitors. Nature reviews Cancer 9(1):28-39 doi:10.1038/nrc2559

CURRICULUM VITAE

CURRICULUM VITAE

PERSONAL DATA

Name Franziska Paech

INDUSTRIAL EXPERIENCE

05/2018 – present **Basilea Pharmaceutica International Ltd., *Basel, Switzerland***

- ADMET Scientist

01/2018 **Pharmaceutical Consulting, *Roche Pharma AG, Grenzach, Germany***

- Medical Writer

07/2014 – present **Pharmaceutical Consulting, *Basilea Pharmaceutica International Ltd., Basel, Switzerland***

- Planning of PK sample collection on an ongoing Phase 1 oncology study
- Working with a validated documentation system
- Literature research for the pharmacology and toxicology group

EDUCATION

06/2013 – 12/2017 **PhD, *University Basel, Switzerland***

- PhD Thesis: „Molecular Mechanisms of Tyrosine Kinase Inhibitors-associated Hepatotoxicity“
- Summa cum laude (best mark)
- Advisor: Prof. Stephan Krähenbühl
- Mitochondrial toxicity and Hepatotoxicity *in vitro* and *in vivo*
- Methods: Cell culture, Animal study, Isolated mitochondria, Oxygen consumption, Western Blot, RT-PCR, FACS, Radioactive assays, Spectrophotometric assays, Microscopy, Histology

09/2014 – 06/2016 **MSc Toxicology, *University Basel, Switzerland***

- 6.0 (best mark)
- Theoretical requirements for the registration as a professional toxicologist of the Swiss and European Register for Toxicologists
- Courses in Immunotoxicology, Reproductive Toxicology, Neurotoxicology, Animal Testing, Alternatives to Animal Testing, Biostatistics, Cancer, and Clinical Toxicology
- Master thesis: „Hepatotoxicity of the novel drug FP1912"

09/2011 – 02/2013 **MSc Medicinal and Industrial Pharmaceutical Sciences, *ETH Zurich, Switzerland***

- 5.46
- Courses in Regulatory Affairs, Patents, Drug Product Development, Project Management, Marketing, Quality Management, Biopharmacy, Biotransformation of Drugs and Xenobiotics, Clinical Research, Pharmacovigilance
- Master thesis: „Liposomal assay to study lipid bilayer permeation of drugs", PD Dr. Stefanie Krämer

09/2008 – 07/2011 **BSc Pharmaceutical Sciences, *ETH Zurich, Switzerland***

08/2001 – 06/2008 **Abitur, *Max-Steenbeck-Gymnasium-Cottbus, Germany***

FURTHER EXPERIENCE

2014 LTK Module 1: Introductory Course in Laboratory Animal Science in Mice/Rats

FURTHER COMMITMENT

2011 – 2016 **Teaching, *Know-Now AG, Switzerland***

- Private tutoring in Mathematics, Chemistry, Physics and Biology

2015 – present **Volunteer fire company Birsfelden, Switzerland**

2013 – present Athletics Club LC Basel, Switzerland

LANGUAGE SKILLS AND IT

German	Native
English	Fluent, conversational safe, team language
French	Basic knowledge

MS Office	Professional user
GraphPad Prism	Experienced user

HONORS AND AWARDS IN SWITZERLAND

2010 – 2017	Selected member of the Schweizerische Studienstiftung
2013	ETH medal for best master thesis in the pharmaceutical sciences, ETH Zurich, Switzerland
2011 – 2013	Master Scholarship Program, ETH Zurich, Switzerland

INTERESTS

Geocaching, Badminton, Hiking

PUBLICATIONS

- Bouitbir, J., Alshaikhali, A., Panajatovic, M. V., Abegg, V. F., **Paech, F.** and Krähenbühl, S. (2019). Mitochondrial oxidative stress plays a critical role in the cardiotoxicity of sunitinib: Running title: Sunitinib and oxidative stress in hearts. *Toxicology*, *426*, 152281.
- **Paech, F.**, Abegg, V. F., Duthaler, U., Terracciano, L., Bouitbir, J. and Krähenbühl, S. (2018). Sunitinib induces hepatocyte mitochondrial damage and apoptosis in mice. *Toxicology*, *409*, 13-23.
- Woodhead, J. L., **Paech, F.**, Maurer, M., Engelhardt, M., Schmitt-Hoffmann, A. H., Spickermann, J., Messner, S., Wind, M., Witschi, A. T., Krähenbühl, S., Siler, S. Q., Watkins, P. B. and Howell, B. A. (2018). Prediction of safety margin and optimization of dosing protocol for a novel antibiotic using quantitative systems pharmacology modeling. *Clinical and translational science*, *11*(5), 498-505.
- Setz, C., Benischke, A. S., Bento, A. C. P. F., Brand, Y., Levano, S., **Paech, F.**, Leitmeyer, K. and Bodmer, D. (2018). Induction of mitophagy in the HEI-OC1 auditory cell line and activation of the Atg12/LC3 pathway in the organ of Corti. *Hearing research*, *361*, 52-65.
- **Paech, F.**, Mingard, C., Grünig, D., Abegg, V. F., Bouitbir, J. and Krähenbühl, S. (2018). Mechanisms of mitochondrial toxicity of the kinase inhibitors ponatinib, regorafenib and sorafenib in human hepatic HepG2 cells. *Toxicology*, *395*, 34-44.
- Mingard, C., **Paech, F.**, Bouitbir, J. and Krähenbühl, S. (2018). Mechanisms of toxicity associated with six tyrosine kinase inhibitors in human hepatocyte cell lines. *Journal of Applied Toxicology*, *38*(3), 418-431.
- **Paech, F.**, Bouitbir, J. and Krähenbühl, S. (2017). Hepatocellular toxicity associated with tyrosine kinase inhibitors: mitochondrial damage and inhibition of glycolysis. *Frontiers in pharmacology*, *8*, 367.
- **Paech, F.**, Messner, S., Spickermann, J., Wind, M., Schmitt-Hoffmann, A. H., Witschi, A. T., Howell, B.A., Church, R.J., Woodhead, J., Engelhardt, M., Krahenbuhl, S. and Maurer, M. (2017). Mechanisms of hepatotoxicity associated with the monocyclic β-lactam antibiotic BAL30072. *Archives of toxicology*, *91*(11), 3647-3662.
- Hermann, K. F., Neuhaus, C. S., Micallef, V., Wagner, B., Hatibovic, M., Aschmann, H. E., **Paech, F.**, Alvarez-Sanchez, R., Krämer, S.D. and Belli, S. (2017). Kinetics of lipid bilayer permeation of a series of ionisable drugs and their correlation with human transporter-

independent intestinal permeability. *European Journal of Pharmaceutical Sciences*, *104*, 150-161.

- Brecht, K., Riebel, V., Couttet, P., **Paech, F.**, Wolf, A., Chibout, S. D., Pogan, F., Krähenbühl, S. and Uteng, M. (2017). Mechanistic insights into selective killing of OXPHOS-dependent cancer cells by arctigenin. *Toxicology in vitro*, *40*, 55-65.
- Eyer, K.*****, **Paech, F.***, Schuler, F., Kuhn, P., Kissner, R., Belli, S., Dittrich, P.S. and Krämer, S. D. (2014). A liposomal fluorescence assay to study permeation kinetics of drug-like weak bases across the lipid bilayer. *Journal of controlled release*, *173*, 102-109.

IMPORTANT CONGRESSES

2016	55th Congress of the Societies of Toxicology, New Orleans, USA
2015	EUROTOX, Porto, Portugal
2014	Targeting Mitochondria, Berlin, Germany